188(1), 2022

COMBUSTION ENGINES

Czołowy producent agregatów prądotwórczych w Polsce

FOGO®

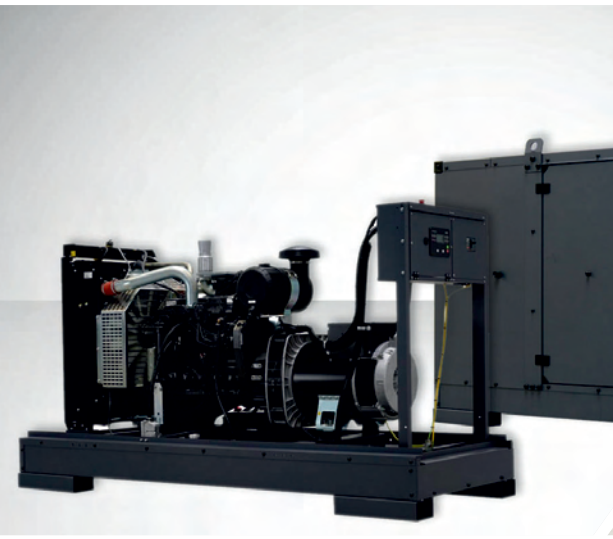

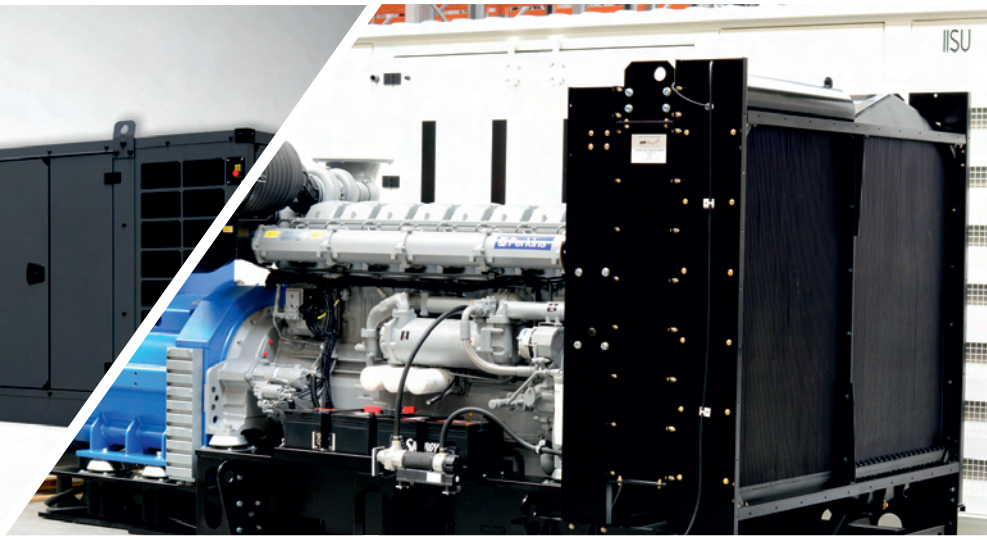

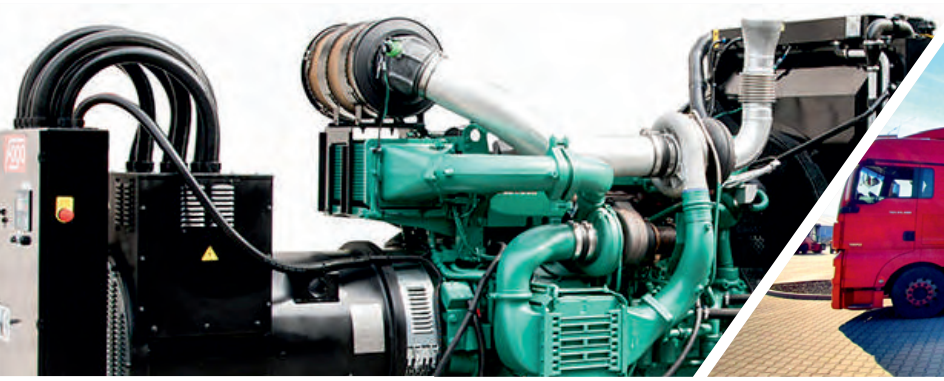

pewna **ENERGIA**

www.fogo.pl

PTNSS Supporting Members
Członkowie wspierający PTNSS

BOSMAL Automotive Research and Development Institute Ltd
Instytut Badań i Rozwoju Motoryzacji BOSMAL Sp. z o.o

Motor Transport Institute
Instytut Transportu Samochodowego

Institute of Aviation
Sieć Badawcza Łukasiewicz – Instytut Lotnictwa

Automotive Industry Institute
Sieć Badawcza Łukasiewicz – Przemysłowy Instytut Motoryzacji

Sieć Badawcza Łukasiewicz – Poznański Instytut Technologiczny

AVL List GmbH

Solaris Bus & Coach S.A.

Air Force Institute of Technology
Instytut Techniczny Wojsk Lotniczych

Military Institute of Armoured & Automotive Technology
Wojskowy Instytut Techniki Pancernej i Samochodowej

Toyota Motor Poland Ltd. Sp. z o.o.

RADWAG Balances and Scales
RADWAG Wagi Elektroniczne

MS Mechatronic Solutions Group

FOGO Sp. z o.o.

COMBUSTION ENGINES

A Scientific Magazine

2022, 188(1)

Year LXI

PL ISSN 2300-9896
PL eISSN 2658-1442

Publisher:

Polish Scientific Society of Combustion Engines
60-965 Poznan, pl. M. Skłodowskiej-Curie 5, Poland
tel.: +48 61 6475966, fax: +48 61 6652204
E-mail: sekretariat@ptnss.pl
WebSite: http://www.ptnss.pl
Papers available on-line: http://combustion-engines.eu

Contents

Publisher:
Polish Scientific Society of Combustion Engines
60-965 Poznan, pl. M. Sklodowskiej-Curie 5, Poland
tel.: +48 61 6475966, fax: +48 61 6652204
E-mail: sekretariat@ptnss.pl
WebSite: http://www.ptnss.pl

Subscriptions
Send subscription requests to the Publisher's address.
Cost of a single issue PLN 40.

Preparation for print
ARS NOVA Publishing House
60-782 Poznan, ul. Grunwaldzka 17/10A

Circulation: 100 copies

Printing and binding

Zakład Poligraficzny Moś i Łuczak, sp. j.,
Poznań, ul. Piwna 1

The journal is registered and listed in the Polish and international database

BazTech · INDEX COPERNICUS INTERNATIONAL · Crossref · EBSCO · DOAJ DIRECTORY OF OPEN ACCESS JOURNALS · POL-index Polska Baza Cytowań · SHERPA/RoMEO · ROAD

Papers published in the
Combustion Engines
quarterly receive 70 points as stated by the Notification of the Minister of Science and Education dated 1 December 2021.

Declaration of the original version
The original version of the Combustion Engines journal is the printed version.

Cover
I – Chevrolet Corvette Z06 LS6 C8 engine *(motortrend.com)*; background *(photo by KEHN HERMANO from Pexels)*
IV – Corvette Z06 LS6 C8 combustion chamber *(www.biznewspost.com)*

Article citation info:
FURMANEK, M., KROPIWNICKI, J. Stirling engines – the state of technology development and computational models. *Combustion Engines*. 2022, **188**(1), 3-12. https://doi.org/10.19206/CE-142027

Mariusz FURMANEK
Jacek KROPIWNICKI

Combustion Engines
Polish Scientific Society of Combustion Engines

Stirling engines – the state of technology development and computational models

ARTICLE INFO

Received: 12 August 2021
Revised: 31 August 2021
Accepted: 8 September 2021
Available online: 13 September 2021

Stirling engines represent a technologically important solution in combined heat and power systems. Their use enables the achievement of over 90 percent efficiency in the management of the primary energy source with a very high durability of the device, mainly due to the lack of contact of the working gas with external factors and a very small number of mechanical components. The use of a Stirling engine may be equally important when applying renewable energy sources or waste heat from other processes. The first part of the work presents an overview of available commercial Stirling engine solutions. The second part of the work presents an overview of numerical models of Stirling engine operation, which enable the correct selection of the main geometrical features of the devices and the improvement of the structure in order to maximize efficiency or power.

Key words: *Stirling engines, numerical models, commercial designs, low temperature sources, renewable energy sources*

1. Introduction

Stirling engines are one of the possible technological solutions enabling the management of the renewable and waste energy sources [10]. Currently, their main commercial application, however, is the production of heat and electricity from conventional energy sources, such as natural gas, diesel oil [8, 11, 20]. One of the most important technical problems related to the use of Stirling engines to generate electricity from low-temperature energy sources is the need to meet two basic countercurrent requirements, minimizing the dead volume associated with transporting the working gas between the compression and expansion spaces, and maximizing the heat exchange surface to provide the right amount of heat to the system with a low-temperature difference [18, 21, 25]. The optimization of the Stirling engine design requires very precise mapping of the influence of the above-mentioned design features on the efficiency and power of the system. For this purpose, computational models with varying degrees of details and accuracy are used. The paper presents an overview of the technology development of these structures.

2. Preview of commercial solutions

Stirling engine is powered from external source (an external chamber engine). This fact allows using heat for two simultaneous processes - heating and electricity production. The ability of supplying from the technological process as well (i.e. chemical or metallurgy industries) leads to reduce emission of carbon dioxide and consumption of fossil fuels. The Stirling engine is able to support process of electricity production with solar energy. Commercial systems aim at only electricity production or cogeneration working. These systems might be supplied by solid fuels, gas fuels and liquid fuels. Some commercial constructions have been presented below (Table 1).

Company Genoa offers engines in two variants [11, 12]. In the first configuration engines have one cylinder (configuration beta) and reach 1 kW (Fig. 1).The second configuration is equipped with two cylinders (configuration alpha) of power 3 kW (Fig. 2). Nitrogen is a working medium in both engines. Biomass and natural gas is a source of heat. These engines require 700°C to start up, the heat source should have at least 850°C.

Fig. 1. Two-cylinder Stirling engine Genoa, ML3000, power 3 kWe [13]

Fig. 2. One-cylinder Stirling engine Genoa ML1000, power 1 kWe [19]

Microgen products are based on one cylinder beta type Stirling engine. Available is setup with 1 kW and 2 kW electric power and heat might be generated in an external combustion chamber produced by burning natural gas or solid fuels. These engines belong to group free piston Stirling engines. Linear generator converts motion of piston on electric energy. This engine starts from about 180°C (working medium temperature). In Fig. 3 a view of Microgen Stirling engine has been presented.

Fig. 3. One-cylinder Microgen, power 1 kWe [5]

System of Inspirit Company includes generation of heat and electricity. In this solution the beta Stirling engine with free piston has been used. Overall efficiency equals to 92% including 16% of electric efficiency. In this case the heat of source is limited to natural gas. Version 3.1 is offered on the market. Previous versions of the engine generating lower power, i.e. Inspirit Charger 2.0 1–2 kWe and 5–10 kWt and Charger 3.0 1–3 kWe and 5–15 kWt. The last revision 3.1 offers up to 6.4 kWe and 15 kWt. In Fig. 4 Stirling engine of Inspirit (view on heater) has been presented.

Fig. 4. CHP Inspirit Stirling engine, power 1 kWe [8]

WhisperGen is distinguished by a lower electric power. In comparison with the engines previously presented, product of WhisperGen is prepared for working on land and sea. WhisperGen PPS 16 reaches 750 W of electric power and 5 kW of thermal power. The upper limit of the heat source is set to 550°C. In Fig. 5 the WhisperGen PPS 16 has been presented.

Fig. 5. Stirling engine Whispergen PPS16, power 0.75 kWe [28]

Engines of Powergen series are based on the beta free piston Stirling engines with linear generators also in two variants of power, respectively 1.2 kWe and 5.65 kWe (Fig. 6). Produced heat exceeds 2 to 3 times electricity production. Electric efficiency is estimated on 30% (the highest value for analyzed construction). The working gas temperature in the heater can operate in the range 400–800°C. Engines of Powergen Company use helium as a working gas.

Fig. 6. Stirling engine Qnery PowergGen 1200/5650, power 1.2 kWe/5.65 kWe [15, 16]

In the Table 1 has been presented engines specification of Genoa and Microgen. In the Table 2 has been presented engines specification of WhisperGen, Qnergy and Inspirit Charger.

Table 1. Technical specification of Genoa Stirling and Microgen

Parameter	Unit	Genoa ML3000	Genoa ML1000	Microgen 1 kW	Microgen 2 kW
Electric power	kWe	3.3	1.1	1.05	2
Thermal power	kWt	18.6	10	4	8
Electric efficiency	%	14	14	15.5–23	15.5–23
Power supply	–	Gas or biomass	Gas or biomass	Pellet, briquette, wood, natural gas or heating oil	Pellet, briquette, wood, natural gas or heating oil
Working medium	–	Nitrogen (air)	Nitrogen (air)	Air	Air
Working temperature (hot side)	°C	850–900	850–900	180–525	180–525
Cooling medium	–	Water	Water	Air	Air
Working temperature inlet/outlet (cold side)	°C	15/60	15/40	Min. 6/max 70; nominal 30	Min. 6/max 70; nominal 30
Cooling medium flow	dm^3/min	6.5	6.5	Nominal 8 (minimum 7)	Nominal 8 (minimum 7)

Table 2. Technical specification of WhisperGen, Qnergy and Inspirit

Parameter	Unit	WhispeGen PPS16	Qnergy PowerGen 1200	Qnergy PowerGen 5650	Inspirit Charger 3.1
Electric power	kWe	0.75	1.2	5.65	1–6.4
Thermal power	kWt	5	3–4.5	14–20	5–15
Electric efficiency	%	–	30	30	16
Power supply	–	Burning refined paraffin or diesel oil	Natural gas	Burning natural gas, LPG, propane	Natural gas
Working medium	–	Nitrogen	Helium	Helium	–
Working temperature (hot side)	°C	Up to 550	400–800	400–800	–
Cooling medium	–	Glycol	–	–	Water
Working temperature inlet/outlet (cold side)	°C	45/70	–	–	60/80
Cooling medium flow	dm^3/min	–	–	–	–

3. Numerical models of Stirling engine

3.1. Isothermal model

Mathematical model of Stirling engine was shown by Gustav Schmidt in 1871. Two basic assumptions of the model are constant temperature in each selected spaces and sinusoidal changing of volume working gas [1]. A heat included in the working gas is transformed to work. There is no heat transfer between environment and cooler, regenerator and heater. Heat transfer is realized in expansion and compression space. Based on these assumption, the engine works is a constant range of temperatures, the maximum temperature is reached in heater and expansion space, whereas the minimum temperature is observed in cooler and workspace called compression space. Those assumption cannot be met in a real engine because of the expected isothermal processing of the cycle, which requires infinity heat transfer surface in the heat exchangers [3].

It can mark out five work spaces of the engine: compression space c, cooler k, regenerator r, heater h and expansion space e. In Fig. 7 layout of temperature in work spaces was shown.

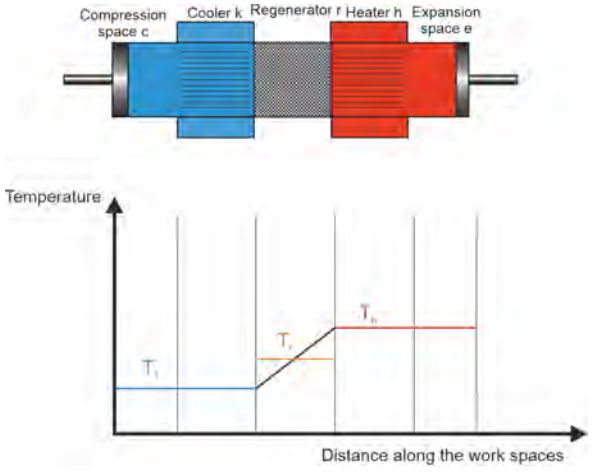

Fig. 7. Temperature profile in workspaces for isothermal model [23]

Assumptions for isothermal model are as follows [23]:

1. The constant gas temperature is over a surface of piston and in heat exchanger i.e. in compression space and in cooler (average temperature of lower heat source) are equal, that is $T_c = T_k$,. The same rule is obeyed in the expansion space and the heater $T_e = T_h$.
2. Rotational speed is constant.
3. The total mass of the working gas is constant (no leakage) in accordance with the following equation (1):

$$M = m_c + m_k + m_r + m_h + m_e \tag{1}$$

where M is the total mass of working gas in the system, m_c is the mass of working gas in the compression space, m_k is the mass of working gas in the cooler, m_r is the mass of working gas in the cooler, m_h is the mass of working gas in the heater and m_e is the mass of working gas in the expansion space.

4. Working gas is considered as an ideal gas.
5. The pressure of the working gas is the same in all spaces.
6. Volume change in the working spaces is sinusoidal.
7. Changes in kinetic and potential energy are negligible.

As a result of the usage of the Clapeyron equation, the total mass of gas equals:

$$M = \frac{P}{R}\left(\frac{V_c}{T_k} + \frac{V_k}{T_k} + \frac{V_r}{T_r} + \frac{V_h}{T_h} + \frac{V_e}{T_h}\right) \tag{2}$$

where P is the working gas pressure, R is the individual gas constant of working substance, V is the volume of working gas and T is the absolute temperature of working gas. After transformation equation (2) the formula of the pressure in the system is defined as:

$$P = \frac{MR}{\left(\frac{V_c}{T_k} + \frac{V_k}{T_k} + \frac{V_r}{T_r} + \frac{V_h}{T_h} + \frac{V_e}{T_h}\right)} \tag{3}$$

Temperature distribution in the regenerator is described by a linear function. In Fig. 8 the distribution of the temperature was shown. On the basis of the assumption there is no heat losses, the change of temperature is the same during heating and cooling process.

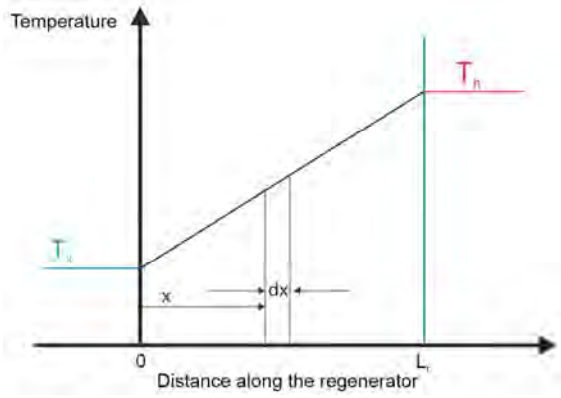

Fig. 8. Temperature distribution in ideal regenerator [24]

The change of temperature along the regenerator can be therefore defined as follows:

$$\frac{T(x)}{x} = \frac{T_h - T_k}{L_r} + T_k \tag{4}$$

where T(x) is the absolute gas temperature away of the inlet and L_r is the regenerator length.

By making transformations, we get:

$$T(x) = \left(\frac{T_h - T_k}{L_r}\right) x + T_k \tag{5}$$

The mass of gas in the regenerator is determined by the following formula:

$$m_r = \int_0^{V_r} \varrho \, dV_r \tag{6}$$

where m_r is the accumulated mass of gas in the workspace of regenerator, ϱ is the gas density and V_r is the volume of the regenerator workspace. The formula of gas density is define based on Clapeyron equation as:

$$\varrho = \frac{RT}{p} \tag{7}$$

Volume of regenerator V_r is equal:

$$V_r = A_r L_r \tag{8}$$

In differential form volume of regenerator equals:

$$dV_r = A_r dx \tag{9}$$

Using equations (7)–(9) the final form of form of equation (6) is given by:

$$m_r = \frac{V_r P}{R} \int_0^{L_r} \frac{1}{T(x) l_r} dx \tag{10}$$

Subsequently using equation (4) we obtain:

$$m_r = \frac{V_r P}{R} \int_0^{L_r} \frac{1}{(T_h - T_k)x + T_k L_r} dx \tag{11}$$

and after integration:

$$m_r = \frac{V_r P}{R} \frac{\ln\left(\frac{T_h}{T_k}\right)}{T_h - T_k} \tag{12}$$

or:

$$m_r = \frac{V_r P}{R T_r} \tag{13}$$

Gas pressure is equal in all spaces, this fact allows calculation of mass based on gas volume and temperature. By summarizing formulas (13) and (7) we obtain:

$$T_r = \frac{T_h - T_k}{\ln\left(\frac{T_h}{T_k}\right)} \tag{14}$$

Work of isothermal process in expansion space equals:

$$W_e = \oint P \, dV_e \tag{15}$$

and respectively work in compression space is calculated by following formula:

$$W_c = \oint P \, dV_c \tag{16}$$

Summarizing generated work in expansion (15) and compression space (16), leads to the total work of engine:

$$W = W_e + W_c = \oint P dV_e + \oint P \, dV_c \tag{17}$$

According to first law of thermodynamics for open system [2]:

$$dQ + \left(C_p T_i m_i' - C_p T_o m_o'\right) = dW + C_v d(mT) \tag{18}$$

where dQ is the heat transferred from the environment to workspace of cylinder, C_p is the specific heat by the constant pressure, T_i is the inlet gas temperature, m_i' is the inlet gas mass, T_o is the outlet gas temperature, m_o' is the outlet gas mass, dW is the work transferred into the environment and C_v is the specific heat by the constant volume. In the Fig. 9 the scheme of the cylinder workspace was shown.

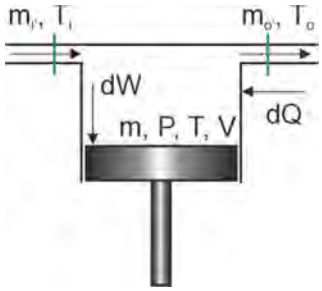

Fig. 9. Scheme of the cylinder workspace [7, 23]

Isothermal model is leading to simplification of formula (18), because the inlet temperature and the outlet temperature are equal ($T_i = T_o$). The formula describing difference between the inlet mass (m_i) and the outlet mass (m_o) is replaced by the parameter dm. Finally it can be described as:

$$dQ + C_p T dm = dW + C_v T dm \tag{19}$$

Correlation between c_p and c_v is described as $c_P = c_v + R$, which reduces formula (19) to the form:

$$dQ = dW + RT dm \tag{20}$$

Amount of the heat transferred into gas working during engine cycle equals integer dQ (20). After integration, the following equations are obtained:

$$Q_c = W_c, \; Q_e = W_e, \; Q_k = 0, \; Q_h = 0, \; Q_r = 0$$

where Q_c is the heat generated during gas compression, W_c is the work of compression process, Q_e is the heat generated during gas expansion, W_e is the work generated during gas expansion, Q_k is the heat derived from cooler into environment, Q_h is the heat rejected from environment, Q_r is the heat losses in regenerator.

The following conclusions can be drawn from the above considerations:

1. The heat exchange is processed only in compression and expansion space.
2. There is no heat losses in the regenerator.
3. In the heater and the cooler there is no heat transfer.

3.2. Adiabatic model

The novel approach in the field of modelling Stirling engine was caused by the adiabatic model developed by Finkelstein [26]. From the point of view of modelling process – compression and expansion cause a significant change. These processes are described by an adiabatic model. The heat transfer into cooler and heater is modelled by the isothermal model. Calculated efficiency based on the isothermal model is higher by about 20–30% in comparison to adiabatic model [9].

Isreaeli Urieli and Dave Berchowitz [26] developed quasi static model of ideal Stirling engine with adiabatic expansion and compression. The assumptions of model are as follows:

1. All processes are realized in a steady state.
2. The rotational speed is constant.
3. The working gas is treated as an ideal gas.
4. Process of compression and expansion are conducted without the heat transfer with the environment.
5. Instantaneous pressure in expansion and compression space is equal.
6. Temperature of gas in the cooler and heater is constant.
7. The change of temperature in regenerator is linear.
8. Kinetic and potential energy is negligible.
9. Heat transfer takes place only in the cooler and heater.
10. Total gas mass in the system is constant.
11. Heat loss as the result of flow between workspaces (compression and expansion) and also heat loss into the environment is negligible.
12. There is no gas leakage.

Split of workspaces was shown in Fig. 10, between workspaces implemented four domains (boundary areas): compression space-cooler ck, cooler-regenerator kr, regenerator-heater rh and heater-expansion space he.

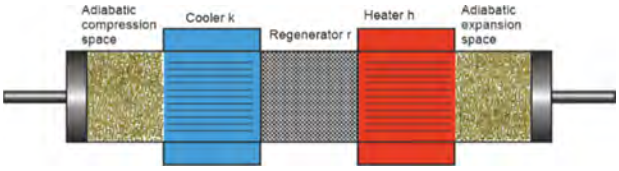

Fig. 10. Scheme of workspaces for adiabatic model [22]

Temperature profile in workspaces with split on domains was presented in Fig. 11.

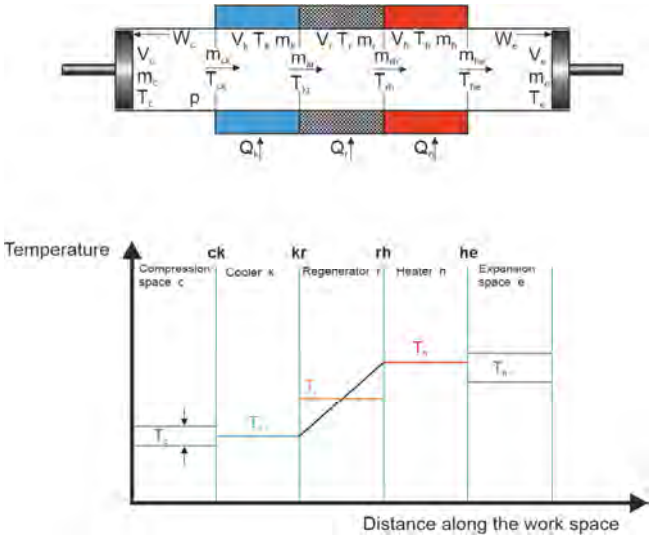

Fig. 11. Temperature profile in workspaces for adiabatic model [22]

The values of temperature on the domain is conditioned by flow direction. Mass flow rate flowing through the domain ck equals m_{ck}'. Positive mass flow rate means gas flow to expansion space, whereas negative is correlated with flow in opposite direction. The value of temperature is determined by direction flow with following equations (21)–(24) [3]:

$$T_{ck} = \begin{cases} T_c \text{ for } \dot{m}_{ck} > 0 \\ T_k \text{ for } \dot{m}_{ck} < 0 \end{cases} \tag{21}$$

$$T_{kr} = \begin{cases} T_k \text{ for } \dot{m}_{kr} > 0 \\ T_r \text{ for } \dot{m}_{kr} < 0 \end{cases} \tag{22}$$

$$T_{rh} = \begin{cases} T_r \text{ for } \dot{m}_{rh} > 0 \\ T_h \text{ for } \dot{m}_{rh} < 0 \end{cases} \tag{23}$$

$$T_{he} = \begin{cases} T_h \text{ for } \dot{m}_{he} > 0 \\ T_e \text{ for } \dot{m}_{he} < 0 \end{cases} \tag{24}$$

where T_{ck} is the gas temperature, m_{ck} is the mass of working gas on the edge compression space and cooler. In the adiabatic model gas mass is constant (similar isothermal model):

$$M = m_c + m_k + m_r + m_h + m_e \tag{25}$$

Working substance is considered as an ideal gas, according to Clapeyron equation in each compartment relationship with thermodynamical parameters are defined:

$$PV = mRT \tag{26}$$

After differentiating Clapeyron equation (26) has taken the following form:

$$\frac{dP}{p} + \frac{dV}{V} = \frac{dm}{m} + \frac{dT}{T} \tag{27}$$

Mass balance of system is written as:

$$dm_c + dm_k + dm_r + dm_h + dm_e = 0 \tag{28}$$

Total gas mass equals:

$$M = \frac{P}{R}\left(\frac{V_c}{T_k} + \frac{V_k}{T_k} + \frac{V_r}{T_r} + \frac{V_h}{T_h} + \frac{V_e}{T_h}\right) \tag{29}$$

Transforming formula (29), is the following formula has been obtained:

$$P = \frac{MR}{\left(\frac{V_c}{T_k} + \frac{V_k}{T_k} + \frac{V_r}{T_r} + \frac{V_h}{T_h} + \frac{V_e}{T_h}\right)} \tag{30}$$

Temperature and volume is constant in the heat exchangers (cooler, regenerator and heat) and therefore the formula (27) is reduced to:

$$\left.\frac{dm}{m}\right|_{k,r,h} = \left.\frac{dP}{P}\right|_{k,r,h} \tag{31}$$

Ideal gas equation in differential form is written as:

$$dm = dP\frac{V}{RT} \tag{32}$$

After substitution (31) in equation (28) mass balance equals:

$$dm_c + dm_e + dP\left(\frac{m_k}{p} + \frac{m_r}{p} + \frac{m_h}{p}\right) = 0 \tag{33}$$

Modification equation (33) by substitution of Clapeyron equation leads to notation:

$$dm_c + dm_e + \frac{dP}{R}\left(\frac{V_k}{T_k} + \frac{V_r}{T_r} + \frac{V_h}{T_h}\right) = 0 \tag{34}$$

Separated section of analyzed spaces (compression space and cooler) was presented in Fig. 12.

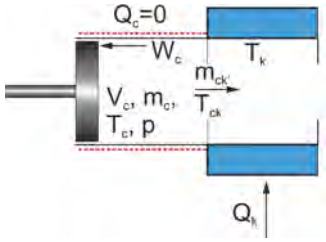

Fig. 12. Scheme of adiabatic compression space and cooler [22]

Compression space is insulated to environment and hence – form of change of internal energy took place only for work. In energy balance for compression space piece of equation related with gas flow in direction cooler occurred [6].

$$-C_p T_{ck} \dot{m}_{ck} = PdV_c + C_V d(T_c m_c) \tag{35}$$

The gas flow is realized from compression space to cooler thus expression (35) changed their form:

$$C_p T_{ck} m_c = PdV_c + C_V d(T_c m_c) \tag{36}$$

Using assumptions about ideal gas, relationship between specific heat by constant pressure and specific heat by constant volume is related with individual gas constant in next form [19]:

$$R = C_p - C_v \tag{37}$$

$$\kappa = \frac{C_p}{C_V} \tag{38}$$

where κ is the heat capacity ratio. Accumulated gas mass into compression space equals:

$$dm_c = \frac{PdV_c + \frac{V_c dP}{\kappa}}{RT_{ck}} \tag{39}$$

and in expansion space:

$$dm_e = \frac{PdV_e + \frac{V_e dP}{\kappa}}{RT_{he}} \tag{40}$$

Combining dependencies (37)–(40) a differential equation is obtained describing pressure in system:

$$dP = -\frac{P\kappa\left(\frac{dV_c}{T_{ck}} + \frac{dV_e}{T_{he}}\right)}{\frac{V_c}{T_{ck}} + \kappa\left(\frac{V_h}{T_h} + \frac{V_k}{T_k} + \frac{V_r}{T_r}\right) + \frac{V_e}{T_{he}}} \tag{41}$$

Determining equation of change of pressure (41) creates a system of nonlinear differential equations including parameters for compression space i.e. T_c, m_c and expansion T_e, m_e. Determination of pressure and mass allows gathering other parameters, volumes in workspaces dV_c, dV_k, dV_h and dV_e which are marked based on kinematic equations. Equation of state gas form compression space has got the following form:

$$T_c = \frac{PV_c}{m_c R} \tag{42}$$

After differentiating state equation (33) equals:

$$dT_c = \frac{V_c}{m_c R} dP + \frac{P}{m_c R} dV_c - \frac{PV_c}{R} \frac{1}{m_c^2} dm_c \tag{43}$$

hence:

$$dT_c = \frac{T_c}{p} dP + \frac{T_c}{V_c} dV_c - \frac{T_c}{m_c} dm_c \tag{44}$$

Final form equation of determining temperature in compression space:

$$dT_c = T_c\left(\frac{dP}{p} + \frac{dV_c}{V_c} - \frac{dm_c}{m_c}\right) \tag{45}$$

In compression space gas temperature is obtained by formula:

$$dT_e = T_e\left(\frac{dP}{p} + \frac{dV_e}{V_c} - \frac{dm_e}{m_e}\right) \tag{46}$$

Using the energy balance equation for heat exchangers (constant temperature and volume of working gas) and equation state of an ideal gas (26), equation energy balance is written as:

$$dQ + \left(C_p T_i m_i' - C_p T_o m_o'\right) = C_v T dm \tag{47}$$

and:

$$dQ + \left(C_p T_i m_i' - C_p T_o m_o'\right) = V dP \frac{C_V}{R} \tag{48}$$

Amount of heat transferred in cooler equals:

$$dQ_k = V_k \frac{C_V}{R} dP - C_p(T_{ck} m_{ck}' - T_{kr} m_{kr}') \tag{49}$$

and in regenerator:

$$dQ_r = V_r \frac{C_V}{R} dP - C_p(T_{kr} m_{kr}' - T_{rh} m_{rh}') \tag{50}$$

also in heater:

$$dQ_h = V_h \frac{C_V}{R} dP - C_p(T_{rh} m_{rh}' - T_{he} m_{he}') \tag{51}$$

The temperature of gas is on the permanent level [3]:

$$\begin{cases} T_{kr} = T_k \\ T_{rh} = T_h \end{cases} \tag{52}$$

Total quantity of work is a sum of a produced work in each cylinder:

$$W = W_e + W_c \tag{53}$$

processes are described by adiabatic model hence work of cycle equals:

$$dW = pdV_e + pdV_c \tag{54}$$

3.3. CAFS – Combined Adiabatic–Finite Speed

Mathematical model developed by Hosseinzadeh and other [7] is an amplification adiabatic model [26], additional elements are mechanical losses and finite speed thermodynamic.

The idea of thermodynamic with finite speed was presented in 50's of 20th century [14]. The assumption of FST is the analysis of real processes which occurred in thermodynamical systems of piston engines towards optimization (increase power and efficiency) and it included irreversible phenomena.

The main task of thermodynamic with finite speed is to describe the interaction between piston (moving with speed w_p) and gas molecules located in the system (moving with average speed of sound c).

Petrescu and other [14] demonstrated that in consequence of piston motion gas pressure being over piston surface are different from instantaneous mean pressure in cylinder. This fact means that compression and expansion work are different to calculated work based on the classical thermodynamic. It causes that work generated by engine is

lower than received work by classical thermodynamic. On account of piston motion local disorder of gas placed in work space is generated leading to make an acoustic wave and as a consequence of this phenomena pressure drops [4]. The propagation of wave took place with the speed of sound [7].

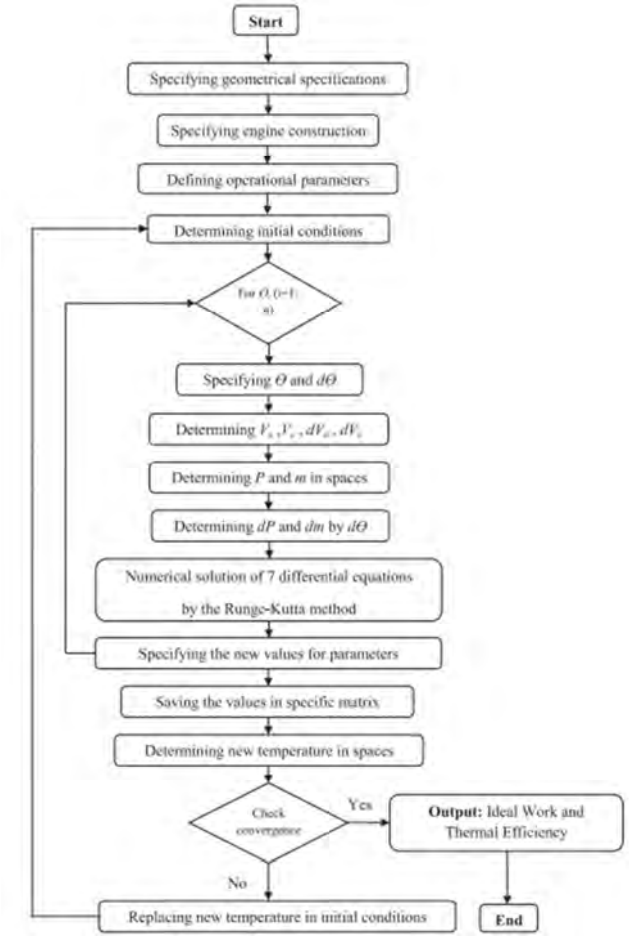

Fig. 13. Flow chart of the algorithm of ideal adiabatic model [7]

The first law of thermodynamics for process with finite speed in a closed system is written as (the scheme of workspace is presented in Fig. 9):

$$dU = \delta Q - p\left(1 \pm \frac{aw_p}{c} \pm \frac{fr\Delta p_f}{p_m}\right) dV \tag{55}$$

where dU is the change of internal energy, δQ is the transferred heat between cylinder and environment, p is the instantaneous mean pressure over piston, a is the coefficient $a = \sqrt{3\kappa}$ [4], w_p is the piston speed, c is the speed of sound $c = \sqrt{3RT}$ [4]. Friction factor fr is a range of from 0 to 1. For fr = 0 heat transfer took place to environment (compression space), heat is keep in the system while fr = 1.

One of the assumption is that the present model is adiabatic process during expansion and compression, hence expression $\delta Q = 0$. Based on equation (58) work is equal change of internal energy with negative sign:

$$dU = -p\left(1 \pm \frac{aw_p}{c} \pm \frac{\Delta P_f}{p_m}\right) dV \tag{56}$$

hence equation (56) is written:

$$mC_v dT = -p\left(1 \pm \frac{aw_p}{c} \pm \frac{\Delta P_f}{p_m}\right) dV \tag{57}$$

Work of irreversible process is obtained:

$$\delta W_{FST} = p\left(1 \pm \frac{aw_p}{c} \pm \frac{\Delta p_f}{p_m}\right) dV \tag{58}$$

where δW_{FST} is calculated irreversible work with using FST. Sign (+) is applicated in equations (55)–(58) for describing expansion process, sign (–) occurs while compression process.

Drop pressure ΔP_f is caused by mechanical losses (friction) ΔP_f. it is computed by equation [4]:

$$\Delta P_f = \frac{(0.4+0.0045w_p)10^5}{3\zeta}\left(1 - \frac{1}{cr}\right) \tag{59}$$

where ζ is the constant value [5]:

$$\zeta = 1 - \frac{1}{cr} \tag{60}$$

where cr is the compression ratio. Total work of engines (with throttle losses) equals [5]:

$$\delta W_{total} = \delta W_{FST} + \Delta P_{th} dV \tag{61}$$

where δW_{total} is generated work by engine with considered finite piston speed, mechanical friction losses and throttle phenomena in heat exchangers, ΔP_{th} is the drop pressure in heat exchangers, V is the instantaneous gas volume.

Drop pressure in heater and cooler are significantly lower than in regenerator. According to Darcy-Weisbach drop pressure equals [27]:

$$\Delta P = fr\frac{\varrho}{2}\frac{L}{D_H}u^2 \tag{62}$$

where fr is the friction coefficient, ϱ is the gas density, L is length, D_H is hydraulic diameter and u is the speed of gas flow.

Drop pressure of throttling is obtained in result of summarizing drop pressure in regenerator, cooler and heater:

$$\Delta P_{th} = \Delta P_r + \Delta P_k + \Delta P_h \tag{63}$$

The efficiency regenerator is calculated based on number of thermal unit (NTU) [7]:

$$\varepsilon = \frac{NTU}{1+NTU} \tag{64}$$

where ε is the regenerator efficiency, NTU is the number thermal unit is determined based on formula:

$$NTU = \frac{StL_r}{D_{hr}} \tag{65}$$

where St is Stanton number, L_r is length of regenerator and D_{hr} is regenerator hydraulic diameter. Stanton number is determined based on Reynolds and Prandtl number [13]:

$$St = 0.023Re^{-0.2}Pr^{-0.6} \tag{66}$$

Hydraulic diameter is calculated in the following way [7]:

$$D_{hr} = \frac{4\Pi}{\Phi(1-\Pi)} \tag{67}$$

where Π is the porosity regenerator, Φ is the coefficient shape is related with volumen and surface:

$$\Phi = \frac{A_{wg}}{V_{mr}} \tag{68}$$

where A_{wg} is the wetted surface and $V_{mr}$is the volume of wires regenerator. Gas temperature in heater and cooler is received by solving equations [7]:

$$T_h = T_{wh} - \frac{fr[Q_h + Q_r(1-\varepsilon_r)]}{\alpha_h A_h} \tag{69}$$

$$T_k = T_{wk} - \frac{fr[Q_k + Q_r(1-\varepsilon_r)]}{\alpha_k A_k} \tag{70}$$

where T_h is the gas temperature in heater, T_{wh} is the wall temperature in heater, fr is engine frequency, Q_h is heat supplied to the heater, Q_r is heat exchanged in regenerator, ε_r is regenerator efficiency, α_h is heat transfer coefficient in heater, A_h is heat transfer surface in heater, T_k is gas temperature in heater, Q_k is heat removed from the cooler, α_k is the heat transfer coefficient in cooler and A_k is the heat transfer surface in cooler. Heat transfer coefficient is obtained using the following equation [7]:

$$\alpha = \frac{0.0791 \mu C_p Re^{0.75}}{2 D_h Pr} \tag{71}$$

where α is heat transfer coefficient, μ is dynamic viscosity, C_p is the specific heat and D_h is hydraulic diameter.

3.4. PSVL – Polytropic model Stirling with various losses

Babaelahi and other [1] developed their model based on the adiabatic model. Energy balance according to first law of thermodynamic for open system is as follows [1]:

$$dQ - dQ_{poli} - dQ_{sh} + \left(m_i C_{p,i} T_i - m_o C_{p,o} T_o\right) = \\ = dW + C_V d(mT) \tag{72}$$

where dQ is transferred heat between working gas and environment, dW is network generated by engine, dQ_{poli} is heat emitted in compression and expansion space by polytropic model and dQ_{sh} is transferred heat by displacer from expansion to compression space shuttle effect of piston [1]:

$$dQ_{sh} = \frac{\pi S^2 \lambda_t D_{dis}(T_e - T_c)}{8 J L_{dis}} \tag{73}$$

where S is stroke, λ_{dis} is the displacer thermal conductivity D_{dis} is diameter of displacer, J is size of the gap between the displacer and the cylinder, L_{dis} is length of displacer. The fourth piece of left side equation (73) is related with enthalpy change of the working substance. The second piece of right side energy balance equation concerns change of internal energy in volume. Transferred heat into environment dQ_{poli} in compression and expansion chamber is obtained [8]:

$$Q_{poli} = mC_n(T_0 - T) \tag{74}$$

where C_n is the specific heat polytropic, T_0 is the ambient temperature and T is the temperature in controlled space. Differential form of equation energy balance is written as:

$$dQ_{poli} = C_n(T_0 - T)dm - mC_n dT \tag{75}$$

Polytropic specific heat is determined in the following way [17]:

$$C_n = C_V \frac{n-k}{n-1} \tag{76}$$

According to the polytropic equation:

$$PV^n = const \tag{77}$$

whereas differential form of polytropic equation equals:

$$P(nV^{n-1}dV) + nV^n dP = 0 \tag{78}$$

hence polytropic exponent:

$$n = -\frac{VdP}{PdV} \tag{79}$$

After modification we get a formula describing the change of mass gas:

$$dm_c = \frac{\left[\left(\frac{PdV_c + \frac{V_c}{\kappa}dP}{RT_{ck}}\right) - \left(\frac{C_{nc} m_c}{C_p T_{ck}} dT_c\right) - \left(\frac{Q_{sh}}{C_p T_{ck}}\right)\right]}{\left[\left(\frac{C_{nc}}{C_p}\right)\left(\frac{T_0 - T_c}{T_{ck}}\right) + 1\right]} \tag{80}$$

where C_{nc} is the polytropic exponent in compression space and C_{ne} is the polytropic exponent in expansion space, thus $dm_c = \dot{m}_{ck}$. An analogous description is retained for the expansion space

$$dm_e = \frac{\left[\left(\frac{PdV_e + \frac{V_e}{\kappa}dP}{RT_{he}}\right) - \left(\frac{C_{ne} m_e}{C_p T_{ck}} dT_e\right) - \left(\frac{Q_{sh}}{C_p T_{he}}\right)\right]}{\left[\left(\frac{C_{ne}}{C_p}\right)\left(\frac{T_0 - T_e}{T_{he}}\right) + 1\right]} \tag{81}$$

By ordering the expressions (80) and (81), the equation defining the change in pressure dP is obtained:

$$dP = \frac{-\kappa\left[\underbrace{\frac{PdV_e}{T_{he}} - \frac{RC_{ne} m_e}{C_p T_{he}} dT_e + \frac{RQ_{sh}}{C_p T_{he}}}_{B_1} + \underbrace{\frac{PdV_c}{T_{ck}} - \frac{RC_{nc} m_c}{C_p T_{ck}} dT_c + \frac{RQ_{sh}}{C_p T_{ck}}}_{B_2}\right] + Rm_w}{\frac{V_c}{T_{ck} B_1} + \frac{V_e}{T_{he} B_2} + \kappa\left(\frac{V_k}{T_k} + \frac{V_h}{T_h} + \frac{V_r}{T_r}\right)} \tag{82}$$

where:

$$B_1 = \left(\frac{C_{nc}}{C_p}\right)\left(\frac{T_0 - T_c}{T_{ck}}\right) + 1 \tag{83}$$

$$B_2 = \left(\frac{C_{ne}}{C_p}\right)\left(\frac{T_0 - T_e}{T_{he}}\right) + 1 \tag{84}$$

Working gas temperature in compression space is calculated based on following expression:

$$dT_c = T_c\left(\frac{dP}{p} + \frac{dV_c}{V_c} - \frac{dm_c}{m_c}\right) \tag{85}$$

Gas temperature in expansion space is computed in a similar way:

$$dT_e = T_e\left(\frac{dP}{p} + \frac{dV_e}{V_c} - \frac{dm_e}{m_e}\right) \tag{86}$$

Transferred heat into the heat exchanger equals respectively [9]:

$$dQ_k = V_k \frac{C_V}{R} dP - C_p(T_{ck}\dot{m}_{ck} - T_{kr}\dot{m}_{kr}) \tag{87}$$

$$dQ_h = V_h \frac{C_V}{R} dP - C_p(T_{rh}\dot{m}_{rh} - T_{he}\dot{m}_{he}) \tag{88}$$

$$dQ_r = V_r \frac{C_V}{R} dP - C_p(T_{kr}\dot{m}_{kr} - T_{rh}\dot{m}_{rh}) \tag{89}$$

Generated work by gas in compression space:

$$dW_c = pdV_c \tag{90}$$

and expansion space:

$$dW_e = pdV_e \tag{91}$$

Overall work was produced by engine is a sum of work made by gas in compression and expansion space.

$$W = \int dW_c + \int dW_e \tag{92}$$

Engine efficiency is quotient of work engines (92) and delivered heat into system (88):

$$\eta_{\text{netto}} = \frac{W}{Q_h} \tag{93}$$

The assumption of nonideal heat transfer in regenerator means that efficiency is lower than 100 percent. Regenerator efficiency ε is defined as its ability to change gas enthalpy that is a real change of enthalpy to the theoretical maximum change of gas enthalpy. Included heat loss, amount of heat delivered to the heater and taking from cooler equals:

$$Q_h = Q_{hid} + Q_{rl} = Q_{hid} + Q_{rid}(1-\varepsilon) \tag{94}$$

$$Q_k = Q_{kid} - Q_{rl} = Q_{kid} - Q_{rid}(1-\varepsilon) \tag{95}$$

Element $Q_{rid}(1-\varepsilon)$ represents heat loss in the regenerator. In comparison with formulas (94)–(95) in this analyze it is regarded regenerator efficiency ε. Regenerator efficiency with assumption linear profile of temperature [26] as function inlet and outlet temperature [1]:

$$\varepsilon = \frac{1}{1+\frac{\delta T}{T_{h_i}-T_{h_o}}} \tag{96}$$

where ε is the regenerator efficiency, δT is the difference temperature between flowing gas from heater in regenerator and flowing gas from cooler, T_{h_i} is the inlet gas temperature to regenerator from heater and T_{h_o} is the outlet gas temperature from regenerator. According to the equation (96) the increase of regenerator efficiency occurs when outlet gas temperature T_{h_o} reaches lower temperature (supplying regenerator from heater side – in regenerator more heat is located). Heat balance of the flowing gas equals $\dot{m}C_p\left(T_{h_i} - +T_{h_o}\right) = \alpha A_{wg}\delta T$. In consequence regenerator efficiency is defined as:

$$\varepsilon = \frac{1}{1+\frac{\dot{m}C_p}{\alpha A_{wg}}} = \frac{1}{1+\frac{1}{NTU}} = \frac{NTU}{1+NTU} \tag{97}$$

where $\dot{m}$ is the mass flow rate, C_p is the specific heat of gas, α is heat transfer coefficient, A_{wg} is the wetted surface by gas.

It is impossible to implement the isothermal model in reality. Hence this model might be only used in order to determine maximum efficiency for the examined engine. This model is based on algebraic equation, this fact allows calculation in an easy way. In other words, results of the isothermal model is upper limit in regarding reached values of the power and efficiency.

Adiabatic model is closer to real engines than isothermal one because in expansion and compression space temperature change occurs but in the heat changers there is still a constant temperature. In the real engines heat transfer appears mainly in the heat exchanger, in significantly small scale in cylinder, so this model is discrepant from real conditions. Adiabatic model is basic for modern models.

In Combined Adiabatic model with Finite Speed an assumption is included that the change of temperature in heat exchangers, nonideal regenerator and mechanical (friction) losses, pressure losses (throttling) and thermodynamics with finite speed. Polytropic model is development of this approach.

One of serious restriction for CAFS and PVSL is necessary awareness of exact specification. Full technical specification often is restricted by producers. CAFS and PVSL (and other models with nonisothermal processes in heat exchangers and cylinders) might be used for modelling real machines.

Isothermal and simple adiabatic model might be only applicable for tentative calculations – estimating power and efficiency for set parameters.

Conclusions

So far devices with Stirling engines offered nowadays on market are mostly not designed to supply with low-temperature heat sources, usually they are equipped with a combustion chamber allowing supply with conventional fuels such as compressed natural gas or mixture of propane and butane. Heaters of such kind of engines c cannot be directly used to supply with contaminated flue gas due to the small cross-sectional area of slots, which the gas passes.

Few examples of devices that enable the use of waste energy, require proper operation of the temperature of energy source no lower than 500°C. Such restrictions have two main reasons: the first one, of a technical nature, heavy mechanical losses in the SE caused by high pressure of working gas, often exceeding 60 MPa [29]. The second reason is of economical nature, SE supplied with low temperature heat source will have extremely long period of return on investment (» 20 years).

The key improvements, which must be done before commercialization of SE supplied with low temperature renewable sources are lowering the mechanical losses in the SE, rising performance of the flue gases – working gas heat exchanger and developing low cost manufacturing technology that ensures low cost of production.

The analysed numerical models of SE operation have a different level of complexity and describe the processes taking place in a real device with a different degree of idealization. Depending on the stage of development of structures powered by low-temperature energy sources, the presented models can be effectively used to determine the direction of changes in the design parameters of the device. The first of them the isothermal model (section 3.1) enables the analysis of the main design parameters of the device without the necessity to take into account the empirical coefficients that are difficult to collect at the initial design stage of design. In engines powered by low-temperature energy sources, it is extremely difficult to design a structure, in which the heat is delivered in the expansion space and not through an external heat exchanger. Hence, the adiabatic model (section 3.2) will be characterized by a higher accuracy, but still does not require the use of hard-to-obtain empirical coefficients. This kind of model is unfortunately more computationally demanding. The next CAFS model – Combined Adiabatic-Finite Speed (section 3.3) should be applied, when the structural details of the designed device are known, the computational base is the adiabatic model, however, a number of hydraulic losses are also taken into account. Experimental coefficients are required for the calculations. The last model, with the most

complexity, PSVL – Polytropic model Stirling with various losses (section 3.4), enables a more detailed description of the phenomena occurring in the area of compression and expansion by using a polytropic model instead of the adiabatic one. It takes into account a similar model of hydraulic losses as previously described, and at the same time requires the greatest number of experimental factors.

Nomenclature

CAFS	Combined Adiabatic Finite Speed
FST	Finite Speed Thermodynamics
NTU	Number of transfer units
PSVL	Polytropic model Stirling with Various Losses
SE	Stirling Engine

Bibliography

[1] BABAELAHI, M., SAYYAADI, H. A new thermal model based on polytropic numerical simulation of Stirling engines. *Applied Energy*. 2015, **141**, 143-159. https://doi.org/10.1016/j.apenergy.2014.12.033

[2] BABAELAHI, M., SAYYAADI, H. Modified PSVL: A second order model for thermal simulation of Stirling engines based on convective-polytropic heat transfer of working spaces. *Applied Thermal Engineering*. 2020, **85**, 340-355. https://doi.org/10.1016/j.applthermaleng.2015.03.018

[3] CHEN, N.C.J., GRIFFIN, F.P. Review of Stirling-engine mathematical models. Oak Ridge, TN 1993. https://doi.org/10.2172/5948203

[4] COSTEA, M., PETRESCU, S., HARMAN, C. Effect of irreversibilities on solar Stirling engine cycle performance. *Energy Conversion and Management*. 1999, **40**(15), 1723-1731. https://doi.org/10.1016/S0196-8904(99)00065-5

[5] Engines, Microgen. https://www.microgen-engine.com/engines/

[6] GARCÍA, M.T., TRUJILLO, E.C., GODIÑO, J.A.V. et al. Thermodynamic model for performance analysis of a Stirling engine prototype. *Energies*. 2018, **11**(10). https://doi.org/10.3390/en11102655

[7] HOSSEINZADE, H., SAYYAADI, H. CAFS: The combined adiabatic-finite speed thermal model for simulation and optimization of Stirling engines. *Energy Conversion and Management*. 2014, **91**, 32-53. https://doi.org/10.1016/j.enconman.2014.11.049

[8] Inspirit Charger https://www.inspirit-energy.com/the-inspirit-charger/

[9] INVERNIZZI, C.M. Closed power cycles: Thermodynamic fundamentals and applications. *Lecture Notes in Energy*. 2013, **11**. https://doi.org/10.1007/978-1-4471-5140-1

[10] KROPIWNICKI, J. Analysis of start energy of Stirling engine type alpha. *Archives of Thermodynamics*. 2019, **40**(3), 243-259. https://doi.org/10.24425/ather.2019.130004

[11] ML3000, Genoa Stirling. https://genoastirling.com/eng/engine-ml3000.php

[12] ML1000, Genoa Stirling. https://genoastirling.com/eng/engine-ml1000.php

[13] ORGAN, A.J. The Regenerator and the Stirling Engine. *Wiley–Blackwel*. 1997.

[14] PETRESCU, S., COSTEA, M., FEIDT, M. et al. Advanced thermodynamics of irreversible processes with finite speed and finite dimension. *AGIR Publishing House Bucharest* 2015, 259-273.

[15] PowerGen 1200, Protek Safety & Control. https://www.proteksc.com/pdf/PowerGen-1200.pdf

[16] PowerGen 5650, Protek Safety & Control. https://www.proteksc.com/pdf/PowerGen-1200.pdf

[17] PUDLIK, W. Termodynamika. *Gdansk University of Technology Publishing House*. Gdańsk 2011.

[18] SCHMIDT, G. Classical analysis of operation of Stirling engine. 1871, 15. A report published in German engineering union.

[19] STANDARD ENGINE CATALOG, Genoa Stirling. https://genoastirling.com/attach/Catalogo_2017_ENG.pdf

[20] Stirling generators, Sunnytek. http://www.sunnytek.se/solenergi/termoelektrisk-energiteknik/stirling-generators.pdf

[21] URIELI, I. Chapter 3a – Ideal Isothermal Analysis. https://www.ohio.edu/mechanical/stirling/isothermal/isothermal.html

[22] URIELI, I. Chapter 4a – Ideal Adiabatic Analysis. https://www.ohio.edu/mechanical/stirling/adiabatic/adiabatic.html

[23] URIELI, I. Energy analysis – ideal isothermal model. www.ohio.edu/mechanical/stirling/isothermal/energy.html

[24] URIELI, I. Regenerator mean effective temperature. https://www.ohio.edu/mechanical/stirling/isothermal/regenT.html

[25] URIELI, I. Stirling engine ideal adiabatic analysis (updated 1/15/10). https://www.ohio.edu/mechanical/stirling/adiabatic/adiabatic.html

[26] URIELI, I., BERCHOWITZ, D. Stirling Cycle Engine Analysis. *Hingham: Adam Hilger Ltd*. 1994.

[27] WAJS, J., MIKIELEWICZ, D., JAKUBOWSKA, B. Performance of the domestic micro ORC equipped with the shell-and-tube condenser with minichannels. *Energy*. 2018, **157**, 853-861. https://doi.org/10.1016/j.energy.2018.05.174

[28] Whispergen PPS 16. https://www.victronenergy.com/Manuals/WhisperGen/UserManual/UserBookDO40015D.pdf

[29] WU, C., CHEN, L., CHEN, J. Recent advances in finite-time thermodynamics. *Nova Science Publishers*. 1999.

Mariusz Furmanek, MEng. – Faculty of Mechanical Engineering, Gdańsk University of Technology.
e-mail: *mariusz.furmanek@pg.edu.pl*

Jacek Kropiwnicki, DSc., DEng. – Faculty of Mechanical Engineering, Gdańsk University of Technology.
e-mail: *jkropiwn@pg.gda.pl*

Article citation info:
CHOJNOWSKI, J., KARCZEWSKI, M. Analysis of the market structure of long-distance transport vehicles in the context of retrofitting diesel engines with modern dual-fuel systems. *Combustion Engines*. 2022, **188**(1), 13-17. https://doi.org/10.19206/CE-142167

Janusz CHOJNOWSKI
Mirosław KARCZEWSKI

Combustion Engines
Polish Scientific Society of Combustion Engines

Analysis of the market structure of long-distance transport vehicles in the context of retrofitting diesel engines with modern dual-fuel systems

ARTICLE INFO

Received: 15 July 2021
Revised: 17 August 2021
Accepted: 12 September 2021
Available online: 15 September 2021

This work contains considerations on the structure of the road tractor market in Poland in the context of their types of fuel supply systems and the possibility of adapting modern dual-fuel solutions in them. The current injection solutions in most vehicles available on the market indicate the possibility of highly effective use of modern dual-fuel or RCCI fuel supply solutions.

Key words: *truck market, fuel supply systems, dual-fuel, RCCI*

1. Introduction

The history of dual fuel systems is long, but it has never been popularized. Adapting a diesel engine to a dual-fuel system with additional gaseous fuel is not an easy task. There were many reasons for this: from infrastructure problems to technical problems such as inadequate advancement of original diesel fuel supply systems or problems with valve opening timing overlap and difficulties with methane oxidation by the exhaust gas aftertreatment system, resulting in increased total hydrocarbons (THC) emissions [2]. These are the main reasons why retrofit diesel engines are not popular. The development of electronics led to the popularization of high-pressure injections systems such as Common Rail (CR) and pump injection unit (PD) systems. The technological advances of these systems bring the modern dual fuel solutions (controlled by diesel injection signals) and idea of Reactivity Controlled Compression Ignition (RCCI) power supply back to life. RCCI is an ignition method in which highly reactive fuel is injected directly into the cylinder [1]. It mixes with the air and self-ignites, thereby initiating the ignition of poorly reactive fuel, which is delivered via indirect injection to the combustion chamber earlier in the process as shown on Fig. 1.

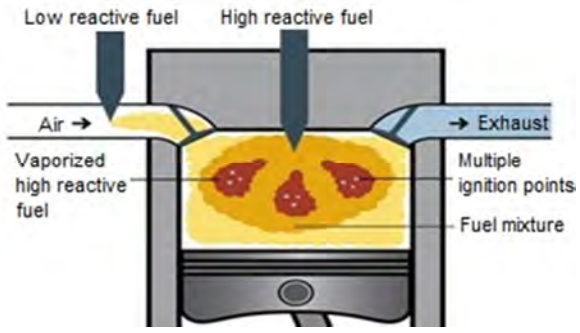

Fig. 1. Ignition and combustion in RCCI engine (based on [18])

The same method of fueling the engine is characteristic of a classic dual-fuel engine, where the difference is that the fuel-air mixture is not homogeneous. The possibility of implementing precise pilot doses and emulating the operation of CR and PD injectors opens up new prospects for high rates of replacement (50–70% or modern type dual-fuel system or 90–99% for RCCI) of the basic fuel with gaseous fuel in such a system [2, 19]. High replacement coefficient ratios directly affect the benefits of such a solution of fueling a diesel engine, through lower emission of harmful exhaust components [1, 2]. This is significantly different from the systems currently available on the market using simplified versions of dual-fuel systems, which most often use a simplified method of "cutting" diesel doses by emulating the acceleration pedal or manifold absolute pressure (MAP) sensors, as shown in Fig. 2 [20].

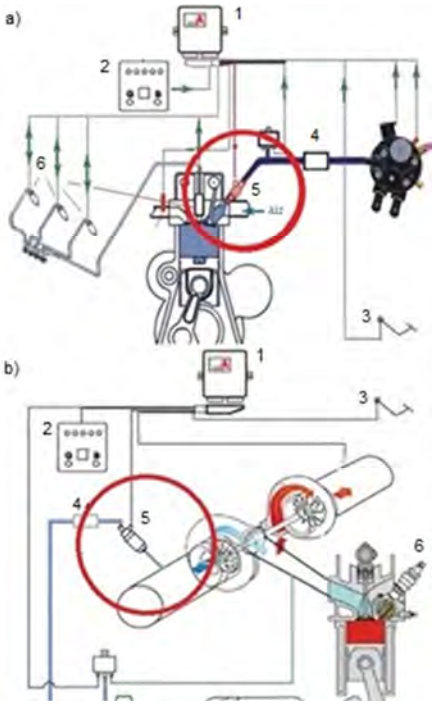

Fig. 2. Comparison of dual fuel systems: a) sequential gas injection pre-intake valve (controlled by diesel injection signals), b) pre-turbocharger gas injection: 1 – gas ECU, 2 – operation mode switch, 3 – acceleration pedal, 4 – gas filter, 5 – gas injector, 6 – diesel injector (based on [10, 20])

Manufacturers of such vehicles offer similar solutions in brand new vehicles, the market of used cars with factory installed systems is quite narrow. Therefore, this work focuses on the analysis of the polish structure of long-distance road transport in the context of the means of transport used by these companies (tractor units) and the possibility of using modern dual-fuel systems in them with the use of the original diesel injection system as a highly reactive fuel dispachers.

2. The structure and the use of road tractors in the Polish transport companies

The last report on the long-distance road transport market issued by the Polish Automotive Industry Association indicated that in Poland in 2019, 372.7 thousand road tractors were registered in Poland (data adjusted for vehicles excluded from use in Polish Central Register of Vehicles and Drivers database). The share of the oldest, over 20 years old, amounted to 5%. The youngest – up to four years old reached 30%. Similarly, tractors from five to ten years of age accounted for 30% of the machine park at the end of 2019. Thus, cars up to 10 years old constitute 60% of all vehicles. Those from eleven to twenty years remained the most numerous and accounted for 35% of the fleet. The average age of truck tractors was 8.9 years, with a median of 8 years [3]. At the end of 2019, in the updated part of the park, the number of road tractors registered in Poland was by 88 thousand. greater than the number of registered trucks (complete chassis, not including tractors and special vehicles) with a maximum permissible weight of more than 3.5 tons. For the first time, truck tractors outnumbered trucks in 2015 [3, 5]. This reflects the scale of investments of carriers specializing in international road transport. The year 2020 brought a decrease in sales, in all segments of commercial vehicles weighing more than 3.5 tons. The piling up of a handful of industry problems, led by the pandemic theme, has resulted in one of the worst results in the past few years [17]. Table 1 shows the registrations by manufacturers of new tractor units in 2020, 2019 and 2018 in Poland [6, 17].

Table 1. Registration of new road tractor units in Poland [6, 17]

Brand	2020	2019	2018
DAF	3 812	5 597	6 358
Scania	2 644	5 269	4 901
MAN	2 221	4 519	5 295
Volvo	2 644	4 235	4 439
Mercedes-Benz	2 226	3 961	3 916
Renault	581	1 405	1 734
Iveco	534	382	731
Ford Trucks	146	23	-
Total	14 808	25 391	27 375

Apart from new trucks, the market structure may also be illustrated by imported used tractor units. In 2020, 29 503 used commercial vehicles were imported to Poland, which, however, is a decrease by 6.2% compared to 2019 (–1948 units), of which 27 174 are road tractors – this segment also recorded a decrease by –3.8% (–1,070 units y/y) [6, 17]. To illustrate the structure of the demand for used vehicles by their manufacturers (it does not have to be a measure of the real demand for used trucks), data from the search engine were used. The data comes from the portal that sells used trucks in Poland. The data provided is presented in the Fig. 3.

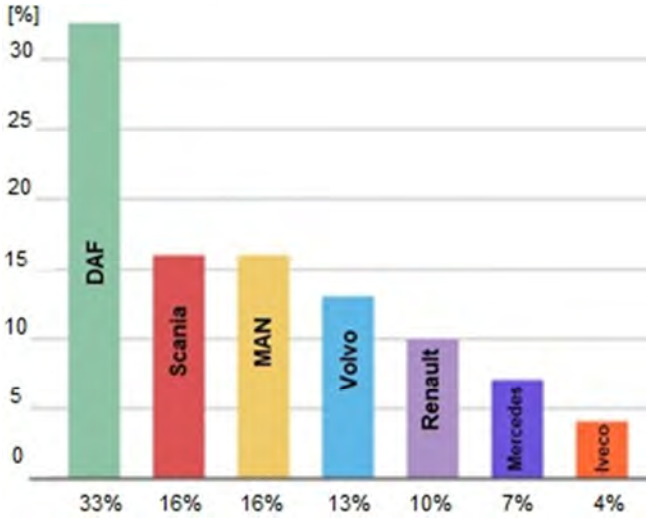

Fig. 3. The popularity of searches by brand for used tractor units [21]

Reliability is an important factor in using truck. Therefore, among the used vehicles, the most popular are road trucks not older than 7 years [4, 9]. The search data for used tractor units by their year of manufacture may also indicate when selling a vehicle makes the best economic sense. Figure 4 shows the percentage of searches for used tractor units by age.

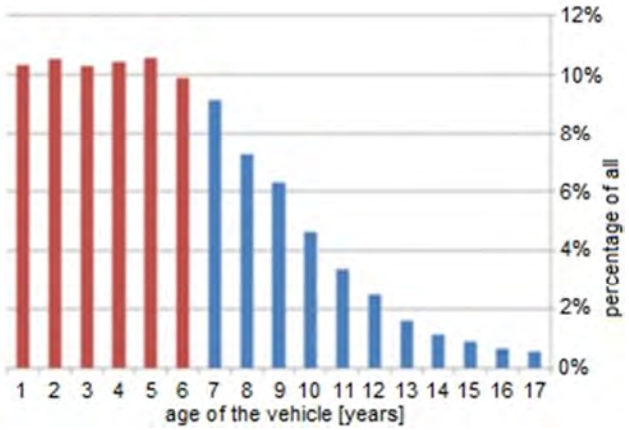

Fig. 4. Searching for used tractor units by their age [21]

Mentioned above data concerning the search preferences for used vehicles according to their year of production are indirectly reflected in the average time of use of a tractor unit in road transport companies. Of course, it is difficult to clearly define the economically justified service life of a tractor unit, as it depends on factors such as the intensity of use, annual mileage, type of work, etc. However, it is assumed that in the case of international long-distance transport it is about 5–7 years, national and local 10–15 years. Vehicles with specialized bodywork are in service the longest. including city ones, incl. garbage

trucks, sweepers, cranes, concrete pumps, etc. In Poland, there were 44% of specialist vehicles over 20 years old [3, 6].

Summing up, a typical Polish long-distance road transport company uses tractor units of the following brands: DAF, Scania, MAN, Volvo, Mercedes-Benz, Renault, Iveco (Ford Truck due to the beginning of entering the market will be omitted in further considerations) not older than 7 years for transport international or 15 years for domestic transport.

The analysis of the types of fuel supply systems in long-distance vehicle engines, presented in the following paragraph, focuses on the group of trucks mentioned above.

3. Engines used in road tractors and types of fuel supply systems used in them

3.1. DAF [7, 8, 15]

The Paccar MX engines were introduced in 2006 with XF105 road truck model. They have a displacement 12.9 liters and maximum powers of 408, 462 and 510 horsepower (hp). Thanks to the use of selective catalytic reduction (SCR), they meet the Euro IV or Euro V standards. They have 4 valves per cylinder, turbocharging and charge air cooling. They use single-section PD injection pumps with the pressure increased from 1500 to 2000 bar. As a result, there is no need for a diesel particulate filter in the exhaust system. Successor of the model XF105 in 2014 introduced upgraded Paccar MX engines in two displacement variants. They are 10.8 liters with 440 hp and 12.0 liters with 410, 460 and 510 hp respectively. Thanks to the use of SCR, they comply with the Euro VI standards. Like the previous engines, they have 4 valves per cylinder, turbo charging and charge air cooling. They use single-section Common Rail injection pumps with a pressure increased from 2,000 to 2,500 bar. As a result, there is no need for a diesel particulate filter in the exhaust system.

3.2. Scania [7, 8, 14]

Scania use engines equipped with XPI (short for "extra high-pressure") common-rail fuel system developed in cooperation with Cummins since 2003 in their models of road tractors from series R and S. These vehicles have a wide range of engines depending on the year of production and the needs of use. These are, respectively, units:

- In-line five-cylinders 9.0 liters 250/280/320/340/360 hp,
- In-line six-cylinders 13.0 liters 370/410/450/480/490 hp,
- V8 16.0 liters 500/520/580/730 hp,

3.3. MAN [7, 8, 13]

Models from series TGS and TGX since 2007 are powered by engines of the D20, D26, D36 series with the following power ratings and exhaust standards:

- Euro V with 360 hp, 400 hp, 440 hp, 480 hp, 540 hp and 680 hp.
- EURO V EEV (Enhanced Environmentally Friendly Vehicles) with 360 hp, 400 hp, 440 hp, 480 hp and 680 hp.
- Euro VI with 440 hp, 480 hp, 520 hp, 560 hp and 640 hp (the last 3 variants are the new inline 6-cylinder 15.2 liters engine D38).

In the fuel supply system of these units, injection pump systems are used for some units that meet Euro V and Common Rail Euro V and Euro VI standards.

The TGX series (the most popular long-distance MAN tractor units on the Polish market) uses six-cylinder in-line engines from the MAN D20 (10.5 liters) and D26 (12.4 liters), Euro VI series, in four power ranges: 360 and 400 hp (D20) and 440 and 480 hp (D26) obtained in the range of 1600–1800 rpm. In most cases, these trucks have a Common Rail power system.

3.4. VOLVO Trucks [7, 8, 12]

In September 2012, Volvo Trucks launched the production of a new generation FH model with many technical improvements. These tractors use 3 engine variants: D13C (unit injection, and Common Rail after july 2015), D13K (Common Rail), D13TC (Common Rail) in power variants from 360 to 540 hp. A variant is also available with the D16 engine with 550, 650 or 750 hp and a torque of up to 3550 Nm. All variants powered by CR.

3.5. Renault Trucks [7, 8, 12]

The T Series tractor units were presented in 2013 as the first of the new line of vehicles for the company and offers two six-cylinder Euro VI engines, 11.0 liters – DTI11 (380, 430 and 460 hp) and 13.0 liters DTI13 (440, 480 and 520 hp). All engines are variants taken from previous Premium and Magnum trucks. These are modified Volvo's D series engines. The fuel supply systems used in them are unit injection and Common Rail.

3.6. Mercedes-Benz Truck [7, 8, 16]

The Mercedes-Benz Actros MP4 made its debut on 30 September 2011. The fourth version of the Actros model offers several engine options in the Euro V or Euro VI variant. Euro VI uses a six-cylinder in-line engine, both OM471 series with 12.8 liters engines with output power: 422 hp to 530 hp and the OM473 from 15.6 liters engine with output power: 517 hp to 626 hp. Both engines use the X-Pulse injection system, which uses the Common Rail system equipped with a system that increases the injection pressure and the function of easy injection modification. The maximum fuel rail pressure is 1160 bar, which makes the maximum injection pressure 2700 bar.

3.7. IVECO Trucks [7, 8, 11]

The Stralis model is equipped with 6-cylinder engines with four valves per cylinder. They come in three variants of capacity, achieving different power parameters:

- Cursor 8, 7.8 liters: 310–360 hp
- Cursor 10, 10.3 liters: 420–450 hp
- Cursor 13, 12.9 liters: 500–560 hp

Changes in this engines took place in 2013 with the introduction of new engines meeting the EURO VI exhaust gas standard. All cursor engines after this date use the common rail system.

4. Discussion

The demands placed on commercial vehicles are constantly increasing. European legislation has forced commercial vehicle manufacturers to develop ever more powerful and dynamic engines with low fuel consumption. With

the appearance of exhaust gas purity standards, truck manufacturers realized that it was necessary to improve the fuel supply system so that the combustion process was more efficient. To achieve this, the fuel injected into the cylinders had to be finer in order to mix more easily with air. High-pressure unit injection systems have proved to be a good and reliable solution. They are also relatively cheap to produce and less prone to fuel contamination. Many years and millions of failure-free kilometers traveled on unit injectors effectively distracted some users and producers from the Common Rail system. Exhaust gas standards and increasing consumer expectations forced manufacturers to take another step in their development, i.e. the need for more precise fuel injection control. The development of electronics enabled the creation of PD and CR fuel supply systems, which were designed to reduce emissions and improve the operation of the diesel engine. These systems enable the feeding of the fuel dose in several portions – including the amount of the afterburner – which makes this type of fuel system an advantage in meeting the high requirements of exhaust gas purity for the EURO VI standard. Since all types of diesel fuel are characterized by the so-called delay of ignition – the use of a small pilot dose before top dead center (TDC) allows to apply the correct dose to the ignition area of the pilot dose – which makes the engine work softer and quiet – while maintaining high thermodynamic efficiency of the engine. The achievements of this technology indicate the potential of its use in a highly effective way, also in modern dual-fuel and RCCI power systems. Adequate control of pilot doses of highly reactive fuel (diesel fuel) to low reactive fuel (gaseous fuel) may be the key to using the original engine fuel supply system for retrofit modifications. Figure 5 shows the theoretical method of implementing such an injection in dual-fuel operation mode.

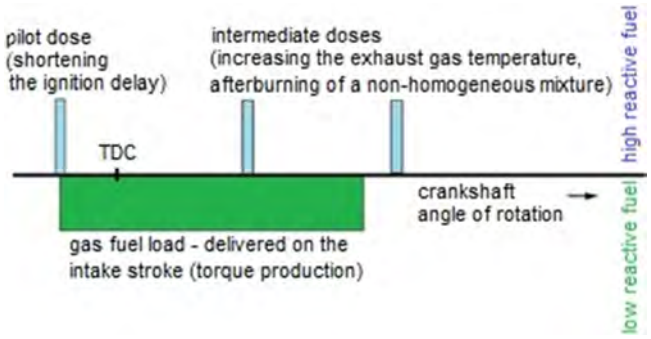

Fig. 5 Diagram of the co-combustion strategy with the use of multiple fuel injection (based on [1, 2, 18])

All mentioned above drastically reduce the cost of such a modification, which in turn gives a greater economic justification for the use of such solutions also in used road tractors, exactly like nowadays with the modification of passenger cars for LPG fueling, which is popular in Poland for many years.

The strict emission limits also leave no choice to the producers. The Common Rail system, although more expensive to produce and operate due to very precise cooperating elements, seems to be a solution that will eventually replace other fuel injection solutions in compression ignition engines. There are also electric and hydrogen solutions on the horizon, but at the moment the high energy consumption of road transport does not indicate a quick displacement of self-ignition engines. The future of road tractors' powertrains systems is uncertain. Strict emission limits leave no choice to manufacturers. The Common Rail system, although more expensive in production and operation (due to the very precise cooperating elements), has in principle already replaced and will eventually replace all other conventional fuel injection solutions in self-ignition engines. At least for a while. The overriding goal is to completely postpone the combustion of conventional fossil fuels. Temporarily, it is possible to use dual-fuel and RCCI solutions as less pollutant emitting solutions. At the moment, there is a lot of work on the use of modern dual-fuel or Reactivity Controlled Compression Ignition instead of regular diesel fuel injection only. The conversion to retrofit was successfully made, for example, by Arena Red in a vessel [19] and in more others. There are also electric and hydrogen solutions for truck tractors on the horizon, but at the moment the high energy consumption of road transport does not indicate a quick replacement of compression ignition units with alternative power sources [2].

5. Conclusion

- Dual fuel solutions for diesel engines are known, but due to their problems, they never gained popularity.
- New types of dual-fuel installations (originally used in factory vehicles) and Reactivity Controlled Compression Ignition systems can be used as retrofit installations in used vehicles such as Pump injection unit and Common Rail thanks to the use of modern diesel injection systems.
- The structure of the market for long-distance road transport vehicles indicates that the use of vehicles is not older than 7 years for transport international or 15 years for domestic transport. Which indicates the market's readiness (its absorptive capacity) to use modern dual-fuel solutions.
- All road tractors from the group of vehicles used in road transport have injection systems that enable the use of new dual-fuel and Reactivity Controlled Compression Ignition systems.
- Due to the pressure of the legislator and certification, the use of propulsion sources in vehicles is changing. Modern dual-fuel and Reactivity Controlled Compression Ignition releases may, in the factory edition as well as retrofit, prove to be an intermediate link before the full displacement of fossil fuels and their replacement with hydrogen electric powertrains or their combination.

Acknowledgements

This work was financed by Military University of Technology under research project UGB 880/2021.

Nomenclature

CR common rail
ECU Electronic Control Unit
EURO IV, V, VI European emission standards
EN European Norm Standards
MAP manifold absolute pressure
PD pump injection unit
RCCI Reactivity Controlled Compression Ignition
TDC top dead center
THC total hydrocarbons

Bibliography

[1] GARCIA, A., CARLUCCI, P., MONSALVE-SERRANO, J. et al. Energy management optimization for a power-split hybrid in a dual-mode RCCI-CDC engine. *Applied Energy*. 2021, **302**, 117525. https://doi.org/10.1016/j.apenergy.2021.117525

[2] HEYWOOD, J.B, Internal Combustion Engine Fundamentals. Second Edition. *McGraw-Hill Education*. New York 2018. https://www.accessengineeringlibrary.com/content/book/9781260116106

[3] KOŹLAK, A. Struktura sektora transportu drogowego w Polsce i ocena jego wyników ekonomicznych na tle państw, Unii Europejskiej. *Studia i Prace Kolegium Zarządzania i Finansów*. 2018, **166**, 59-75. https://econjournals.sgh.waw.pl/SiP/article/view/805/707

[4] URBANYI-POPIOŁEK, I. Ekonomiczne i organizacyjne aspekty transportu. *Wyższa Szkoła Gospodarki w Bydgoszczy*. Bydgoszcz 2019.

[5] REPORT of the Polish Central Statistical Office: GUS–Transport: wyniki działalności 2019.

[6] REPORT of the Polish Automotive Industry Association: PZPM – Branża motoryzacyjna, raport 2020/2021.

[7] Press data from the manufacturer's website.

[8] Data from diagnostic programs: TEXA Truck version 51.0.0 IDC5 (2021) and Bosch ESI [tronic] 2.0 Truck (2021).

[9] MOBILITY AND TRANSPORT. Road Safety. https://ec.europa.eu/transport/road_safety/specialist/knowledge/fatique/risk_groups/professional_and_truck_drivers (accessed on 5.09.2021).

[10] SKA-TECH, Auto Gaz Miszewo. https://eko-pal.com.pl/diesel-na-gaz/ (accessed on 5.09.2021).

[11] IVECO STRALIS. https://en.wikipedia.org/wiki/Iveco_Stralis (accessed on 27.08.2021).

[12] List of Volvo Trucks engines. https://en.wikipedia.org/wiki/List_of_Volvo_Trucks_engines (accessed on 27.08.2021).

[13] MAN TG-range. https://en.wikipedia.org/wiki/MAN_TGX (accessed on 05.09.2021).

[14] Scania series R. https://en.wikipedia.org/wiki/Scania_series_R (accessed on 27.08.2021).

[15] PACCAR Powertrain. https://paccarpowertrain.com/engines/mx-13/ (accessed on 5.09.2021).

[16] Daimler Truck AG. https://roadstars.mercedes-benz-trucks.com/pl_PL/magazine/transport/03-2014/the-new-om-473-the-man-behind-the-engine.html (accessed on 6.09.2021).

[17] Truck Focus.pl. https://truckfocus.pl/nowosci/58046/podsumowanie-sprzedazy-pojazdow-ciezarowych-w-2020-roku (accessed on 3.09.2021).

[18] Arena Red. Engine Management Systems. https://www.arenared.nl/cpbc+~+rcci (accessed on 27.08.2021).

[19] KHL Group Americas LLC. https://www.dieselgasturbine.com/news/A-Commercial-First-For-RCCI-Retrofits/7011943.article (accessed on 5.09.2021).

[20] Gascar.pl. http://www.gascar.pl/diesel-na-cng/ (accessed on 3.09.2021).

[21] Getruck.eu. https://www.getruck.eu data obtained courtesy of the portal.

Janusz Chojnowski, MSc. – Faculty of Mechanical Engineering, Military University of Technology, Poland.
e-mail: *janusz.chojnowski@wat.edu.pl*

Mirosław Karczewski, DEng. – Faculty of Mechanical Engineering, Military University of Technology, Poland.
e-mail: *miroslaw.karczewski@wat.edu.pl*

Article citation info:
NAKASHIMA, K., UCHIYAMA, Y. Influence of piston surface treatment on piston assembly friction in an eco-mileage vehicle engine. *Combustion Engines*. 2022, **188**(1), 18-23. https://doi.org/10.19206/CE-142552

Kohei NAKASHIMA
Yosuke UCHIYAMA

Combustion Engines
Polish Scientific Society of Combustion Engines

Influence of piston surface treatment on piston assembly friction in an eco-mileage vehicle engine

ARTICLE INFO

Received: 9 August 2021
Revised: 22 September 2021
Accepted: 23 September 2021
Available online: 3 October 2021

This study investigated the effect on piston assembly friction after treating piston surfaces with a fine particle bombarding process, using a friction measurement apparatus with a floating cylinder liner, similar to an eco-mileage vehicle engine. Friction was measured in four conditions: (1) no treatment (standard piston in a commercially-available engine), (2) micro dimple treatment (45 μm ceramic particles were air-blasted onto the piston surface), (3) molybdenum disulfide (MoS_2) shot treatment (1 μm MoS_2 particles were air-blasted onto the piston surface), and (4) combination of the previous two micro dimple and MoS_2 shot treatments (first 45 μm ceramic particles and then 1 μm MoS_2 were air-blasted onto the piston surface). Results indicated that friction decreased in the following order: no treatment > micro dimple treatment > MoS_2 shot treatment > combination of micro dimple and MoS_2 shot treatments.

Key words: *eco-mileage vehicle engine, floating cylinder liner, fine particle bombarding, piston, piston assembly friction*

1. Introduction

In eco-mileage vehicles, reducing engine friction is an effective means for improving fuel efficiency. Because the piston assembly friction (the friction between the piston, the piston rings, and the cylinder liner) makes a significant contribution to engine friction [1, 3, 4, 6], it is important to reduce this piston assembly friction. The friction between the piston and the cylinder liner accounts for more than 50% of the piston assembly friction, and its ratio increases with increasing engine speed and decreasing engine load [7]. There have been reports on reducing piston assembly friction by applying a surface treatment on the piston skirt [2, 5, 9–11, 13–15]. One approach plates a piston with tin [5]. Tin not only reduces friction, but also simplifies the break-in run. However this tin plating wears out during protracted engine operation, losing the friction reduction effect. Another approach plates a piston with a resin coating in which molybdenum disulfide (MoS_2) and polytetrafluoroethylene (PTFE) are dispersed in a resin binder [2, 5, 15], a resin coating in which fine hard particles are dispersed in a resin binder [14], or a resin coating of two layers in which MoS_2 is dispersed in a resin binder in the upper layer and graphite is dispersed in the lower layers [13]. This rein does not wear out even during protracted engine operation, achieving sustainable friction reduction. But the performance of slide and transfer of solid lubricants such as MoS_2 and PTFE, is suppressed by the resin binder [10]. In addition, the thickness of these resin coatings is approximately 10 μm, so it is necessary to design the piston with advance consideration of the final coating thickness. Yet another approach uses a micro dimple treatment (by air-blasting fine ceramic particles at a high speed) [9, 11] and a MoS_2 shot treatment (by air-blasting fine MoS_2 particles at a high speed) [10, 11] on the piston surface using a fine particle bombarding (FPB) process. This approach reduces friction even during protracted engine operation, and has minimal effect on piston dimension. This process (of micro dimple and MoS_2 shot treatments with FPB) can be easily applied to the piston in an eco-mileage vehicle engine, where it can be expected to reduce friction even during protracted operation. Our previous study developed a friction measurement apparatus with a floating cylinder liner, by using components of an eco-mileage vehicle engine as much as possible [8]. This study employs that measurement apparatus to quantify the effect on piston assembly friction of piston surface treated with a FPB process.

2. Experimental apparatus and method

Figure 1 shows the apparatus to measure piston assembly friction with the floating liner, as developed in our previous study [8]. This measurement apparatus was designed to be similar as possible to an actual eco-mileage vehicle engine. So it employed a commercially-available, four-stroke, air-cooled, horizontal, single-cylinder, gasoline engine, displacing 49 mL, with a bore diameter of 39 mm and a stroke of 41.4 mm. The crankcase of this engine was cut, and a cover was attached to the cut of the crankcase. The engine was turned from horizontal to vertical. The floating liner was produced by machining the outer periphery of the air-cooled cylinder (aluminum finned cylinder casting cast-iron liner). This floating liner was installed in the aluminum cylinder block. Joint plates were installed in the grooves on the outer periphery of the floating liner at both the thrust and the anti-thrust sides. Then the joint plates, as well as load washers of piezo type, were mounted in the cylinder block, as shown in Fig. 2. To suppress lateral displacement due to piston thrust force, clamping bolts were mounted to the cylinder block at four sides: thrust, anti-thrust, front, and rear. Heaters were installed in the cylinder block at the thrust, anti-thrust, and rear sides, and thermocouples were installed into the clamping bolts at the front and rear sides so that the bore surface temperature of the floating liner could be measured and adjusted. In addition, an oil tank was set outside the engine, and a heater and a thermocouple were installed into the oil tank to adjust the oil temperature to a fixed temperature. The heated oil was

then pumped from the oil tank to a pipe in the upside of the crankcase, and supplied from there to the crankshaft at a flow rate of 600 mL/min.

Figure 3 shows the four experimental pistons and the surface shapes on the piston skirts. The piston without surface treatment (1) is standard part of a commercially-available engine, and has a streaked sliding surface (Ra 2.4 µm) and three grooves in the skirt. In the micro dimple treatment (2) ceramic particles with a diameter of 45 µm were air-blasted on the standard piston surface. In the MoS_2 shot treatment (3) MoS_2 particles with a diameter of 1 µm were air-blasted on the standard piston surface. In the combination of micro dimple and MoS_2 shot treatments (4) first ceramic particles with a diameter of 45 µm were air-blasted on the standard piston surface, and then MoS_2 particles with a diameter of 1 µm were air-blasted onto it. There was no difference in the outer diameter, measured with a micrometer, at each position of the pistons with and without surface treatments.

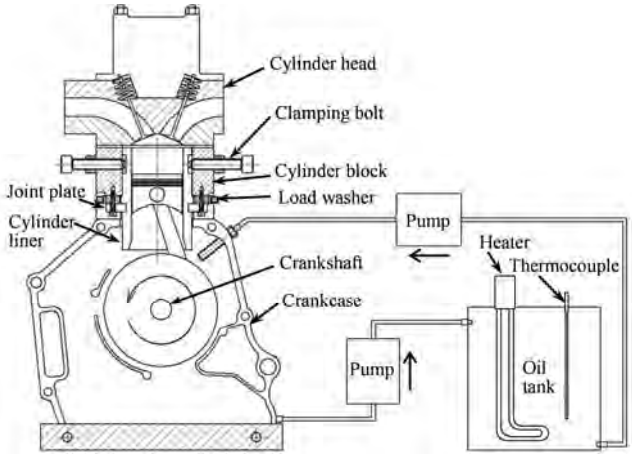

Fig. 1. Measurement apparatus of piston assembly friction

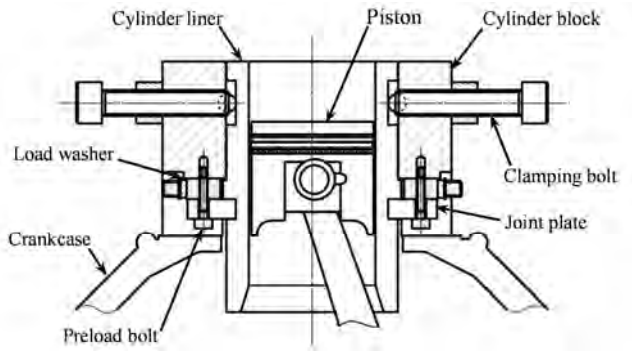

Fig. 2. Measurement unit of piston assembly friction with floating liner

Table 1 shows the experimental rings, which are standard parts of a commercially-available engine. These rings had been fully run earlier [8].

The floating liner had been also fully operated earlier [8]. The roughness of the sliding surface on the liner bore was Rz_{JIS} 1.22~1.34 µm (Ra 0.20~0.22 µm).

In the experiment, the intake and exhaust valves were not activated (no cylinder pressure was applied) while the engine was operated by motoring. Using the same rings and floating liner, each experimental piston was installed in the engine. Before measuring piston assembly friction, the engine was run in for 20 hours, at an engine speed of 1600 rpm, with temperatures of the liner bore and lubricant of 80°C. Then the piston assembly friction was measured at temperatures of 40°C, 60°C and 80°C, and at engine speeds from 800 rpm to 1600 rpm every 200 rpm. Table 2 shows the kinematic viscosities of the experimental lubricant (Honda genuine Ultra Green) at each temperature, measured with the Redwood viscometer.

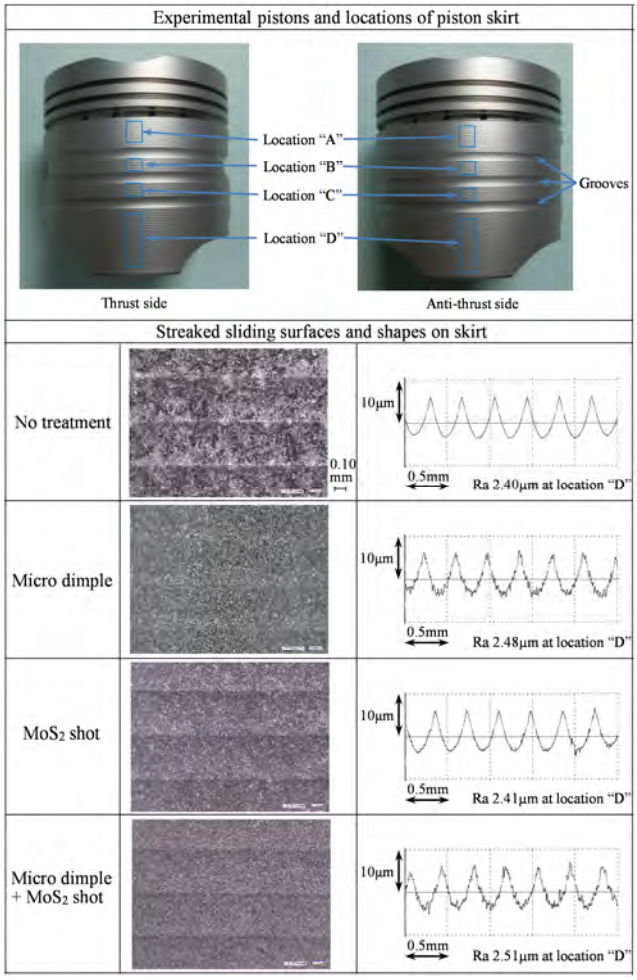

Fig. 3. Experimental pistons and the surface shapes on the piston skirts

Table 1. Experimental piston rings

[mm]

Top ring	Second ring	Oil ring
1.7, 0.78	1.7, 0.78, 1°46'	1.04, 0.3, 0.3
End clearance 0.08 mm Tension 3.2 N Chrome plating	End clearance 0.15 mm Tension 4.4 N Phosphate	End clearance 0.52 mm Tension 11.2 N Chrome plating

Table 2. Kinematic viscosities of experimental lubricant

Temperature	Kinematic viscosity
40°C	30.3 mm^2/s
60°C	15.8 mm^2/s
80°C	10.4 mm^2/s

3. Results and discussion

Figures 4 to 6 show the measurement results of the piston assembly friction at an engine speed of 1000 rpm and at temperatures of 40°C, 60°C and 80°C, respectively. In Figs 4 to 6, crank angles of 0º and 360º represent engine top dead center (TDC), and 180º bottom dead center (BDC). Since the intake and exhaust valves were not activated, only two strokes of the piston (downward stroke and upward stroke) are indicated. At each temperature, not only near TDC and BDC but also near the center of the stroke, friction decreased in the following order: no treatment > micro dimple treatment > MoS_2 shot treatment > combination of micro dimple and MoS_2 shot treatments. As the temperature increased, the friction reduction ratio of each surface treatment (compared to no treatment) decreased, especially near TDC and BDC.

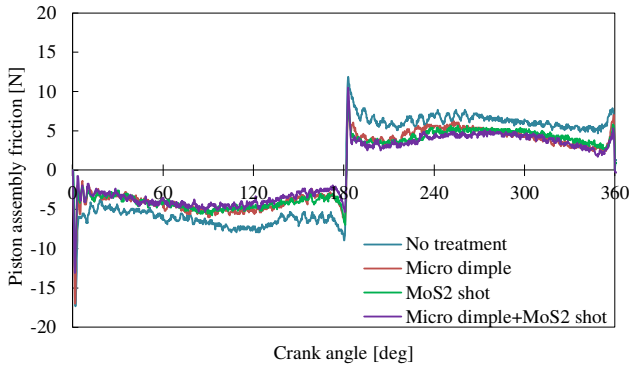

Fig. 4. Piston assembly friction at 40°C (1000 rpm)

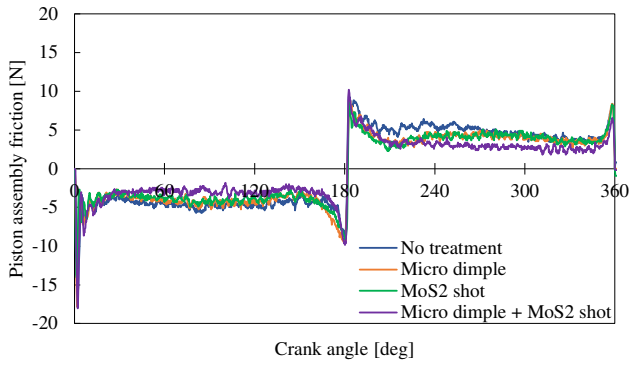

Fig. 5. Piston assembly friction at 60°C (1000 rpm)

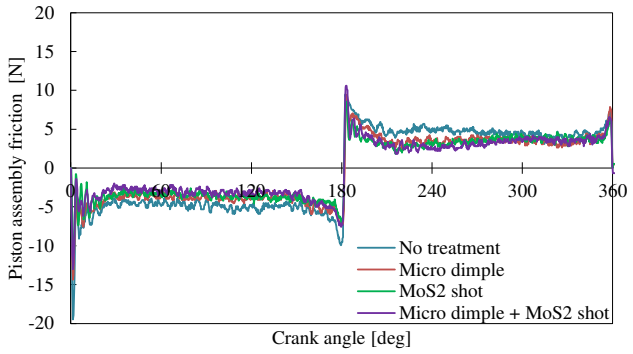

Fig. 6. Piston assembly friction at 80°C (1000 rpm)

Figures 7 to 10 show the Stribeck diagrams (at 1000 rpm with crank angles of 3° to 177° and 183° to 357°) for each piston corresponding to the friction measurement results in Figs 4 to 6. Here the friction coefficient was obtained by dividing the absolute value of friction by the sum of the thrust force of the piston (which was obtained by multiplying the inertial force of the piston by the tangent of the tilt angle of the connecting rod) and the normal force of the rings (which was obtained by multiplying the ring surface pressures by the outer peripheral surface areas of the rings). The lubrication parameter was also obtained by multiplying the lubricant viscosity, μ, by the piston speed, U, and dividing by W, the sum of the surface pressures of the piston skirt (one skirt side) and the rings. In Figs 7 to 10, fluid lubrication was dominant at lower temperatures, but mixed lubrication was dominant at higher temperatures. In all lubrication regions, friction coefficient again tended to decrease in the following order: no treatment > micro dimple treatment > MoS_2 shot treatment > combination of micro dimple and MoS_2 shot treatments.

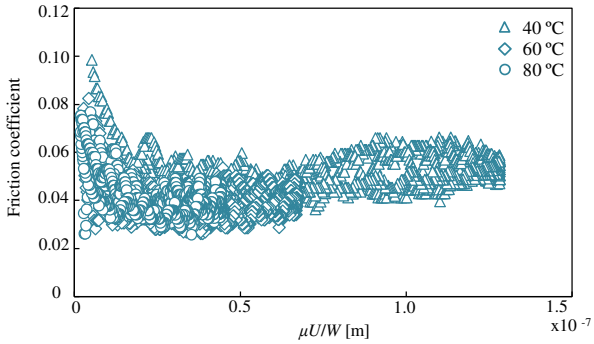

Fig. 7. Stribeck diagram in no treatment (1000 rpm)

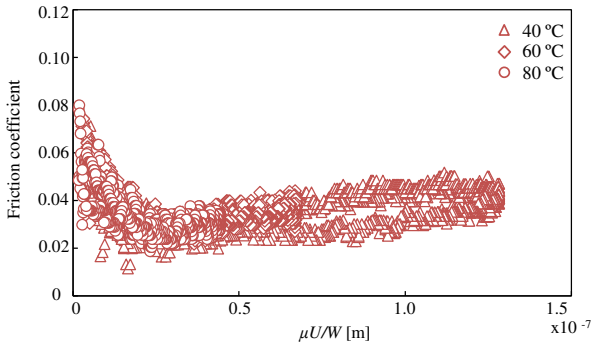

Fig. 8. Stribeck diagram in micro dimple treatment (1000 rpm)

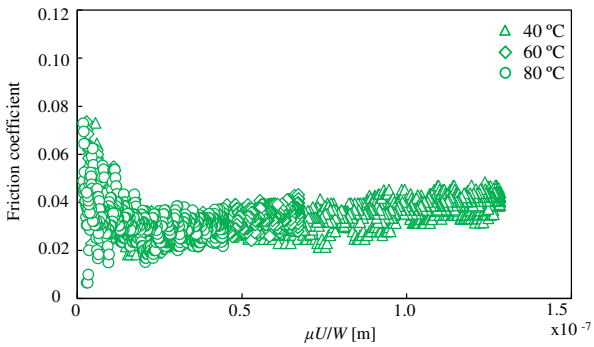

Fig. 9. Stribeck diagram in MoS_2 shot treatment (1000 rpm)

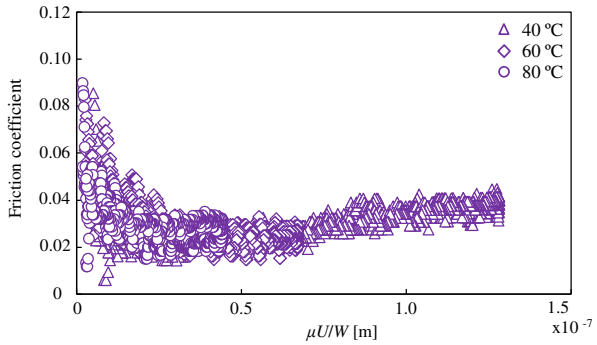

Fig. 10. Stribeck diagram in combination of micro dimple and MoS_2 shot treatments (1000 rpm)

Figures 11 to 13 show the friction mean effective pressure (FMEP) at 40°C, 60°C and 80°C, respectively. Here the FMEP was obtained by integrating the absolute value of friction at crank angles of 0° to 360° and dividing by the stroke volume. At each temperature and engine speed, the FMEP also tended to decrease in the following order: no treatment > micro dimple treatment > MoS_2 shot treatment > combination of micro dimple and MoS_2 shot treatments. At a lower temperature, as the engine speed increased, fluid lubrication became dominant, so the FMEP increased in each piston. At a higher temperature, when the engine speed increased from 800 rpm to 1200 rpm, boundary contact decreased, and the FMEP decreased in each piston. But when the engine speed further increased from 1200 rpm to 1600 rpm, fluid lubrication became dominant, and the FMEP tended to increase in each piston. Here, the FMEP was reduced by 31% to 45% for the combination of micro dimple and MoS_2 shot treatments, compared to no treatment.

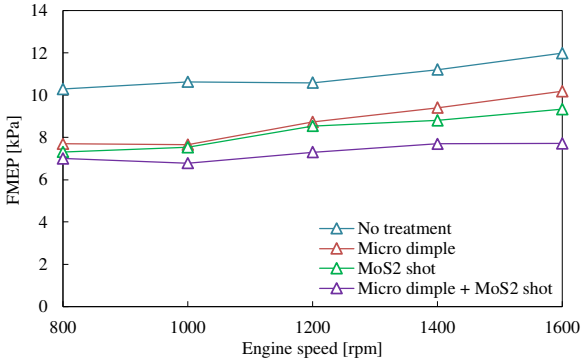

Fig. 11. FMEP at 40°C

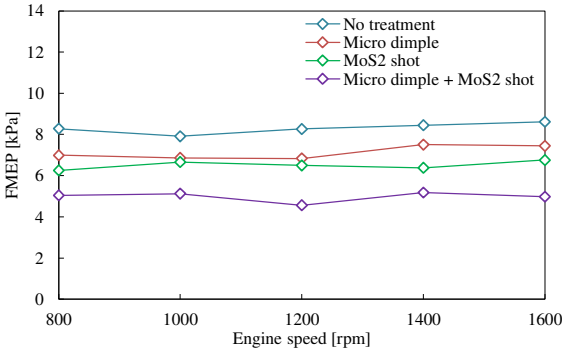

Fig. 12. FMEP at 60°C

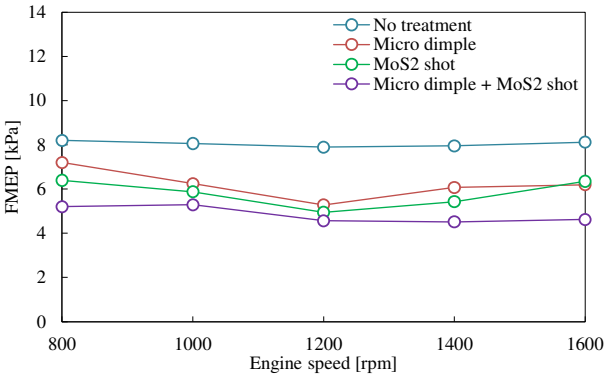

Fig. 13. FMEP at 80°C

Figure 14 shows the maximum amount of wear on the streaked sliding surface at location "C" of each piston skirt after the friction measurement. All pistons had the maximum amount of wear on the streaked sliding surface at the piston skirt "C" at both the thrust and the anti-thrust sides. In Fig. 14, except for the micro dimple treatment, there was no significant difference in the maximum amount of wear on each piston skirt. Except for the micro dimple treatment, the maximum amount of wear at the anti-thrust side was larger than that at the thrust side. At the thrust side, the maximum amount of wear with the micro dimple treatment was greater than that of all other treatments, including no treatment. It was considered that the outer diameter of the streaked surface became larger due to the micro dimple treatment. Figure 15 shows the observation results of the streaked surface at the piston skirt "C" on the anti-thrust side. In Fig. 15, the micro dimples remained even on the worn surface of the streak, with both the micro dimple treatment and the combination of the micro dimple and the MoS_2 shot treatments. In all pistons, the amount of wear on the streaked sliding surface at locations (skirt "A," "B" and "D") other than skirt "C" was 0~1 μm, and there was no significant difference in the amount of wear.

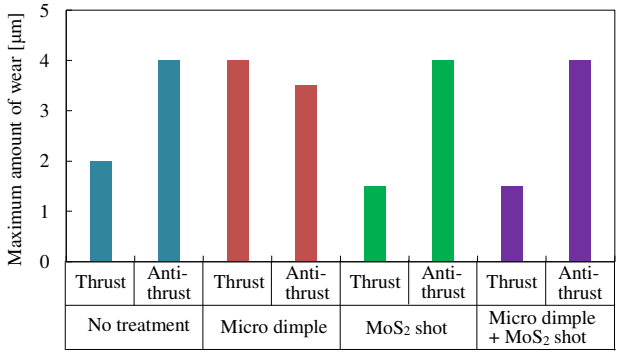

Fig. 14. Maximum amount of wear on streaked sliding surface at part of "C" after friction measurement

The micro dimple treatment reduced friction compared to no treatment. The micro dimples also remained on the worn surface of the streak with the micro dimple treatment. It is thought that, in the mixed lubrication region, the lubricant in the valley between streaks circulated through micro dimples as a passage, covering not only the actual sliding

surfaces but also those micro dimples there, reducing friction [9]. It is also considered that, in the fluid lubrication region, the shear force of the lubricant between the sliding surfaces became smaller due to the formation of a vortex inside each micro dimple, reducing friction [12].

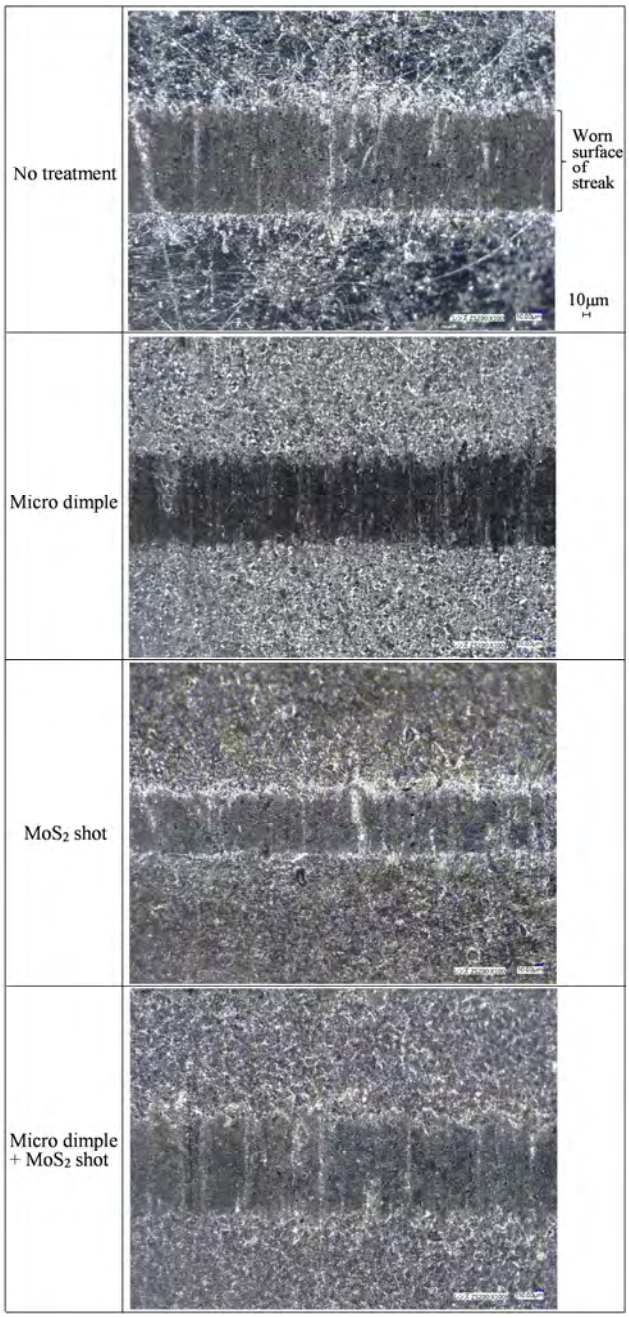

Fig. 15. Observation results of streaked surface at piston skirt "C" at anti-thrust side after friction measurement

The MoS_2 shot treatment further reduced friction, more than both no treatment and the micro dimple treatment. The MoS_2 has a hexagonal layered crystal structure, and in each layer a plane of molybdenum (Mo) atoms is sandwiched by planes of sulfur (S) atoms. The covalent bonds between the Mo and S atoms within layers are relatively strong, while the van der Waals forces cohering S and S atoms between layers are considerably weaker. Therefore the shear force acts between these layers, so interlayer sliding occurs, reducing friction. However, as shown in Fig. 14, the streaked surface at the piston skirt "C" had a maximum wear of 4 μm, which corresponded to approximately the depth of the treatment of MoS_2 shots. Here, Ogihara [10, 11] examined the worn part of the streaked MoS_2 treated piston skirt, after engine motoring, using Field Emission Scanning Electron Microscopy/Energy Dispersive X-ray Spectroscopy (FE-SEM/EDX), and confirmed the remaining presence of MoS_2 both on the worn surface and deep inside the surface. This is because the MoS_2 particles are repeatedly cleaved and transferred to other areas. As in Ogihara [10, 11], this study considered that the cleaved MoS_2 particles were transferred to the worn surface. In the mixed lubrication region, the sliding force acted between MoS_2 layers, facilitating interlayer sliding and reducing friction. It seems that, in the fluid lubrication region, the cleaved MoS_2 particles decreased the shear force of the lubricant, reducing friction.

The combination of the micro dimple and the MoS_2 shot treatments further reduced friction in all regions. It was thought that, in the mixed lubrication region, not only the MoS_2 interlayer sliding occurred (by the sliding force acting between layers) but also lubricant was supplied to the sliding surface through micro dimples, further reducing friction. In the fluid lubrication region, the shear force of the lubricant between the sliding surfaces decreased, due to both the cleaved MoS_2 particles and the vortices generated inside the micro dimples, further reducing friction.

4. Conclusions

Using a friction measurement apparatus with a floating cylinder liner, similar to an eco-mileage vehicle engine, the effect of piston surface treatment with the FPB process on piston assembly friction was investigated. Results indicated that, the micro dimple and the MoS_2 shot treatments reduced friction. The MoS_2 shot treatment reduced friction more than the micro dimple treatment. Finally, the combination of both the micro dimple and the MoS_2 shot treatments further reduced friction. This combination of micro dimple and MoS_2 shot treatments reduced friction from 31% to 45%, compared to no treatment.

Acknowledgements

We would like to thank Fujikihan Co., Ltd. for treating the piston surfaces with the FPB process.

Nomenclature

BDC bottom dead center
FE-SEM/EDX Field Emission Scanning Electron Microscopy/Energy Dispersive X-ray Spectroscopy
FMEP friction mean effective pressure
FPB fine particle bombarding
Mo molybdenum
MoS_2 molybdenum disulfide
Ra calculated average roughness
Rz_{JIS} 10-point average roughness
S sulfur
TDC top dead center

Bibliography

[1] HOSHI, M. Reducing friction losses in automobile engines. *Tribology International*. 1984, **17**(4), 185-189. https://doi.org/10.1016/0301-679X(84)90017-3

[2] KANAI, S., TARESAWA, C., FUJIWARA, N. Friction reduction technology of the piston for gasoline engine. *Transactions of the Society of Automotive Engineers of Japan*. 2013, **44**(2), 381-386. https://doi.org/10.11351/jsaeronbun.44.381 (in Japanese).

[3] KOVACH, J., TSAKIRIS, E., WONG, L. Engine friction reduction for improved fuel economy. *SAE Technical Paper* 820085. 1982. https://doi.org/10.4271/820085

[4] MATSUMOTO, K. Friction reduction in an internal combustion engine. *Journal of the Japan Society of Mechanical Engineers*. 1976, **79**(694), 870-876. https://doi.org/10.1299/jsmemag.79.694_870 (in Japanese).

[5] MURAKAMI, M., KONOMI, T., NOHIRA, H. et al. Analysis of piston frictional force under engine firing condition. Effects of surface characteristics of piston skirt on friction. *Transactions of the Society of Automotive Engineers of Japan*. 1991, **22**(4), 70-73. (in Japanese).

[6] NAKADA, M. Trends in engine technology and tribology. *Tribology International*. 1994, **27**(1), 3-8. https://doi.org/10.1016/0301-679X(94)90056-6

[7] NAKANISHI, K., OKADA, Y., SERA, K. et al. Teardown analysis for piston assembly friction with optimization controls. *Honda R & D Technical Review*. 2010, **22**(1), 154-159.

[8] NAKASHIMA, K., UCHIYAMA, Y. Experimental development of apparatus to measure piston assembly friction in an eco-mileage vehicle engine. *Combustion Engines*. 2019, **177**(2), 55-59. https://doi.org/10.19206/CE-2019-210

[9] OGIHARA, H., KIDO, T., YAMADA, H. et al. Technology for reducing engine rubbing resistance by means of surface improvement. *Honda R & D Technical Review*. 2000, **12**(2), 93-98.

[10] OGIHARA, H. Modification of piston sliding surface for internal combustion engine by fine particle peeing of solid lubricant. *Tribologist*. 2002, **47**(12), 895-900. (in Japanese).

[11] OGIHARA, H. Research into surface improvement for low friction pistons. *SAE Transactions Journal of Engines*. 2005, **114**(3), 1182-1190. https://doi.org/10.4271/2005-01-1647

[12] PODGORNICK, B., VILHENA, L., SEDLACEK, M. et al. Effective and design of surface texturing for different lubrication regimes. *Meccanica*. 2012, **47**, 1613-1622. https://doi.org/10.1007/s11012-012-9540-7

[13] SASAKI, M., TAKAHASHI, N., SATO, T. et al. Development of low friction solid film lubricant for piston (First report) Development of double layer solid film lubricant, *2010 JSAE Annual Congress (Spring) Proceedings*, 2010, **82**(10), 7-10. (in Japanese).

[14] SUGIMURA, K. Development of piston treatment for internal combustion engine. *SAE International Journal of Materials and Manufacturing*. 2008, 1(1), 824-831. https://doi.org/10.4271/2008-01-1462

[15] TAKIGUCHI, M., TAKIMOTO, T., ASAKAWA, E. et al. A study of friction force reduction on piston skirt (Effect of width, roughness and resin coating). *Transactions of the Japan Society of Mechanical Engineers B*, 1997, **63**(611), 2587-2592. https://doi.org/10.1299/kikaib.63.611_2587 (in Japanese).

Prof. Kohei Nakashima, DEng. – Department of Vehicle and Mechanical Engineering, Meijo University, Japan.
e-mail: *nakasima@meijo-u.ac.jp*

Yosuke Uchiyama, MEng. – Department of Vehicle and Mechanical Engineering, Meijo University Graduate School, Japan.
e-mail: *150446017@ccalumni.meijo-u.ac.jp*

Article citation info:
CHMIELEWSKI, Z. Assessment of the kinetics of changes in selected physicochemical indicators of engine oil in operation. *Combustion Engines*. 2022, **188**(1), 24-29. https://doi.org/10.19206/CE-141337

Zbigniew CHMIELEWSKI

Combustion Engines
Polish Scientific Society of Combustion Engines

Assessment of the kinetics of changes in selected physicochemical indicators of engine oil in operation

ARTICLE INFO

Received: 13 July 2021
Revised: 6 August 2021
Accepted: 17 August 2021
Available online: 15 September 2021

The article presents the results of operational tests of engine oil, including the observation of changes in the values of selected physicochemical parameters of oil in subsequent operation cycles, in accordance with the service life specified by the vehicle manufacturer. Preliminary analysis of defined indicators characterizing the condition of engine oil were performed in terms of their suitability for the ongoing monitoring of the technical condition of the engine. On the basis of the values of selected indicators of fresh oil recorded in the course of operational tests and during replacement, one indicator was selected, the kinematic viscosity at 100°C, for which an unambiguous trend of changes was observed during the tests. The last stage was to verify the hypothesis about the correlation between the observed changes in the value of the indicator and the mileage of the engine–vehicle.

Key words: *internal combustion engine, cylinder liner, engine oil, kinematic viscosity*

1. Introduction

Lubricating oils used in tribological systems of combustion engines are a mixture of organic compounds and enriching additives, while the physical structure of the oil is not sufficiently explained. Hence, an unambiguous description of their condition and the current assessment of their properties as a lubricant are difficult. Therefore, the characteristics of the oil are not a set of precise quantitative and qualitative data of the chemical composition, chemical structure, or the values of characteristic physical quantities. The characteristics of oil as a lubricant, an element of the tribological system, are expressed using indicators that indicate the possibility of its application in specific kinematic nodes [16].

The description of the lubricant condition cannot be made in isolation from the tribological system. Hence, this concept is understood not only as a description of a state in the physical sense, defined as a set of values of quantities characterizing the macroscopic properties of a system, but also a set of values related to basic functions fulfilled in the system. The condition description must therefore reflect the individual and functional (collective) properties of the lubricant. In practice, these properties are most often assessed by measuring specific parameters – indicators included in the relevant standards for lubricants.

Research is carried out on the behavior of engine oil in operation, however, it concerns only the analysis of the oil itself without taking into account the technical condition of the tribological system in which it worked [1, 3, 5, 8, 9, 14, 15].

Engine oil is a component of the tribological system, the operating conditions of which change over time. It is subjected to variable mechanical and thermal loads resulting from the tasks performed, but it is also subject to variable and usually unfavorable loads due to the wear of the components of the piston-rings-cylinder (PRC) system with time. Among all the elements of the tribological system, engine oil is subject to the most intense physical and chemical changes during operation. This is due to the effect of the system on the oil. The size of the excitations acting on engine oil is related to, inter alia, with the technical condition of the PRC system, expressed by the amount of clearances in this combination [6, 7]. The increase in the amount of blow-by of exhaust gases into the engine crankcase caused by the increasing clearance, as well as the increase in the amount of oil entering the combustion chamber and the amount of unburned fuel entering the oil sump cause the indicators describing the condition of the engine oil to change over time. The kinetics of this process is the result of the occurring tribological phenomena and wear of the PRC system. The analysis of the process of changes taking place in the engine oil in operation and an attempt to describe them mathematically requires to take into account not only the typical forces acting on the oil, but also the changing operating conditions of the system, resulting from the natural wear process of the elements of the PRC tribological system.

The results of the research compliant with the indicated postulate are presented below. Changes in the engine oil were observed and recorded in relation to selected physicochemical indicators at intervals related to its periodic replacement and the progressive wear of the PRC system components. Based on the research results, a mathematical model of the kinetics of changes in selected physicochemical indicators of oil in operation was proposed, correlated with the vehicle mileage.

2. Models of kinetics of changes in oil properties

The aging processes are cumulative and have specific features. During the operation of the oil, partial renewal procedures are performed, regeneration of properties resulting from the need to refill the oil to the volume recommended for a given lubrication system and to use oil filtration in the engine itself [12].

Refreshing by topping up is a discrete process, while regeneration by filtering is a continuous but also random process. In the latter, the randomness is the random trap-

ping of particles that make up the oil contaminants. On the other hand, the purification device itself (filter) operates continuously with varying efficiencies.

When analyzing the kinetics of changes in oil properties, the following issues should generally be considered:

1. All the physical and chemical processes that take place during its use (aging).
2. The process of regeneration (refreshing) by adding fresh oil.

Physico-chemical processes take place under all conditions of oil use, but their intensity depends both on the type and type of oil, as well as on the physical parameters determined by the conditions of using the oil in a given system (temperature, pressure, volume). On the other hand, the refreshing process is a natural consequence of the loss of oil as a result of its combustion, as well as possible leaks from the system.

Taking into account that in reality not only oil quality changes over time due to the refreshing process, but also physical and chemical processes occurring in the oil volume, it seems that the most appropriate image of the kinetics of changes may be exponential curves. Such a situation is presented in Fig. 1. However, it is also a certain approximation of an averaging nature, but having the advantage of reflecting relatively well the general tendency of changes, which is an expression of the influence of both considered.

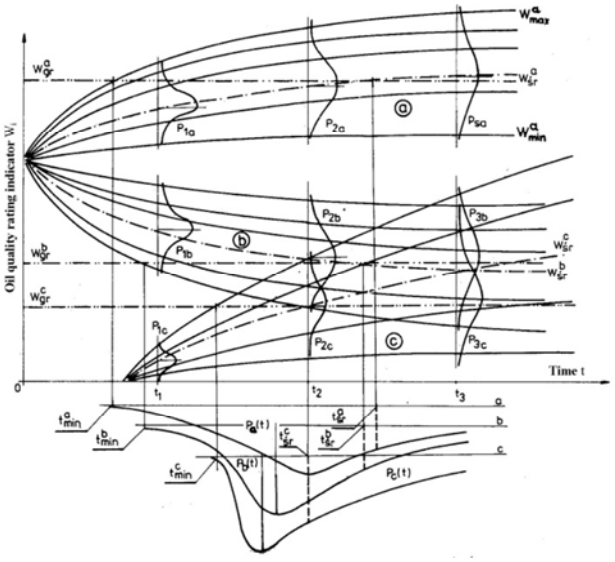

Fig. 1. Kinetics of changes in oil quality assessment indicators [11]

Thus, for research and comparative purposes, it is necessary to propose a mathematical model describing the changes taking place in the used engine oil. This model, with high probability, should take into account the kinetics of changes in relation to selected physicochemical parameters of oil essential for the proper functioning of the tribological system. Such research has been conducted for a long time.

For example, in the work [13] it was assumed that the absolute difference in the values of fresh oil and oil properties after a specified operation time allows the assessment of changes in the properties of the aged oil in comparison with the properties of fresh oil. The course of these changes has a specific character of an exponential sequence with the limit (1) and (2):

$$\lim_{n\to\infty}|P_0 - P_i|_P = \alpha \cdot \Delta t \tag{1}$$

and

$$\lim_{n\to\infty}\sum_1^n k^n = \alpha \cdot \Delta t \cdot \frac{k}{1-k} \tag{2}$$

where: α – the slope of the straight line, Δt – continuous operation time between successive additions of mechanical, n – the number of cycles of the fluid and the number of further additions, k – the unit volume of fresh oil to the lubrication while each additions, P – analyzing the property of the lubricating oil , which for fresh oil takes the value of P_0 and during aging, without taking into account refreshing, changes rectilinearly as a function of working time to the final value of P_i in the next working cycle.

The presented model allowed the authors to state that the analyzed lubricating oil aging process does not have a limit state as a function of time.

The problem remains open and research on the kinetics of changes in selected properties of engine oil in operation is still carried out. The results of tests of engine oils in service presented in [17] allowed for the development of a statistical model using the basic mathematical model – a linear function. The obtained model based on changes in the kinematic viscosity at 100ºC of engine oils under operating conditions can be used to predict the behavior of engine oil during operation. It should be noted, however, that in order to obtain a complete picture of changes taking place in the oil, it is advisable to interpret the kinematic viscosity in addition to the dynamic viscosity (HTHS), the degree of oxidation and the acid number. These properties can affect the reliability of the entire engine, and it is therefore important to continue observing the degradation state of the engine oil. Moreover, the research, as the authors point out, mainly covered vehicles operated in conditions that can be described as "difficult", i.e. frequent engine start, short distances, prolonged idling. Hence, the proposed model of the kinetics of changes in kinematic viscosity at 100ºC of engine oils does not necessarily reflect the changes taking place in the engine operated under statistically average load conditions.

According to the author, the mathematical models proposed so far do not fully reflect the actual changes taking place in the engine oil. Due to the limitations occurring during the operational tests or the adopted boundary conditions, the proposed model does not fully reflect the actual changes taking place in the engine oil between its changes, especially with the increase of the engine mileage. Therefore, it is important to observe and analyze the changes taking place in the oil in subsequent cycles of its replacement, taking into account the actual mileage of the engine and the mutual correlation of these parameters.

3. Research method

Among the physicochemical and functional indicators characterizing the condition of the lubricating oil, in operational tests the most frequently used (apart from the contamination content) is kinematic viscosity. The conditions of cooperation of the elements: piston, piston rings, cylin-

der liner are primarily determined by the viscosity of the lubricant between them. It determines the nature of friction, both in a cold and warm engine [10]. It is also important during engine start-up [2]. Moreover, the viscosity of engine oil changes significantly during its service life. It is related to, inter alia, with the leakage of unburned fuel to the engine oil pan, which in turn is largely conditioned by the tightness (wear) of the PRC connection. The increase in clearance between the piston and the cylinder liner, observed along with the mileage of the vehicle–engine, favors the penetration of more and more fuel and faster dilution of the engine oil. The simultaneous processes causing the increase in oil viscosity do not neutralize the above tendency, and moreover, their intensity is not closely correlated with the progressive wear of the PRC system. Their occurrence is mainly related to the aging processes of the oil taking place in the high-temperature zone of the engine, i.e. the lubricating layer on the cylinder liner surface. Thus, the process of diluting engine oil during operation is observed [4], and it intensifies with the mileage of the vehicle. The kinetics of changes in oil viscosity is thus reflected in the decreasing function with absolute increases with the vehicle mileage.

However, the changes taking place in the exploited oil include not only its degradation, as a result of the system's impact, but also the refreshing phenomenon through "refills". The image of the physicochemical state of the used oil just after topping up is strongly distorted. A portion of fresh oil improves the properties of the lubricant, bringing them closer to the initial values. Hence, the moment of the analysis is an important issue.

The actual condition of the used oil is observed at the time of its replacement. Observations of users' behavior indicate that they do not make any top-ups of oil before its soon planned oil change. Thus, the condition of engine oil at the time of its replacement well reflects the resultant of the forces acting on the engine oil in the next, full cycle of its operation.

The model of the kinetics of changes in the properties of engine oil in operation, proposed by the author, also takes into account the correlation between the phenomenon of cylinder liner wear, which is a continuous process observed for the same kinematic pair, and the oil degradation process taking place for subsequent, new portions of oil after each oil change. Moreover, the actual oil service life may be different for subsequent changes, although statistically, with high service culture, its expected value will be close to the recommended by manufacturer.

The above requirements take into account the proposed index of the intensity of changes in C_W oil properties. It is characterized by the relationship (3):

$$C_W = \frac{W_p - W_k}{t_{ol}} \quad \text{for } t > 0 \tag{3}$$

where: W_p – value of the measured index of oil condition assessment for fresh oil, W_k – value of the measured oil condition assessment index for used oil (at the time of replacement), t_{ol} – engine oil operation time to be changed, C_w – index of intensity of changes in oil properties.

This indicator provides average information about the intensity of the engine's impact on the oil. It does not take into account periodic changes in the measured value of the oil parameter, but reflects the long-term tendency of the observed changes.

The operational tests have shown that the best indicator of the intensity of changes in kinematic viscosity at 100°C – C_{V100} for the purposes of the presented method.

The last stage is to verify the hypothesis on the correlation between the observed changes in the kinematic viscosity of the used engine oil, expressed with the C_{V100} kinematic viscosity change intensity index, and the engine–vehicle mileage.

4. Operational research

4.1. Research object and methodology

The object of the operational tests were five 110 kW diesel engines installed in medium-duty trucks. The tests were carried out under supervised operational test conditions. The tests were carried out after factory-new engines were installed in the vehicles, and their initial technical condition was known (cylinder liners micrometers were carried out to the extent possible after the cylinder head had been disassembled, the compression pressure, crankcase exhaust gas blow – by and exhaust smoke were measured). The vehicles were part of the fleet. The average load of the load box was 5000 kg and never exceeded the permissible load capacity of the vehicle. The daily mileage of the cars was from 240 to 350 km. The cars were operated in urban and non-urban driving conditions. The engine lubrication system uses engine oil of API CE/SF quality class and SAE 15W/40 viscosity class. This oil was used throughout the research period and came from one production batch. All technical maintenance of engines was performed in accordance with the manufacturer's recommendations.

The method of evaluation of the physicochemical and functional parameters of the oil was used to assess changes in oil properties. The chemical analysis of fresh oil as well as used oil samples, collected at the time of replacement, and used oil were carried out in one laboratory with the use of a commissioned system. This allowed to maintain the repeatability of the measurement methods used, and thus increase the reliability of the obtained test results. Selected physicochemical properties of fresh oil are presented in Table 1.

Table 1. Physical and chemical properties of 15W40 oil

The parameter under study		Unit	Value
Kinematic viscosity at 40°C		mm^2/s	99.52
Kinematic viscosity at 100°C		mm^2/s	14.21
Base number		mg KOH/g	10.84
Carbon residue according to Conradson		%	1.38
Sulphated ash		%	1.10
Flash point in a closed cup		°C	190
The content of elements derived from improvers	calcium – Ca	%	0.33
	zinc – Zn	%	0.13
	phosphorus – P	%	0.12

The actual mileage between exchanges did not differ by more than 10%. During the exchange, a sample of used oil

was taken (about 1 dm^3). Additionally, the content of elements derived from the engine's structural elements was determined for the used oil (iron – Fe, copper – Cu, lead – Pb).

4.2. Results and analysis

The analysis of changes in the condition of oil in operation was carried out as an assessment of the kinetics of changes in the selected oil index. The basis was information on:

- the value of the selected condition assessment indicator for fresh oil,
- values of the selected condition assessment indicator for used oil (at the time of replacement),
- oil service time (car mileage between oil changes).

This information is related to the indicator of the intensity of changes in C_W oil properties (3). The following oil condition indicators were assessed in terms of changes occurring during operation.

Among the physicochemical indicators:

- kinematic viscosity at temperature 40°C – ν_{40},
- kinematic viscosity at temperature 100°C – ν_{100},
- base number – LZ,
- carbon residue according to Conradson,
- sulphated ash,
- flash point in a closed cup,
- the content of elements derived from improvers: Ca, Zn, P. of the functional indicators:
- the content of metallic elements originating from the engine's structural elements: Cu, Fe, Pb.

The analysis of changes in engine oil was carried out for the mileage above 10,000 km. This allowed to eliminate errors related to the running-in process of kinematic pairs in the engine. Only the period of stabilized wear was included in the analysis (Lorentz curve).

The calculated values of the intensity index of oil properties changes C_{Wi} (i = 1, 2, ..., n, where n – the number of the next oil change) for each of the above-mentioned oil condition indicators were related to the vehicle mileage corresponding to the time of measurement (vehicle mileage in when the oil is changed). Using the STATISTICA® program, the correlations between the C_{wi} index for each of the observed oil condition indexes and the vehicle mileage were determined. Initially, the data was fitted with a linear regression model estimated using the maximum likelihood method under the socalled generalized least squares method. The application of the above-mentioned method made it possible to include in the estimation process a theoretically justified assumption about the correlation of successive measurements of oil parameters. This assumption was introduced by assuming that the random term in the regression model is subject to a continuous first-order autoregressive process. However, in the course of further analyzes and as a result of the sensitivity analysis, it was shown that the use of the above-described advanced statistical apparatus changed the results of the analysis to a minimal degree in relation to the classical model of normal linear regression. As a result, in order to simplify the presentation of results and facilitate interpretation, the linear regression models were estimated using the classical method of least squares. The second type of regression lines were used to initially estimate the dependencies sought. The results of the calculations are summarized in Table 2 (the determined correlations are significant at the confidence level of $1-\alpha = 0.95$ assumed as the border value of the acceptable error level [18]).

Table 2. List of linear correlation coefficients for the assessment of oil condition changes in relation to the vehicle mileage

Oil condition change assessment indicators C_{wi}	The value of Pearson's linear correlation coefficient r	Coefficient of determination R^2	Test probability value p
Kinematic viscosity at 40°C	–0.71	0.532	0.00044
Kinematic viscosity at 100°C	–0.81	0.628	0.00006
Base number	correlation irrelevant		
Carbon residue according to Conradson	0.46	0.28	0.00541
Sulphated ash	correlation irrelevant		
Flash point in a closed cup	correlation irrelevant		

Exemplary waveforms are shown in Figs 2–4.

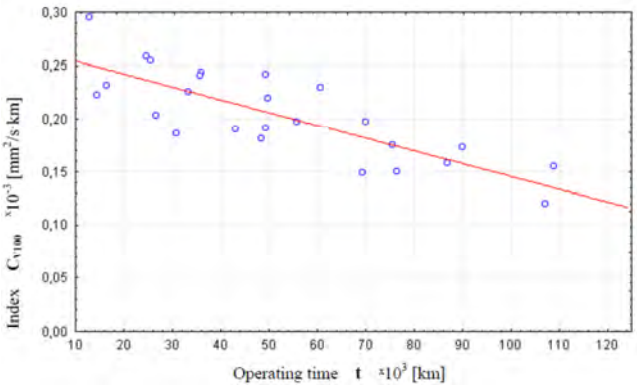

Fig. 2. The course of the kinematic viscosity change intensity index at 100°C C_{V100} as a function of operating time

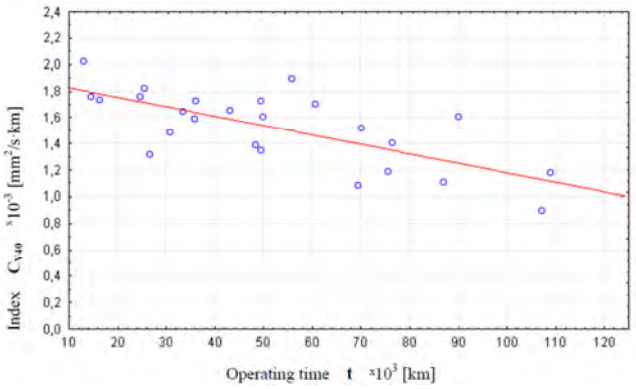

Fig. 3. The course of the kinematic viscosity change intensity index at 40°C C_{V40} as a function of operating time

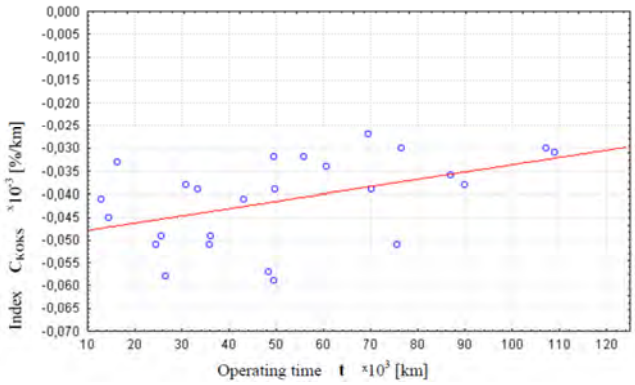

Fig. 4. Course of the change intensity index of coking residues according to Conradson C_{KOKS} as a function of operating time

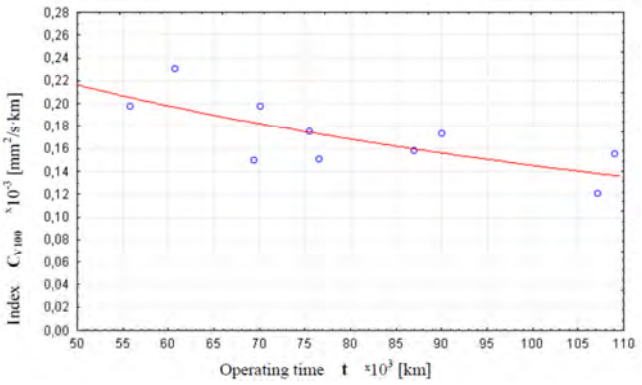

Fig. 5. Power regression model of the C_{V100} index in relation to the vehicle mileage

Thus, among the oil condition indicators observed in operation, the highest value of the linear correlation coefficient with respect to the vehicle mileage was obtained for the kinematic viscosity change intensity index at 100°C C_{V100}. This result confirms the correctness of the theoretical analysis carried out. By limiting ourselves to this parameter of engine oil, the C_{V100} index curves were determined in relation to the operating time. The highest value of the curvilinear correlation coefficient, at the level of R = 0.741, was obtained for the regression line described by the power function (the panel of the STATISTICA program was used). Thus, the course of changes of the C_{V100} index in relation to the operating time can be described by the relationship (4):

$$C_{V100} = (3.277) - (2.142) \cdot t^{(0.033)} \left[\frac{mm^2}{s \cdot km}\right] \quad (4)$$

where: t – engine operation time (mileage) [km].

The course of the determined dependence is shown in Fig. 5.

This dependence, apart from the highest value of the correlation coefficient, well reflects the physical interpretation of the observed phenomenon. Changes in the properties of engine oil tend to a certain limit but do not reach it, which perfectly correlates with the course of the power function. The results of the analysis, verified in operational tests, confirm the relationship between the changes taking place in the used engine oil in terms of kinematic viscosity at 100°C, and the mileage of the vehicle–engine.

5. Conclusions

Based on the analysis of the factors influencing the phenomenon of engine oil degradation in operation, it can be concluded that:

1. The changes in selected physicochemical properties recorded in the engine oil tests confirm the thesis about the correlation between the value of the observed parameter and the vehicle mileage.
2. The conducted operational tests confirm the correctness of the theoretical analysis performed and indicate that the changes taking place in the used engine oil are, among others, as a result of wear of the PRC system components. In this approach, among the physicochemical and functional indicators characterizing the condition of the used lubricating oil, only the kinematic viscosity at 100°C sufficiently reflects the degradation processes occurring in this combination. It has also been shown that there is a close relationship between changes in the kinematic viscosity of the used engine oil, expressed by the intensity index of changes in kinematic viscosity at 100°C C_{V100}, and the mileage of the vehicle–engine.
3. As a result of the tests, no relationship was found between the vehicle mileage and the content of elements derived from engine components in the tested engine oil. It can therefore be concluded that the methods of spectroscopic analysis of the content of metallic elements in engine oil can only be an auxiliary means in assessing the condition of the engine. They can be of key importance in estimating the acceptable wear of lubricated kinematic pairs.

Nomenclature

API	American Petroleum Institute
C_w	index of intensity of changes in oil properties
C_{V100}	kinematic viscosity change intensity index at 100°C
HTHS	High Temperature High Shear rate
p	test probability value
PRC	Piston-Rings-Cylinder
r	the value of Pearson's linear correlation coefficient
R^2	coefficient of determination
R	curvilinear correlation coefficient
SAE	Society of Automotive Engineers
t_{ol}	engine oil operation time to be changed
W_k	value of the measured oil condition assessment index for used oil (at the time of replacement)
W_p	value of the measured index of oil condition assessment for fresh oil

Bibliography

[1] ALBERTSON, W.C., STALEY, D.R., MCDONALD, M.M. et al. Engine oil viscosity diagnostic system and methods. *United States Patent*. 2008, 20080223114.

[2] DROŹDZIEL, P., IGNACIUK, P. Ocena zmian własności oleju silnikowego w trakcie stanowiskowych rozruchów silnika spalinowego. *Tribologia*. 2004, **2**, 117-128.

[3] GOMÓŁKA, I., AUGUSTYNOWICZ, A. Evaluation of applicability of dielectric constant in monitoring aging processes in engine oils. *Eksploatacja i Niezawodnosc – Maintenance and Reliability*. 2019, **21**(2), 177-185. https://doi.org/10.17531/ein.2019.2.1

[4] JAKÓBIEC, J., BUDZIK, G. Czynniki mające wpływ na stopień degradacji oleju silnikowego w okresie eksploatacji. *Archiwum Motoryzacji*. 2007, **3**. 209-216.

[5] KARPOVICH, I.A., ODZHAYEV, V.B., AZARKO, I.I. et al. Universal device for motor-oil quality control. *11th International Conference Microwave and Telecommunication Technology*. IEEE Cat. No.01EX487. 2001, 673-674. https://doi.org/10.1109/CRMICO.2001.961712

[6] KOSZAŁKA, G. Model of operational changes in the combustion chamber tightness of a diesel engine. *Eksploatacja i Niezawodnosc – Maintenance and Reliability*. 2014, **16**(1), 133-139.

[7] KOSZAŁKA, G., SUCHECKI, A. Changes in performance and wear of small diesel engine during durability test. *Combustion Engines*. 2015, **162**(3), 34-40. https://doi.org/10.19206/CE-116863

[8] KUMBAR, V., VOTAVA, J. Differences in engine oil degradation in spark-ignition and compression-ignition engine. *Eksploatacja i Niezawodnosc – Maintenance and Reliability*. 2014, **16**(4), 622-628.

[9] LEWI, A., PEEW, D. On the evaluation of exploitation qualities of PristaSuper 25W40 motor oil with DIA method. *Eksploatacja i Niezawodnosc – Maintenance and Reliability*. 2011, **4**, 11-14.

[10] MAZURKOW, A., WITKOWSKI, W., KALINA, A. et al. The effect of oil feeding type and oil grade on the oil film bearing capacity. *Eksploatacja i Niezawodnosc – Maintenance and Reliability*. 2021, **23** (2), 381-386. http://doi.org/10.17531/ein.2021.2.18

[11] NADOLNY, K. Możliwości wyznaczania uzasadnionych okresów eksploatacji oleju. *Technika Smarownicza*. 1979, **3**.

[12] NADOLNY, K. Niezawodnościowe problemy eksploatacyjnych zmian jakości silnikowych olejów smarowych. *Politechnika Poznańska, Rozprawy nr 164*, Poznań 1985.

[13] SOBAŃSKA, K., LEWIŃSKA I.B., HEBDA, M. et al. Matematyczny model przebiegu procesu starzenia olejów smarowych pracujących w urządzeniach mechanicznych II typu. *Materiały Konferencyjne KONMOT*. 1978.

[14] Standard test method for low temperature, low shear rate, viscosity/temperature dependence of lubricating oils using a temperature-scanning. *Technique. West Conshohocken*. ASTM International, 2005.

[15] URZĘDOWSKA, W., STĘPIEŃ, Z. Wybrane zagadnienia dotyczące zmian właściwości silnikowego oleju smarowego w eksploatacji. *Nafta-Gaz*. 2012, **12**(LX), 1102-1110.

[16] WOLAK, A., JANOCHA, P. Zmiany właściwości użytkowych olejów silnikowych w warunkach eksploatacji – analizy FTIR. Nowoczesne środki smarowe do specjalistycznych zastosowań w urządzeniach przemysłowych, transporcie i komunikacji. *Kraków: Instytut Nafty i Gazu – Państwowy Instytut Badawczy*. 2015, **201**, 84-105.

[17] WOLAK, A, ZAJĄC, G. The kinetics of changes in kinematic viscosity of engine oils under similar operating conditions. *Eksploatacja i Niezawodnosc – Maintenance and Reliability*. 2017, **19**(2), 260-267. https://doi.org/10.17531/ein.2017.2.14

[18] StatSoft, Electronic Statistics Textbook. https://www.statsoft.pl/textbook/

Zbigniew Chmielewski, DEng. – Faculty of Mechanical Engineering, University of Technology and Humanities in Radom.

e-mail: *zbigniew.chmielewski@uthrad.pl*

Article citation info:
KAMIŃSKA, M., ANDRZEJEWSKI, M., DASZKIEWICZ, P. Research of ecological indicators of two-way vehicle in stationary conditions. *Combustion Engines*. 2022, **188**(1), 30-34. https://doi.org/10.19206/CE-142169

Michalina KAMIŃSKA
Maciej ANDRZEJEWSKI
Paweł DASZKIEWICZ

Combustion Engines
Polish Scientific Society of Combustion Engines

Research of ecological indicators of two-way vehicle in stationary conditions

ARTICLE INFO

Received: 6 August 2021
Revised: 25 August 2021
Accepted: 12 September 2021
Available online: 15 September 2021

The presented article concerns the research on the emission of pollutants of a rail-road tractor in two stationary research tests. The purpose of the tests was to carry out control tests of pollutant emissions and their analysis. The object used during the works was approved in accordance with the Stage V standard, which requires measurements of emissivity both in stationary, dynamic and real conditions. Despite the requirement to test engines installed on a vehicle during their normal duty cycle with PEMS, the emission limits measured in this test have not yet been defined. Therefore, the work below focuses on the stationary test cycle. The measurements were carried out in accordance with the internal combustion engine operating points described in the approval test, and then compared with the modernized NRSC test. It contains modified measuring points and rotational speeds of the crankshaft, adopted on the basis of the most common operating parameters of agricultural tractor combustion engines in real operating conditions. The measurements were performed with the use of a mobile dynamometer and devices for measuring emissions of harmful exhaust gas compounds and recording on-board data. In the performed test, the vehicle drive system worked at fixed operating points, with defined values of crankshaft rotational speed and load. Based on the recorded data on the concentrations of pollutants in the exhaust gases, the unit emission of the tested object was determined. In the final stage of the work, these data were used to perform a comparative analysis with the emission limits contained in the standard.

Key words: *exhaust emission, rail-road vehicle, NRSC, PEMS, NRMM*

1. Introduction

One of the key factors contributing to the deterioration of the natural environment are combustion engines in means of transport, which are the source of exhaust gases. Research by the European Environment Agency shows that transport generates 20% of all global CO_2 emissions, almost 10% of PM10 and 39% of NO_x [5]. Despite the introduction of increasingly more stringent exhaust emission norms, the number of vehicles in use is increasing annually, which obviously affects the air quality. This contributes to the formation of smog in urban agglomerations and causes climate change as a result of the greenhouse gases (GHG) released. According to World Health Organization (WHO) reports, over 90% of the world's population lives in regions where the limits of harmful compounds concentration in the air are exceeded [20]. Our World in Data research team has shown that in 2017, air pollution was the fourth largest in terms of numbers (after high blood pressure, smoking, high blood sugar and obesity) cause of illness and death or disability in the world. It is estimated that 3.4 million people died prematurely as a result of this pollution, which accounts for about 6% of deaths worldwide. This indicates that it is one of the world's biggest health and environmental problems to date [12].

Off-road vehicles have a significant impact on the environmental pollution due to their operating characteristics and how they are used [6]. The main problem of these types of vehicle is the type-approval tests carried out on an engine dynamometer. The literature widely describes the problem of the unrepresentativeness of laboratory tests performed on specially prepared measuring stands [9, 11, 13, 16, 18, 19]. In this type of test, the real operating conditions of the vehicles are simulated in standardized tests. It has been shown, however [7, 8, 14, 15, 17], that the test cycles used in type approval do not reflect the real conditions of the engine's actual operation. This is mainly due to the wide variety and diversity among machines and vehicles classified under the NRMM (*Non-Road Mobile Machinery*) group. This contributes to the differences between the qualitative and quantitative measurements of exhaust emissions in stationary tests and the real exhaust emissions in operation. In order to obtain reliable results, it becomes necessary to conduct field work on real objects performing real tasks. Currently, road tests are compulsory for passenger cars and heavy vehicles all over the world. Measurements in RDE (*Real Driving Emissions*) tests are performed using specialized exhaust gas analyzers from the PEMS group (*Portable Emissions Measurement Systems*). This makes it possible to perform reliable measurements in real operating conditions, and thus to verify the ecological indicators of vehicles in a wide spectrum of operation of their drive systems.

Based on the NRSC (*Non-Road Stationary Cycle*) test and field measurements, it is possible to modify and adjust the current test procedures. A set of changes to the static engine tests were proposed in [6], based on the similarity of the operating conditions of the engines, and where the phase coordinates were selected arbitrarily based on the author's knowledge and experience. This test was described in more detail and used to conduct comparative analyzes in the section discussing the measurement results.

2. Method

A rail-road tractor was used for the tests (Fig. 1, Table 1) equipped with a 6-cylinder VGT (*Variable Turbo Geometry*) turbocharged engine with a displacement of 6.8 dm^3 and a maximum power of 107 kW at 2000 rpm. The maximum torque of the engine was 640 Nm at 1500 rpm. The engine was supplied by direct injection of Common Rail

fuel at a pressure of 1800 bar. It should also be noted that the tractor was equipped with a continuously variable transmission, which was a combination of a two-stage planetary gear, a clutch assembly and a hydrostatic transmission. This solution to optimize the power flow, and additionally boasts a simple design and two internally changed gears. According to the manufacturer's data, the vehicle complied with the Stage V exhaust emission norm. It was equipped with an EGR (*Exhaust Gas Recirculation*) system, so that part of the engine exhaust is mixed with the intake air in the form of exhaust gas recirculation. As a result, the combustion process in the engine is slower and, at the same time, its temperature is lower. The vehicle also had a DOC (*Diesel Oxidation Catalyst*) and DPF (*Diesel Particulate Filter*) system, allowing for the reduction of both hydrocarbon and particulate emissions in the exhaust gas. In addition, the vehicle also uses SCR (*Selective Catalytic Reduction*) to reduce the content of nitrogen oxides in the exhaust gases, which are converted into nitrogen and water vapor using an aqueous solution of urea (Adblue).

Fig. 1. Test vehicle with the drive system highlighted [10]

Table 1. The main technical parameters of the test vehicle [10]

Vehicle parameters data sheet	
Engine type	Diesel
Fuel supply system	Common Rail
Number of cylinders	6
Displacement	6.8 dm^3
Nominal power at engine speed	107 kW/2000 rpm
Nominal torque at engine speed	640 Nm/1500 rpm
Turbocharging	VGT
Exhaust aftertreatment systems	EGR, DOC, DPF, SCR
Exhaust emission norm	Stage V

The aim of the research was to determine the differences in the exhaust emissions measurements carried out in stationary conditions. The vehicle was tested according to two different measurement test methods, and the actual ecological indicators of the test vehicle were determined based on the comparative analysis of the results obtained from these tests. As shown in [7, 8, 14, 15, 17] tests carried out in laboratory conditions on engine dynamometers and test benches do not reflect the real exhaust emission values that occur in real vehicle operation. The NRSC test procedures according to which off-road vehicles are normally tested do not sufficiently reflect the actual engine operating parameters.

The test vehicle was connected with a mobile dynamometer using a power take-off (PTO) shaft, which made it possible to set the engine to achieve assigned operating points (Fig. 2 (II)). The dynamometer was equipped with an air-cooled electric machine (generator), which enabled a two-way power take-off. The maximum dynamometer rotational speed was 3600 rpm and the maximum received torque was 7200 Nm. The engine operating parameters read from the on-board diagnostics system were recorded using the TEXA Navigator TXT device. Additionally, during the tests, the emission of pollutants from exhaust gases was measured with the use of devices from the PEMS group (Fig. 2 (I)).

Fig. 2. Test stand: I – exhaust emissions measurement device, II – connection between the PTO and the mobile dynamometer

3. Results

The exhaust emission measurements of toxic gases was carried out in the process of performing two measurement tests. The first was the stationary NRSC test cycle used for testing off-road machines (Fig. 3, Table 2). It is a part of the Stage I, II, III A, III B and IV exhaust emission norms for diesel engines with a net power of 19 kW ≤ P ≤ 560 kW, operating at constant or variable speeds. It consists of 8 phases of different rotational speed and load points, which are chosen to correspond with the typical operating range of diesel engines in machines of this type [1, 2, 4].

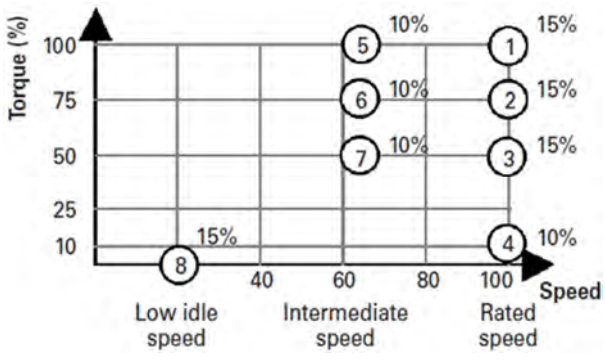

Fig. 3. NRSC test procedure measurement points (test 1) [3]

Table 2. The NRSC test parameters [3]

Parameters	Test phase number							
	1	2	3	4	5	6	7	8
load [%]	100	75	50	10	100	75	50	0
load [Nm]	**465**	**350**	**230**	**45**	**600**	**425**	**300**	**0**
n	n_{rated}				$n_{intermediate}$			n_{idle}
n [rpm]	**2000**				**1200**			**800**
Phase weighing factor	0.15	0.15	0.15	0.10	0.10	0.10	0.10	0.15

The rail-road tractor was also tested in accordance with the modified NRSC test for all engines (Fig. 4, Table 3). The modified version of the NRSC test was developed by Lijewski [6]. Proposition (II) results from the combination of two tests taking into account the individual character of the engine operation for the tested vehicles. The first group consists of engines which, in real operating conditions, operate in the entire rotational speed range. The second group consists of engines operating typically at a constant rotational speeds. This test was chosen because agricultural tractors belong to both engine groups simultaneously, depending on how the vehicle is used and which type of task it performs. The procedure consisted of 7 speed and load phases which depend on the engine used.

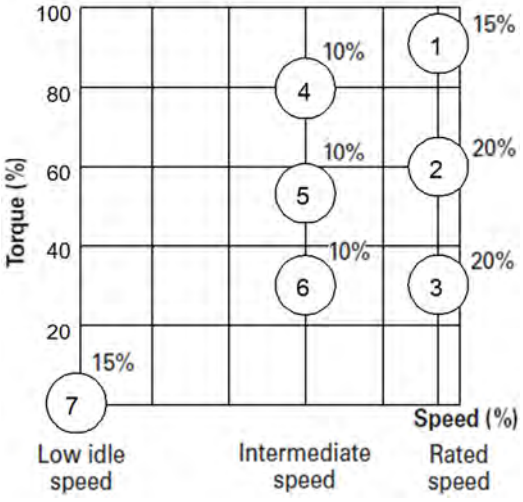

Fig. 4. The modified NRSC test (test 2) [6]

Table 3. Parameters of the modified NRSC test designed for all engines [6]

Parameters	Test phase number						
	1	2	3	4	5	6	7
load [%]	90	60	30	80	55	30	0
load [Nm]	**420**	**280**	**135**	**475**	**320**	**175**	**0**
n	n_{rated}			$n_{intermediate}$			n_{idle}
n [rpm]	**2000**			**1200**			**800**
Phase weighing factor	0.15	0.20	0.20	0.10	0.10	0.10	0.15

Based on the performed measurements, carried out in the above-mentioned test phases, the characteristics of the time-variable exhaust emission of harmful exhaust compounds limited by the emission norms were created assigned to the defined engine operating points. From the obtained results, a similarity in the way the results are distributed could be observed. In both cases, there is a downward trend for each of the monitored toxic exhaust compounds. Thus, it can be concluded that the resulting exhaust emission was closely related to the rotational speed and the load of the vehicle engine. The obtained results differed, however, to some extent. In the case of the modified NRSC test, the obtained results were about 30% lower than in the NRSC homologation test. These deviances were 27.8% for carbon monoxide, 34.2% for nitrogen oxides and hydrocarbons, and 30.3% for particulate matter, respectively. This was due to the fact that the load for all the tested phases, as defined in test 2, was characterized by lower values. The characteristics have been shown in Figs 5 and 6. For better clarity of the results, the PM values were multiplied by 10000.

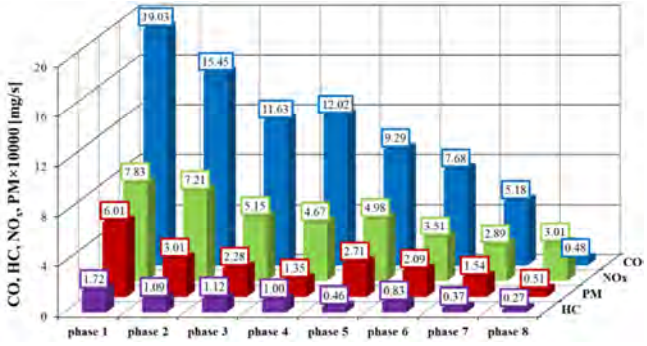

Fig. 5. Exhaust emission characteristics in each second obtained in the NRSC test

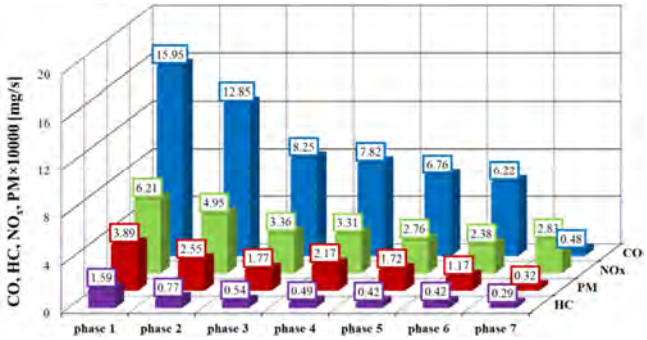

Fig. 6. Exhaust emission characteristics in each second obtained in the modified NRSC test

The performed analysis was supplemented with the characteristics of the specific emissions obtained in the entire tests, together with the reference to the Stage V emission norm for engines in the power range $56 \leq P < 130$ kW, based on which the test vehicle received type approval (Fig. 7). The obtained results show that the Lijewski test (test 1) shows a more favorable exhaust emission values of all toxic gas compounds per unit of work. The smallest difference (9.2%) was obtained for hydrocarbons. The value for test 1 was 0.25 g/kWh and for test 2 it was 0.23 g/kWh. In both cases, the Stage V emission limit value of 5 g/kWh was not met.

The largest difference (29.3%) was found for particulate matter, the values were 5.01×10^{-5} g/kWh for the NSRC test and 3.54×10^{-5} g/kWh for the modified NRSC test, respectively. In both cases, the exhaust emission standard of 0.015 g/kWh was met. For nitrogen oxides, the difference was

11%, and for carbon monoxide 22% (2.35 g/kWh NO_x, 1.26 g/kWh CO – test 1, 2.09 g/kWh NO_x, 0.98 g/kWh CO – test 2). The limit values were 0.4 g/kWh for NO_x (not met in both tests) and 0.5 g/kWh for CO (met in both tests), respectively. On the basis of the obtained results, it can therefore be concluded that using modified research tests characterized by different engine operating points to test off-road vehicles has scientific merit.

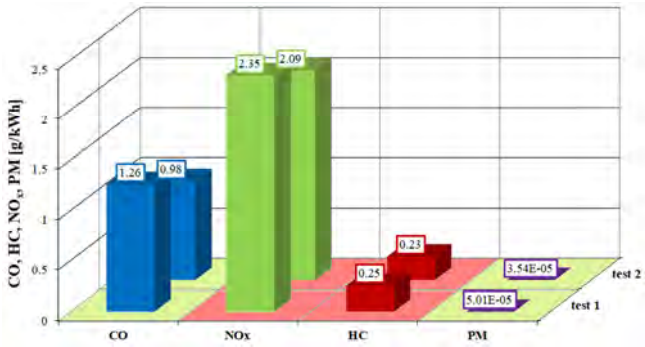

Fig. 7. Characteristic of the specific emission obtained in the tests

6. Conclusions

The considerations discussed in this article concern exhaust emission tests of toxic compounds during the engine dynamometer braking tests of an off-road vehicle. The eight-phase NRSC test and its modified original seven-phase variant were performed. As part of the research carried out, ecological indicators of the engine were determined, based on which a comparative analysis was conducted. The specific exhaust emission values of pollutants obtained as a result of the measured data were compared to the limit values defined in the Stage V emission norm, for which the tested vehicle received the type approval.

In order to present the differences between the obtained measurement results, the article uses the proposed measurement procedure described in [6]. The two performed tests were characterized by a similar distribution of results, which can be seen thanks to the characteristics of the exhaust emission in time for each of the defined test phases. They confirmed the relation between the ecological indicators and the engine speed and load. The obtained results of the emission per second (lower by about 30%) and the values of the specific emission (differences at the level of 10–20%) indicate the advantage of the modified NRSC test. In terms of CO and PM emissions, the Stage V emission standard was met, while the HC and NO_x indicators were exceeded. Special attention should be brought to the last of the given toxic compounds, because normally this compound's emission in real operating conditions most often reaches different – higher values, as compared to stationary tests.

The modified test procedure used by the authors allows for testing vehicles equipped with engines in their entire operating range of rotational speed as well as those operating at a constant rotational speed. Thanks to its versatility, it is possible to implement this solution for engines installed in all off-road vehicles. Therefore, further work of the authors will concern similar considerations and tests done for other machines of this category. In addition, plans are considered for conducting measurements on a wider group of vehicles in order to create a new original research test proposal.

Nomenclature

CO	carbon monoxide
CO_2	carbon dioxide
DOC	diesel oxidation catalyst
DPF	diesel particulate filter
EGR	exhaust gas recirculation
GHG	greenhouse gas
HC	hydrocarbons
NO_x	nitrogen oxides
NRMM	non-road mobile machinery
NRSC	non-road stationary cycle
PEMS	portable emissions measurement systems
PM	particulate matter
PTO	power take-off
RDE	real driving emissions
SCR	selective catalytic reduction
VGT	variable turbo geometry
WHO	World Health Organization

Bibliography

[1] COMMISSION DIRECTIVE 2010/26/EU of 31 March 2010 amending Directive 97/68/EC of the European Parliament and of the Council on the approximation of the laws of the Member States relating to measures against the emission of gaseous and particulate pollutants from internal combustion engines to be installed in non-road mobile machinery.

[2] COMMISSION DIRECTIVE 2012/46/EU of 6 December 2012 amending Directive 97/68/EC of the European Parliament and of the Council on the approximation of the laws of the Member States relating to measures against the emission of gaseous and particulate pollutants from internal combustion engines to be installed in non-road mobile machinery.

[3] Delphi Technologies. Worldwide emissions standards. On and off-highway commercial vehicles, 2018/2019.

[4] DIRECTIVE 2004/ 26/EC OF THE EUROPEAN PARLIAMENT AND OF THE COUNCIL of 21 April 2004 amending Directive 97/68/EC on the approximation of the laws of the Member States relating to measures against the emission of gaseous and particulate pollutants from internal combustion engines to be installed in non-road mobile machinery.

[5] European Environment Agency. European Union Emission Inventory Report 1990–2016; Publications Office of the European Union: Luxembourg, 2018., European Environment Agency. Greenhouse Gas Emissions from Transport in Europe; European Environment Agency: Copenhagen 2019.

[6] LIJEWSKI, P. Studium emisji związków toksycznych spalin z silników o zastosowaniach pozadrogowych. Rozprawa ha-

bilitacyjna. *Wydawnictwo Politechniki Poznańskiej*. Poznań 2013.
[7] LIJEWSKI, P., MERKISZ, J., FUĆ, P. et al. Air pollution by the exhaust emissions from construction machinery under actual operating conditions. *Applied Mechanics and Materials*. 2013, **390**, 313-319. https://doi.org/10.4028/www.scientific.net/AMM.390.313
[8] KAMIŃSKA, M., RYMANIAK, Ł., DASZKIEWICZ, P. et al. Test guidelines for evaluation real driving emission two-way vehicles. *MATEC Web of Conferences*. 2019, **294**, 02009-1–02009-8. https://doi.org/10.1051/matecconf/ 201929402009
[9] KHAN, T., FREY, H.C. Comparison of real-world and certification emission rates for light duty gasoline vehicles. *Science of the Total Environment*. 2018, **622**, 790-800. https://doi.org/10.1016/j.scitotenv.2017.10.286
[10] Manufacturer's technical data – agricultural tractors produced in 2018-2020.
[11] O'DRISCOLL, R., STETTLER, M.E.J., MOLDEN, N. et al. Real world CO_2 and NO_x emissions from 149 Euro 5 and 6 diesel, gasoline and hybrid passenger cars. *Science of the Total Environment*. 2018, **621**, 282-290. https://doi.org/10.1016/j.scitotenv.2017.11.271
[12] Our World in Data Website. Available online https://ourworldindata.org (accessed on 05.2021).
[13] PATHAK, S.K., SOOD, V., SINGH, Y. et al. Real world vehicle emissions: Their correlation with driving parameters. *Transportation Research Part D: Transport and Environment*. 2016, **44**, 157-176. https://doi.org/10.1016/j.trd.2016.02.001
[14] RYMANIAK, Ł., DASZKIEWICZ, P., MERKISZ, J. et al. Method of determining the locomotive engine specific fuel consumption based on its operating conditions. *AIP Conference Proceedings*. 2019, **2078**(1), 020053-1–020053-8. https://doi.org/10.1063/1.5092056
[15] RYMANIAK, Ł., LIJEWSKI, P., KAMIŃSKA, M. et al. The role of real power output from farm tractor engines in determining their environmental performance in actual operating conditions. *Computers and Electronics in Agriculture*. 2020, **173**, 105405-1–105405-7. https://doi.org/10.1016/j.compag.2020.105405
[16] SCHROEDER, F., BREUER, B., PREISS, H., WEIDHAAS, G. Motorcycle noise and exhaust emissions-statutory testing methods versus real traffic situations. presented at the small engine technology. *SAE Technical Paper* 1999-01-3255. 1999. https://doi.org/10.4271/1999-01-3255
[17] SIEDLECKI, M., SZYMLET, N., LIJEWSKI, P. et al. Emissions from NRMM vehicles in real operating conditions in relation to the number of vehicles in use in the Poznan city agglomeration. *SAE Technical Paper* 2020. 2020-01-2218. https://doi.org/10.4271/2020-01-2218
[18] THOMAS, D., LI, H., WANG, X. et al. A comparison of tailpipe gaseous emissions for RDE and WLTC using SI passenger cars. *SAE Technical Paper* 2017-01-2391. https://doi.org/10.4271/2017-01-2391
[19] TSAI, J.-H., CHIANG, H.-L., HSU, Y.-C. et al. Development of a local real world driving cycle for motorcycles for emission factor measurements. *Atmospheric Environment*. 2005, **39**, 6631-6641. https://doi.org/10.1016/j.atmosenv.2005.07.040
[20] World Health Organization Website. Available online: http://www.who.com (accessed on 05.2021).

Michalina Kamińska, MEng. – Faculty of Civil and Transport Engineering, Poznan University of Technology.
e-mail: *michalina.kaminska@put.poznan.pl*

Maciej Andrzejewski, DEng. – Łukasiewicz Research Network – Rail Vehicle Institute "TABOR", Poland.
e-mail: *maciej_andrzejewski@op.pl*

Paweł Daszkiewicz, DEng. – Łukasiewicz Research Network – Rail Vehicle Institute "TABOR", Poland.
e-mail: *pawel.daszkiewicz@tabor.lukasiewicz.gov.pl*

Article citation info:
BRZEŻAŃSKI, M., MARECZEK, M., NOGA, M. The concept of a maintenance-free drive-thru inspection station for commercial vehicles. *Combustion engines*. 2022, **188**(1), 35-41. https://doi.org/10.19206/CE-141180

Marek BRZEŻAŃSKI
Michał MARECZEK
Marcin NOGA

Combustion Engines
Polish Scientific Society of Combustion Engines

The concept of a maintenance-free drive-thru inspection station for commercial vehicles

ARTICLE INFO

Received: 17 July 2021
Revised: 28 July 202
Accepted: 10 August 2021
Available online: 15 September 2021

The article presents the concept of a maintenance-free inspection station intended for conducting drive-thru tests of commercial vehicles. The main purpose of building this type of diagnostic line is to carry out non-invasive, preliminary tests of heavy-duty vehicles entering the vehicle service area in terms of parameters affecting the safety of their operation in relation to the applicable standards. The main parameter to be assessed will be the concentration of toxic exhaust components, measured using remote sensing methods. In addition, the proposed diagnostic line can be supplemented with additional remote measurement systems, such as, for example, systems for assessing the condition of vehicle lighting, loads on individual axles and individual wheels of the vehicle, tire pressure, thermal load of the brake system, as well as a system for detecting leaks of fluids from the vehicle. Based on the carried out work, it has been shown that using the current specialist knowledge and the components of measurement systems available on the market, it is possible to develop an innovative diagnostic line using remote measurement methods.

Key words: *exhaust emissions, screening tests, vehicle inspection, remote sensing*

1. Introduction

At the present stage of the development of the road transport means, all kinds of activities relating to their impact on the environment play an extremely important role [3]. In this area, a number of legal regulations have been established regarding the conditions of admitting vehicles to roads and a number of control regulations that determine the day-to-day operation of vehicles [4, 10]. However, due to the very diversified car fleet and very different conditions of vehicle operation, the existing control regulations do not always effectively and quickly identify vehicles that are operated with faults that endanger their safe operation or exceed the established emission limits.

In June 2019, in Cracow, as the first city in Poland, emissions from the streams of passing vehicles were tested using optical methods. Initial estimates showed that approx. 3% of vehicles are responsible for approx. 40% of traffic pollution [11]. These vehicles often did not meet the requirements in force during periodic technical inspections. For this reason, it is important to further develop and disseminate methods enabling effective detection of sources of air pollution as well as systems enabling the construction of databases and statistics in still not fully recognized area.

Therefore, it is advisable to develop a concept of a maintenance-free inspection station intended for non-invasive, initial screening of vehicles involved in the road. The main idea of creating this type of diagnostic tool is to perform screening tests addressed to domestic and foreign shippers operating in the European Union. The results of this type of research will be particularly important in terms of meeting the EU requirements, both for domestic forwarding companies and for vehicles from outside the EU, which are subject to other types of regulations in this area.

The effect of the project may be the protection of the EU area in terms of adverse effects of road transport, which is inconsistent with the applicable standards.

Ultimately, the operational experience of the diagnostic line can be used in the development of standard control procedures used in real road traffic, e.g. for the so-called motorway gates, entrances to urban agglomerations, etc.

The legal and logistic concept of developing this type of diagnostic station will require a separate analysis.

2. Assumptions for the proposed concept

The concept proposed by the research team from the Department of Automotive Vehicles at the Cracow University of Technology is based on the use of spectrophotometric and thermovision techniques as well as computer image analysis to identify exhaust gas composition and the opacity. It is based on the optical detection of the exhaust cloud near the vehicle and the spectral analysis of the light in the infrared and UV range to register individual compounds in the cloud. According to the assumptions, the measurements are to be non-contact, remote and immediate.

The diagnostic line based on the concept proposed by the team from the Cracow University of Technology, may become one of the first installations operating for in the long term conditions on Polish roads, having a beneficial effect on the protection of the natural environment against automotive pollution. An innovative approach in the proposed concept is the use of computer image analysis, which will allow to determine with high accuracy the location of the source of the emitted exhaust gases, i.e. around the end of the tail pipe outlet. A targeting of the measuring beam at the exhaust gas cloud with the lowest possible dilution by air, will allow to obtain the most reliable results.

A further goal of building this type of diagnostic line is to conduct preliminary, non-invasive screening tests of commercial vehicles in terms of all parameters affecting the safety of their operation in relation to the applicable standards. The assumed diagnostic procedure will take place

during one run along the designated measuring track with appropriately selected characteristics.

The main parameter to be assessed will be the concentration of toxic exhaust gas components measured by remote sensing. This parameter is of key importance for the assessment of the technical condition of the vehicle's powertrain, mainly the fuel system, as well as the technical condition of the exhaust gas aftertreatment system. In addition, the proposed diagnostic line can be supplemented with additional remote measurement systems, such as:

- vehicle lighting condition assessment system,
- system for detecting leaks of operating fluids from the vehicle,
- system for assessing the load of axles and individual wheels of the vehicle,
- tire pressure estimation system,
- system for estimation the thermal load of the brake system components.

Those types of tests are aimed at making an initial, comprehensive assessment of the technical condition of selected vehicle components and identifying the most important faults that affect operational safety. According to the assumptions, the entire diagnostic procedure should take place during one run along a designated measuring track with appropriately selected characteristics. The result of the tests will be forwarded to the vehicle driver by a message displayed at the end of the diagnostic line.

The proposed approach differs from that used in road emission tests, e.g. in the USA, in that it applies to selected vehicles whose drivers volunteer for screening, not all vehicles passing the road section under test. This reduces the number of vehicles tested, but on the other hand allows a much more complete assessment of the technical condition of commercial vehicles, which has a significant impact on road safety and overall automotive emissions.

3. The concept of remote measurement of the concentration of exhaust gas components

The role of screening control for automotive exhaust gases is to detect irregularities in the level of harmful components emitted by the vehicle. Exceeding the permissible values may indicate a failure of the engine, fuel system or exhaust gas aftertreatment system. It is not intended to precisely determine the composition of exhaust gases, nor to diagnose the cause of a failure. The result of such inspection is to be a suggestion that the vehicle should be directed to a service or for further tests to a vehicle inspection station.

The main features of the screening control of exhaust are its non-invasive nature and the least possible involvement of third parties, including the driver. Measurements must be automated. The only requirement is that the vehicle must run in such a way that it is possible to take a sample of the exhaust gases. The most beneficial place to sample exhaust gases is at the outlet of the vehicle's tailpipe. However, the need to locate it and place the measuring probe in it, additionally while the vehicle is in motion, excludes the possibility of direct measurement. The outlet of the tailpipe is often placed under the vehicle at some distance from the vehicle's contour. Therefore, it was assumed that the measurement would be made in the vicinity of the exhaust gas outlet, taking into account the dilution of the exhaust gas with ambient air. However, it still does not completely eliminate the problem of locating the exhaust gas outlet. For this purpose, it is necessary to use the technique of computer image analysis.

When analyzing the available measurement methods, it was necessary to choose the most appropriate one for remote tests, in which reliability and maintenance-free are also an important factor. Table 1 summarizes the basic measurement methods with their main features.

Table 1. Methods of measuring the concentration of the components of exhaust gases [5]

Method	Advantages	Disadvantages
Optical spectroscopy	– direct and fast, – selective with good sensitivity, – minimal measurement drift, – no effect on other gases	– the need to define carefully selected areas of the radiation spectrum
Gas chromatography	– very accurate and selective	– continuous measurement difficult to implement, – gas sample delivering needed, – very expensive
Semiconductor sensors	– low cost, – possible exposure measurements, – very sensitive (ppm)	– poisoning effect possible, – is subject to irreversible wear, – measurement susceptible to the influence of other gases, – sensitive to moisture
Catalytic (pellistor)	– low cost, – detects the presence of flammable gases	– possible poisoning effect, – sensitive to gas groups, – errors under the influence of other flammable gases, – zero error (ppm)

Among the methods used in industry, there are also thermally conductive sensors (TDC), electrochemical sensors and sensors based on the phenomenon of surface acoustic wave (SAW). Optical measurement methods themselves, usually based on emission or absorption spectroscopy, constitute a numerous group of solutions [7]. The above-mentioned methods of remote measurement of the concentration of carbon monoxide, hydrocarbons, nitrogen oxides and smoke in exhaust gases were initially analyzed in laboratory conditions in the Department of Automotive Vehicles at the Cracow University of Technology.

Measurement methods are marked with international symbols:

- NDIR (Non-Dispersive Infrared Spectroscopy),
- FTIR (Fourier Transform Infrared Spectroscopy),
- TDLS (Tunable Diode Laser Spectroscopy),
- CRDS (Cavity Ring-Down absorption Spectroscopy),
- DOAS (Differential Optical Absorption Spectroscopy),
- DIAL (Differential Absorption Lidar),
- PAS (Photoacoustic Spectroscopy),
- MUPASS (Multipass Spectroscopy), etc.

Optical gas concentration measurement (NDIR) is widely used in the automotive industry, but not only [9]. The popular solutions used so far, however, did not allow for the study of the exhaust cloud from vehicles traveling on the road. In recent years, due to the interest in the problems

of urban traffic pollution, solutions are developed and implemented that enable monitoring of the air condition [1]. There are portable systems recording passing vehicles together with an estimated assessment of the composition of the exhaust gases emitted by them.

4. Verification of the proposed concept of remote measurement of the concentration of exhaust gas components in real conditions

In order to pre-verify the proposed concept of a remote-sensing diagnostic line appropriate measurements were made to quantify the assumptions for selected exhaust components. Measurements of CO_2 and O_2 concentrations were made for two exemplary vehicles – a Mercedes Actros 1842 truck and a Mercedes Tourismo coach (Fig. 1). The tested Mercedes Actros truck had a mileage of approximately 500,000 km, while the Mercedes Tourismo coach was a brand new vehicle. Both were technically sound. The aim of the measurements was to determine the area around the outlet of the exhaust system within which it is possible to measure the concentration of toxic exhaust components with a diagnostic analyzer.

Fig. 1. Test vehicles – Mercedes Actros 1842 truck (top) and Mercedes Tourismo coach (bottom)

The Capelec Cap 3201 analyzer used for the measurements consisted of two modules: a five-gas exhaust gas analyzer and an opacimeter (Fig. 2).

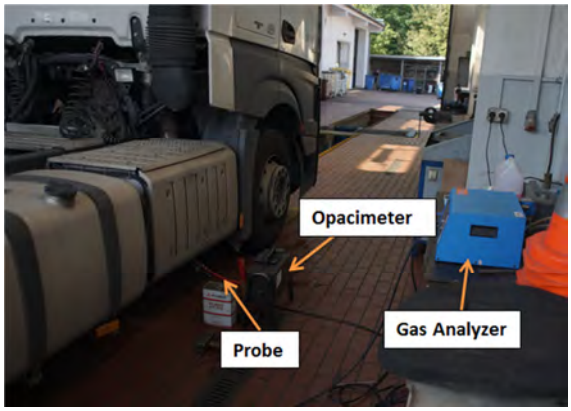

Fig. 2. A general view of the stand for measuring the composition and opacity of exhaust gases

The measurements were carried out for both vehicles while the engine was idling. The limit line was considered to be the achievement of 0.2% of CO_2 concentration, which is the lower measurement threshold of the popular analyzers, however lower values are achievable [2]. In the case of a truck, the outlet of the exhaust pipe is located on the right side of the vehicle (Fig. 3). In the case of the coach, the exhaust gases come out from the bottom of the vehicle, in the left rear part of the body (Fig. 4). The Mercedes Actros truck is equipped with a diffuser-shaped exhaust pipe with a flattened shape and several nozzles. This results in the dispersion of the exhaust gas stream and a significant dilution of the sample with the ambient air.

Fig. 3. View of the outlet of the exhaust system – Mercedes Actros truck

Fig. 4. View of the outlet of the exhaust system – Mercedes Tourismo coach

Figures 5 and 6 show the schemes for measuring the volumetric concentration of carbon dioxide CO_2 and oxygen O_2 in the exhaust gas for both tested vehicles at differ-

ent distances from the outlet of the exhaust system. For screening tests, the area beyond the outline of the vehicle to which exhaust gases are emitted is important.

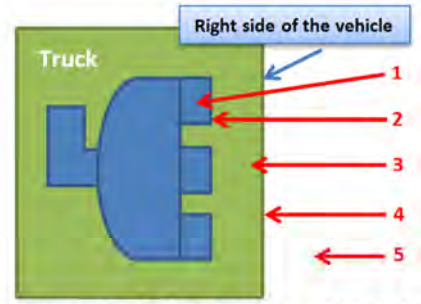

Concentration (vol.) at the point:	% CO_2	% O_2
1. Inside the exhaust system	1.8	17.3
2. Edge of the outlet of muffler	0.7	19.3
3. 10 cm from the outlet edge	0.5	19.7
4. At the vehicle's lateral contour	0.4	19.9
5. 35 cm from the outlet edge	0.2	20.2

Fig. 5. Distribution of CO_2 and O_2 concentration as a function of distance from the exhaust outlet of the Mercedes Actros truck

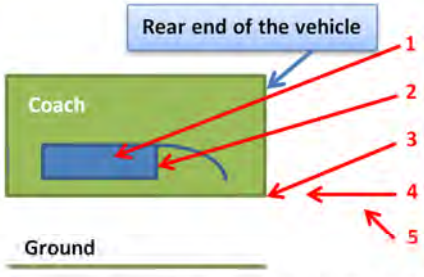

Concentration (vol.) at the point:	% CO_2	% O_2
1. Inside the exhaust system	2.3	16.4
2. Edge of the outlet of muffler	2.3	16.3
3. At the vehicle's rear contour	0.4	19.9
4. 10 cm from the vehicle's contour	0.3	20.0
5. 50 cm from the vehicle's contour	0.2	20.3

Fig. 6. Distribution of CO_2 and O_2 concentration as a function of distance from the exhaust outlet of the Mercedes Tourismo coach

The concentration of carbon dioxide CO_2 is in this case taken as a reference value allowing the identification of the exhaust gas cloud. It is important to locate the area where the concentration of carbon dioxide CO_2 is higher than 0.2%. In the case of a vehicle with an efficient exhaust aftertreatment system, the remaining exhaust components, such as carbon monoxide CO, nitrogen oxides NO_x, HC hydrocarbons and NH_3 ammonia, may remain at the analyzer measurement threshold, which is acceptable in the case of screening tests. The measurements show that in the area up to approx. 30–50 cm from the contour of the vehicle, at the height of the exhaust pipe, it is possible to measure the exhaust gas with sufficient accuracy, using an analyzer for diagnostic tests.

In order to evaluate the performed measurement, it is necessary to find the correlation between the concentration of CO_2 and O_2 and the toxic components of the engine exhaust as a function of the engine load and the place of sampling. Measurement of the opacity of the exhaust gases, taken with a standard opacimeter, did not show any measurable values, however it is planned to implement exhaust opacity testing in the final version of the system. That will require additional exploratory research. The value of the exhaust gas temperature at the end of the exhaust pipe as indicated by the analyzer was 50–60°C. In the case of the NDIR measurement method used in the diagnostic exhaust gas analyzer, the time needed to stabilize the measurement is about 30 seconds.

5. Measurement techniques in the proposed concept of remote measurements

During the preliminary tests the NDIR detector was used to determine the CO_2 concentration in the exhaust gas cloud. It is important as it is a method based on spectrophotometric measurement. However, the NDIR analyzer, the general scheme of which is shown in Fig. 7, imposes certain limitations in a typical design, preventing remote measurement.

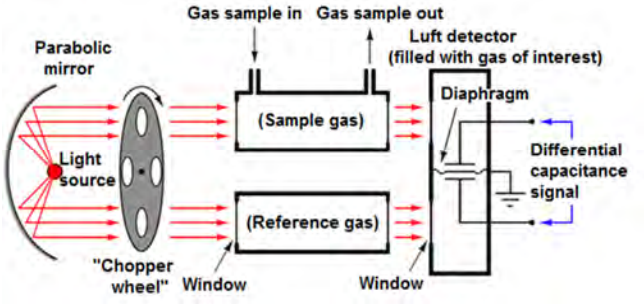

Fig. 7. NDIR gas analyzer working principle – prepared basing on [12]

The principle of operation uses the effect of the absorption of a narrow band of electromagnetic radiation by the tested chemical compound. The proportion of the amount of light passing through the measuring tube with the tested gas and the reference tube in which the light passes through the reference gas is proportional to the concentration of the tested gas in the reference gas. In the case of bench tests, the reference gas is air taken from the environment. In order to carry out such a measurement, a sample of the tested gas mixture should be delivered to the measuring tube. The radiation energy passing through the measuring tube and the reference tube heats the measuring chamber unevenly. The pressure difference in the measuring chamber is read as the concentration of a given compound. The need to deliver the tested gas to the measuring tube is related to the location of the probe in the flue gas stream. It would be a complex problem in the field of automation and mechanics when the test vehicle is driven through the test stand. The second limitation is the mere fact of the time it takes the sample to get to the measuring tube and properly heat the measuring chamber. Assuming that the vehicle is in motion during the measurements, which is necessary to cause the engine load, this seems to be an additional argument in the search for other solutions.

The proposed concept assumes the identification of the exhaust gas cloud and the determination of its composition based on the analysis of the image recorded in the infrared and ultraviolet UV spectrum. This method will consist in

comparing the selective spectra of the band in the range of 2–11 μm and the UV radiation generated by the radiator and passing through the exhaust gas cloud in the immediate vicinity of the tested vehicle [6]. Figure 8 shows a general diagram of the measuring system.

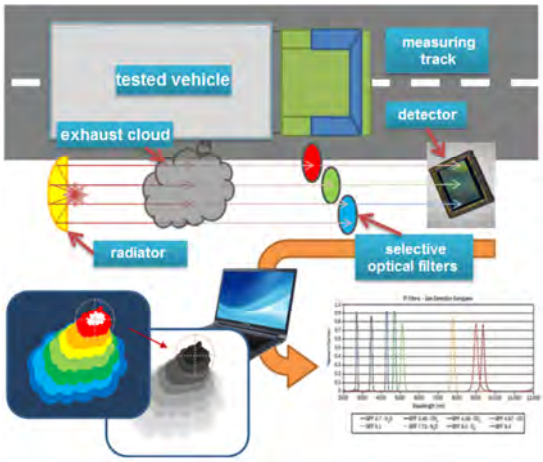

Fig. 8. General diagram of the stand for spectral measurements of exhaust gas composition

It is assumed that the vehicle traverses the measurement path with a forced engine load. A specially profiled track is set for the vehicle to travel. The image of the vehicle surroundings is to be recorded in real time during the test and analyzed at the same time. This approach differs from usually used in inspection station conditions, but the forced engine load gives a much better opportunity to reveal possible malfunctions. The result of the measurements from a given sample will be displayed on the monitor screen after the completion of the test track.

The principle of the measurement is based on comparing the spectrum of radiation incident directly on the detector and the spectrum after passing through the exhaust gas cloud. The gas contained in the exhaust cloud absorbs a certain part of the spectrum, strictly defined for a given chemical compound. The amount of radiation that reaches the detector after passing through the narrowband optical filter is proportional to the energy absorbed by the gas, and therefore to its concentration. Figure 9 shows a spectral diagram of the absorption of individual exhaust gas compounds from internal combustion engines.

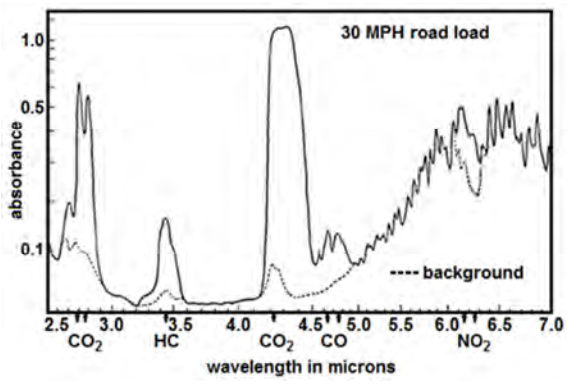

Fig. 9. Absorption spectrum for exhaust gases of motor vehicles – prepared basing on [8]

The areas of the spectrum where individual components of the exhaust gas have a high absorption capacity are clearly marked. Figure 10 shows the image recorded by a thermal imaging camera, additionally equipped with an optical filter with a band corresponding to carbon dioxide CO_2.

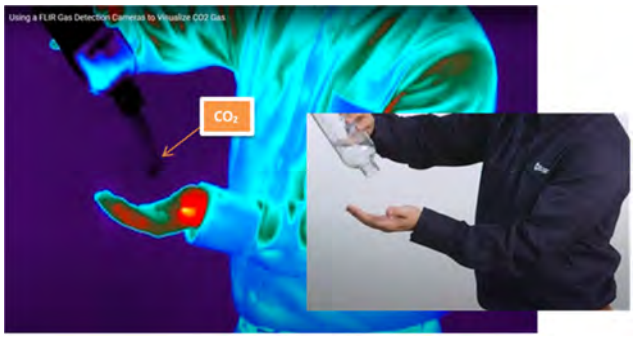

Fig. 10. Image from a thermal imaging camera and a standard camera showing the outflow of carbon dioxide CO_2 from a bottle [13]

Contemporary thermal imaging techniques operate in a wide range of infrared radiation. Combining high sensitivity and resolution, they enable the creation of accurate images in real time, which allows for even better analysis, especially in the case of dynamic changes in the engine load.

6. The concept of an integrated data analysis system from subsequent stages of vehicle diagnostics

The project of an innovative diagnostic line using remote measurement methods for diagnostic screening tests of commercial vehicles entering the area of vehicle service stations assumes the creation of a uniform system for the acquisition and processing of measurement data. It is planned to develop this type of system in the LabView programming environment, consisting of acquisition and computing modules.

The first stage of processing data from all measurement modules will be their synchronization as a function of the measurement time and their collection with division into individual measurement blocks. Then, they will be used to select the data that is important from the point of view of interaction with data from other measuring blocks and requires processing according to the developed algorithms.

Calculated data from all measurement modules will be subject to verification on the basis of established ranges of values assumed as correct or exceeding the adopted range. The final data, resulting from the examination along the entire diagnostic track, will be archived in memory modules and stored at the time determined by the owner of the facility. The remaining intermediate data collected during the research procedure will be deleted from the computer system.

It is planned to develop a general calculation algorithm using measurement and calculation data, the final effect of which will be to provide information on the technical condition of the analyzed vehicle components. Limit values of the tested vehicle parameters will be established, the exceeding of which requires further analysis in a specialist

vehicle service station. The values of the measured and calculated operational parameters of the vehicle being tested on the designed diagnostic track will be subject to basic verification based on the criteria related to the regulations authorizing the vehicle to travel on the roads of the European Union. Additional criteria for the evaluation of the test results will be criteria related to the vehicle manufacturer's standards.

The diagnostic system under development has as a priority the identification of vehicle faults or ailments in screening tests, which are important from the point of view of the vehicle operation and the applicable regulations in the field of admitting the vehicle to traffic on public roads. It is assumed that test result information will be displayed on the monitor at the end of the diagnostic track. It is also possible to make a printout of the course of the study. As the proposed system will have a diagnostic potential that goes beyond the above-mentioned criteria, an additional effect of this type of research will also be the identification of other deficiencies that affect the durability and reliability of the vehicle's operation. This additional information will encourage vehicle users to use this type of diagnostic line.

7. Conclusions

The article presents the concept of assessing the concentration of selected exhaust gas components measured remotely using remote sensing methods. This parameter is of key importance for assessing the technical condition of the vehicle's powertrain, mainly the fuel system, as well as the technical condition of the exhaust gas aftertreatment system. In addition, the proposed diagnostic system has further development potential and can be supplemented with additional remote measurement systems for many other vehicle parameters responsible for its proper operation and road safety.

The analysis of the existing solutions shows that so far no similar system of automated vehicle screening tests has been implemented. The target assumption of the developed concept is the creation of an automatic diagnostic line that would enable screening of possible irregularities in commercial vehicles to the extent similar to periodic mandatory technical inspections carried out at vehicle inspection stations. For this reason, vehicle test stations may, to some extent, be a reference for the developed concept of vehicle diagnostic screening lines. The main differences between the developed concept of the diagnostic line and the test procedure carried out in vehicle inspection stations are that this innovative concept assumes a completely automatic vehicle testing procedure, which enables a quick diagnosis of the technical condition to be carried out at any time. The report generated for the user of the vehicle after the test will contain information whether any irregularities that require repair or adjustment have been discovered within individual areas of control. On this basis, the vehicle user will decide on the further treatment of the vehicle and may have it inspected and repaired at a vehicle service station. For this reason, the proposed concept of a diagnostic line for vehicle screening is characterized by a very high level of innovation. The implementation of such solutions will certainly have a significant impact on increasing the level of road safety and reducing the environmental nuisance of commercial vehicles.

The presented concept showed that, based on the current specialist knowledge and the components of measurement systems available on the market, it is possible to develop an innovative diagnostic line using remote measurement methods intended for diagnostic screening tests of vehicles participating in road traffic. It is estimated that at the time of preparing the article, the proposed system had reached the technology readiness level 3. It means that the adopted solutions have proved successful, but a lot of efforts still need to be made to develop a ready-made system.

The measurable effect of launching this type of diagnostic line may have a significant impact on increasing the safety of vehicle operation, reducing the environmental burden and controlling the applicable standards.

Nomenclature

CRDS	cavity ring-down absorption spectroscopy
DIAL	differential absorption lidar
DOAS	differential optical absorption spectroscopy
FTIR	Fourier Transform Infrared Spectroscopy
MUPASS	multipass spectroscopy
NDIR	non-dispersive infrared spectroscopy
PAS	photoacoustic spectroscopy
SAW	surface acoustic wave
TDC	thermally conductive sensors
TDLS	tunable diode laser spectroscopy

Bibliography

[1] HAWE, E., DOOLY, G., FITZPATRICK, C. et al. Measuring of exhaust gas emissions using absorption spectroscopy. *International Journal of Intelligent Systems Technologies and Applications*. 2008, **3**(1-2), 33-51. https://doi.org/10.1504/IJISTA.2007.014125

[2] HUMMELGÅRD, CH., BRYNTSE, I., BRYZGALOV, M. et al. Low-cost NDIR based sensor platform for sub-ppm gas detection. *Urban Climate*. 2015, **14**(3), 342-350. https://doi.org/10.1016/j.uclim.2014.09.001

[3] KOSZAŁKA, G., SZCZOTKA, A., SUCHECKI, A. Comparison of fuel consumption and exhaust emissions in WLTP and NEDC procedures. *Combustion Engines*. 2019, **179**(4), 186-191. https://doi.org/10.19206/CE-2019-431

[4] MERKISZ, J., RYMANIAK, Ł. Determining the environmental indicators for vehicles of different categories in relation to CO_2 emission based on road tests. *Combustion Engines*. 2017, **170**(3), 66-72. https://doi.org/10.19206/CE-2017-310

[5] MIKOŁAJCZYK, J., BIELECKI, Z., STACEWICZ, T. et al. Detection of gaseous compounds with different techniques. *Metrology and Measurement Systems*. 2016, **23**(2), 205-224. https://doi.org/10.1515/mms-2016-0026

[6] TRAN, D., NEHMETALLAH, G., GORIUS, N. et al. Low-cost, compact and robust gas abundance sensor package. *Proceedings of SPIE*. 2018, **10641**, https://doi.org/10.1117/12.2304639

[7] OMAR, M.F. et al. FTIR spectroscopy characterization of Si-C bonding in SiC thin film prepared at room temperature by conventional 13.56 MHz RF PECVD. *Malaysian Journal of Fundamental and Applied Sciences*. 2012, **8**(5), 242-244. http://dx.doi.org/10.11113/mjfas.v8n4.156

[8] TWISS, S.B., TEAGUE, D.M., BOZEK, J.W. et al. Application of infrared spectroscopy to exhaust gas analysis. *Journal of the Air Pollution Control Association*. 1955, **5**(2), 75-83. https://doi.org/10.1080/00966665.1955.10467692

[9] WEN, D-M., CHEN, M-X., ZHAO, L. et al. Use of thermal imaging and Fourier transform infrared spectroscopy for the pre-symptomatic detection of cucumber downy mildew. *European Journal of Plant Pathology*. 2019, **155**, 405-416. https://doi.org/10.1007/s10658-019-01775-2

[10] ZIÓŁKOWSKI, A., FUĆ, P., LIJEWSKI, P. et al. Analysis of RDE emission measurements in rural conditions from heavy-duty vehicle. *Combustion Engines*. 2020, **182**(3), 54-58. https://doi.org/10.19206/CE-2020-309

[11] Innowacyjne badania spalin w Krakowie, https://www.krakow.pl/zalacznik/350036 (accessed on 2021.07.07)

[12] Luft detector Principle. https://instrumentationtools.com/luft-detector-principle/ (accessed on 2021.07.06)

[13] Using a FLIR Gas Detection Cameras to Visualize CO_2 Gas. https://www.youtube.com/watch?v=O1fJ3UuSFaU (accessed on 2021.07.06)

Prof. Marek Brzeżański, DSc., DEng. – Faculty of Mechanical Engineering, Cracow University of Technology.
e-mail: *marek.brzezanski@pk.edu.pl*

Michał Mareczek, DEng. – Faculty of Mechanical Engineering, Cracow University of Technology.
e-mail: *michal.mareczek@mech.pk.edu.pl*

Marcin Noga, DSc., DEng. – Faculty of Mechanical Engineering, Cracow University of Technology.
e-mail: *marcin.noga@pk.edu.pl*

Article citation info:
KALOCIŃSKI, T. Modern trends in development of alternative powertrain systems for non-road machinery. *Combustion Engines*. 2022, **188**(1), 42-54. https://doi.org/10.19206/CE-141358

Tomasz KALOCIŃSKI

Combustion Engines
Polish Scientific Society of Combustion Engines

Modern trends in development of alternative powertrain systems for non-road machinery

ARTICLE INFO

Received: 29 July 2021
Revised: 11 August 2021
Accepted: 18 August 2021
Available online: 16 September 2021

The main goal of the paper is to review available alternative powertrain technologies for non-road machinery. Based on that, to propose adequate classification and recognise main trends within this area. The paper presents various powertrain propositions alternative to internal combustion engine and solely mechanical powertrain developed by manufacturers over a course of years. The article explains actual legislative situation regarding environmental challenges connected to the powertrain solutions and reiterates the need for development in that area. Both commercially available and only presented at fairs or at early development stages solutions have been analysed. Depending on the load conditions and work patterns multiple benefits as well as challenges to the reviewed concepts have been discussed. Certain classification of existing powertrain solutions have been proposed taking into account its design and functionality.

Key words: *powertrain technology, alternative drive, hybrid, agricultural, construction*

1. Introduction

Increasingly stringent environmental protection laws and reduction of fossil fuels dependency are the main objectives of modern economies. Development of new powertrain systems faces two major challenges. First is to increase working parameters of the powertrain with simultaneous reduction of fuel consumption and the second to stay compliant with current environmental protection laws. Very often these two conditions are contradictory to each other and are difficult to fulfill [1–4].

Continuous decrease of CO_2 emissions thus reduction of fuel consumption are the main drivers for search of new powertrain solutions. Some countries have introduced specific limits and presented specific laws focused on reduction CO_2 emission. The European Union also have introduced first CO_2 limit standards for example for passenger cars in 2009. In 2015 this limit was set at 130 g/km, and in 2020 at 95 g/km as an average emission calculated for new car fleet [5, 6].

For non-road machinery new Stage V emissions standards have been phased in already in 2018 in European Union. These regulations limit emission of CO, HC, NO_x, PM and PN [7, 8].

Multiple technologies have been put in place over last years to already meet previous limits, especially on NO_x and PM. Namely, high pressure common rail injection, cooled exhaust gas recirculation, diesel oxidation catalyst, selective catalytic reduction and exhaust particulate filter [9, 10].

Use of electric, electrified or hybrid drives can also significantly increase efficiency of powertrains and therefore reduce emissions. Moreover, introduction of mentioned solutions may expand vehicle flexibility and create new functionalities. Together with fast development of machine automatization, precision farming and use of satellite positioning system for farming operation continuously increase interest in alternative drives. Mainly due to ease control of speed and torque and due to system simplification in comparison to mechanical or hydraulic solutions [11, 12].

Starting at mid 1950s manufacturers have already tried alternative powertrain solutions, for instance: IH Farmall 450 with additional electric generator for power output or Allis-Chalmers with fuel cell powered tractor (Fig. 1). Later in 1970s, Terex presented Titan mining dump truck with diesel-electric powertrain. Mentioned examples of alternative solutions have not created significant demand and have been abandoned for next decades [13].

No.	Year	Manufacturer	Model	Alternative drive type	Energy store
1	1954	IH Farmall 450	IH ElectrAll	Electrified components	NO
2	1959	Allis-Chalmers	Fuel cell	FCEV	NO
3	1974	Terex	Titan	Diesel-electric	NO
4	1998	Eltrac/Schmetz GmbH	E135	Diesel-electric	NO
5	2005	IH Case	ProHybrid EECVT	HEV	YES
6	2007	John Deere	7430/7530 E premium	Electrified components	NO
7	2008	Caterpillar	D7E	Diesel-electric	NO
8	2009	Belarus	3023	Diesel-electric	NO
9	2010	Agco	ElectRoGator 1386	Diesel-electric	NO
10	2011	New Holland	NH2	FCEV	YES
11	2011	John Deere	6210 RE	Electrified components	NO
12	2011	Rigitrac	EWD 120	Diesel-electric	NO
13	2012	Komatsu	HB205-1	HEV	YES
14	2013	John Deere	644K	Diesel-electric	NO
15	2013	Merlo	40.7 Hybrid	PHEV	YES
16	2013	Fendt	X Concept	Electrified components	NO
17	2014	Belaz	75710	Diesel-electric	NO
18	2015	Multi Tool Track	N/A	REX	YES
19	2016	Claas	Arion 650 hybrid	HEV/electrified auxiliaries	YES
20	2016	John Deere	SESAM	BEV	YES
21	2016	Kramer	5055e	BEV	YES
22	2016	ZF	Terra +	Electrified components	NO
23	2017	Fendt	e100	BEV	YES
24	2017	Farmtrac	26E	BEV	YES
25	2018	John Deere	GridCON	Electric drive	NO
26	2019	Steyr	Konzept	PHEV	NO
27	2019	Rigitrac	SKE 50	BEV	YES
28	2019	John Deere	1RE	BEV	YES
29	2019	John Deere	Joker	BEV	YES
30	2019	John Deere	8370 eAutoPowr	Electrified components	NO
31	2020	Case	580 EV	BEV	YES
32	2020	JCB	525-60E	BEV	YES
33	2021	John Deere	E-power backhoe	BEV	YES

Fig. 1. List of selected alternative powertrain solutions for non-road machinery

New approach to the alternative powertrain solutions appeared again in early 2000s. In 1998 Schmetz GmbH created test diesel-electric powertrain based on New Holland tractor. Later, with initiative of Universities in Munich

and Regensburg, together with AGCO, Wiedemann and Fraunhofer-Geselschaft, project MELA (Mobile Electrische Leistungs- und Antriebstechnik) have started with goal to create high efficiency electric components for diesel-electric powertrains [14].

Similarly, project TEAM (Entwicklung von Technologien fur energiesparende Antriebe mobiler Arbeitmaschinen) created with RWTH University in Aachen and Universities in Karlsruhe and Dresden together with many manufacturers, e.g. AGCO, Claas, Deutz, Wirtgen, CAT, Liebherr, Rexroth and others resulted in works on high speed electric motors and electric components for non-road machinery drives [14].

Since mid 2000s more companies experimented with different types of alternative powertrains, either prototype ones like Belarus with its diesel-electric model 3023, Case with hybrid-electric ProHybrid EECVT or large-scale production like John Deere 7430/7630 E Premium with electrified auxiliaries [13–16].

From 2010s onwards increasingly higher interest in alternative powertrains have been seen. More large companies like John Deere, New Holland or AGGO would create prototypes and large-scale production machines. However, also smaller companies like Rigitrack, Merlo or Farmtrack have started creating its own solutions [12, 13, 17].

Examples of the alternative powertrains selected by author can be seen in Fig. 1. List of selected alternative powertrain solutions for non-road machinery.Fig. 1. List of selected alternative powertrain solutions for non-road machinery

The year of presentation, manufacturer and model as well as type of powertrain have been indicated to present the variety of solutions developed by the manufacturers.

2. Alternative powertrain solutions

Alternative powertrain solutions can vary and encompass different concepts from electrified auxiliary power outputs, diesel-electric and diesel-hydraulic solutions through many hybrid layouts to the battery-electric, fuel cell-electric and many other variations.

Classification and unified definitions of this solutions its needed to understand the differences between them as well as their advantages and challenges for the practical use of them. More in-depth systematization of alternative powertrain solutions for non-road machinery will be presented in this chapter. Proposed classification is author's approach to the subject.

To determine different definitions for alternative powertrain solutions, first definition of the opposite: the conventional drive needs to be clarified. For the non-road machinery traditionally, the conventional powertrain would consist of internal combustion engine and mechanical or hydro-mechanical transmission.

Proposition for non-road machinery classification can be seen on Fig. 2.

2.1. In-series drive

In series drive is the powertrain architecture where prime mover and drive components are connected to each other in a way that one propels the next one and transfers the torque to the driving wheels. For non-road machinery prime mover would typically be diesel internal combustion engine (ICE).

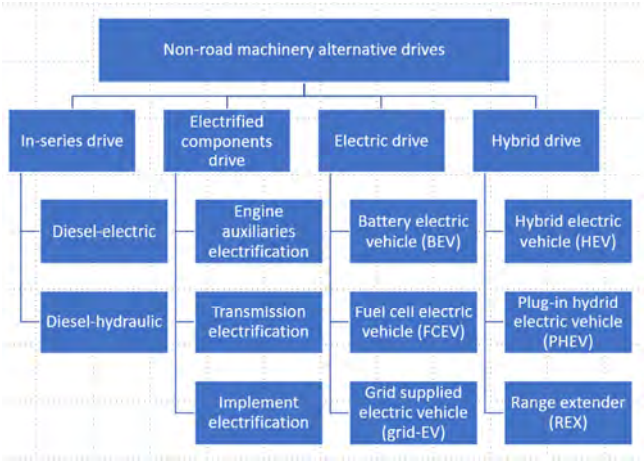

Fig. 2. Non-road machinery alternative drive classification

Fist type of the in-series drive is the diesel-electric drive. In this solution diesel drives the electric generator and sends the electric power straight to the electric motor and further to the transmission or final drive. Alternatively, electric energy can be sent to multiple electric motors mounted on driving axles or even directly on driving wheels. This solution is well known and used within marine, rail and other industries.

The second type of in-series drive used in non-road machinery is the diesel-hydraulic drive. In this solution prime mover supplies torque to the hydraulic pump or pumps and sends the hydraulic power to the hydraulic motors. Similarly, to the previous solution hydraulic motor can drive the gearbox, axles or directly driving wheels. Powertrain of this type is also well known and widely used for instance in agricultural sprayers, telehandlers, harvesting machines and others.

Main advantage of both those solutions is that transmission or gearbox of any type in not required. However, quite often the transmission is used anyway to increase the powertrain possibilities.

It is worth to mention this solution cannot be considered as a hybrid drive. Mainly because it lacks an energy store of any form or source of power other than mainly diesel in this case. In other words, the vehicle cannot be operated if the prime mover is stopped, unlike to a hybrid drives [4].

2.2. Electrified components drive

This alternative powertrain type is sometimes considered to be the first step to the machine hybridization, namely micro-hybridization. Main idea behind the solution is to integrate electric generator within certain areas of the existing, mainly classical powertrain, e.g. on a flywheel. Generated electrical energy can be used to supply components within the machine itself or be sent to the attached implements.

First type of this solution deals with engine auxiliaries electrification. Some systems components within the internal combustion engine (ICE) can be successfully driven by electric motors instead of mechanical or hydraulic drives. This increases ease of control and expands the possibility

for new functionalities, e.g. radiator fan reverse for cleaning purposes.

Next type is the transmission electrification. Main objective of this solution is to increase the efficiency and sensitivity of hydraulic or mechanic-hydraulic transmission. Higher efficiency of electric generator and motor successfully increases total efficiency of the transmission in comparison to the use of hydraulic pump and hydraulic motor [3].

The third solution is the implement electrification. Similarly, to the previous two drives, mechanical or hydraulic transmission of energy to the implement can be change for the electric energy. In order to achieve that generator needs to be placed somewhere on a driveline and be able to supply external receivers connected to the machine. Typically, that would be fly wheel or side generator.

In practice, those three solutions can be incorporated within one machine and use common generator to satisfy those three types of needs.

2.3. Electric drive

Purely electric drive cab be another solution for the non-road machinery. In this case power transferred to the driving wheels comes from electric motor and goes either through some sort of transmission or final drive or goes directly to the driving hubs. Electric drive gives wide possibilities for torque and speed control as well as ease of operation.

Electric energy supplied to the electric motor or motors can come from different sources which usually limits the machine range or operational time.

Machine supplying energy to the electric motor from the battery or rechargeable energy storage system (RESS) would be called battery electric vehicle (BEV). Within this powertrain machine uses the energy from the battery which needs to be recharged when minimal state of charge (SOC) is achieved. Therefore, size of the battery simply limits the operational time of the machine.

Other solution offers energy to the electric motor from different source of electricity, namely: fuel cell. Thus: fuel cell electric vehicle (FCEV). This option is based on the idea that electricity is supplied to the electric prime mover through chemical process. Hydrogen stored on a vehicle connects with the oxygen from the ambient air creating: electricity, heat and water. That kind of electric powertrain can be supplied with battery and plug-in option, however not necessarily [1, 2].

The third mentioned type of alternative non-road machinery powertrain supplies electric motor of the machine directly from the electric grid next to the working area. Within presented classification indicated as grid-EV. For machines working mainly stationary or within relatively small radius that solution seems to be rational. For more mobile machinery, e.g. agricultural tractor this solution might be a more of a challenge.

2.4. Hybrid drive

The definition of hybrid drive is a coexistence of primary and secondary drive within a vehicle. Most of the hybrid vehicle solutions consists of internal combustion engine (ICE) as a primary source of drive and electric motor with battery as a secondary drive. Many variants and configurations of the hybrid drives are possible, nevertheless two sources of drive to propel the vehicle is the definition of a hybrid drive [1, 2].

Variety of hybrid drives creates a need for systematization. Different criteria can be taken into account to do so, e.g. architecture or functional.

In terms of architecture hybrid drives can be divided as seen on Fig. 3:

1. Series hybrid drive: drive is supplied by electric motor using energy delivered by internal combustion engine to the battery,
2. Parallel hybrid drive: drive is supplied by internal combustion engine or/and electric motor,
3. Series-parallel hybrid drive: usage of advantages of both, series and parallel drive in order to transmit power and torque.

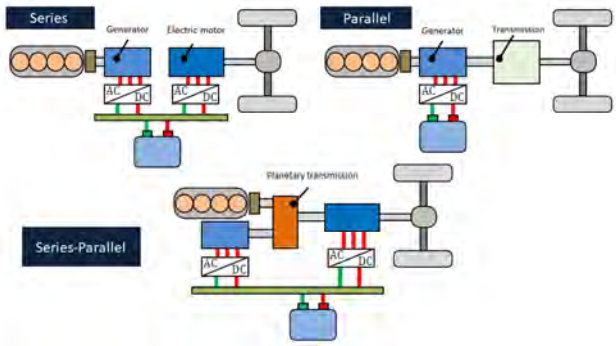

Fig. 3. Hybrid drive architectures [1]

In terms of functional features hybrid drives can be divided into:

1. Micro hybrid drive: the simplest hybrid drive, enables only start and stop of the internal combustion engine when operational parameters are suitable for that, uses only modified engine starting systems,
2. Mild hybrid drive: equipped with electric machine able to support internal combustion engine and recover energy from braking events,
3. Full hybrid drive: drive with full usage of internal combustion engine and electric machine as a motor and generator, simultaneous or separate work of both sources of drive is possible.

Important factor used to describe degree of hybridization of a powertrain is called the hybridization factor (HF) and is defined as a power of electric drives within the powertrain over sum of electric and internal combustion engine drive. According to the description above for micro-hybrid: $0 < HF < 0.1$, mild hybrid: $0.1 < HF < 0.25$, full hybrid: $0.25 < HF < 0.5$, PHEV: $0.5 < HF < 0.7$. The $HF = = 1$ refers to pure electric vehicle and $HF = 0$ to conventional non-hybrid powertrain.

One of the most common types of hybrid is hybrid electric vehicle (HEV). This solution is usually referred as internal combustion engine and electric motor with battery designed within one of the architectures mentioned earlier.

Another common solution is plug-in hybrid electric vehicle (PHEV) which is a extension of the HEV by adding possibility of charging a battery from external source (grid).

Specific solution of hybrid drive is range extender (REX). Idea of this drive is a small internal combustion

engine with electric generator charging batteries only when needed, otherwise internal combustion engine does not operate. Separate electric motor supplies drive to the wheels [1, 2, 4].

3. Alternative powertrain – selected examples

This paper does not encompass all types of alternative and especially hybrid drives available but just the ones encountered during the study of existing non-road machinery drives and selected as the most significant. Other types of alternative powertrain solutions as hydraulic hybrid vehicle (HHV) or photo-voltaic hybrid vehicle (PVEV) have not been recognized as significant examples in this study [18].

Description of existing examples of powertrain solution within classification in Fig. 2 will be carried out within this chapter.

3.1. In-series drive

Terex in 1974 presented Titan, a 320 tons dump truck. Equipped with 16-cylinder, approx. 2200 kW internal combustion engine and 10-pole AC generator supplying through rectifier DC voltage to the four electric traction motors [19].

Fig. 4. Eltrac E 135 [20]

In 1998, Eltrac E135, first modern agricultural tractor with diesel-electric drive was built by Schmetz GmbH (shown in Fig. 4). Based on New Holland M135 with 6-cylinder, turbocharged Iveco diesel with power of 100 kW and torque of 612 Nm. As shown in Fig. 5, air cooler electric generator supplied power to the electric motor which drive tractor gearbox [20].

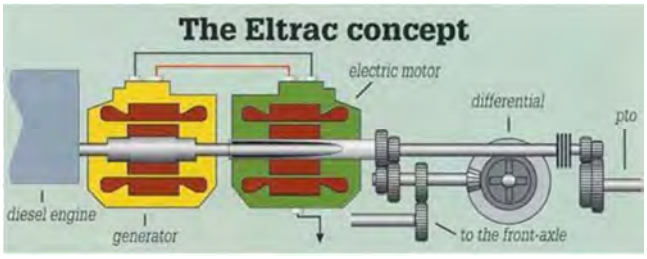

Fig. 5. Eltrac E 135 powertrain diagram [48]

Caterpillar, presented in Fig. 6. have also used diesel-electric drive in 2008 for their D7E bulldozer. Internal combustion engine of 175 kW drives an AC generator sending electric power to two traction motors [21]. Caterpillar claims fuel consumption reduction in this model in compare to its conventional predecessor D7R2 from 10% up to 30% [21].

The emissions of D7E in comparison to the conventional D7R2 appeared to range from 28% lower to 2% higher when it comes to CO_2 and from 7% to 21% higher in terms of NO_x [22].

In 2009 Belarus designed prototype of model 3023 as in Fig. 7. Diesel-electric with 220 kW diesel engine and 172 kW generator supplying power to transmission, electric engine fan drive, front PTO and 380 V power output sockets. Belarus claims 15% to 20% reduction in fuel consumption in comparison to its classical counterpart [23]. Plough field tests showed specific fuel consumption of 10.8 kg/h for the diesel-electric powertrain and 13.2 kg/ha for its conventional version. As result 18% of fuel consumption reduction has been proved [24].

Fig. 6. Caterpillar D7E dozer [21]

Fig. 7. Belarus 3023 with electro-mechanical powertrain [23]

AGCO presented in 2010 self-propelled sprayer ElectRoGator 1386 with 229 kW CAT diesel engine supplying 650 V DC from the 200 kW, water-cooled generator with 1500 rpm. Alternatively, 240 kW with 1900 rpm. Electric motors with 84 kW of power and 700 Nm of torque mounted on each of four wheels (Fig. 8). Lifetime of the electric motors was estimated for 50,000 h which is longer than a lifetime of the traditional sprayer [13, 15].

AGCO claims that electric version o the sprayer featured 36% higher torque, 6% more power. On the prototype of the machine braking energy was dissipated into heat. Development works are conducted to recover this energy as well [23]. In comparison to conventional hydrostatic version, this electrified powertrain reduced fuel consumption in field tests from 20% in a summer up to 30% in autumn [13].

Fig. 8. AGCO ElectRoGator 1386 [23]

Swiss manufacturer Rigitrack together with Technische Universitat Dresden developed diesel-electric tractor EWD 120 (Fig. 9) equipped with 91 kW Deutz engine and 85 kW, 650 V DC liquid-cooled generator came to the public in 2011. Permanent magnet synchronous motors of 33 kW each mounted directly on wheels allowed to control torque transmission on each of axles as shown in Fig. 10. Additional electric output socket was available [17, 23].

Fig. 9. Rigitrac EWD 120 [23]

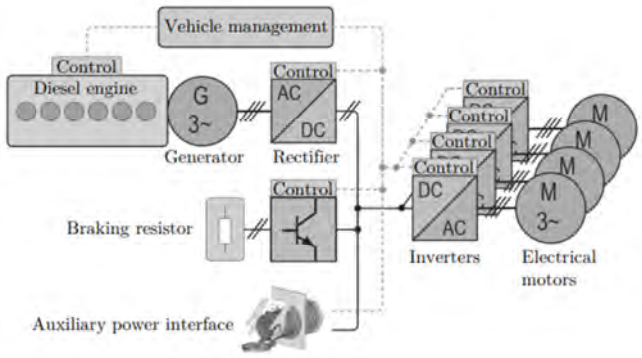

Fig. 10. Rigitrac EWD 120 powertrain architecture [52]

John Deere have introduced in 2013 loader 644K (Fig. 11) with their John Deere 6.8 dm^3, 6-cylinders diesel engine of 167 kW, 985 Nm driving two brushless, oil-cooled AC generators. Electric power is further supplied through solid state, inverters to the four also brushless, oil-cooled AC motors, one for each wheel. Six inverters, one for each of the electric machines are based on insulated gate bipolar transistor (IGBT) technology.

Fig. 11. John Deeer 644K Hybrid loader [27]

Powertrain does not feature energy store, but it is equipped in two water-cooled brake resistors to dissipate brake energy to be used for boom or bucket functions reducing load on the internal combustion engine and reducing fuel consumption (Fig. 12). Larger version of this machine is also available with similar powertrain architecture, model 944K [26]. John Deere claims 25% of fuel consumption reduction in comparison to the conventional powertrain of this machine [23, 27].

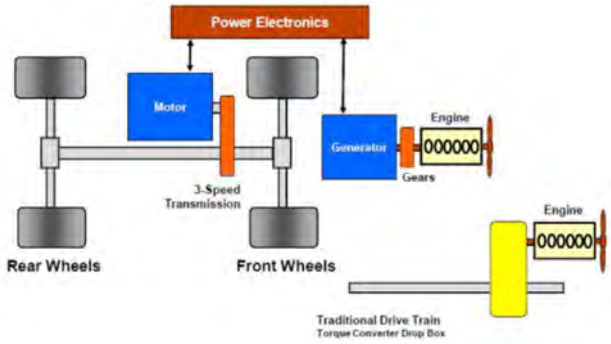

Fig. 12. John Deere 644K loader powertrain diagram, hybrid and traditional [27]

In 2014 Belaz showed their 75710 (Fig. 13) diesel-electric dump truck. This also was the largest dump truck produced with 450 tons of payload prepared to work in difficult conditions and temperatures ranging from –50°C to +50°C. Belaz put two 1704 kW alternators and connected them to four traction motors, 1200 kW each. Alternators driven by two diesel MTU DD 16V4000 engines with rated power of 1715 kW.

Fig. 13. Belaz 75710 [25]

3.2. Electrified components drive

In 1954 IH Farmall presented model IH ElectrAll as in Fig. 14. Regular agriculture tractor based on conventional powertrain architecture but with generator attached in parallel to the internal combustion engine ready to supply external receivers. Generator was a 3-phase, 120/208 V, 10 kW electric machine [14].

Fig. 14. IH Farmall 450 ElectrAll [14]

John Deere introduced in 2007 models 7430 E Premium and 7530 E Premium with standard 121 kW and 132 kW engines respectively. Tractors with conventional architecture featured additional 3-phase, 480 V, 20 kW electric generator mounted on an engine's fly wheel. Part of the electric power from the generator was consumed by electrically driven engine auxiliaries: radiator fan and A/C compressor. This allowed precise control of duty time and speed of these devices. Additionally, electric energy is available on external sockets in a form of 1-phase 230 V, and 3-phase, 400 V (Fig. 15). This power can be used to supply external devices up to 5 kW when tractor is standing still. Mentioned solution resulted in a 5% reduction in a fuel consumption in comparison to the conventional version of those machines [13, 15, 28].

Field tests of electrified and conventional version of 7530 tractor in harrowing and towing a trailer were conducted. Results yielded 4% of fuel consumption reduction in harrowing and 16% in towing a trailer on the road [29].

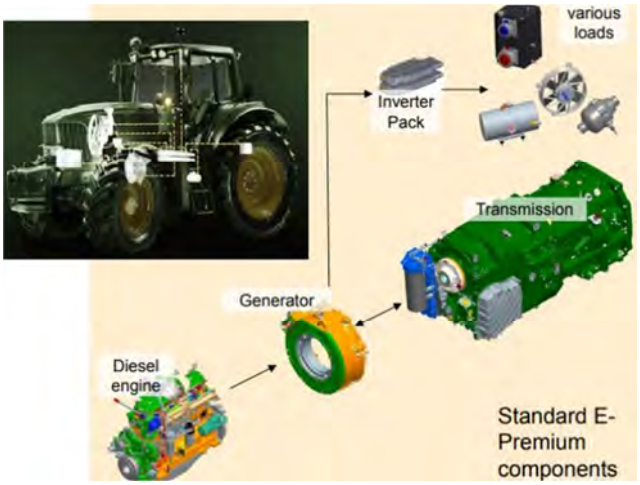

Fig. 15. John Deere 7530 E Premium components [30, 33]

Again, John Deere repeated similar solution and expanded its capabilities in 2011with model 6210 RE. This time architecture was similar to the solutions from 2007 however now 20 kW of electric power was available for driving external machines also when tractor was moving (Fig. 16). Available electric power parameters were 480 V DC and 3-phase, of 750 V AC with max. current of 200 A [13, 15, 30, 31].

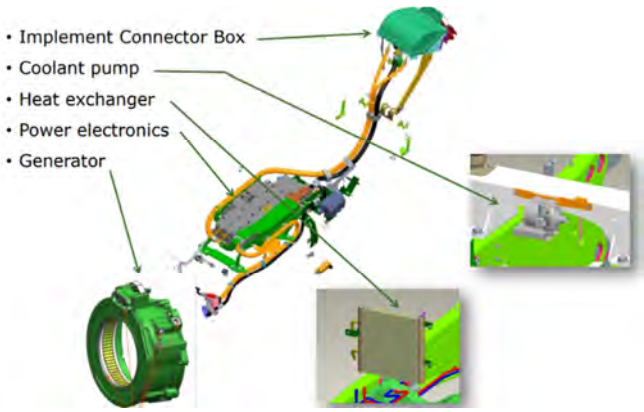

Fig. 16. John Deere 6210 RE powertrain components [30]

Similar solution was presented by Fendt in 2013 with model X Concept (Fig. 17) based on conventional Fendt 722 Vario with 147 kW diesel engine. Fendt has integrated AC generator o 130 kW, 700 V DC on the engine output supplying power to the engine auxiliaries: radiator fan and coolant pump and to the external sockets available to power implements [15, 23].

Fig. 17. Fendt X Concept powertrain components [15]

Other example of similar ready to use technology is a solution prepared by ZF with TERRA + product line ranging from 3-phase, 400 V electric motor hubs through 80 kW generators ready to be integrated between engine and a gearbox of existing machines to full size transmissions with 50 kW and 70 kW generators build in (Fig. 18). Generator is ready to supply energy to implements. Additionally, with deployment of energy store this can create hybrid system with recovery braking capabilities as presented in Fig. 19. The ZF also offers PTO driven generator to be fitted to the existing machine with capacity of supplying energy to two 25 kW electric motors [23, 32].

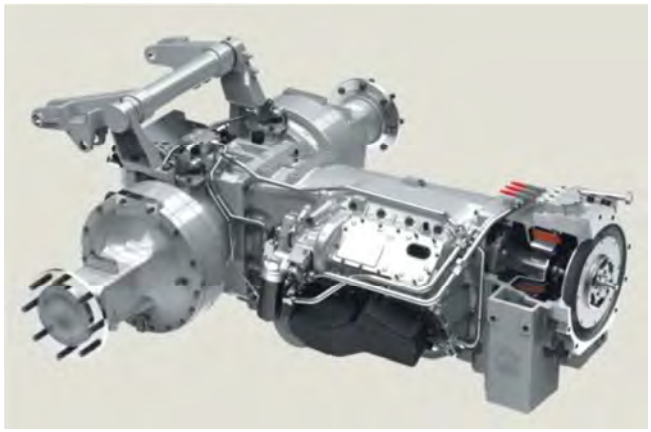

Fig. 18. ZF TERRA+ starter generator with transaxle [23]

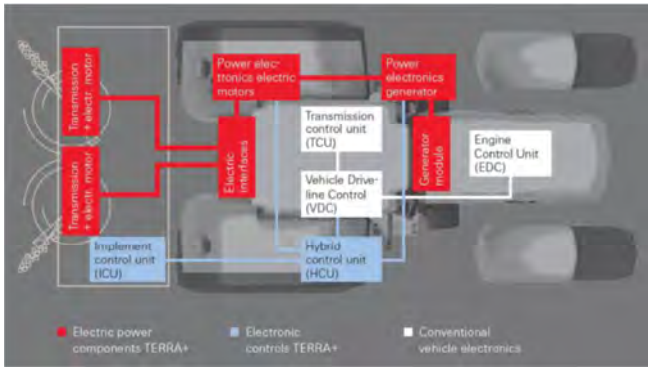

Fig. 19. ZF TERRA+ possible architecture [23]

In 2019 again John Deere presented new solution in their 8370 R eAutoPowr as in Fig. 20. Based on regular tractor architecture with 275 kW, 6-cylinder engine and continuously variable transmission (CVT). However, in this electrified solution hydraulic pump and motor have been changed for electric machines increasing significantly transmission efficiency. Additionally, AC brushless generator capable of supplying 100 kW power to the external implements through sockets on a back of the machine in a form of 700 V DC or 3-phase, 480 V AC. Originally the project was developed together with trailer manufacturer Joskin to support their 100 kW electric motor mounted to the trailer axle [34, 35].

Taking into account that CVT not always supports machine with transmission efficiencies similar to the gear transmission this electrified option seems promising [23].

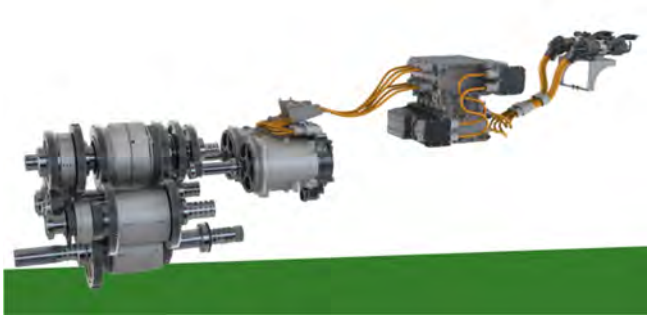

Fig. 20. John Deere eAutoPowr transmission [34]

3.3. Electric drive

In 1954 Alli-Chalmers presented first fuel cell powered electric tractor (Fig. 21). It featured 1008 cells arranged in 112 units of 9 cells each within 4 banks generating 15 kW of electric energy transferred to the electric drive motor.

Fig. 21. Allis-Chalmers AC D-12 fuel cell tractor [14, 23]

First practical use of fuel cell electric vehicle (FCEV) in terms of tractor was presented by New Holland in 2011 (Fig. 22). Tractor named NH_2 was based on conventional T6.140 model and featured fuel cell module of 100 kW with efficiency of 96% and 2 electric motors, one for PTO drive, other for tractor drive. Each motor performed 100 kW of power and 950 Nm of torque. Quantity of 8.2 kg of hydrogen was stored under 350 bars of pressure. This

powertrain solution featured a Li-Ion battery working with 300 V and size of 12 kWh with peak power output of 50 kW [13, 17, 23].

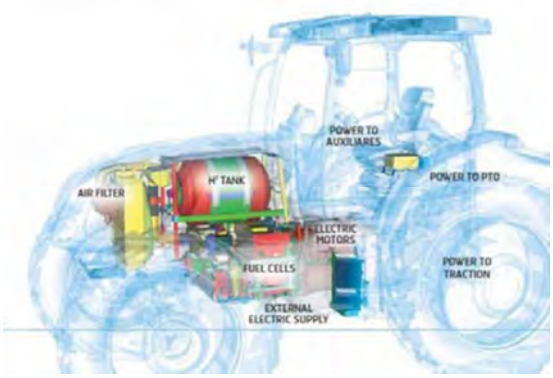

Fig. 22. New Holland NH2 hydrogen-powered tractor [23]

Proposition of prototype battery electric vehicle (BEV) was developed in 2016 by John Deere with a model called SESAM (Sustainable Energy Supply for Agricultural Machinery). Tractor was based on Mannheim's 6R frame and was equipped in 130 kWh, 670 V, Li-Ion battery and 2 electric motors 150 kW each (Fig. 23). One of the motors drives Direct Drive transmission and the second drives PTO. Tractor has capacity of work continuously for approx. 4 h or travel distance of 55 km. Charging of the battery takes about 3 h. Battery is designed for 3100 charging cycles [12, 36].

Fig. 23. Battery pack of John Deere SESAM [36]

Fig. 24. Kramer 5055e loader [17]

In 2016 Kramer presented their first fully electric loader 5055e (BEV). It consists of 2 electric motors, one for the machine drive 15 kW and second for hydraulic drives 22 kW (Fig. 24). Battery works on 80 V and has capacity of 416 Ah. Operational time on one charging depends on load and range between 5 h and 8.5 h [17, 37].

Next fully electric tractor shown by Fendt in 2017, model e100 Vario featured power output of 50 kW with Li-Ion battery of 100 kWh and voltage of 650 V (Fig. 25). Operational time was estimated at 5h under moderate load [12, 38].

Fig. 25. Fendt e100 Vario [38]

Also, in 2017 Indian manufacturer Escorts launched its BEV tractor Farmtrac 26E prepared mainly for vineyards and horticulture presented in Fig. 26. In this solution electric motor of 19 kW drives standard transmission with 21 kWh, Li-Ion battery. This supports 6 h of working time [12].

Fig. 26. Escorts Farmtrac 26E [12]

Very interesting solution for the electric vehicle (EV) have been proposed by John Deere in 2018. Autonomous tractor without the cab called GridCON with constant connection to the electric grid from the site of the field. Tractor is equipped with special spool with 1 km of supply cable mounted in a front of the machine as shown in Fig. 27. Mentioned cable supplies two electric motors, one 100 kW for tractor drive and second 200 kW for power output to the implement. Mass of the tractor is 8.5 t which is an equivalent to the John Deere model 6195R. Max. speed of the machine is 20 km/h. Electric power supply need to be 2.5

kV however tractor power bus is 700 V DC. John Deere claims that running costs of this powertrain solution are reduced by half in comparison to the BEV [39, 40].

Fig. 27. John Deere GridCON [39]

Fig. 28. Rigitrac SKE50 [41]

In 2019 Swiss manufacturer Rigitrac proposed new solution for the fully electric tractor BEV, model SKE 50 (Fig. 28). In this powertrain solution one Li-Ion, 400 V, 80 kWh battery supplies 4 electric motors, one for front axle, second for rear axle, third for front PTO and fourth for rear PTO [12, 41].

John Deere in 2019 shown two fully electric machines, with little information provided. First one, model 1RE, fully electric prototype of small compact tractor with expected operational time of 4.5 h on one charge (Fig. 29).

Fig. 29. John Deere 1 RE [42]

Second one is the John Deere Joker, prototype of fully electric and fully autonomous machine as in Fig. 30. Tractor is featuring no cab and power output of 500 kW. No information about the battery have been provided yet [42].

Fig. 30. John Deere Joker [40]

In 2020 Case and JCB showed their fully electric machines (BEV) for construction industry presented in Fig. 31. For Case that is "Project Zeus" 580 EV backhoe loader powered with 480 V, 90 kW Li-Ion battery pack supplying separately drive and hydraulic components. Single charge will support 8 h of operational time [43].

Fig. 31. Case 580 EV „Project Zeus" [43]

The JCB introduced whole fleet of construction battery electric vehicles. To name one: telehandler 525-60e (Fig. 32). With Li-Ion battery of 24 kWh and 3 charging options: 110 V, 230 V, 415 V. One charge supports entire day of operational time [44].

Fig. 32. JCB 525-60e telehandler [44]

John Deere in January 2021 also presented fully electric backhoe loader called E-power backhoe developed together with National Grid – an electricity and natural gas provider.

The machine it is to perform on the same level as its conventional counterpart, model 310L [45].

In 2021, additionally to described developments, John Deere have already conducted field tests on autonomous machines working in swarm as in Fig. 33. In this particular example John Deere GridCON has supplied power to the single John Deere Joker machine. However, the idea is to supply energy to several machines [46, 47].

Fig. 33. John Deere GridCON and John Deere Joker [47]

3.4. Hybrid drive

First practical full hybrid electric (HEV) powertrain solution for non-road machinery was presented in 2005 Case ProHybrid EECVT (Fig. 34). Tractor based on conventional Case MXM with 120 kW, 800 Nm engine and two electric machines, 50 kW each. One electric machine working as a generator supplies energy to the second one working as a motor. Surplus of energy can be stored in 11.5 kWh, 456 V DC battery. Additionally, energy from braking can be recovered and sent to the battery. In this powertrain solution tractor can work in full electric mode or in a hybrid mode with diesel engine and electric motors together through CVT [14, 48].

Fig. 34. Case ProHybrid EECVT [14]

In 2012, Komatsu introduced full hybrid (HEV) model HB205-1. Because of hybrid architecture diesel engine can be downsized form 6-cylinder to 4-cylinder. Electric generator/motor is placed at the engine output and supplies power to the capacitor as shown in Fig. 35. Electric swing motor/generator moves the upper structure of the machines and recovers energy from when the structure slows down sending it to capacitor. Energy from capacitor can be used to support the diesel engine by the means of motor/ generator placed on the engine output. Komatsu claims fuel consumption reduction between 25–41% [13, 23].

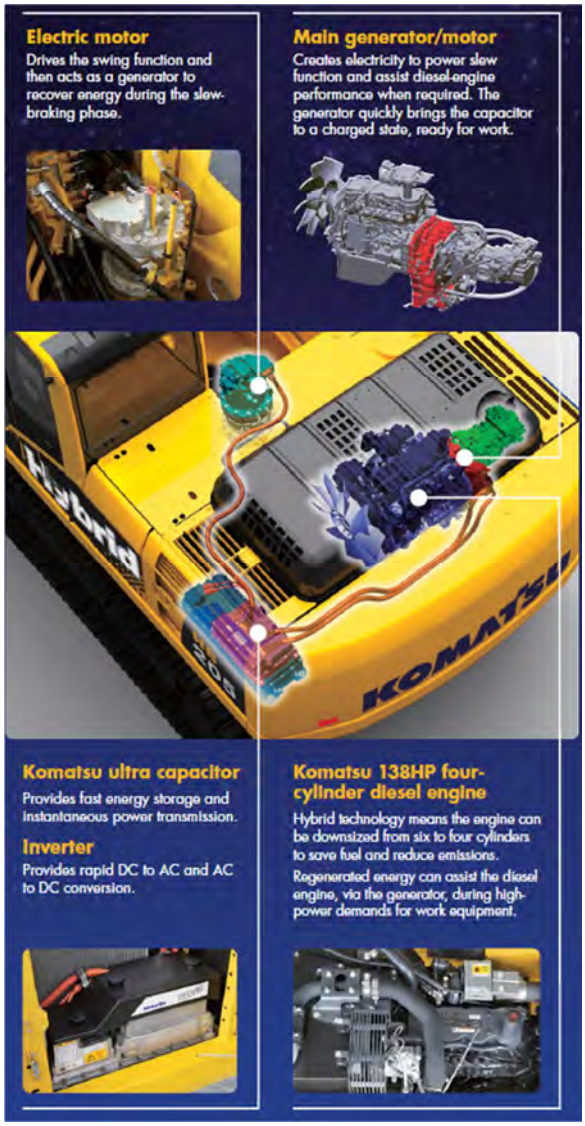

Fig. 35. Komatsu HB205-1 powertrain components [49]

Merlo presented in 2013 their 40.7 plug-in hybrid electric vehicle (PHEV). In fully electric mode the energy is supplied from 30 kWh, Li-Ion battery (Fig. 36). In hybrid mode internal combustion engine working at a constant speed supplies energy to the machine drive and charges the battery. In this architecture diesel output can be reduced in a half without the reduction in machine performance. In case of low-load work or idling, machine can work solely electric and reduce fuel consumption and CO_2 emission up to 30% Merlo claims. Machine can be also charged from the grid as a plug-in hybrid [17, 48].

Fig. 36. Merlo 40.7 hybrid telehandler [48]

Different type of hybrid vehicle (REX) used by Multi Tool trac company from Netherlands as in Fig. 37. This powertrain uses 6-cylinder, 160 kW diesel engine driving 140 kW generator supplying energy to the Li-Ion, 30 kWh battery. This supports 0.5 h of continuous work. Electric energy is supplied from the battery to 4 electric motors at wheels [16].

Fig. 37. Muli Tool Trac [16]

Claas have shown in 2016 full hybrid machine (HEV) based on model Arion 650. The Claas Arion 650 Hybrid. The prime mover in powertrain was a 129 kW, 6.8 dm^3 diesel engine driving 90 kW permanent magnet synchronous generator. The generator was located between engine and EQ200CVT transmission (Fig. 38). Second source of energy in this powertrain was 5.75 kWh, 635 V battery [16, 50].

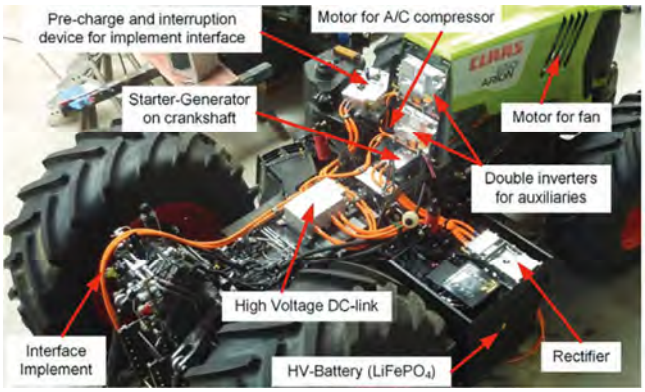

Fig. 38. Class Arion 650 Hybrid powertrain components [16, 50]

In 2019 Steyr presented its Konzept PHEV tractor as shown in Fig. 39. All hydraulics and PTO were electrically driven, external power output socket with 48 V and 700 V available as well. Energy from breaking was recovered and sent to battery. Charging from grid possible. Energy from the battery drives 4 electric motors at wheels [51].

Fig. 39. Steyr Konzept [51]

4. Conclusions

In this paper main known alternative powertrain solutions within non-road machinery area have been presented. Classification for the mentioned examples have been undertaken and described. Together with indication of differences between given solutions. Based on that specific conclusions can be drawn:

1. Alternative powertrain solutions for non-road machinery are getting increasingly more attention, especially electric drives and start to play visible role within market of high tech solutions for this industry segment.
2. Significant rise in development works regarding alternative powertrain solutions started in early 2000s and increased in 2010s.
3. Different structure within development works on alternative powertrain types over course of years is visible with direction moving from experimenting with many solutions to focus on the BEVs.
4. Many alternative powertrain solutions are not limited only to the machine powertrain but also expanded on supplying power to the implement as well.
5. Although pace of development works on alternative powertrains, mainly BEVs seems to be very fast, the limitations to the battery capacity therefore, operational time are still existing.
6. Alternative powertrains for non-road machinery are not making any significant impact on whole industry market now but mentioned pace of development works, also on battery technology puts this kind of solutions into near future perspective.

Nomenclature

AC	alternating current
A/C	air conditioning
BEV	battery electric vehicle
CVT	continuously variable transmission
DC	direct current
EV	electric vehicle
FCEV	fuel cell electric vehicle
HEV	hybrid electric vehicle
HF	hybridization factor
HHV	hybrid hydraulic vehicle
ICE	internal combustion engine
IGBT	insulated gate bipolar transistor
PHEV	plug-in hybrid electric vehicle
PTO	power take-off
PVEV	photovoltaic electric vehicle
RESS	rechargeable energy storage system
REX	range extender
SOC	state of charge

Bibliography

[1] MERKISZ, J., PIELECHA, I. Układy mechaniczne pojazdów hybrydowych. *Wydawnictwo Politechniki Poznańskiej.* Poznań 2015.

[2] MERKISZ, J., PIELECHA, I. Układy elektryczne pojazdów hybrydowych. *Wydawnictwo Politechniki Poznańskiej.* Poznań 2015.

[3] RENIUS, K.T. Fundamentals of tractor design. *Springer.* 2020.

[4] Automotive Handbook. *Robert Bosch GmbH.* 2014.

[5] RYMANIAK, Ł., LIJEWSKI, P., KAMIŃSKA, M. et al. The role of real power output from farm tractor engines in determining their environmental performance in actual operating conditions. *Computers and Electronics in Agriculture,* 2020, **173**, 105405. https://doi.org/10.1016/j.compag.2020.105405

[6] Regulation (EC) No 443/2009 of the European Parliament and of the Council of 23 April 2009 setting emission performance standards for new passenger cars as part of the Community's integrated approach to reduce CO_2 emissions from light-duty vehicles. http://eur-lex.europa.eu/legal-content/EN/ALL/?uri=celex%3A32009R0443

[7] Regulation (EU) 2016/1628 of the European Parliament and of the Council of 14 September 2016 on requirements relating to gaseous and particulate pollutant emission limits and type-approval for internal combustion engines for non-road mobile machinery, amending Regulations (EU) No 1024/2012 and (EU) No 167/2013, and amending and repealing Directive 97/68/EC. http://eur-lex.europa.eu/legal-content/EN/TXT/PDF/?uri=CELEX:32016R1628&from=LV

[8] European Stage V non-road emission standards. *International Council of Clean transportation*. 2016. http://theicct.org/sites/default/files/publications/EU-Stage-V_policy%20update_ICCT_nov2016.pdf

[9] FEBIG, M., WIARTALLA, A., HOLDERBAUM, B. et al. Particulate emissions from diesel engines: correlation between engine technology and emissions. *Journal of Occupational Medicine and Toxicology.* 2014, **9**(6). https://doi.org/10.1186/1745-6673-9-6

[10] CWIKOWSKI, P., TEODORCZYK, A. The latest achievements in gasoline and diesel injection technology for the internal combustion engines. *Journal of KONES Powertrain and Transport*. 2009, **16**(2), 79-90. http://yadda.icm.edu.pl/yadda/element/bwmeta1.element.baztech-article-BUJ5-0032-0016

[11] DZIUBINSKI, M., DROZD, A., ADAMIEC, M. et al. Energy intensity of the electric vehicle. *Advances in Science and Technology Research Journal.* 2017, **11**(4), 27-34. https://doi.org/10.12913/22998624/78516

[12] MALIK, A., KOHLI, S. Electric tractors: survey of challenges and opportunities in India. *Materials Today: Proceedings*. 2020, **28**, 2318-2324. https://doi.org/10.1016/j.matpr.2020.04.585

[13] MOREDA, G.P., MUNOZ-GARCIA, M.A., BARRIEIRO, P. High voltage electrification of tractor and agricultural machinery – a review. *Energy Conversion and Management*. 2016, **115**, 117-131. https://doi.org/10.1016/j.enconman.2016.02.018

[14] WEYMANN, S. Electric drivelines for tractors and agricultural machinery. Part 1. *Agricultural, Horticultural and Forest Engineering*. 2016, **61**(4), 6-8.

[15] WEYMANN, S. Electric drivelines for tractors and agricultural machinery. Part 2. *Agricultural, Horticultural and Forest Engineering*. 2016, **61**(5), 8-10.

[16] WEYMANN, S. Electric drivelines for tractors and agricultural machinery. Part 3. *Agricultural, Horticultural and Forest Engineering*. 2016, **61**(6), 9-11.

[17] WEYMANN, S. Electric drivelines for tractors and agricultural machinery. Part 4. *Agricultural, Horticultural and Forest Engineering*. 2017, **62**(1), 11-14.

[18] MOUSAZADEH, H., KEYHANI, A., JAVADI, A. et al. Optimal power and energy modeling and range evaluation of a solar assist plug-in hybrid electric tractor (SAPHT). *American Society of Agricultural and Biological Engineers. Transactions of the ASABE.* 2010, **53**(4), 1025-1035. https://doi.org/10.13031/2013.32586

[19] DREW, D. Terex Titan. It was a big one. *Earthmovers Magazine*. http://www.earthmoversmagazine.co.uk/digger-man/view,terex-titan-it-was-the-big-one-blog-post-revisited_252.htm (accessed on 10.06.2021).

[20] BERNHARD, B. Untersuchungen zur Bewegung Stufenloser Fahrantriebe für Mahdrescher. *Universitat Hochenheim.* 2011. http://opus.uni-hohenheim.de/volltexte/2012/648/pdf/Dissertation_Bjoern_Bernhard.pdf

[21] Caterpillar trade press media representatives. Updated Cat D7E features advanced technology to boost productivity. 2014. http://www.cat.com/en_GB/news/machine-press-releases/updated-cat-d7e-featuresadvancedtechnologytoboostproductivityand.html (accessed on 10.06.2021).

[22] JOHNSON, K.C., BURNETTE, A., CAO, T. et al. Hybrid off-road equipment in-use emission evaluation. FY 2010-11 air quality improvement project. Hybrid off-road equipment pilot project. *California Air Resources Board.* 2013.

[23] HOY, R., ROHRER, R., LISKA, A. et al. Agricultural industry advanced vehicle technology: Benchmark study for reduction in petroleum use. *Idaho National Laboratory.* 2014.

[24] PUHOVOY, A.A. Agricultural tractor with pure electromechanical drivetrain. *SAE International Journal of Commercial Vehicles.* 2011, **4**(1), 275-285. https://doi.org/10.4271/2011-01-2296

[25] Belaz. http://belaz.by/en/products/products-belaz/dumpers/dump-trucks-with-electromechanical-transmission/dumpers-series-7571/ (accessed on 10.06.2021).

[26] Construction Equipment. http://www.constructionequipment.com/john-deere-644k-hybrid-wheel-loader (accessed on 10.06.2021).

[27] SOBOTZIK, J. Electrische Antriebstechnik. Eine neue Chance in Mobile Arbeitmaschinen. *VDI Workshop Electrification.* Wieselburg. 2013.

[28] HAHN, K. High voltage electric tractor-implement interface. *SAE International Journal of Commercial Vehicles.* 2009, **1**(1), 383-391. https://doi.org/10.4271/2008-01-2660

[29] PESSINA, D., FACCHINETTI, D. Gemelli diversi. *Macchine Agricole*. 2009, **7**, 44-51. http://www.researchgate.net/publication/303142160_Gemelli_diversi

[30] KRAH, J.O., SOBOTZIK, J., HAMBLOCH, M. Tractor/implement electrification. Opportunities and challenges. *EtherCat in Mobile Applications.* Frankfurt. 2013.

[31] STOSS, K.J, SHI, B., SOBOTZIK, J. et al. Tractor power for implement operation – mechanical, hydraulic, and electrical: An overview. *Agricultural Equipment Technology Conference,* Kansas City. 2013.

[32] BUNING, E.A. Electric drives in agricultural machinery. An approach from the tractor side. *Bologna, EIMA International,* 2015.

[33] MUNCH, P. Sensorik und Elekrifirizierung bei Landmachinen. *John Deere.* 2013.
[34] Eautopowr Eroffnet neue Traktorbe-triebsweisen. http://flurundfurche.de/eautopowr-eroeffnet-neue-traktorbetriebsweisen/ (accessed on 10.06.2021).
[35] Das Gullefass Arbait mit. http://www.deere.de/de/blog/articles/technik/eautopowr-john-deere-elektrisches-getriebe-power-off-boarding/ (accessed on 10.06.2021).
[36] John Deere SESAM-batterie-traktor. http://www.topagrar.com/technik/news/john-deere-sesam-batterie-traktor-9365391.html (accessed on 10.06.2021).
[37] Into the future with new drive. http://www.kramer-online.com/en/product/model/5055e/ (accessed on 10.06.2021).
[38] Fendt e100 Vario. Unser antrieb fur the zukunft. http://www.fendt.com/at/e100-vario (accessed on 10.06.2021).
[39] An der Langen Leine. http://www.faz.net/aktuell/technik-motor/motor/john-deere-forscht-am-elektrischen-traktor-15961820.html (accessed on 10.06.2021).
[40] PICKEL P. Trends in tractor development. *John Deere ETIC*. Wieselburg. 2020
[41] Rigitrac Traktorenbau AG. http://www.rigitrac.ch/produkte-1/rigitrac-ske-40-electric/ (accessed on 10.06.2021).
[42] Future of farming. http://www.deere.co.uk/en/agriculture/future-of-farming/ (accessed on 10.06.2021).
[43] The industry's first fully electric backhoe loader-The Case 580 EV http://www.casece.com/northamerica/en-us/products/backhoe-loaders/580ev-project-zeus (accessed on 10.06.2021).
[44] The new electric JCB 525-60e compact telehandler. http://www.jcb.com/en-gb/products/telescopic-handlers/525-60e-hi-viz (accessed on 10.06.2021).
[45] John Deere joint its first electric powered backhoe with National Grid. http://www.deere.com/en/our-company/news-and-announcements/news-releases/2021/construction/2021jan06-electric-powered-backhoe/ (accessed on 10.06.2021).
[46] The autonomous swarm tractor from John Deere. http://thefurrow.co.uk/the-autonomous-swarm-tractor-from-john-deere/ (accessed on 10.06.2021).
[47] Farmer.pl http://www.farmer.pl/technika-rolnicza/maszyny-rolnicze/ciagnik-na-prad-z-przewodu-john-deere-zadziwia,108905.html (accessed on 10.06.2021).
[48] CABAN, J., ZARAJCZYJ, J., SZMIGIELSKI, M. et al. Hybrid drive as a future in agricultural technology. *Proceedings of the Institute of Vehicles.* 2018, **3**(177), 19-27.
[49] Komatsu customer support materials. Komatsu hybrid excavator. World-first hybrid technology. http://www.komatsu.com/ (accessed on 10.06.2021).
[50] TETZLAFF, S. System-wide electrification and appropriate functions of tractor and implement. *Landtechnik.* **70**(5), 203-216. 2015. http://doi.org/10.15150/lt.2015.2676
[51] Steyr traktoren. http://www.steyr-traktoren.com/en-distributor/agriculture/technologie/steyr-konzept (accessed on 10.06.2021).
[52] OSINENKO, P. Optimal slip control for tractors with feedback of drive torque. *Technische Universitat Dresden.* 2014.

Tomasz Kalociński MEng. – Manager Training Center & Training Shared Services at John Deere, Faculty of Civil and Transport Engineering, Poznan University of Technology.
e-mail: *tomaszkalocinski@gmail.com*

Article citation info:
CIEŚLIŃSKI, J.T., KRZYŻAK, J., KROPIWNICKI, J. et al. Experiments on compression ignition engine powered by nano-fuels. *Combustion Engines*. 2022, **188**(1), 55-59. https://doi.org/10.19206/CE-142281

Janusz T. CIEŚLIŃSKI
Jan KRZYŻAK
Jacek KROPIWNICKI
Zbigniew KNEBA

Combustion Engines
Polish Scientific Society of Combustion Engines

Experiments on compression ignition engine powered by nano-fuels

ARTICLE INFO

Received: 15 July 2021
Revised: 14 September 2021
Accepted: 14 September 2021
Available online: 16 September 2021

The use of nanoparticles in fuels provides new opportunities for modification of fuel properties, which may affect the operational parameters of engines, in particular the efficiency and fuel consumption. The paper presents comparison of compression ignition engine performance fuelled with neat diesel and nano-diesel. Alumina (Al_2O_3) was used as nanoparticles. Surface-active substances, including Span 80 surfactant, as well as water admixture were used to improve the stability of the produced fuel. Measurements of the thermal conductivity and dynamic viscosity of the produced mixtures were conducted. In this study was used naturally aspirated, water cooled, four-stroke diesel engine. Addition of Al_2O_3 nanoparticles result in 4% reduced fuel consumption, addition of TiO_2 nanoparticles result in 10% reduced fuel consumption with respect to neat diesel fuel.

Key words: *nano-fuels, compression ignition engine, fuel consumption, turbidity, fuel optical transparency*

1. Introduction

Nanofluid is a suspension consisted of the base liquid and metallic or non-metallic nanoparticles with sizes significantly smaller than 100 nm. Despite the small share of nanoparticles – from a few ppm to several percent of volume or mass concentration, the nanofluids exhibit completely different thermophysical properties than the so-called base fluids.

In recent years, attempts have been made to produce engine fuels that are mixtures of liquid fuels and nanoparticles. The studies were primarily concerned with diesel-based nanofuels although some attempt were made to fabricate and test the gasoline based nanofuels. Comprehensive state-of-the-art reviews regarding nanofuels have been presented in the literature [1–3]. Several fundamental aspects connected with nanofuels have been studied. First of all thermophysical properties of the nanofuels. It is well established that addition of nanoparticles to the base fluid increases both the thermal conductivity and viscosity [4, 5]. Viscosity increase causes poor atomization, dispersion and lower penetration of fuel which is responsible for poor mixing of air and fuel inside the cylinder [6]. In order to utilize the potential benefits of nanoparticle addition it is essential to produce stable and homogeneous nanofuels. It is known fact that poorly stabilized nanofuels always deteriorates the overall operating characteristics of an engine. Moreover, aggregation of nanoparticles not only causes the problem of settlement of particles but also increases the chances of clogging of fuel injection system. Two methods are promising in stabilization of nanofuels: application of surfactants [7] and emulsification of fuels [8, 9]. Another very carefully studied aspects are ignition and combustion of nanofuels [10]. Published studies revealed that addition of nanoparticle to fuel acts as combustion catalyst and improves combustion behavior [11]. It was found that burning rates of hydrogen with diesel fuel in the presence of aqueous aluminum were quite high. The reason can be attributed due to small aluminum particle size and high oxidation rates which provides larger contact surface areas for decomposition of more hydrogen from water [12, 13]. It was pointed out that metal particles are always covered with a natural oxide layer, which limits the oxidation process at low temperatures and also have a marked influence on ignition and combustion process [14]. For instance, it was shown that the presence of nanoboron particles in the fuel reduces the ignition delay which could be responsible for more complete combustion of hydrocarbon fuels [15]. Physics of nanofuel droplet combustion is investigated as well [11]. It was established that nanoscale suspension are permeable porous and uniformly distributed structure which is responsible for the early occurrence of micro explosion phenomenon [16]. Evaporation characteristics of nano-droplets was studied as well [17]. It is almost common consensus that metal nanoscale additives enhanced catalytic activity during combustion process and as a consequence leads to the better *engine characteristics* defined by such parameters as brake power (BP), brake thermal efficiency (BTE) and brake specific fuel consumption (BSFC). Literature data indicate slightly higher engine brake power [18, 19]. Experimental studies conducted with metallic, metal oxides and carbon nanotubes as additives to diesel fuel show higher brake thermal efficiency [20, 21]. Finally, addition of nanoparticles to diesel fuel results in lower engine brake specific fuel consumption [9, 22, 23]. It is necessary to stress, that the enhancement of BP and BTE or reduction of BSFC were observed up to a certain load of nanoparticles. The better performance is attributed to high surface area of nanoparticles which provides better heat transfer rates and further accelerates the combustion process provides fast oxidation, which promotes combustion reactions. Further it was observed that up to certain rpm value, there exist a linear relationship between brake power output and the amount of nanoparticle concentration in liquid fuels. Proper selection of type of nanoparticle with accurate concentration in liquid fuels should essentially be required for optimizing the engine performance parameters. Research studies report that addition of nanoparticles to diesel fuel results in significant decrease of exhaust gas emission and soot emissions of a diesel engine [24, 25]. The emission reduction level is directly related to the type

and concentration of nanoparticles. It was known that CO emission mainly depends on equivalent air fuel ratio, though diesel engines generally operates with lean air fuel mixtures. It was shown that addition of nanoparticles to diesel fuel decreases CO emission up to a certain load limit [26, 27] and possible explanation of this phenomenon is that metal oxide nanoparticles during combustion behave as oxygen donating catalyst which augments the oxidation rate of CO. The combustion in CI engine is connected with NO_x emission, that depends upon number of factors, but first of all combustion temperature. It has been established that addition of nanoparticles to diesel fuel reduces NO_x emissions significantly [22, 28]. Possible explanation of this fact is the increased chemical reactivity of nanofluid that reduces the ignition delay period that would result in low peak combustion temperatures and low peak cylinder pressures which further reduces the NO_x emission [27]. Experimental studies show that addition of nanoparticles to diesel fuel accelerates the flame propagation inside the cylinder, which lowers the carbon activation temperature and promotes more complete combustion (because nanoparticles act as oxidizing catalyst). These factors mainly inhibit the hydrocarbon emissions [29]. Lower smoke emission was observed by many authors due to higher evaporation rate and reduced ignition delay of nanofuels [9, 28, 30].

As it was stated in [3, 31, 32] limited experimental studies have been performed on diesel engine to investigate the engine performance parameters using nanofluid fuels and present paper supplements the data in the relevant literature.

Alumina (Al_2O_3) was used as nanoparticles. Surface-active substances, including Span 80 surfactant, as well as water admixture were used to improve the stability of the produced fuel. Measurements of the thermal conductivity and dynamic viscosity of the produced mixtures were conducted.

2. Experiment

2.1. Experimental stand

Figure 1 shows scheme of the used experimental stand, to investigate engine characteristic. In this study was used naturally aspirated, water cooled, four-stroke diesel engine, technical details of engine is given in Table 1.

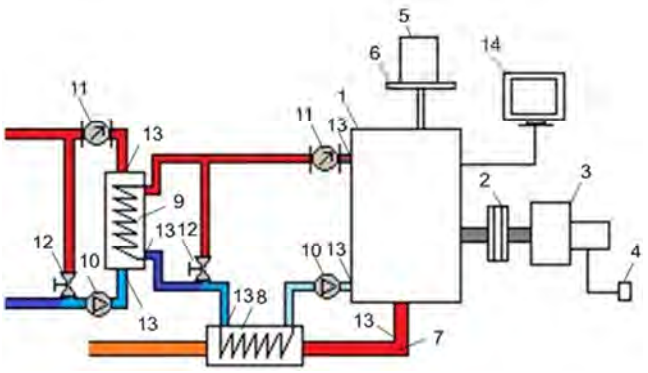

Fig. 1. Schematic diagram of experimental stand: 1 – engine, 2 – coupling, 3 – non-synchronous electric generator, 4 – electricity meter, 5 – fuel tank, 6 – scale, 7 – exhaust line, 8 – heat exchanger, 9 – cooler, 10 – pump, 11 – flow meter, 12 – valve, 13 – thermocouples, 14 – computer

The fuel was supplied by a mechanically controlled injection system from a tank, in which diesel fuel mixed with nanoparticles in appropriate proportions was stored. The internal combustion engine powered a generator which allowed the engine to be loaded at a constant rotational speed. Due to the mechanical load control system used, it was not possible to achieve full repeatability of the load for the three tested fuel types at one of the operating points (8 kW). The resulting discrepancies in the load settings did not, however, noticeably affect the characteristics of the analysed engine operating parameters.

Table 1. Test engine specification

Test engine/type	Andoria S320
Number of cylinder	1
Bore	120 mm
Stroke	160 mm
Engine volume	1810 cm^3
Compression ratio	17:1
BSFC	258 g/kWh
Power	13.2 kW
Max torque	84.4 Nm
Rotational speed	1500 rev/min

2.2. Preparation and characterization of the tested nanofluids

Nanofuels were prepared by direct mixing and ultrasonification. Two types of nanoparticles were used in the research: Al_2O_3 and TiO_2. Nanoparticles were supplied from SigmaAldrich, size below 50 nm. Nanoparticles suspended in base fluid result in changes in optical properties. Figure 2 presents change in optical transparency in nanofuel Al_2O_3 50 ppm compared to neat diesel fuel. On the left show neat diesel fuel, letters behind sample are sharp, on the right show nanofuel consist of diesel fuel – Al_2O_3 50 ppm mass concentration. Sample on the right is cloudy and letters are fuzzy.

Fig. 2. Comparison optical transparency, a) neat diesel fuel b) nanofuel – Al_2O_3 50 ppm, turbidity ~30 NTU

As an example illustrating the influence of the fuel preparation method on its properties, the results of nonofuel Al_2O_3 tests are presented in Fig. 3 Turbidity value was measured by infrared Turbidimeter Al250T-IR. Figure 3 presents variation of nanofuel turbidity with respect to sedimentation time, for different preparation methods. Turbidity changes could be described by two slope curves, in first period after preparation turbidity decrease rapidly, after three days turbidity decrease slowly. The results show

that method of preparation greatly influences the turbidity value. Direct mixing resulted in the lowest value of turbidity, only small part of particles was suspended in diesel fuel. Ultrasonification and combination of ultrasonification before direct mixing give comparable results, application direct mixing after ultrasonification result in slight increase of turbidity value. Combination of direct mixing before ultrasonification result in the highest turbidity value. The research did not include the measurement of the viscosity of fuels due to the lack of availability of measuring equipment adapted to the research in this area of nanofuels.

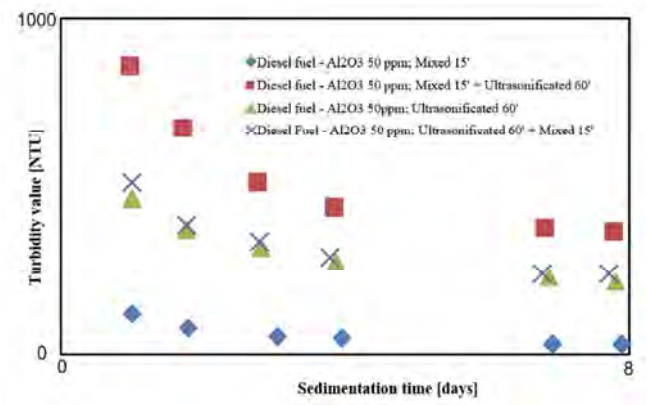

Fig. 3. Variation of nanofuel turbidity value with respect to sedimentation time for different preparation methods

3. Results

Figure 4 presents effect of nanoparticles on fuel consumption. Fuel consumption increases with the power increase The points are fitted into line, therefore linear approximation allow estimate effect nanoadditives on fuel consumption. Linear approximation curves are almost parallel, therefore comparing value of shifts between curves allow estimate changes in fuel consumption. Addition of Al_2O_3 nanoparticles result in 4% reduced fuel consumption, addition of TiO_2 nanoparticles result in 10% reduced fuel consumption with respect to neat diesel fuel.

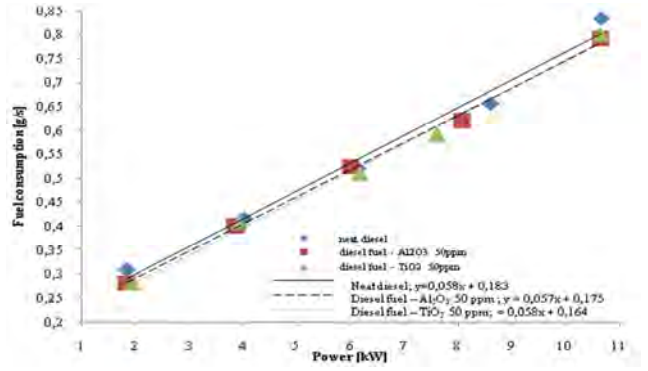

Fig. 4. The effect of nanoparticles on fuel consumption

The Figure 5 present effect of nanoparticles on brake specific fuel consumption. Brake specific fuel consumption decreases withe the power increase, values of BSFC are approaching to the value BSFC from engine specification Table1. In maximum power point, diesel fuel obtain BSFC = 281 g/kWh, nanodiesel Al_2O_3 reduced about 4.9% BSFC to 267 g/kWh with respect to neat diesel, nanodiesel TiO_2 reduced about 3.9% BSFC to 270 g/kWh with respect to neat diesel.

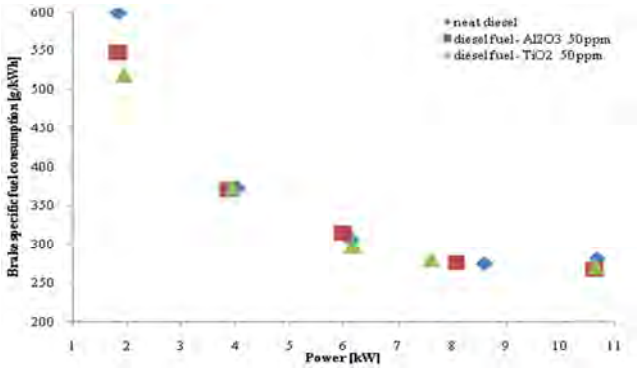

Fig. 5. Effect of nanoparticles on brake specific fuel consumption

Figure 6 presents effect nanoparticles on exhaust gas temperature. Exhaust gas temperature increase with the power increase. The points are fitted into line. There are no noticable changes in exhaust gas temperature after addition nanoparticles.

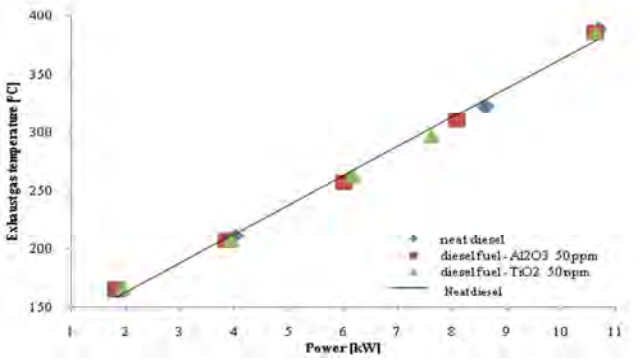

Fig. 6. Effect of nanoparticles on exhaust gas temperature

4. Conclusions

The use of nanoparticles as additives to diesel fuel may, according to the reported research results, bring a noticeable change in the course of the combustion process, mainly by modifying the thermal conductivity of the fuel. The tests carried out with the use of two types of nanofuels and net diesel oil as the reference fuel, allowed to conclude that the use of even small amounts of additives modifies the combustion process, leading to changes in the operational parameters of the engine. Nanoaddtives reduced fuel consumption, nanofuel – Al_2O_3 50 ppm reduced fuel consumption about 4%, nanofuel – TiO_2 50 ppm reduced fuel consumption about 10%. It is worth noting that the change in fuel consumption is several orders greater than the change in fuel density resulting from the use of nanoparticles. There are not observed changes in the exhaust gas temperature after addition of nanoparticles.

Bibliography

[1] SHAAFI, T., SAIRAM, K., GOPINATH, A. et al. Effect of dispersion of various nanoadditives on the performance and emission characteristics of a CI engine fuelled with diesel, biodiesel and blends — a review. *Renewable and Sustainable Energy Reviews*. 2015, **49**, 563-573. https://doi.org/10.1016/j.rser.2015.04.086

[2] KHOND, V.W., KRIPLANI, V.M. Effect of nanofluid additives on performances and emissions of emulsified diesel and biodiesel fueled stationary CI engine: a comprehensive review. *Renewable and Sustainable Energy Reviews*. 2016, **59**, 1338-1348. https://doi.org/10.1016/j.rser.2016.01.051

[3] SAXENA, V., KUMAR, N., SAXENA, V.K. A comprehensive review on combustion and stability aspects of metal nanoparticles and its additive effect on diesel and biodiesel fuelled C.I. engine. *Renewable and Sustainable Energy Reviews*. 2017, **70**, 563-588. https://doi.org/10.1016/j.rser.2016.11.067

[4] CIEŚLIŃSKI, J.T., KRYGIER, K., SMOLEŃ, S. Measurement of temperature-dependent viscosity and thermal conductivity of alumina and titania thermal oil nanofluids. *Archives of Thermodynamics*. 2015, **36**(4), 35-47. https://doi.org/10.1515/aoter-2015-0031

[5] CIEŚLIŃSKI, J.T. Wpływ nanocząstek na własności paliw silnikowych. *XXIII Zjazd Termodynamików*. Abstracts. 2017, 69-70.

[6] VAIRAMUTHU, G., SUNDARAPANDIAN, S., KAILASANATHAN, C. et al. Experimental investigations on the effects of cerium oxide nanoparticle on Calophyllum inophyllum (PUNNAI) biodiesel blended with diesel fuel in DI diesel engine modified by nozzle geometry. *Journal of the Energy Institute*. 2015, **5**, 1-5. https://doi.org/10.1016/j.joei.2015.05.005

[7] METHA, R.N., MORE, U., MALEK, N. et al. Study of stability and thermodynamic properties of water-in-diesel nanoemulsion fuels with nano-Al additive. *Applied Nanoscience*. 2015, **5**, 891-900. https://doi.org/10.1007/s13204-014-0385-3

[8] YANG, W.M. Impact of emulsion fuel with nano-organic additives on the performance of diesel engine. *Applied Energy*. 2013, **112**, 1206-1212. https://doi.org/10.1016/j.apenergy.2013.02.027

[9] BASHA, J.S., ANAND, R.B. Performance, emission and combustion characteristics of a diesel engine using Carbon Nanotubes blended Jatropha Methyl Ester Emulsions. *Alexandria Engineering Journal.* 2014, **53**, 259-273. https://doi.org/10.1016/j.aej.2014.04.001

[10] SHAAFI, T., VELRAJ, R. Influence of alumina nanoparticles, ethanol and isopropanol blend as additive with diesel-soybean biodiesel blend fuel: combustion, engine performance and emissions. *Renewable Energy.* 2015, **80**, 655-663. https://doi.org/10.1016/j.renene.2015.02.042

[11] MEHTA, R.N., CHAKRABORTY, M., PARIKH, P.A. Nanofuels: combustion, engine performance and emissions. *Fuel*. 2014, **120**, 91-97. https://doi.org/10.1016/j.fuel.2013.12.008

[12] KAO, M.J., TING, C.C., LIN, B.F. et al. Aqueous aluminum nano fluid combustion in diesel fuel. *Journal of Testing and Evaluation*. 2008, **36**, 186-190. https://doi.org/10.1520/JTE100579

[13] MEHTA, R.N., CHAKRABORTY, M., PARIKH, P.A. Impact of hydrogen generated by splitting water with nano-silicon and nano-aluminum on diesel engine performance. *International Journal of Hydrogen Energy*. 2014, **39**, 8098-8105. https://doi.org/10.1016/j.ijhydene.2014.03.149

[14] WEN, D. Nanofuel as potential secondary energy carrier. *Energy & Environmental Science*. 2010, **3**, 591-600. https://doi.org/10.1039/B906384F

[15] KARMAKAR, S., HANBERRY, J., DOOLEY, K.M. et al. Pre and post-combustion characteristics of boron nanoparticles in an ethanol spray flame. *International Journal of Energetic Materials and Chemical Propulsion*. 2011, **10**, 1-17. https://doi.org/10.1615/IntJEnergeticMaterialsChemProp.2012002669

[16] GAN, Y., QIAO, L. Combustion characteristics of fuel droplets with addition of nano and micron-sized aluminum particles. *Combustion and Flame*. 2010, **158**, 354-368. https://doi.org/10.1016/j.combustflame.2010.09.005

[17] GAN, Y., LIM, Y.S., QIAO, L. Combustion of nanofluid fuels with the addition of boron and iron particles at dilute and dense concentrations. *Combustion and Flame*. 2012, **159**, 1732-1740. https://doi.org/10.1016/j.combustflame.2011.12.008

[18] NADEEM, M., RANGKUTI, C., ANAUR, K. et al. Diesel engine performance and emission evaluation using emulsified fuels stabilized by conventional and gemini surfactants. *Fuel*. 2006, **85**, 2111-2119. https://doi.org/10.1016/j.fuel.2006.03.013

[19] GUMUS, S., OZCAN, H., OZBEY, M. et al. Aluminum oxide and copper oxide nanodiesel fuel properties and usage in a compression ignition engine. *Fuel*. 2016, **163**, 80-87. https://doi.org/10.1016/j.fuel.2015.09.048

[20] MIRZAJANZADEH, M., TABATABAEI, M., ARDJMAND, M. et al. A novel soluble nano-catalysts in diesel-biodiesel fuel blends to improve diesel engine performance and reduce exhaust emissions. *Fuel*. 2015, **139**, 374-382. https://doi.org/10.1016/j.fuel.2014.09.008

[21] LENIN, M.A., SWAMINATHAN, M.R., KUMARESAN, G. Performance and emission characteristics of a DI diesel engine with a nanofuel additive. *Fuel*. 2013, **109**, 362-365. https://doi.org/10.1016/j.fuel.2013.03.042

[22] KESKIN, A, METIN, G, ALTIPARMAK, D. Influence of metallic based fuel additives on performance and exhaust emissions of diesel engine. *Energy Conversion and Management*. 2011, **52**, 60-65. https://doi.org/10.1016/j.enconman.2010.06.039

[23] NARINDER, S., BHARJ, R.S. Effect of CNT-emulsified fuel on performance emission and combustion characteristics of four stroke diesel engine. *International Journal of Current Engineering and Technology*. 2015, **5**(1), 477-485. http://inpressco.com/category/ijcet/

[24] DEBNATH, B.K., SAHA, U.K., SAHOO, N. A comprehensive review on the application of emulsions as an alternative fuel for diesel engines. *Renewable and Sustainable Energy Reviews*. 2015, **42**, 196-211. https://doi.org/10.1016/j.rser.2014.10.023

[25] NORHAFANA, M., NOOR, M.M., SHARIF, P.M. et al. A review of the performance and emissions of nano additives in diesel fuelled compression ignition-engines. *1st International Postgraduate Conference on Mechanical Engineering (IPCME2018), IOP Conference Series: Materials Science and Engineering*. 2019, **469**, 012035. https://doi.org/10.1088/1757-899X/469/1/012035

[26] SHAFII, M.B., DANESHVAR, F., JAHANI, N. et al. Effect of ferrofluid on the performance and emission patterns of a four stroke diesel engine. *Advances in Mechanical Engineering*. 2011, **3**, 1-5. https://doi.org/10.1155/2011/529049

[27] SARVESTANY, S.N., FARZAD, A., BAJESTAN, E.E. et al. Effects of magnetic nanofluid fuel combustion on the

performance and emission characteristics. *Journal of Dis-Dispersion Science and Technology*. 2014, **8**, 1745-1750. https://doi.org/10.1080/01932691.2013.874296

[28] KANNAN, G.R., KARVEMBU, R., ANAND, R. Effect of metal based additive on performance emission characteristics of diesel engine fuelled with biodiesel. *Applied Energy*. 2011, **88**, 3694-3703. https://doi.org/10.1016/j.apenergy.2011.04.043

[29] SAJITH, V., SOBHAN, C.B., PETERSON, G.P. Experimental investigations on the effects of cerium oxide nanoparticle fuel additives on biodiesel. *Advances in Mechanical Engineering*. 2010, **36**, 1-16. https://doi.org/10.1155/2010/581407

[30] SELVAN, V.A.M., ANAND, R.B., UDAYAKUMAR, M. Effects of cerium oxide nanoparticle addition in diesel and diesel, biodiesel, ethanol blends on the performance and emission characteristics of a CI engine. *Journal of Engineering and Applied Sciences*. 2009, **4**, 1-6.

[31] JAMO, H.U., UMAR, I.D., YUSUF, B. et al.: Enhancement of physical properties of biodiesel extracted from palm oil by the addition MgO nano particles. *International Journal in Physical and Applied Sciences*. 2019, **6**(5), 1-9.

[32] KEGL, T., KOVAČ, KRALJ A., KEGL B. et al. Nanomaterials as fuel additives in diesel engines: A review of current state, opportunities, and challenges. *Progress in Energy and Combustion Science*. 2021, **83**, 100897. https://doi.org/10.1016/j.pecs.2020.100897

Prof. Janusz T. Cieśliński, DSc., DEng. – Faculty of Mechanical Engineering, Gdańsk University of Technology.
e-mail: *jcieslin@pg.gda.pl*

Prof. Jacek Kropiwnicki, DSc., DEng. – Faculty of Mechanical Engineering, Gdańsk University of Technology.
e-mail: *jkropiwn@pg.gda.pl*

Jan Krzyżak, Eng. – Faculty of Mechanical Engineering, Gdańsk University of Technology.
e-mail: *rebusteed@gmail.com*

Prof. Zbigniew Kneba, DSc., DEng. – Faculty of Mechanical Engineering, Gdańsk University of Technology.
e-mail: *zkneba@pg.gda.pl*

Article citation info:
PSZCZÓŁKOWSKI, J. The model for cylinder charge parameters during engine starting. *Combustion Engines*. 2022, **188**(1), 60-66. https://doi.org/10.19206/CE-142029

Józef PSZCZÓŁKOWSKI

Combustion Engines
Polish Scientific Society of Combustion Engines

The model for cylinder charge parameters during engine starting

ARTICLE INFO

Received: 2 August 2021
Revised: 24 August 2021
Accepted: 8 September 2021
Available online: 17 September 2021

The process of cylinder charge – air sucked into the cylinder – transformation during engine start-up phase is characterized. Heat exchange and air flow through piston-cylinder group leakage processes are described as factors influencing the gas thermodynamic parameters. The Woschni formula based on similarity theory was finally used as equation describing heat transfer in combustion engines cylinder. The computational model for cylinder charge parameters in the whole engine cycle during its starting at low temperature is presented. Some taken assumptions and characteristics of partial processes resulting from the computations are shown. There are indicated the possibilities of using the model at internal combustion engine diagnostic process.

Key words: *combustion engine, low temperature start-up, cylinder charge parameters*

1. Introduction

It is known that difficulties in obtaining the start of piston combustion engines increase at lowered temperature conditions. Lowering abilities of a diesel engine to undertake the independent operating at low temperature result from its influence on exploitation materials, engine systems properties, and directly from lowering the temperature of the air sucked-up into the engine cylinders. In the first phase of a difficult start the starter drives the engine crankshaft with a certain rotational speed. Then in the engine cylinders there are no ignitions of the injected fuel, but there are created the conditions suitable for its appearing. The requirement of the engine start-up is to initiate a cyclical, automatic repetition of the combustion processes in cylinders. There are two factors deciding of the injected fuel combustion occurrence: thermodynamic parameters (temperature and pressure) of air charge in the engine cylinders and the fuel spraying quality [4]. Thus, the knowledge about the thermodynamic state of the charge contained in engine cylinders is important for evaluation of air-fuel mixture properties and combustion processes characteristics during engine starting. It was the reason for which a model for cylinder air charge in starting conditions has been worked out.

The problems of engine start-up mathematical modelling have been widely discussed, e.g. [1, 5, 11, 18]. Computation procedures include a considerable number of parameters resulting from experimental data or complete experiment enabling to receive additional information basing on an indicator diagram. One of the most important parameters of such a model is the heat transfer coefficient of the air charge with the cylinder walls. The first heat transfer equation for combustion engines based on similarity theory was formulated by Woschni. It is still in use today [12]. There are also presented the new heat transfer correlations for the Engines [2]. In the paper [6] there is done the modified wall heat transfer equation which correctly reflects the transient, spatially averaged wall heat losses for SI-engines and DI-diesel combustion engines without any adjustments of empirical calibration factors.

These correlations are used in models for engine starting conditions. Effects of cold start control strategy on cold start performance of the diesel engine based on a comprehensive preheat diesel engine model are presented in [3]. The change in the temperature field of the charge at compression was numerically studied [9], taking into consideration the vortex flows that arise when a charge forms in the engine's cylinder. It was necessary to substantiate the new method for facilitating the cold start of the diesel engine. The paper [14] presents the different issue of thermal loads of a piston in a combustion engine during start-up. There were conducted simulation research based on the results of engine tests in the low temperature test chamber. There are also presented in the literature [8] the results of in-cylinder measurements of gas temperatures and pressures during a cold start.

It could be necessary to tune the coefficients of empirical formulas during the model calibration process if a formula is not accurate enough in the case of a specific combustion engine [19]. In the case of commercially available software the capability of the standard heat transfer models is limited due to model calibration constrains. It is possible to increase the capability of the simulation tool using the user model linked to the main solver or constituting an independent, own solution of the author prepared for a specific purpose.

The article presents such author's own study of the model for cylinder charge parameters during engine starting – cranking by the starter system designed for engine-battery-starter system diagnosis.

2. Cylinder air charge changes in engine starting conditions

In the case of a diesel engine starting the fuel autoignition may occur if in the compression process the air charge reaches the suitable values of thermodynamic parameters and appropriate fuel atomizing appears. The autoignition process of the sprayed fuel is characterized by selfignition delay. The autoignition delay is a function of the temperature and pressure and increases when their values decrease. That is why it is necessary to know air charge parameters

during engine starting. The gas transformation process can be described using the energy conservation law – often called the first thermodynamic law in the differential form for an open system:

$$dU = -pdV + dQ + idm \tag{1}$$

where: $dU = mdu + udm$ – air charge internal energy change, pdV – elementary work of volume change, dQ – heat quantity exchanged between air and the walls surrounding it, i – specific gas enthalpy ($I = U + pV$).

The gas total energy change and charge parameters at any moment of the process can be evaluated by equation (1) integration. The quantity of exchanged heat can be specified applying expression:

$$Q = \int dQ = \iint_{Ft} \alpha(T - T_S)dFdt \tag{2}$$

where: α – the surface film conductance, F – the surface of heat exchange, T – the air temperature, T_S – the temperature of the surface surrounding the air volume, t – the heat exchange time.

The fundamental importance for the heat exchange processes between air charge and the piston, engine head and cylinder walls has the choice of an appropriate formula describing surface film conductance value. There are well-known many empirical formulae for computing its value in engine compression chambers (for example formulae according to Woschni and Zapf) [16]. They usually have a similar general character (they differ only with constant parameters values):

$$\alpha = A(v_t p)^a (d)^b (T)^c \tag{3}$$

where: A, a, b, c – constant parameters, v_t – average piston speed, d – cylinder diameter.

There was carried out the analysis of some formulae of this type. The course of computed, using some formulae, surface film conductance values as a function of crankshaft rotation angle are presented in Fig. 1. During the computations there were taken the same values of air temperature and pressure for each formula and technological data for AD4.236 engine. In the Sitkei formula d does not mean the cylinder diameter but the so-called equivalent combustion chamber diameter evaluated as: $d = 2Dh/(D + 2h)$, where D is the cylinder diameter and h the height of the combustion chamber over the piston. The dependence presented in [1] is very different in its character:

$$\alpha = 406 \cdot \rho^{0,4} \qquad \left[\frac{W}{m^2 \cdot K}\right] \tag{4}$$

The air density is in [kg/m^3]. This formula gives much more enlarged surface film conductance values equal 460 to 980 [W/(m^2·K)] in the conditions assumed for the discussed computations.

Taking into account that the Zapf formula gives enlarged values of the surface film conductance, and it was elaborated in principle for cylinder charge exchange periods, but Sitkei formula gives its values a bit decreased, for the subsequent considerations (after some verifications) there was accepted the Woschni formula.

In each engine operating conditions a part of the compressed air charge flows to the crankcase through piston-cylinder group leakage. The proportion of this part of charge is higher when the rotational speed of engine crankshaft is lower, especially in the range of speed extorted by starter. Because of it the air flow in crankshaft driving conditions should be taken into account.

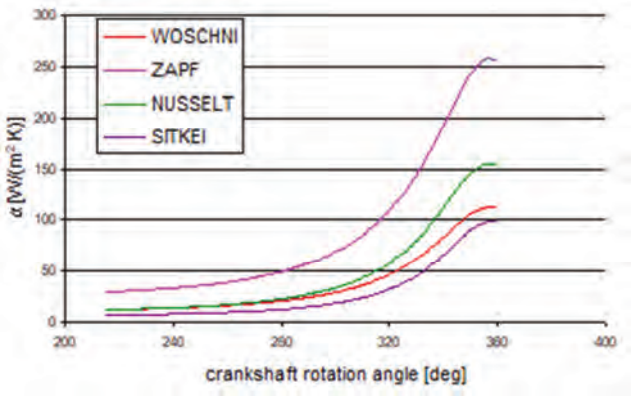

Fig. 1. The dependence of surface film conductance value on crankshaft rotation angle in AD4.236 engine compression chamber computed according to the formulae of: Zapf, Nusselt, Woschni, Sitkei

Application of an appropriate formula and constant parameter for describing the air flow through piston-cylinder leakage is also important. The air flow can be treated as an incompressible viscous fluid flow by the speeds of 0,6 M (Mach) [17]. Then the flow is expressed by a formula describing the equilibrium of static and dynamic pressure in chosen pipe section where the flow exists:

$$\Delta p = \frac{1}{2}\xi \cdot \rho \cdot w^2 \tag{5}$$

where: ξ – the coefficient of flow drag, ρ – density of the flowing fluid, Δp – static pressures difference between the ends of pipe, w – velocity of fluid flowing.

From this it is possible to determine the flowing fluid velocity:

$$w = \sqrt{\frac{1}{\xi}}\sqrt{\frac{2\Delta p}{\rho}} = \mu\sqrt{\frac{2\Delta p}{\rho}} \tag{6}$$

where: μ is the intensity of flow coefficient.

There is used one orifice as a model of air flow. By the high pressure difference between engine cylinder and crankcase volume, the air flow should be treated as supercritical viscous fluid flow. In this case the speed of air flowing to the crankcase can be evaluated on the base of energy conservation law. For the isentropic flow of compressive fluid, by assumption that the initial fluid speed equals "0", the final speed *w* can be computed as [16]:

$$w = \sqrt{2\frac{\kappa}{\kappa-1}p_1 v_1\left[1 - \left(\frac{p_2}{p_1}\right)^{\frac{\kappa-1}{\kappa}}\right]} \tag{7}$$

where: κ – the average value of adiabatic exponent, v_1 – the initial specific volume of flowing fluid, p_1 – initial static pressure of the fluid, p_2 – the static pressure in the final flowing section.

It is necessary, for the real viscous fluid flow, to introduce into the equation (7) the coefficient of flow velocity

(because of friction losses). This coefficient is experimentally determined for a given orifice. For model needs there was defined the specific (unitary) linear coefficient of volume flow intensity – μ_l. "μ_l" is the only one constant parameter in the model (apart from the formula describing the heat exchange process), which is determined using the experimental data. So, the elementary air volume ΔV, which flows through piston-cylinder leakage at Δt time can be determined as:

$$\Delta V = \mu_l \pi d \Delta t w \tag{8}$$

3. Computational model characteristic

The presented model is a numerical approach using integration procedures of the first thermodynamic law (1). The computations are realized by iteration method, where computing accuracy is obtained in the internal cycle. The model initial basic assumption is that the temporary rotational speed of the crankshaft has a constant value. The values of parameters characterizing air physical properties, depending on a chosen computing option, can be taken as constant or dependent on its temperature and pressure (air specific heat by constant volume c_v, adiabatic exponent κ, air density). Piston relocation and substitute height of combustion chamber are determined according to the kinematic dependences for piston-connecting-rod system. As the initial piston location (0 degrees of crankshaft rotation) its TDC at the beginning of intake stroke was taken.

Moreover, there were made some additional assumptions in the model, such as:

1. cylinder charging with fresh air and gas outflow are processes which proceed at a constant pressure value equal to the ambient pressure,
2. at the moment of the exhaust valve opening the immediate pressure equalization between cylinder charge and engine ambient takes place (gas being present in cylinder is subjected to the adiabatic process and a suitable mass of air flows into the cylinder).

Depending on the chosen option the computer program can realize the following procedures:

– gas adiabatic process by iteration method or Runge-Kutt's approach and comparing the results with the computed parameters using the adiabatic equation,
– gas change process at engine start-up conditions with taking into account (or not) heat exchange and blow-by of gas processes,
– evaluation of the engine minimum starting rotational speed dependence on temperature.

The input data include technological data concerning the engine, initial parameters of air and the engine, and conditions for processes involving the air. Output data include the current parameters of air charge in cylinder, such as temperature, pressure, temporary value of surface film conductance and specific heat, mass of the air charge. Moreover, there are computed some summarizing data, for example the average equivalent value of polytropic exponent for compression and decompression processes. Computation results can be presented on a computer display screen, printer or text file and then be transformed using computer software.

4. Initial verification of the model

The main goals of the initial model verification were to evaluate, which of the partial processes have a decisive influence on charge parameters and to evaluate specific (unitary) linear coefficient of volume flow intensity. The presented results concern the diesel engine AD4.236 of a farm tractor, which was also experimentally tested. Computations were carried out for the data:

– inlet air temperature – 260 K,
– ambient pressure – 1 atm = 0.101325 MPa,
– average crankshaft speed – 120 rpm.

The accepted above for computations value of rotational speed of the crankshaft is due to the fact that driven by the starting system crankshaft speed varies significantly from about 80 rpm for compression ignition engines and from 40 rpm for spark ignition engines to about 300 rpm [13].

For evaluation, which factor has a decisive influence on air parameters in engine cylinder, there were carried out different computational processes of air parameters change applying the discussed model.

In Fig. 2 there are presented the results of computed temperature values for various types of cylinder charge change:

1. adiabatic process without taking into account the temperature influence on air specific heat and adiabatic exponent (κ = const = 1.4) – marked with a in Fig. 1,
2. adiabatic process with taking into account the temperature influence on air properties (specific heat and adiabatic exponent) – b,
3. change process with taking into account the heat exchange between air charge and the walls surrounding it according to Woschni formula (and temperature influence on air properties) – c,
4. change process with taking into account the heat exchange according to Woschni formula and blow-by of gas by leakage of the piston-cylinder group – e.

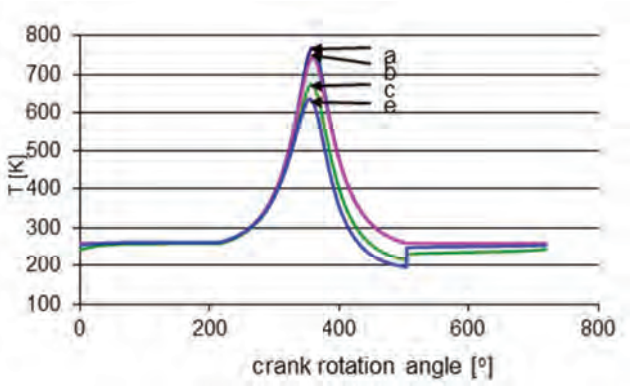

Fig. 2. The results of air temperature computation for various charge changes in AD4.236 engine cylinder

It is necessary to underline the change of air temperature values at the moment of outlet valve opening for gas change processes with taking into account the heat exchange and gas flow through leakage (curve e). At the final period of air charge decompression stroke its temperature and pressure decrease till much lower values than parameters of the engine environment. In this case the charge tem-

perature before outlet valve opening equals about 194 K, so it is 66 K lower than ambient temperature.

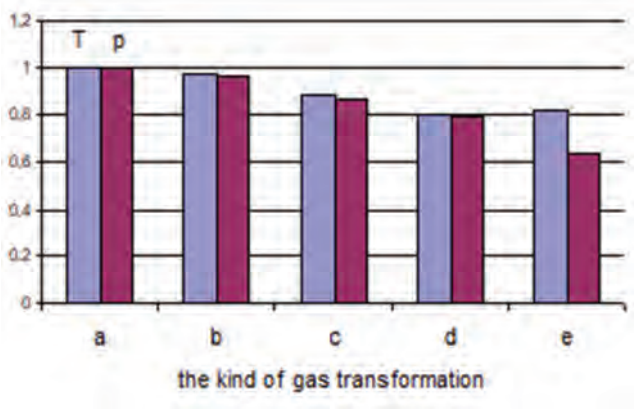

Fig. 3. The quotient values of temperature and pressure for different types of air change in comparison to adiabatic process at piston location in TDC

The comparative data illustrating the temperature and pressure quotient values for every type of change in comparison to their value in the adiabatic process with adiabatic exponent κ = const = 1.4 at piston location in TDC (360°) are presented in Fig. 3. In this figure there are also presented data for process in which there were taking into account the heat exchange according to Zapf formula – d. The presented dependences indicate the degree of individual factor influence on computed thermodynamic gas parameters.

It is worth noticing that taking into account only the temperature influence on air properties causes the noticeable decrease of cylinder charge thermodynamic parameters. Heat exchange phenomenon causes air charge temperature and pressure lowering, in comparison to adiabatic process, practically at the same degree. Air flow through piston-cylinder group leakage influences the temperature and pressure values obtained during air transformation in engine cylinder at different degree. The fact that heat exchange and gas flow influence air charge thermodynamic parameters at different degree can be useful in independent determining constant parameter values which characterize these processes in crankshaft driving conditions. It is important that the equivalent compression polytropic exponent for air change, where surface film conductance is described with Zapf's formula without additional air flow through leakage is lower than during the process described by Woschni formula and taking into account mass losses (in Fig. 3 the quotient of air temperature in d is lower than in e case). There was made an attempt to determine the reason for difference of surface film conductance expressed by Woschni and Zapf formulae. The different values of this parameter cause visible difference between air parameters obtained using the two formulae. In Fig. 4 there is presented the course of their quotient values as crank angle function in the case if constant A in both formulae has the same value and surface film conductance was evaluated for the same values of air temperature and pressure.

It is easily seen that the basic reason for the difference between both coefficients of surface film conductance are various values of constant A. If the constant A has the same value, the highest relative difference of temperature values in the processes described by such dependences does not exceed 3.5%. The criterion for determining the specific (unitary) linear coefficient of volume flow intensity – μ_l was the equality of air charge maximum pressure evaluated using the model and the one determined experimentally.

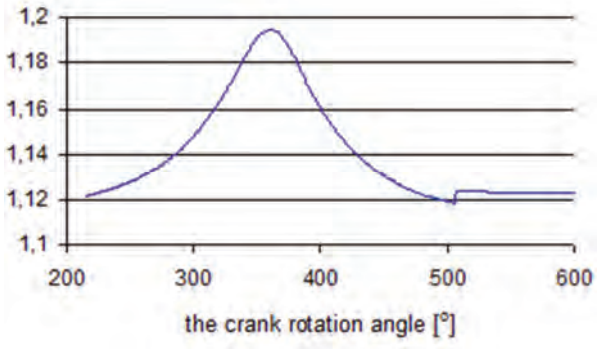

Fig. 4. The quotient values of temperature and pressure for different types of air change in comparison to adiabatic process at piston location in TDC

It is easily seen that the basic reason for the difference between both coefficients of surface film conductance are various values of constant A. If the constant A has the same value, the highest relative difference of temperature values in the processes described by such dependences does not exceed 3.5%. The criterion for determining the specific (unitary) linear coefficient of volume flow intensity – μ_l was the equality of air charge maximum pressure evaluated using the model and the one determined experimentally.

The final verification concerns the influence of the kind of air flow through the leakage and the temporary crankshaft speed changes on the computation results. Because the crankshaft rotational speed cannot be computed using the model (because of lack of suitable experimental data), there were taken into account the results of its measurements. Because the difference in obtained results are difficult to distinguish in the complete diagram of engine cycle, in Fig. 5 there is presented a fragment of the course of the computed charge temperature values (in the surroundings of TDC) for the different conditions of air flow through piston-cylinder group leakage and the changes of temporary crankshaft speed:

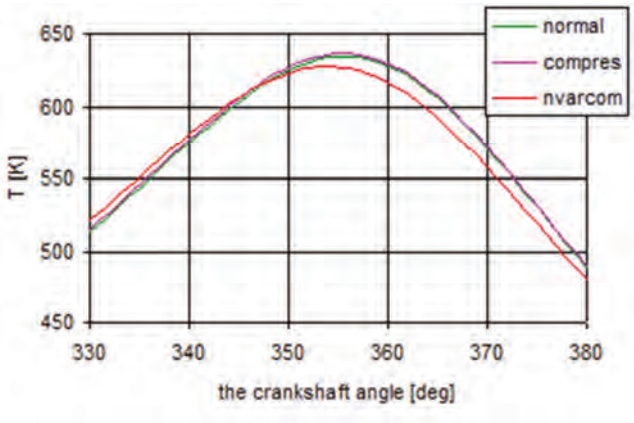

Fig. 5. The fragment of the computed temperature values dependence on the crankshaft rotation angle for different conditions of air flow and crankshaft temporary rotational speed changes

– normal – incompressible fluid flow, constant crankshaft rotational speed value,
– compres – compressible fluid flow, constant speed value,
– nvarcom – compressible fluid flow, changeable speed value.

It was necessary to assume the appropriate specific linear coefficient of volume flow intensity value for each examined process according to the maximum pressure criterion.

It is easily seen that in the crankshaft rotation angle interval, in which the processes of creating and ignition of air-fuel mixture take place, the differences between the computed temperature values are inconsiderable. So, independently of the assumed rules of air flow and the crankshaft temporary speed changes the obtained results, in aspect of the air temperature influence on engine starting properties, are comparable. The maximum relative differences of the parameters values characterizing the air change processes in relation to the process with incompressible air flow are:

– for the process taking into account the compressible fluid flow at constant speed value: temperature – 0.55%, pressure – 2% (after TDC, about 430 deg), mass losses – 1.5%,
– for the process taking into account the compressible fluid flow at changeable speed value: temperature – 2.3%, pressure – 9% (after TDC, about 430 deg), mass losses – 8% (about 430 deg).

5. Using the model in engine diagnostic process

As it was marked before, the developed and presented model for cylinder charge parameters during engine crankshaft driving could be used for engine-battery-starter system diagnosis, especially for analysis of the compression in the cylinders of an internal combustion engine. Changes in tightness of an internal combustion engine combustion chamber may be determined based on: the measurement results of maximum compression pressure in the cylinders, pressure drop measured using a cylinder leakdown tester, and the blow-by flow rate at different engine operating conditions. Also, the comparative compression in the cylinders of an engine may be tested by analyzing the changes of current drawn from battery when the engine is cranked by the starter motor with ignition or fuel inhibited.

Each engine cycle has a positive current peak due to a compression stroke in specific cylinder. Missing a positive current peak indicates a very low compression in one cylinder. The current cycles could be integrated and the integrals compared to detect compression imbalance. The base level of integration is equal to the level of an adjacent negative current peak (see Fig. 7). In the same way for engine cylinders relative compression diagnosis can be used battery voltage [7] or even engine crankshaft rotational speed, in inverse relationship of the positive and negative peaks. The analysis of the possibility of using the results of measurements of the instantaneous rotational speed and its derivative – crankshaft acceleration to assess the condition of a compression-ignition engine is presented in [15].

For the purpose of internal combustion engine diagnostics, there are new possibilities to use the parameters of crankshaft driving by the electric starting system: the current drawn by the starter, the voltage at the battery terminals, the crankshaft rotational speed. For the diagnostic use of these parameters it is necessary to build mathematical models of all objects – especially cylinder charge transformation process. The intensity of the current consumed by the starter, the voltage at the battery terminals and the rotational speed of the crankshaft are the response of the engine-starter-the starting battery set to the forcing, which is the internal combustion engine crankshaft driving by the starter. In the diagnostic test, the values of the system's state characteristics should be determined on the basis of the features of the output signals – system response to external extortion, which include:

– the intensity of the current consumed by the starter – it characterizes the battery's ability to return current under load conditions, it depends on the state of the starter characterizing the relationship between the current consumption and the generated torque, contains information about the combustion engine resistance of motion,
– voltage at the loaded battery (or starter) terminals – it contains information on the state of the energy source feeding the starter. The voltage value is dependent on the nominal battery capacity, current consumption, temperature and its status,
– rotational speed of the crankshaft forced by the starter – it is the resultant of the following features: the engine motion torque of resistance, the electromechanical characteristics of the starter and the starting capacity of the battery.

The variable component of the engine resistance torque, when the crankshaft is driven by the starter, depends on the compressed air pressure in the engine cylinders. An example of the course of the charge pressure in the engine cylinder during crankshaft driving is shown in Fig. 6.

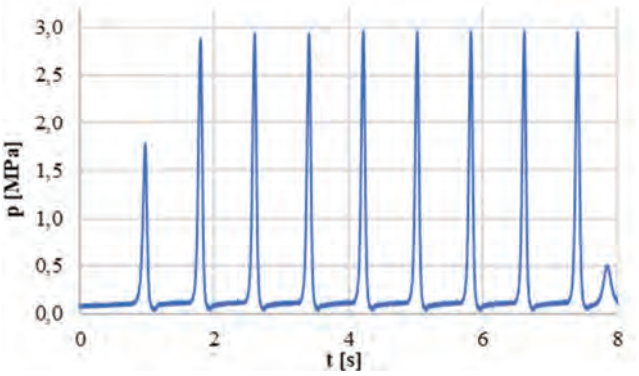

Fig. 6. The course of the compression pressure in the cylinder of the engine being tested

The variable component of the starter current (resistance torque) can be the premise for determining the value of the air compression pressure in the engine cylinders. To determine the value of the compression pressure, it is necessary to build a model for the engine crankshaft driving that allows correlating the pressure value and the current drawn by the starter. An example of the course of current during the engine crankshaft driving is shown in Fig. 7.

The condition of the engine in terms of its resistance torque can be determined by comparing the value of the

resistance torque determined during experiment (driving the crankshaft) and on the basis of the analytical formula.

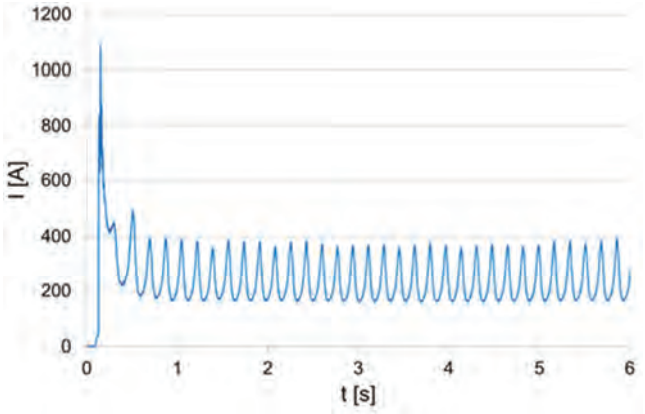

Fig. 7. The course of the current taken by the starter during the engine crankshaft driving

The voltage at the battery terminals characterizes its ability to give off energy. At a given current consumption, the voltage at the battery terminals depends on its nominal capacity Q, the electrolyte temperature T and the battery state k, which can be identified with the technical condition of the energy source. The voltage on the battery terminals U dependence on the characterizing its state parameters can be assumed as a linear function of these parameters. Battery condition assessment can be made based on comparison the voltage values in engine crankshaft driving conditions and determined from the analytical model. An example of the voltage course at the battery terminals while driving the engine crankshaft is shown in Fig. 8.

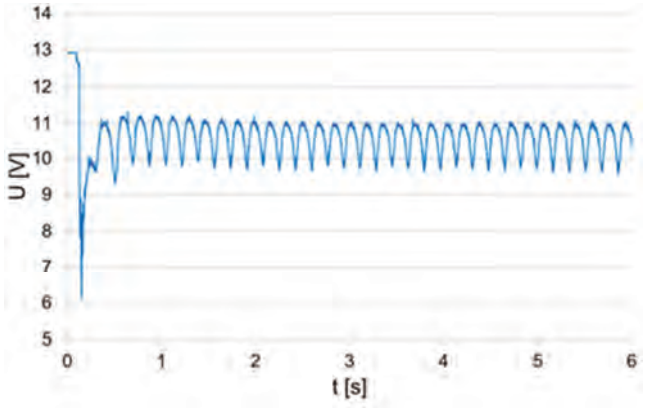

Fig. 8. The course of voltage measured at the terminals of a loaded battery

To assess the state of the electric starter, it is necessary to know the engine resistance torque. The basic meaning in the proposed method of the starter state assessment is to determine its actual power characteristic. The course of the power characteristics of the starter similar to the parabola indicates the possibility of their description using the second-degree polynomial in depending on the current.

The value of engine crankshaft rotational speed driven by the starting system can be used to determine the actual starter power, if its torque value is determined on the basis of the current. The power of the starter in given operating conditions is the basic parameter of the assessment of its technical condition (it must be related to its actual power characteristic). An example of the course of rotational speed of the engine crankshaft driven by starter is shown in Fig. 9.

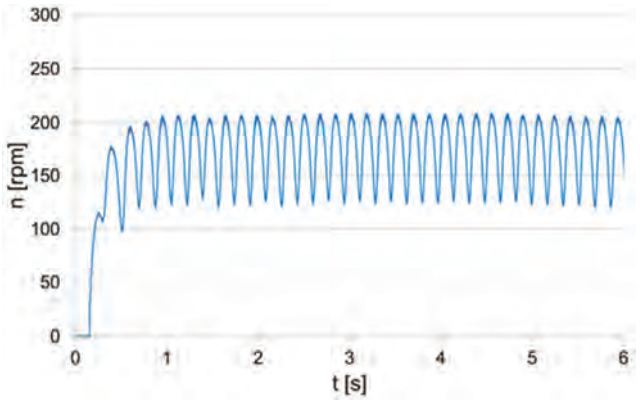

Fig. 9. The course of the engine crankshaft rotational speed driven by the starting system

The signals of the engine crankshaft driving through the electric starting system show significant similarities and correspondence of their variability phases. This is due to the existence of causal relationships between their values resulting from:

– battery characteristics, as a voltage source of electric current, which relate to one another recorded courses of voltage and current,
– a set of starter characteristics, as an electric motor, which uniquely bind the torque of force with the current and rotation speed of the starter shaft with the voltage of the power source.

6. Closing remarks

The article presents the principles of the author's own model for calculating the parameters of the cylinder charge while driving the crankshaft by the starting system and the essence of the new proposed system diagnostic method: acid battery – electric starter – internal combustion engine with the use of models of the diagnosed objects.

The mathematical model of any technical object or process presents its formalized, simplified description. The model can replace a real object or a process in such way that its testing can be the source of additional information on the object. The model allows controlling extortion parameters and conditions of object operation and to obtain information and dependencies, measuring of which during the experiment can be impossible, laborious or costly. The goal of working out of the presented model is to assist in experimental studies and to obtain dependencies, which are not provided by an experiment. The presented design for computing of thermodynamic air parameters in engine cranking conditions can be a part of the whole engine start-up or diagnostic model. The model should be still developed to increase its accuracy and to close computational procedures to the real conditions of engine driving. First of all, it is necessary to take into account the crankshaft speed non-uniformity. The Woschni formula seems to be the best for surface film conductance evaluation in engine cylinder

in cranking conditions. The air flow through the piston-cylinder group leakage, due to high pressure difference between cylinder volume and the engine crankcase should be treated as supercritical compressible fluid flow and described using expression (7). The presently obtained results indicate that these data can be used to qualitative and quantitative evaluation of piston engines starting and at the engine diagnostic process.

The originality of the diagnostic method lies in the fact that it enables the assessment of the complete system condition, and above all, the determination of the absolute value of the charge compression pressure in the cylinder. The principle of the relative compression test is based on tracking the battery current, voltage or crankshaft rotational speed changes during cranking to determine the comparative compression values of all cylinders. Proposed method requires the construction and integration into one whole of mathematical models of the battery, electric starter, cylinder charge compression and a model of resistance to driving the crankshaft by the starting system.

Nomenclature

dU	air charge internal energy change	pdV	elementary work of volume change
dQ	the exchanged heat quantity	T	temperature

Bibliography

[1] DIATLOV, E.G., ROMANOV, G.I. Influence of the reduced compression ratio on the starting qualities of a high-speed diesel engine. *Engine building*. 1990, **7**. (In Russian).

[2] CHANG, J., GURALP, O., FILIPI, Z. et al. New heat transfer correlation for an HCCI engine derived from measurements of instantaneous surface heat flux. *SAE Technical Paper* 2004-01-2996, 2004. https://doi.org/10.4271/2004-01-2996

[3] DENG, Y., LIU, H., ZHAO, X. et al. Effects of cold start control strategy on cold start performance of the diesel engine based on a comprehensive preheat diesel engine model. *Applied Energy*. 2018, **210**, 279-287. https://doi.org/10.1016/j.apenergy.2017.10.093.

[4] DROŹDZIEL, P. Rozruch samochodowego silnika o zapłonie samoczynnym. *Politechnika Lubelska*. Lublin 2020.

[5] GARDNER, T.P., HENEIN, N.A. Diesel starting. A mathematical model. *SAE Technical Paper* 880426. 1988. https://doi.org/10.4271/880426

[6] HEINLE, M., BARGENDE, M., BERNER, H. Some useful additions to calculate the wall heat losses in real cycle simulations. *SAE International Journal of Engines*. 2012, **5**(2), 469-482. https://doi.org/10.4271/2012-01-0673

[7] Compression test using battery voltage waveform during cranking. https://patents.google.com/patent/US4126037A/en (accessed on 05.08.2021).

[8] JORGENSEN, S. Compression temperatures in a cold cranking engine. *SAE Technical Paper* 880045. 1988. https://doi.org/10.4271/880045.

[9] KASIMOV, A., KORYTCHENKO, K., DUBININ, D. et al. Numerical study of the process of compressing a turbulized two-temperature air charge in the diesel engine. *Eastern-European Journal of Enterprise Technologies*. 2018, **6**(5), 96, 49-53. https://doi.org/10.15587/1729-4061.2018.150376

[10] KOSZAŁKA, G. Model of operational changes in the combustion chamber tightness of a diesel engine. *Eksploatacja i Niezawodnosc – Maintenance and Reliability*. 2014, **16**(1), 133-139.

[11] LEWICKI, J. Bilans cieplny silnika wysokoprężnego przy rozruchu w niskich temperaturach otoczenia. *Prace Naukowe Politechniki Szczecińskiej*. 1991, **439**.

[12] MOLLENHAUER, K., TSCHÖKE, H. Handbook of diesel engines. *Springer Verlag*. Berlin, Heidelberg 2010.

[13] MYSŁOWSKI, J. Rozruch silników samochodowych z zapłonem samoczynnym. *Wydawnictwo Naukowo-Techniczne*. Warszawa 1996.

[14] MYSŁOWSKI, J., TALAGA, K. Thermal loads of a piston in a diesel engine during startup. *Combustion Engines*. 2008, **133**(2), 20-25. https://doi.org/10.19206/CE-117242

[15] TRAWIŃSKI, G. Analiza możliwości wykorzystania pomiarów chwilowej prędkości obrotowej i przyspieszenia wału korbowego do oceny stanu technicznego silnika o zapłonie samoczynnym. Rozprawa doktorska. *Wojskowa Akademia Techniczna*. Warszawa 2004.

[16] WIŚNIEWSKI, S. Obciążenia cieplne silników tłokowych. *Wydawnictwa Komunikacji i Łączności*. Warszawa 1972.

[17] WIŚNIEWSKI, S. Termodynamika techniczna. *Wydawnictwo Naukowo-Techniczne*. Warszawa 1980.

[18] ZHDANOVSKY, N.S., NIKOLAENKO, A.I., KUZMIN, G.S. Thermodynamic analysis of final compression parameters at start-up of a diesel engine. *Energomashinostroenie*. 1973, **8**.

[19] ŽÁK, Z., EMRICH, M., TAKÁTS, M. et al. In-cylinder heat transfer modelling. *Journal of Middle European Construction and Design of Cars*. 2016, **14**(3), 2-10. https://doi.org/10.1515/mecdc-2016-0009

Józef Pszczółkowski, DSc., DEng. – Faculty of Mechanical Engineering, Military University of Technology.

e-mail: *jozef.pszczolkowski@wat.edu.pl*

Article citation info:
GĘCA, M.J., RADICA, G. Effect of compression ignition engine preheating on its performance under cold start conditions. *Combustion Engines*. 2022, **188**(1), 67-74. https://doi.org/10.19206/CE-142346

Michał Jan GĘCA
Gojmir RADICA

Combustion Engines
Polish Scientific Society of Combustion Engines

Effect of compression ignition engine preheating on its performance under cold start conditions

ARTICLE INFO

Received: 10 August 2021
Revised: 15 September 2021
Accepted: 16 September 2021
Available online: 17 September 2021

This paper examines the effect of an external preheating system for an internal combustion engine on fuel consumption, CO_2 emissions, and cabin temperature of a Euro4 vehicle. A 1 kW electric system powered by 220 V was installed in series in the cooling system of a vehicle with a compression-ignition engine of 2.5 dm^3 capacity. The tests were carried out in simulated urban driving conditions (distance of 4.2 km), extra-urban driving conditions (distance of 17 km), and during idling at cold-start temperatures ranging from –10°C to 2°C. Preheating the engine under simulated city conditions reduces fuel consumption by 2.64 dm^3/100 km and increases the supply air temperature immediately after engine start-up. Due to the preheater being powered from an external power grid, the cost per trip and total CO_2 emissions are increased. Assuming renewable energy sources, CO_2 emissions would be reduced the most for the stationary tests after engine preheating. In contrast, emissions would be reduced the least for extra-urban driving

Key words: *internal combustion engine, engine warm-up, cold start, CO_2 emissions, fuel consumption*

1. Introduction

The main task of an internal combustion engine cooling system is to transfer heat from the engine to the environment. Air-cooling systems are rarely used in today's vehicles; manufacturers usually choose liquid-cooling systems with a cooling medium. It is assumed that at least two-thirds of the energy contained in the fuel is transferred to the environment as heat, among other things by the cooling system. On the basis of the heat released during the combustion process, the overall efficiency of the engine is determined. The highest efficiency of an automobile engine is estimated to be around 40%, but that is also with a limited operating field [1]. Overall efficiency measures the ratio of the effective work done by the engine in one cycle to the heat extracted during that cycle from the fuel burned:

$$\eta_o = \frac{L_e}{Q} \cdot 100\% \quad (1)$$

where: η_o – overall efficiency of the engine, L_e – effective work (in one cycle) [J], Q – heat extracted from fuel [J].

It is estimated that [2] cooling losses from 26% to 32% of supplied heat – it is the energy carried by cooling fluid, it is taken from the engine elements exposed to very high temperatures (even 2000–3000 K) in order to protect them from heat damage.

At the point of friction the temperature must not exceed a certain limit value due to the thermal strength of the oil film. The limit temperature of engine oil is considered to be the piston temperature measured at the bottom of the channel of the first piston ring at 210°C [11].

The second basic function of the cooling system is to maintain the engine temperature within a certain range. The optimum and safe operating temperature for engines used in motor vehicles due to the acceptable heat loads on its components is usually between 85 and 95 degrees Celsius. This temperature is measured on the engine block. One of the reasons why the optimum operating temperature of the engine should be reached as soon as possible is due to constructional limitations. The materials used for the engine components, like all materials, are characterized by thermal expansion. This property changes volume and linear dimensions as a function of temperature. With decreasing temperature the volume and linear dimensions decrease, whereas with increasing temperature the volume and linear dimensions increase. Designers must take thermal expansion phenomenon into account when designing components such as pistons, cylinder head, engine block, etc. [3]. Adequate engine operating temperature is associated with lower power mechanical losses. This is why reaching an operating temperature of about 90 degrees Celsius in the shortest possible time is so important, because only then do the mechanical parts of the engine work together in the most optimal way. At lower temperatures, there can be too much clearance between the mechanically moving parts. In the long run, this can lead to faster wear or damage, generating very high repair costs, as well as temporarily taking the vehicle out of service until it is fully operational.

In order to increase the heating rate of the engine, the cooling system is split into multiple loops (two pumps and two coolers). In such a system, one circuit includes high temperature sources (80–100°C) such as engine head, EGR cooler, and oil cooler and the other circuit includes low temperature sources (35–45°C) such as A/C condenser and second stage intercooler. This approach reduced CO_2 emissions by 5 g CO_2/km and shortened the engine warm-up period by 25%. The direct heating of the cooling liquid by means of exhaust gases was applied by Toyota in spark-ignition engines to support the engine warm-up [16]. The efficiency of the classical cooling system can be increased by improving components such as the thermostat and coolant pump. Authors [12] proposed a comprehensive nonlinear control architecture for transient temperature tracking in multiple cooling circuits. In cooling system of experimental engine and transmission gear have been installed variable-

position smart thermostat valve, two variable-speed electric pumps, and variable-speed electric radiator fan. In paper [13], the effectiveness of an electric pump was tested against a standard mechanical pump in an internal combustion engine cooling system. In paper [14], the effect of centrifugal pump geometry on its performance was analyzed in detail. They observed velocity fluctuations caused by the impeller-diffuser interactions both in the impeller and diffuser regions. In the article [15] 4 automotive cooling system pumps were tested for application in an aircraft compression-ignition combustion engine.

The main function of engine preheating systems is to bring the engine to optimum operating temperature in the shortest possible time and to prepare the engine for one of the operating phases called the working phase, even before it is started during cold weather. Engine pre-heating systems support the cooling system. Depending on the type, they are designed to positively influence the vehicle operation by reducing fuel consumption, reducing harmful exhaust gases to the atmosphere, improving the cold starting performance, reducing mechanical parts wear and tear and improving the comfort of the vehicle operation.

The concentration of pollutants in the exhaust gases is also variable depending on the operating temperature, or the temperature of the engine being cold-started. Internal combustion engine start-ups may be divided into two groups: "cold" start-ups and "hot" start-ups. This division depends on the values of engine and lubricating oil temperature occurring during the vehicle start-up operation [4]. "Hot" start-up of a compression-ignition engine occurs above the temperature of 60°C and when there is no necessity to use a device facilitating the start-up (flame plug, glow plug, etc.). Otherwise, we are dealing with "cold" starting. The decision on using the engine starting aid is made subjectively by the vehicle operator or automatically by the fuel injection control system. On the basis of own research (stationary tests on a 4-cylinder engine), the author of publication [5] proposed additionally to introduce the concept of so-called first daily start of an internal combustion engine. Such a start-up occurs after the vehicle has been parked for a minimum of 8 h overnight in an open space or indoors. The temperature of the first daily start-up of an internal combustion engine is equal to the temperature of the air surrounding the vehicle [6].

During the start-up of a compression-ignition engine, many negative phenomena are observed, which intensify during "cold" start-ups. The energetic properties of the engine starting system decrease and the starting resistant torque increases [7], [8]. Significant resistance to motion causes appearance of large values of current drawn by the starter in a short time. This influences the increase of: engine starting time, fuel consumption and emission. There is an increased emission of toxic components in the exhaust gases due to insufficient atomization and evaporation of the first fuel doses, evaporation of self-ignition, and incomplete and incomplete combustion of the fuel-rich fuel mixture [9].

The purpose of this study was to determine the effect of preheating on vehicle performance parameters such as fuel consumption and CO_2 emissions and whether it would increase comfort in daily vehicle use. Chapter 2 presents the current use of engine preheating systems, Chapter 3 the research object and measurement systems, Chapter 4 the research methodology. Chapter 5 presents the results and analysis of the study. The work is concluded with a summary.

2. Preheating systems

The Figure 1 shows the classification of engine preheat systems. They can be divided into external (mounted as a separate engine system), internal (integrated with the engine), and static (being an external part of the engine bay).

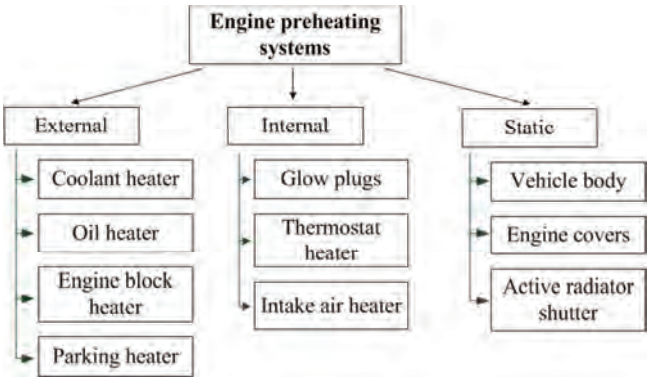

Fig. 1. Combustion engine coolant heat accumulators, pre-heating and temperature maintenance systems

External liquid heaters mounted in series or parallel in a walking circuit are equipped with an internal pump, an electric heating element and a thermostat. They can heat up the cooling system to a maximum of 50°C. LF Bros coolant heaters for passenger vehicles are available in different power versions, with heaters from 1000 W up to 3000 W. DEFA offers, apart from the duct heaters, also heaters mounted directly in the engine block. Heaters mounted in the engine block are only used in vehicles with engines that have a technological hole allowing the heater to be installed. Such holes are plugged with "brokas", in other words engine block plugs. After removing the blanking plug, the engine block heater can be placed in its place. Depending on the way of fixing, we divide engine block heaters into driven, screwed and bolted ones

Engine oil heaters are used to heat up engine oil while the engine is not running. Oil preheating before starting the engine allows to achieve in a shorter time the optimum operating temperature of oil and its better lubricating parameters just after starting the engine. There are systems in the form of a heater, a heating rod in the oil sump or a heater, a heating mat installed underneath the oil sump.

The purpose of a parking heater is to benefit the daily operation of the vehicle. Depending on the solution used, they allow for heating the vehicle cabin, the engine by heating the coolant or heating the cabin and engine simultaneously. In the combustion chamber of the parking heater, fuel supplied from the vehicle's factory fuel tank is burned. It is delivered to the combustion chamber by a fuel pump, which is part of the parking heater kit and operates independently of the fuel pump supplying the engine. The air required to burn the fuel is supplied to the combustion

chamber by an air fan. During fuel combustion, the heat generated is extracted from the combustion chamber by a heat exchanger and transferred to the coolant. The circulation of the coolant through the system is forced by a circulating pump.

Internal systems that facilitate starting include glow plugs, intake air heaters and coolant heaters near the thermostat. The glow plugs have the function of heating the combustion chamber after starting. This prevents the excessive release of soot and harmful combustion compounds and increases the engine's operating comfort. The length of the reheating period depends on the engine temperature.

Intake air heaters are located in the intake manifold. The purpose of the warmer air is to make it easier to start a cold engine and to improve its operation after the engine has been started.

a) b)

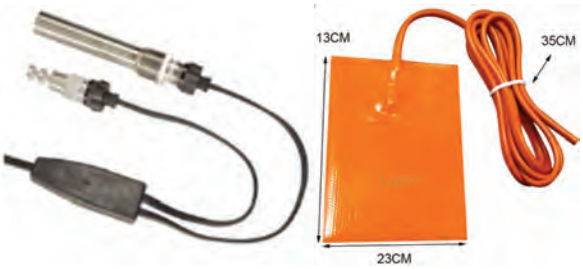

Fig. 2. Engine oil pre-heating system, a) heating rod, b) heating mat [10]

Intake air heaters are located in the intake manifold. The purpose of warmer air is to make it easier to start a cold engine and to improve the quality of operation after it has been started.

In automotive cooling systems, you can find thermostats that allow the coolant to reach temperatures higher than 90 degrees Celsius, the so-called phase thermostats. Phase thermostats are designed to maintain the temperature of the fluid at the most optimal level. The main difference in the principle of operation is that phase thermostats rely on information from the engine controller and the fluid temperature. When the engine load is increased, the ECU sends information to the electric heater, which heats heat extensible element in the thermostat, causing it to fully open as soon as the load is increased.

One way to increase engine warm-up is to use the active radiator shutter. When the cooling demand of the engine is low, the shutter automatically closes the air flow into the engine compartment which allows the engine to warm up faster due to less heat loss to the environment. In addition, body panels provide thermal protection by increasing engine warm-up while the vehicle is in motion and helping the engine to reach its optimum operating temperature. In addition, some vehicle models are equipped with engine guards mounted on the underside of the body. Their main role is to protect the engine from the water and dirt, but it also constitutes a thermal shield for the engine limiting the possibility of heat exchange of the engine compartment with the environment.

3. Research object and measuring instruments

The test vehicle used was a BMW 5 series, model E61, with a compression ignition engine with a displacement of 2497 cm^3, 130 kW, complying with the Euro 4 standard and automatic transmission. The engine used in this vehicle is a four-stroke, six-cylinder in-line 24-valve engine. The powertrain used in the tested vehicle is powered by diesel fuel through a common rail system. According to the manufacturer's data, the tested vehicle has fuel consumption and CO_2 emissions of:

– in urban test – 10.7 dm^3/100 km,
– in extra urban test – 6.3 dm^3/100 km,
– in combined test – 7.9 dm^3/100 km,
– CO_2 emission – 210 g/km.

The engine in the test vehicle has a liquid cooling system of volume 9.6 dm^3 and a lubrication system of volume 8.3 dm^3. Thus, there are about 7 kg of engine oil, 10 kg of coolant and 140 kg of engine metal parts to be heated.

Fig. 3. Tested vehicle BMW E61

Installed in series in the vehicle's cooling system is a coolant heater LF Bros model D-12-8003 with a 1000 W heater, powered by 230 V. The heat is transferred from the heater to the coolant. The circulation of the heated liquid in the system is forced by a pump, which is located inside the heater casing. LF Bros heater model D-12-8003 is equipped with an internal thermostat that turns off the heating element (heater) when the fluid temperature approaches 65–70°C and restarts it when the temperature is around 60°C. Note, however, that the heater shuts off at a given temperature reached by its internal thermostat. Due to heat loss, the motor itself reaches a lower temperature, depending on its capacity and design.

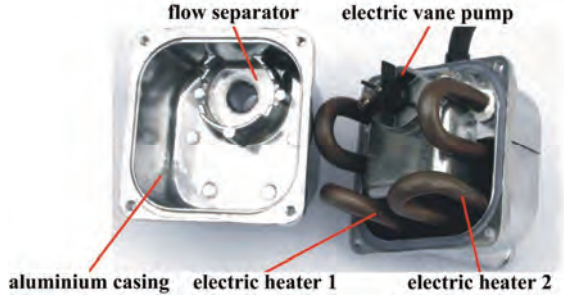

Fig. 4. Construction of LF Bros heater model D-12-8003 with 1000 W heater

The following measuring instruments were used to test the effect of using the installed LF Bros engine preheating system on the performance parameters of the test vehicle:

- GreenBlue GB202 wattmeter,
- ELM327 iCar2 Vgate OBD2 INTERFACE,
- electronic thermometer,
- smartphone with the "Car Scanner" application.

A stationary test bench was made to determine the volumetric flow rate of the LF Bros model D-12-8003 engine preheat system pump.

A wattmeter was used to measure the amount of energy and consumed from the power grid to power the preheater under test. The ELM327 iCar2 Vgate OBD2 INTERFACE connected to the OBD-II socket and allowing communication with the vehicle was used to read out the engine and vehicle operating parameters. In order to display and read out the operating parameters, the ELM327 interface was connected via bluetooth to the free "Car Scanner" application installed on the Android device. During the tests, the application was used to read out data on coolant temperature and average fuel consumption. After finishing a given measurement and disconnecting the application from the interface, the data are automatically saved. The application enables reading of the saved data and its preview in the form of a chart.

Fig. 5. Example of real-time preview of engine operating parameters using the "Car Scanner" application

4. Methodology

The effect of the engine preheating system on engine performance was investigated in 3 test scenarios:

- on a short route of 4.2 km ("urban"),
- over a long distance of 17 km ("extra urban"),
- with the engine switched off.

Each research scenario was repeated 5 times. The test vehicle was driven by the owner, who drives a short and long route on his daily work commute for several years. Driving characteristics show comparable driving values.

The first test track (city) was set entirely in a built-up area and the speed during its passage by the vehicle did not exceed 50 km/h. Moreover, it runs through very little traffic on residential roads and without traffic lights, which allowed to perform similar trips in terms of time and speed. In order to simulate the daily use of the vehicle, the test track had both left and right turns, gradients and sections to be driven at different speeds. Average travel time on urban route (distance 4.2 km) was 8 minutes 38 seconds with average speed 28.19 km/h.

The second test track (the route) was designed to represent a mixed driving cycle, i.e. a combination of driving in built-up areas and outside built-up areas. However, the vast majority of the test track was outside built-up areas. Trial runs were made at late hours or on non-working days to minimize the impact of other traffic on the test results. The route was driven in accordance with applicable traffic regulations and speed limits. Average travel time on extra urban route (distance 17 km) was 18 minutes 30 seconds with average speed 55.14 km/h.

The purpose of the stationary tests was to determine the amount of energy consumed for the tests with the engine preheating system and the amount of fuel consumed for the tests without the engine preheating system to achieve the required Δt [°C] coolant temperature change. The vehicle engine was turned off during the preheater tests. The no heater tests were conducted at engine idle without the cabin heating on and without any other energy sources such as radios or heated seats. These factors have a direct impact on a vehicle's energy consumption, which translates into fuel burn rate and coolant temperature. During the tests, the preheating time was also measured both during engine operation and during tests with the LF Bros engine preheating system.

In addition, the temperature of the air blown into the cabin was measured using an electronic thermometer during the runs. The measuring element (thermocouple) was placed four centimeters deep in the center tunnel of the cabin air intake during the measurements. The display was placed in a prominent position. In order to obtain the most reliable results, during each measurement the value of the cabin heating potentiometer was set to 19°C and the vehicle was heated in "auto" mode. Measurements were performed both for tests, where LF Bros heater was used to preheat the engine and for tests without preheater.

The mean value of the mercury thermometer readings and the outside temperature indicated by the vehicle's on-board computer were used to determine the outside temperature. The fuel consumption is the arithmetic mean of the on-board computer readings and the data obtained from the "Car Scanner" application via OBDII.

To determine the amount of fuel consumed during idling tests, only the value indicated by OBD was used. To determine the external temperature, the mean value of the mercury thermometer and the internal temperature indicated by the vehicle's on-board computer were used.

5. Test results and analysis

The Figure 6 shows the temperature rise of the vehicle's engine coolant during testing with the electric heater alone. The vehicle's engine was turned off. The initial temperature of the engine and ambient was 6°C. The coolant reached a temperature of 39°C after 60 minutes. Using the heater, we can heat the engine to a maximum of 46°C under the

conditions presented. The preheat curve flattens out as the time increases, which means that there is a large heat loss to the environment. When the heater is used for more than 90 minutes, the losses to ambient air exceed the amount of energy released to the vehicle's engine. Under the same ambient conditions, it takes only 6 minutes to preheat the vehicle without the heater to 39°C using only the chemical energy of the fuel (vehicle engine idling).

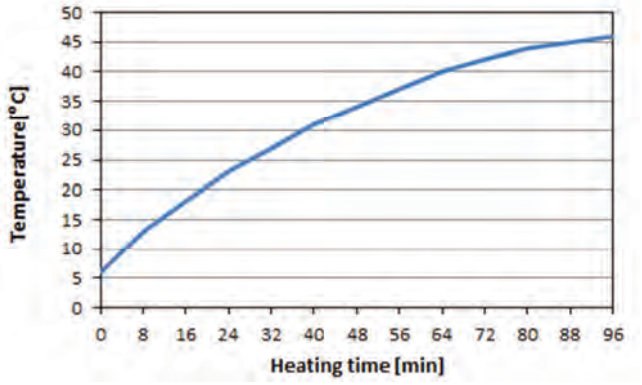

Fig. 6. Coolant temperature as a function of heater on time

The preheating of the engine allowed for an easier start and a more stable maintenance of the idle speed right after the start. Preheating the engine allows also to reduce the idling speed. The difference was definitely noticeable during the tests performed at outdoor temperatures below 0°C. Figure 7 shows the values of the engine speed after start-up, during the test without engine preheating and during the test with engine preheating at an outside temperature of –14°C. The rotational speed of the cold engine was 1250 rpm at the initial stage and then maintained at 1000 rpm. After preheating the engine, the engine speed was about 750 rpm, which allows the engine to consume less fuel just after starting, thus generating less pollution.

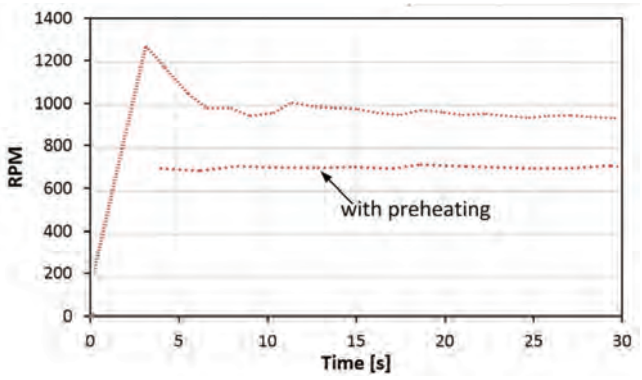

Fig. 7. Engine crankshaft speed at idle after starting with and without preheat system at –14°C

During all of the test runs performed on the test tracks, it can be seen that during runs with the engine preheating system, the vehicle coolant reached a higher temperature at the end of the run than during runs without the system. The Figure 8 shows the increase in coolant temperature for the sample runs without the engine preheat system and with the engine preheat system. The final coolant temperature difference alone for the runs with and without the engine preheat system was not as large, compared to the initial temperature. This was directly related to the heating of the vehicle cabin. During each of the driving tests, to reflect daily vehicle operation, the cabin air intake was set to "auto" mode and the potentiometer was set to 19 degrees Celsius. Due to the low outside temperatures during the tests, the cabin space was heated, which involved taking heat in the heater from the coolant and transferring it to the interior of the vehicle.

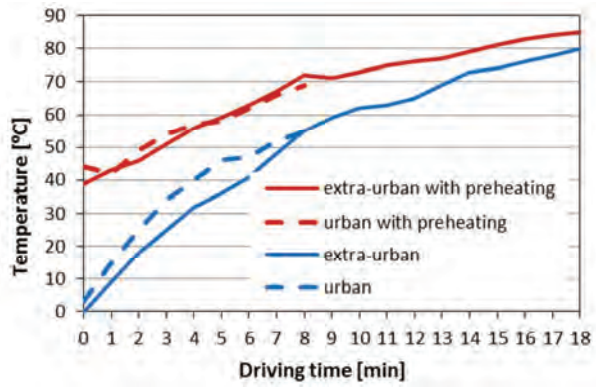

Fig. 8. Increase in engine temperature of the vehicle on the test track "urban" and "extra urban" as a function of driving time with and without engine preheating

Analyzing the graphs shown in Fig. 9 it can be seen that the supply air temperature for the first 8 minutes in the tests after engine preheating was significantly higher. This situation was repeated for the two test runs. Thus, travel comfort was definitely improved after engine preheating.

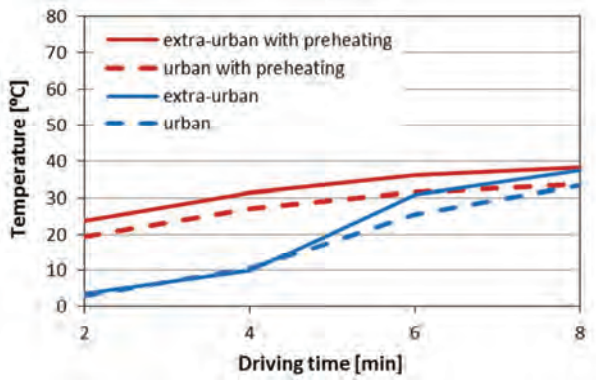

Fig. 9. Temperature increase of the supplied air to the vehicle cabin on the test track "urban" and "extra-urban" as a function of driving time with and without engine preheating

Engine preheating helps to reduce fuel consumption. The Figures 10 and 11 show the average fuel consumption during the "urban" and "extra urban" test under different ambient conditions. The basis for calculating the percentage reduction in fuel consumption was the fuel consumption without the heater. For both the first and second test runs, fuel consumption on average decreased by 8.99% and 1.95%, respectively. Thus, it can be seen that the difference in fuel consumed decreases with the longer trip. This is directly related to the travel time and therefore the engine reaching a temperature closer to its optimum operating

temperature. In the case of the second test track (extra-urban), the difference in fuel consumption between runs with and without the heater was undoubtedly reduced by the fact that most of the test track was outside built-up areas. Driving outside built-up areas is characterized by less fluctuation of the engine load and therefore less fuel consumption. In addition, the fuel consumption of the two test tracks was related to the external temperature recorded during the tests. For the first track and the second track at the lowest temperature of –9°C and –12°C, respectively, the highest combustion of the tested vehicle was observed for both runs with the preheating system without its use. For the urban run, the difference in fuel burned between the highest (19.59 dm^3/100 km) and lowest (17 dm^3/100 km) observed was 13.2% for the tests without the preheater and 6.5% for the tests with the preheater. During the "urban" tests, the difference in fuel burned between the highest (12.3 dm^3/100 km) and lowest (10.5 dm^3/100 km) observed results was 14.6% for the tests without the heater and 13.3% for the tests with the heater.

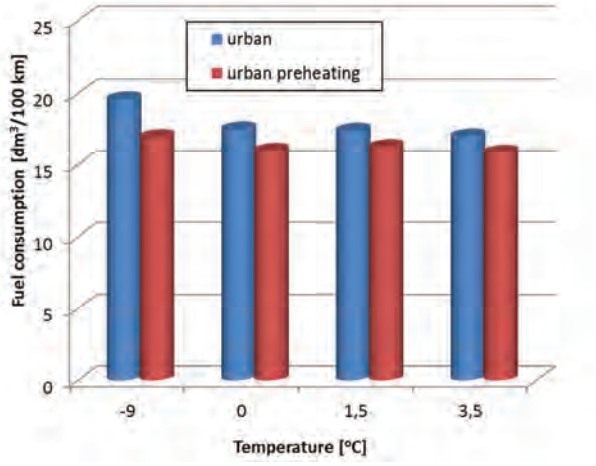

Fig. 10. Average fuel consumption on the „urban" test at different ambient temperatures with and without engine preheating

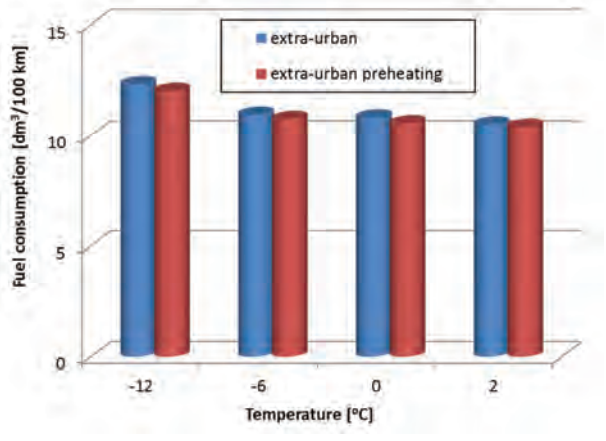

Fig. 11. Average fuel consumption on the „extra urban" test at different ambient temperatures with and without engine preheating

When analyzing the total cost of travel and the CO_2 emissions of a vehicle using an electric engine preheater, it must be remembered that the unit draws its electricity from the grid. Thus, the cost of electricity consumed should be added to the price of the fuel consumed during the runs with the engine preheating system. The following values have been taken as a basis for the calculation of the total cost of the test runs: the average price of diesel fuel of 5.40 PLN/dm^3 and of electricity of 0.75 PLN/kWh. During the tests the heater was run for 95 minutes.

The Table 1 shows the calculated difference in total cost of heating and driving 100 km during the tests with and without electric engine heating. The values shown are the difference in fuel cost consumed by the engine and the electricity cost consumed by the electric heater. For the idle tests, the engine preheating was more economical. The cost of fuel consumed to preheat the engine was greater than the cost of energy consumed to preheat the engine with the heater. The savings ranged from 11.5 PLN to a maximum of 16 PLN and were proportional to the decrease in ambient temperature. The lower the outside temperature, the more economically advantageous it is to use a heater only at idling speed. Table 1 shows that the total cost of electricity consumed by the heater and fuel burned increases the operating costs for both urban and extra-urban routes.

Table 1. The difference in the total cost of driving per test with an electric heater across different test scenarios and ambient temperatures

Test scenario	**Temperature [°C]**		
	–10	**1.5**	**0**
Idling [PLN]	–16	–11.5	–12.2
Urban [PLN/100 km]	+20.5	+26	+24.2
Extra-urban [PLN/100 km]	+6.1	+7.1	+6.4

The cost of driving 100 km with a vehicle whose engine is heated using grid electricity is higher than if the engine is heated using the chemical energy of the fuel burned during both the urban and extra-urban test runs. Although the fuel consumption was lower after using the heater, the cost of the electricity used by the heater added to the fuel cost.

The total cost of trips using the heater on the urban gauge increased by an average of 21.8%, while the extra-urban gauge saw an average increase of 11.2% in the total cost of the trip. This cost decreases as the ambient temperature (initial engine temperature) decreases. Also, this cost is less for the extra-urban trials than for the urban trials. In order to make the cost of the urban and extra urban trials with and without the heater in the test vehicle the same, the engine preheat time would have to be reduced from 95 minutes to 19 minutes. Then the temperature would change by only 15°C.

Another aspect discussed in the analysis is the amount of CO_2 emitted in individual tests with and without engine preheating. Because the preheater is powered from the grid, the amount of CO_2 generated during electricity generation must be added to the tests using the preheater in addition to the CO_2 emitted from the fuel burned. The following data were adopted for the analysis:

- from burned 1 dm^3 of diesel fuel 2.3 kg of CO_2 is generated [17],
- 0.719 kg of CO_2 is emitted during the production of 1 kWh of electricity [18].

The Table 2 shows the calculated difference in total CO_2 emissions during the tests with and without heating the electric vehicle engine. In this case as in the case of the total cost of driving a route section with a preheated engine the CO_2 emissions are higher in all cases. The reduced CO_2 emissions resulting from the reduction in fuel consumption after the engine has been preheated do not compensate for the emissions resulting from the production of electricity consumed by the heater. For the "urban" test, on average, the total amount of CO_2 emitted increased by 41%, while the "extra urban" test saw a 22.6% increase in CO_2 emissions for the heater tests. The highest CO_2 emissions were recorded for low ambient temperatures, which resulted in higher fuel consumption.

Table 2. The difference in the total CO_2 emissions per test with an electric heater powered from the electricity grid across different test scenarios and ambient temperatures

Test scenario	**Temperature [°C]**		
	-10	**1.5**	**0**
Idling [kg CO_2]	+0.41	+0.49	+0.5
Urban [kg CO_2]	+1.17	+1.22	+1.19
Extra-urban [kg CO_2]	+1.23	+1.33	+1.23

Considering the generation of electricity from renewable energy sources (RES) connected to the electricity grid, for example from a wind farm or a photovoltaic plant, we can expect a reduction in CO_2 emissions to the atmosphere after using an electric heater. The Table 3 shows the calculated difference in total CO_2 emissions during the tests with and without heating the electric vehicle engine.

In this case, after using RES to power the heater, the total CO_2 emissions are lower in all cases. Under the assumption of obtaining energy from renewable energy sources, CO_2 emissions would be reduced to the greatest extent for stationary tests after preheating the engine. In contrast, emissions would be reduced the least for the "extra urban" tests because the difference in fuel burned for the tests with and without the heater was less than for the "urban" tests.

Table 3. The difference in the total CO_2 emissions per test with an electric heater powered by renewable energy sources across different test scenarios and ambient temperatures

Test scenario	**Temperature [°C]**		
	–10	**1.5**	**0**
Idling [kg CO_2]	–0.94	–0.85	–0.88
Urban [kg CO_2]	–0.25	–0.11	–0.15
Extra-urban [kg CO_2]	–0.12	–0.04	–0.11

6. Summary

The effect of preheating a compression ignition engine with a 1000 W electric preheater was analyzed. The preheater was run for 95 minutes at three ambient temperatures (coolant temperatures): –10°C, 0°C, 2°C. The device heats up the coolant in the system to maximum 47°C.

The effect of an external preheating system for an internal combustion engine is as follows:

1. Enables faster heating of the engine in relation to the conventional drive.
2. Improves the comfort of vehicle operation by increasing the temperature of supplied air to the cabin to 22°C.
3. the idling speed is reduced to the value of ca. 700 rpm after starting the vehicle.
4. the vehicle start-up system and battery are less loaded during the engine start-up phase.
5. A reduction in fuel consumption and CO_2 emissions was observed at both idle and simulated urban and extra-urban driving conditions (up to 2.64 dm^3/100 km during urban trail and low ambient temperatures).
6. Due to the cost of powering the device from the electricity grid, the total cost of driving 100 km increased in the study vehicle.

The operating cost and CO_2 emissions can be reduced by powering the vehicle's engine preheater from a grid connected renewable energy source.

Nomenclature

CO_2 carbon dioxide
RES renewable energy sources
ECU electronic control unit

Bibliography

[1] KNEBA, Z. Studium problemów zarządzania ciepłem odprowadzanym silnika w samochodach osobowych. *Wydawnictwo Politechniki Gdańskiej*. Gdańsk 2011.
[2] WAJAND, J.A., WAJAND, J.T. Tłokowe silniki spalinowe średnio- i szybkoobrotowe. Wydanie IV. *Wydawnictwa Naukowo-Techniczne*. Warszawa 2005.
[3] GÓRECKI, A. Technologia ogólna: podstawy technologii mechanicznych. *WSiP*. Warszawa 1984.
[4] PSZCZÓŁKOWSKI, J. Charakterystyki rozruchowe silników o zapłonie samoczynnym. *Wyd. SEPP „Cogit*o". 2004.
[5] DROŹDZIEL, P. O rozruchu silnika o zapłonie samoczynnym. *Eksploatacja i niezawodność.* 2007, **2**(34), 51-59.
[6] DROŹDZIEL, P. Wybrane zagadnienia rozruchu samochodowego silnika o zapłonie samoczynnym. *Polskie Naukowo-Techniczne Towarzystwo Eksploatacyjne.* Warszawa 2007.
[7] BUCK, W.H., LOHUIS, J.R. Lubricant effects on low-temperature diesel engine cold starting. *SAE Technical Paper* 940097. 1994. https://doi.org/10.4271/940097
[8] DUVAL, H. Computer model of the lead/acid starter battery in automobiles. *Journal of Power Sources*. 1995, **53**, 351-357. https://doi.org/10.1016/0378-7753(94)02000-S
[9] GĘCA, M., BARAŃSKI, G., MAJCZAK, A. IC CI engine cold start-up facilitating systems tests. *Logistyka*. 2015, **3**, 1452-1458.
[10] PAWO. www.pipewarm.com
[11] OGRODZKI, A. Technika cieplna w pojazdach. *Wydawnictwo Komunikacji i Łączności.* Warszawa 1982.
[12] SALAH, M.H., MITCHELL, T.H., WAGNER, J.R. et al. A smart multiple-loop automotive cooling. *IEEE/ASME Transactions on Mechatronics* 2010, **15**(1), 117-124. https://doi.org/10.1109/tmech.2009.2019723

[13] WANG, X., LIANG, X., HAO, Z. et al. Comparison of electrical and mechanical water pump performance in internal combustion engine. *International Journal of Vehicle Systems Modelling and Testing*. 2015, **10**(3), 205-223. https://doi.org/10.1504/IJVSMT.2015.070155

[14] FENG, J., LUO, X., BENRA, F.K. et al. Experimental investigation of velocity fluctuations in a radial diffuser pump. *Journal of Hydrodynamics.* 2015. **27**(3), 332-339. https://doi.org/10.1155/2014/702318

[15] GĘCA, M.J., PIETRYKOWSKI, K., BARAŃSKI, G. Coolant pump for compression-ignition aircraft engine. *Combustion Engines.* 2019, **179**(4), 52-57. https://doi.org/10.19206/CE-2019-408

[16] KILMAN, G., HARADA, O., WTENABE, K. et al. The 1.8L engine of the new Toyota Prius. *FISITA 2010*. F2010-A-043.

[17] KRÓL, E. Porównanie emisji zanieczyszczeń pojazdów z napędem elektrycznym i spalinowym. *Napędy i Sterowanie*. 2017, 140-143.

[18] Wskaźniki emisyjności CO_2, SO_2, NO_x, CO i pyłu całkowitego dla energii elektrycznej na podstawie informacji zawartych w Krajowej bazie o emisjach gazów cieplarnianych i innych substancji za 2019 rok. *Krajowy Ośrodek Bilansowania i Zarządzania Emisjami*. Warszawa 2020. https://www.kobize.pl/

Michał Jan Gęca, DEng. – Faculty of Mechanical Engineering, Lublin University of Technology.
e-mail: *m.geca@pollub.pl*

Prof. Gojmir Radica, DEng. – Faculty of Electrical Engineering, Mechanical Engineering and Naval Architecture, University of Split, Croatia.
e-mail: *gojmir.radica@fesb.hr*

Article citation info:
KMIEĆ, M., WEBER, M., ROMIJN, M. et al. Application of automotive safety design methodologies to the development of Euro 7 emission control systems including on board monitoring. *Combustion Engines*. 2020, **188**(1), 75-82. https://doi.org/10.19206/CE-141291

Mateusz KMIEĆ
Matthias WEBER
Marcel ROMIJN
Dave MATEWS

Combustion Engines
Polish Scientific Society of Combustion Engines

Application of automotive safety design methodologies to the development of Euro 7 emission control systems including on board monitoring

ARTICLE INFO

Received: 18 July 2021
Revised: 14 August 2021
Accepted: 16 August 2021
Available online: 15 September 2021

Euro7 and California HD-OBD present a shift of approach in emissions control. Legislative bodies concentrate on individual vehicle conformity to standards during its lifetime on top of type approval processes in test environment. The main change is NO_x trackers in software and sensors in the exhaust pipes of all vehicles. As a consequence of constant supervision not only single point faults are taken into account in the analysis, but also cumulative parameter drift of components due to aging. To achieve normative requirements and prevent emission standards violation during exploitation, methodologies known from automotive functional safety domain and SOTIF are used to evaluate and modify a propulsion system design. An illustrative example of analysis is presented in the paper.

Key words: *OBD, Euro 7, emission control, robust design, design evaluation*

1. Introduction

Today's automotive development cycles are around 3 years [1]; new legislation norms can extend to requiring 4 years. Looking into the future, currently negotiated norms have to be considered now; otherwise, it will not be possible to sell the product. The article discusses regulations that will appear in coming years and development methods that are now transferred from other domains into the OBD domain.

For three decades, the emission characteristics of internal combustion engines have been increasingly gaining attention – the focus on clean transportation resulted in several normative and legal requirements which the vehicles need to fulfill [2]. Due to the development of better measurement equipment and increased computing power of ECUs placed on board and detected differences between declared, accredited, and actual measured emission, there is an evolution of emission control design approaches.

The previous generation approach with regulations Euro 5/V, China 5/V and older USA regulations was to design and balance all emission controls to produce valid emission levels of all relevant pollutants. The design was verified on near-series production vehicles on a chassis or engine dyno according to emission cycles. The type approval was conducted with, at minimum, an aged catalytic converter (DOC, SCR, 3W-cat). During this test, CO_2 emission was verified as well.

Since the previous procedure misses real-life exploitation parameters, for current generation Euro 6/VI [3] and China 6/VI, it was decided to include PEMS (Portable Emissions Measurement System) to pre-series cars and verify the emission limits on a public road with RDE (Real Driving Emissions) driving, traffic, and ambient conditions. The procedure applies to measurement with also, at minimum, an aged catalytic converter. To ensure compliance in the In-Service Conformity with Euro 6/VI, US EPA and California ARB [4] demand that PEMS testing is performed on randomly selected series vehicles. Additionally, for Euro VI (heavy-duty), PEMS measurement has also been required with a similar principle as RDE. China VI for heavy-duty has similar requirements with minor differences in the measurement protocol.

As a next step in evolution, regulations have demanded additional means above adding PEMS equipment to have data on real-life emissions systems performance. The California ARB demands that data from the tailpipe NO_x sensor is sorted by engine load and then stored in the vehicle engine management system, readable by the OBDII scan tool. The California ARB can stop any random series vehicle on the road and read out the stored tailpipe NO_x data for analysis, therefore being able to read data from the history of that vehicle. China VI has a very similar requirement, except instead of long-term storage in the vehicle, the data is reported by telematics to a server of the Chinese authorities.

The latest evolution is the demand for OBM (On Board Monitoring) that is part of the proposals for Euro 7/VII [5]. Other than storing data from tailpipe sensors as California and China [6] are demanding, the Euro 7/VII proposal demands a diagnostic in the vehicle software that will trigger a warning to the driver if tailpipe emissions (averaged over a certain driving distance which is still to be defined by legislation) have exceeded a threshold limit. Firstly the tailpipe emission data collection by NO_x sensors will be obligatory. The other sensors are to follow.

Tailpipe monitoring of consumer vehicles serves two purposes:

- Detection of design flaws of the released system. If a significant number of field reports surpass the emission limits, the design was not robust enough, and the manufacturer will have to improve it. The design needs to consider all conditions during vehicle usage and its exploitation up to aging and mileage limit.
- Detection of emission failure of individual vehicles. Regardless if there is a single point failure or combination of parameter drift resulting in violation of thresholds- it will be detected, and the owner will be prompt-

ed. As a result, the owner will have to replace components or drivetrain until the limits are reached again or alternatively purchase a different vehicle.

The practical consequence of new Euro 7 with on-board monitoring design is compared in Table 1.

Table 1. Comparison of analysis depth required for Euro6 and 7 norms

Norm/analysis of the effect on emissions:	Euro 6/VI with OBD	Euro 7/VII with OBM
Aging	Emissions achieved for type approval only with aged catalyst system and mildly aged overall for in service conformity.	Emissions achieved with actual aging overall is monitored for every vehicle for the whole lifetime
Tolerances	Mostly limited to production tolerances (aging = 0)	Production and aging
Failure modes	Norm defined Single point failure/deviation	Multi-point cumulative failures/deviations
Diagnostic capabilities	Only norm defined elements have to be diagnosed	Diagnostic capability over all relevant components of a system- to allow identification and replacement of problematic element

To achieve the required depth of system analysis and reach design goals required with Euro 7 OBM norm, one needs to incorporate a structured design and analysis method. To fulfill the OBM while still offering pinpointing of the root cause, it is also necessary to have a system wide approach to Emission Diagnostics and not a Component or Subsystem Approach as used nowadays in the industry. A structured methodological approach is also recommended as the need for comprehensive knowledge to overlook the complete Emission Reduction System to the detail can only be found in a few Specialists. To assist these experts and enable other engineers to design a comprehensive and complete Emission Reduction System, we suggest using the well-established lifecycle, design, and analysis methods from Functional Safety.

Both Functional Safety/SOTIF and OBD domains have established methods that are fit for this purpose:

– FUSA/SOTIF:
  - Determining safety goals on vehicle level and propagating them down to individual system components, including performance criteria.
  - Comprehensive failure/deviation analysis methods: HARA, FMEA, FTA, FMEDA.
  - Introduce OBD lifecycle based on safety lifecycle of the project;
– OBD
  - Analysis of tolerances combinations and aging effects.

The paper aims to show that mentioned methods are fit for emission domain and emission system development compliant to Euro 7 OBD norm.

2. Method

To show the stated thesis, a simplified model of the emission system is used. The methodology bases on the proven in-use safety lifecycle defined in ISO 26262:2 is used [7].

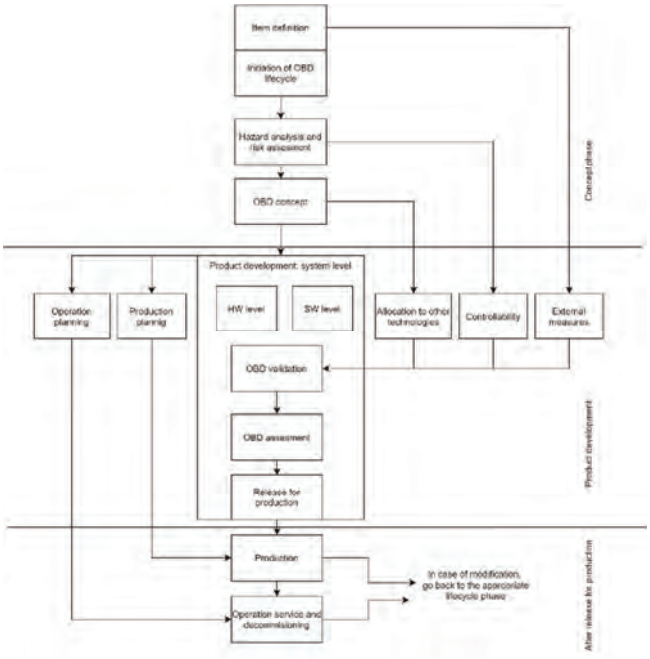

Fig. 1. OBD OBM lifecycle based on FuSa lifecycle [7]

The proposed OBD/OBM lifecycle consists of several steps that ensure systematic analysis of an item and provide argumentation for analysis completeness. The top-down approach is the most straightforward way to ensure complete NO_x supervision. In severe cases of lawsuits, it provides proof of reasonable effort taken to minimize potential risks.

– Item definition:

The very first step to conduct is to define the subject of the analysis. The scope is called an Item. The item is defined by a set of high-level functions, boundaries, interfaces, assumptions, working conditions, and other environmental influences necessary to have a strict description of the item in question. The description shall be comprehensive in the way that the Items function is well understood

– Hazard analysis and risk assessment(HARA):

The HARA procedure consists of defining potential hazards that an item can pose to the user or environment. The identified (emissions compliance) hazards are then evaluated in terms of probability, controllability, and severity. Combining those three numbers (usually rated on a scale of 1–10), one can judge the required emission integrity level (EMIL). Emission Integrity levels span from EMIL 1 to 5 grades. At EMIL 1, there is no or too little impact on emissions and the system so, unless spelled out in the regulation, no OBD monitor is needed. At EMIL 5, there is a potential HW or Mechanical redesign in order. With each EMIL level, there is more care and more amount of analysis and redundancy required. Based on such assessment, the emission goals (EG) are formulated based on hazards. The EGs inherit the required emission integrity level (EMI) from HARA analysis.

– OBD concept:

With the knowledge from previous steps, the OBD concept is developed considering the preliminary architecture of an item. The requirements derived from emission goals are allocated to the elements of the system. The OBM concept is also added here, although that is a given from the regulation. At this level, FMEA analyses are performed on the Function and Interface level.

– Product development at the system level:

In this phase, the system is designed according to the OBD concept and other functional requirements. Also, demands following from the effect of the OBM concept on the system are taken into the design. This step may include external solutions that are out of item boundary. The system architecture and technical requirements are specified. The technical assumptions, human behavior assumptions and hazard assumptions are also validated during this phase. HSI, which is the HW-SW interface, needs to be defined at this stage as well.

– Product development at the hardware and software level:

Inheriting from system design and requirements, the HW and SW detailed design and implementation are conducted. This phase also includes testing and validation on the corresponding level of detail. FMEA analysis is repeated or extended here but at HW/SW level.

– Production, operation, service, and decommissioning:

This part of the process runs parallelly, starting with product development on the system level, ending at the SOP (start of production) date.

Tied into this is the type approval and in service conformity preparation, which includes a dry-run test before actual approval and in-service conformity.

The process part aims to define unique characteristics of the item that are relevant for emission. This includes production repeatability, tolerances, calibration, End Of Line (EOL) tests. Additionally, operation and service instructions and unique characteristics have to be defined as well as decommissioning of faulty or worn out parts.

Most of the mentioned steps will be illustrated based on the proposed exemplary system. The development on HW/SW level and testing will be briefly mentioned due to the demonstrative character of the analysis for which detailed HW/SW solution is not relevant.

In the following chapters, we will apply the methodology to an exemplary system.

3. Example

The chosen system is based on a medium-duty diesel engine emission control system intended for Euro 6d_final/Euro 7 or Euro VI_e/Euro VII norm. Only NO_x emissions will be analysed. The turbocharger section is cut out for clarity. The system consists of two EGR loops for High and Low pressure, two urea dosers with supply, and a series of catalytic converters, including DOC, SDPF, SCR, and AMOX converter. Additionally, the system has several temperature, pressure NO_x and NH_3 sensors.

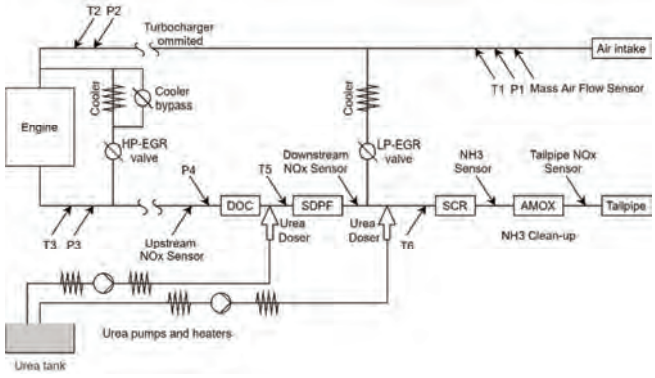

Fig. 2. Medium-duty diesel engine emission control system

3.1. System(item) definition

In the item definition, one needs to define a boundary that separates the system under consideration from the outside world. In our case, it contains engine, intake, and exhaust pipe. Consequently, the interface, which means flows or signals crossing the boundary, is air intake, tailpipe and heat exchange with the surroundings. In this example, we also do not consider the fuel system to simplify the example furtherly.

As this article is a demonstration example, we will only analyse parts relevant for NO_x control.

3.2. System(item) main function

The identification of system main function occurs on abstract level. One shall not consider the technical realisation of the system but its purpose. The system function in our case is to reduce NO_x emission.

3.3. Emission goal definition

According to the methodology of the OBD lifecycle, one should run a HARA analysis over the functionality of the emission reduction system to determine the emission goals. In this example, however, we simplify this step by using the emission goal defined in Euro 7/VII proposals [5].

Table 2. Emission goals

Emission goal ID	Emission goal
EG 1	The system NO_x emission shall not exceed the limit value of X [g/km] over the averaging window of Y km.

3.4. System elements

To analyse potential failures main functions of system elements need to be defined.

Table 3. System elements sub-functions

System element	**Sub-function**
HP-EGR loop	Increase inert gas in combustion chamber
LP-EGR loop	Increase inert gas in combustion chamber
SCR	Neutralize NO_x into harmless components
SDPF	Neutralize NO_x into harmless components shortly after cold start
AMOX	Neutralise NH_3 particles
DOC	Oxidise leftover hydrocarbons, HO and PM
Urea tank	Stores ammonia

Table 3cont.

Sensors	**Sub-function**
AMF	Provides feedback for EGR loop.
Upstream NO_x	Measure NO_x coming from engine
Downstream NO_x	Measure NO_x coming from engine
NH_3	Measure NH_3 level
Exhaust NO_x	Provides final feedback on NO_x elimination efficiency
T1, P1	Provides temp and pressure of incoming air
T2, P2	Provides pressure and temp of gas entering the engine from turbocharger
T3, P3	Provides temperature and pressure of exhaust gases directly at the exhaust manifold.
P4	Provides pressure at the entrance of catalytic chain
T5	Provides gas temperature at the entrance of SDPF
T6	Provides gas temperature at the entrance of SCR
Actuators	**Sub-function**
H-EGR valve	Controls recirculation rate of HP EGR
L-EGR valve	Controls recirculation rate of HP EGR
H-EGR cooler	Controls cooling power of HP-EGR loop
L-EGR cooler	Controls cooling power of HP-EGR loop
Urea Dosers	Controls urea dosing rates
Urea Heaters	Heat the urea to prevent freezing
Urea Pumps	Provide pressure for urea installation

4. OBD concept

4.1. System analysis

The next step is to take exemplary elements and analyse them according to standard failure modes and their effects (FMEA):

Table 4. FMEA of SCR element, function neutralise NO_x

FM ID	Failure mode	Failure Mechanism	Potential Effect
1	Too Long	SCR too cool	Excessive NO_x emissions
2	Too Short	SCR too hot	Faster Aging, Excessive NO_x emissions
3	Too Slow Response	Urea doser underperformance	Excessive NO_x emissions
4	Too Fast Response	Urea doser overperformance	Excessive NH_3
5	Reverse	No effect	No effect
6	Intermittent	Urea doser malfunction/ mixer malfunction	Excessive NO_x emissions
7	Fluctuating	Urea doser malfunction/ mixer malfunction	Excessive NO_x emissions
8	No	SCR clogged	Loss of power
9	Less	SCR coating covered/aged	Excessive NO_x emissions
10	More	No effect	No effect
11	Follow Command with Different Outcome	Urea doser malfunction/ mixer malfunction	Excessive NO_x
12	Follow Command with the same outcome by accident	Urea doser has lower max efficiency than design, but the engine has a low load.	No effect
13	As Well As	NH_3 spillage	Excessive NH_3

Table 5. FMEA of H-EGR valve element, function: controls recirculation rate of HP EGR

FM ID	Failure mode	Failure Mechanism	Potential Effect
14	Too Long	see slow response	No effect
15	Too Short	see slow/fast response	No effect
16	Too Slow Response	slow-moving valve (high resistance)	In transients, the EGR mass flow stays behind
17	Too Fast Response	No effect	No effect
18	Reverse	Incorrect connection/wiring	EGR mass flow is uncontrollable
19	Intermittent	high resistance in moving (PID is struggling) / command transfer is interrupted	In transients, the EGR mass flow stays behind
20	Fluctuating	high resistance in moving (PID is struggling)	In transients, the EGR mass flow stays behind
21	No	valve is stuck in a closed position	EGR mass flow is uncontrollable
22	Less	valve is stuck/blocked below the target/blockage in flow/leakage to ambient	EGR mass flow is less than the target
23	More	valve is stuck/blocked above the target	EGR mass flow is more than the target
24	Follow Command with Different Outcome	Any of the above	EGR mass flow deviated from the target
25	Follow Command with the same outcome by accident	Any of the above	NOTE: If no transient is commanded; if low EGR is requested or high EGR is requested – any of the above failures can be hidden (latent)
26	As Well As	Any of the above	Any leakage or blockage will also impact the pressure to the intake of the turbine

Table 6. FMEA of upstream NO_x sensor element, function: measure NO_x upstream

FM ID	Failure mode	Failure Mechanism	Potential Effect
27	Too Long	No effect	No effect
28	Too Short	No effect	No effect
29	Too Slow Response	deposits on sensor	Too little urea added, L-EGR malcontrol
30	Too Fast Response	noise	Wrong amount of urea
31	Reverse	Wrong value	Excessive NO_x emissions + clogging of ECR
32	Intermittent	Loose wiring	Wrong amount of urea
33	Fluctuating	EMC noise	Wrong amount of urea
34	No	Connection lose	Lack of feedback – Excessive NO_x emissions or clogging of catalysts

Table 6cont.

35	Less	Deposits on sensor	Too little recirculation and amount of urea clogging of catalysts – too big emissions
36	More	To thin wiring	Too significant recirculation, too much urea, clogging of catalysts
37	Follow Command with Different Outcome	No effect	
38	Follow Command with the same outcome by accident	No effect	
39	As Well As	No effect	

Beyond an FMEA (bottom-up), an FTA (top-down) is performed to have evidence of completeness and better insight into relations between failure modes.

With the SCR system, most failure modes lead to excessive NO_x emissions. FM ID 4 and 13 are the exemption as they cause excessive NH_3, but for these situations, the AMOX catalyst is still in place to break down the NH_3. FM ID 12 is a particular case; there can be Excessive NO_x emissions, but current engine out NO_x production is (e.g. due to low load) low enough that the failure mode is not currently violated. In ISO 26262, such a failure is called a Latent failure. This also forms an issue in OBD and OBM, despite previously not having a defined name for it.

The Function FMEA is, in principle, valid for both SDPF and the downstream SCR. There is a difference, however. The SDPF is more exposed to high temperatures and is critical to being operational at the lowest possible temperature following a cold start. Also, it is affected first by any substances from the engine combustion, including substances that can lead to poisoning and coverage of the coating. Should the SDPF fail, however, the downstream SCR is to a certain degree capable of compensating. Therefore, the failure modes are the same, but how they occur and the exact emissions effect they have is deviating between SDPF and downstream SCR.

In the EGR function FMEA, the failure modes correspond to the incorrectness of EGR mass flow. A too low or late EGR mass flow leads to a too-small level of inert gas in the combustion chamber, resulting in increased engine-out NO_x. Too much or too early affects the combustion stability or performance due to an excessive amount of inert gas in the combustion chamber. An EGR failure leading to an increased level of engine-out NO_x does have the benefit that SDPF and SCR can reduce some of the excess NO_x within their abilities. However, a counter effect is that some of the excess NO_x is returned to the intake side via the LP-EGR. A special note is to FM ID 22 and 26 to point out that EGR failures that are leakage or a blockage affect the turbocharger setup. This effect can disturb intake air mass availability to the combustion chamber and enhance the effect. The FM IDs 16, 19, 20, and 25 are all connected to transient operation. In theory, an engine could be operated in steady-state and/or mild transients only, hiding the failure mode of EGR. As previously stated, there is a risk for a latent fault. However, the chances are less as the transient operation does occur in both emissions test cycles and real-life vehicle operations.

The upstream NO_x sensor has a very different Function FMEA in respect to its role. Sensors in themselves are less relevant, but their incorrect reporting of measurements is disturbing the control systems. The upstream NO_x sensor is, just as the middle NO_x sensor, the main parameter for the SCR control of SDPF and SCR, respectively. Their failures disturb the reduction of NO_x.

After discussing the Fault Modes found by the FMEA, an example set of Fault Modes is selected for the further demonstration of the methodology.

In the previous approach of OBD, there was the possibility to discard some of the failure modes as not relevant for the Emission Goal. These failure modes would not be capable of pushing NO_x tailpipe emission above the limit. The OBM approach does not allow this anymore, and all fault modes need to be discussed. While it is still true that some failures on their own would not be able to push tailpipe NO_x over the limit, they would be able to do so in combination. As in this paper, the space is too limited for a complete discussion, a representative set of fault modes is chosen to proceed with the example.

With that, the following is chosen:

OBD: One SCR with reduced efficiency due to coating coverage FM ID 9 that has reached a point where, despite possible compensation of, e.g., downstream SCR, the tailpipe NO_x over an emissions cycle has reached the OBD limit.

OBM 1: An amount of SDPF reduced efficiency due to coating coverage FM ID19. As the failure mode of coating coverage originates from a foreign substance or engine oil, in reality, the SDPF will be affected, but to a lesser degree, the SCR downstream will have reduced efficiency due to coating coverage. In addition, the NO_x sensors upstream of each SCR will be affected as well, which is causing them to fail as slow response (FM ID 29). These effects together reach a tailpipe NO_x value over an average time of driving that exceeds the limit.

OBM 2: The entire NO_x system under consideration has suffered from aging. The EGR systems both suffer from a small level of soot buildup (FM 22 in a minimal degree), both SCRs suffer from the aged coating and aged urea dosers (FM ID 3 and 9), and finally, the sensors have also suffered from age effects (FM ID 29 and 35). None of these deviations on its own is a reason for concern but all combined, they reach tailpipe NO_x value over an average time of driving that exceeds the limit.

The next step is to create OBD and OBM concepts based on the chosen set of fault modes.

4.2. Creating the OBD and OBM concept

For SCR, a common approach is to compare the NO_x sensor upstream and NO_x sensor readings downstream of the concerning SCR, possibly corrected or performed by NH_3 sensor readings. The OBD concept would take the SCR failure at the NO_x OBD limit on the emissions cycle and then develop a concept to detect that specific SCR with that specific failure level. As such approaches are common

in the industry and covered by literature [8], further details are not added.

To extend OBD into the OBM world, one needs to also take into account multi-point faults. This is further split into two classes: this class of faults is characterized by the fact that each fault does not violate the emission goal solely, but the sum of the faults does.

1. Dependent faults
   One fault directly leads to another fault which in turn causes a direct violation of the emission goal.
2. Independent faults
   Statistically independent random faults that combined cause emission goal violation.

The way to proceed is to define abstract failure levels first. One can consider that process a fuzzy logic membership function assignment on an abstract level. Please note that at this stage of analysis, the membership function does not have strict physical meaning. One has to assume normalization of failure level: 0% is the part that runs perfectly, 100% is the part that has failed completely. Then let the normalised deviation be divided into 3 classes: 30%, 60%, 100% where class 30% means the number is less or equal 30%, class 60% is 31–60% and so forth [9]. With this step, we discretize the spectrum so that it is possible to conduct predicate reasoning on clauses [10]. As the next step, the table with combinations of discretized failure levels of elements is constructed according to mentioned OBM. Let the given discrete deviation level be called symptom after Isermann et al. [11].

Table 7. Discretised failure combinations- symptoms and failure judgement, EG violation judgement

Element	30%	60%	100%	Judgement	EG violation
SDPF	1	0	0	normal uniform wear	0
SCR	1	0	0		
SDPF	1	0	0	Accelerated SCR wear – LP-EGR underperformance	0
SCR	0	1	0		
SDPF	1	0	0	SCR Single point failure	1
SCR	0	0	1		
SDPF	0	1	0	Early stage oil contamination	0
SCR	1	0	0		
SDPF	0	1	0	Uniform wear	0
SCR	0	1	0		
SDPF	0	1	0	LP-EGR underperformance	1
SCR	0	0	1		
SDPF	0	0	1	SDPF Single point failure	1
SCR	1	0	0		
SDPF	0	0	1	Late stage oil contamination	1
SCR	0	1	0		
SDPF	0	0	1	Uniform wear	1
SCR	0	0	1		

As can be noticed, the table will grow exponentially with an increased number of elements and failure stages. However, such a bottom-to-top approach ensures analysis of all possible combinations. As a result of analysis, one can be sure which parts of the system have to be supervised either directly or monitored by combining several measurements.

Additionally such structure can be directly converted into set of logical sentences – IF <clause 1> AND <clause2> …<clause N> THEN <Judgement> which are easily implementable in SW. The next step is to design emission monitoring mechanisms that will give the physical base to the abstract statements of failure stages.

The regulator gives the OBM concept. It must be detected when tailpipe NO_x as averaged over a specific driving distance/condition exceeds the limit, regardless of what caused it.

However, if the OBM triggers due to e.g. the late stage oil contamination as in OBM 1 a parallel detection is needed, informing the symptoms of what is wrong and where the effort for repair must go. Our example would be a turbo oil seal or a piston oil ring combined with the SPDF and SCR. This diagnostic must reproduce the OBM result, but with information on the root cause.

In the simplified form, the SCR efficiency is expressed in a ratio of measured NO_x upstream of the SCR and measured NO_x downstream of the SCR. Dynamic effects and NH_3 effects on the sensors are significant disturbances in this monitor, but for the sake of simplicity, these are considered to be captured by averaging for this explanation. Typical SCR OBD algorithms used in today's vehicles use averaging over 60 minutes or more of driving. We will define a perfectly healthy SCR here as one that removes 100% of expected NO_x and 0% failing if the removal is at 98% level. A 30% failing we will define as 94% removal. The 60% failing at 90% removal and 100% failing at 86% removed NO_x or worse.

Restricting to oil contamination, this means:

1. IF SDPF efficiency is 93–90% efficiency AND SCR efficiency is 100–94%, THEN do nothing
2. IF SDPF efficiency is 89% or less AND SCR efficiency is 93–90%, THEN store fault code information that oil or other foreign substance has covered the SCR coating and point towards the relevant repair procedure. Note that the driver likely comes to the workshop with the OBM warning activated.
3. IF SDPF efficiency is 100–94% AND SCR efficiency is 89% or less, THEN store fault code information that single source failure has affected the SCR and point towards the relevant repair procedure. Note that the driver likely comes to the workshop with the OBM warning activated.
4. Etc.

4.3. Realization of the concept

Difference between OBM and OBD

With OBD, the development activities focus on the concept definition of a diagnostic. This diagnostic involves sensors to measure those parameters that indicate the single failure mode that needs to be found. Once the diagnostic concept is created, the concept must also be verified against tolerances within this sensor-to-failure mode relation and the risk for Type I and Type II errors, where Type I is a false alarm and Type II is a genuine error that is not detected [12].

With OBM, the diagnostic is given by the regulator. Here the focus lies very differently because the OEM has

the interest to ensure that failure modes are detected not only by the OBM monitor but also by own diagnostics that ensure efficient repair is possible. This implies that the existing OBD must be in place. However, in addition, a collection of multiple small failures but with a common source (OBM 1: common source is foreign substances or oil) are detected. A big delta to OBD is here that the failure modes of each individual contributing emissions system (EGR, SCR, etc.) are far smaller than in the case of pure single fault OBD. The more minor effects emphasize the issues of sensor tolerances and aging. It needs to be ensured that aging and drift, together with other noise factors, can be distinguished from the actual sensor signal.

In the situation of OBM 2, there is an added complexity. Even though none of the components or systems may be perceived to be having a failure mode, the sum is still enough to trigger tailpipe NO_x limits. Here, an OEM is interested in ensuring that this situation only occurs after at least the minimum mileage and vehicle age for emissions durability (full useful life) have been passed. For consumer satisfaction, however, likely a higher mileage or vehicle age target is demanded.

Allocation

With OBD, the allocation is a non-complicated matter. The SCR diagnostic to detect the single point fault has to be allocated to the SCR software. In that ECU or software section, the correct information is available at the correct accuracy and sample rate.

With the OBM 1 example, the situation becomes more complex. The symptom analysis, however, will help significantly. The symptoms analysis will first remove any combinations of failure modes that are irrelevant or physically impossible. It will highlight those that have a common failure mode.

With OBM 1, the deviation that each part can have due to aging is now defined. In traditional emissions control, this is defined by the aging done to demonstrate the durability of the emissions system on the emissions cycle. In the case of OBM, however, there must be a safety margin added as not every vehicle will age each component the same. Some vehicle will have increased EGR soot loading while other will have more SCR coating aging. The target for the OEM is to define an allowable aging deviation per component.

Analysis of the implementation

To analyse the implementation for OBD, a tolerance investigation is required. This can be based on computational simulation, vehicle measurements, or a mixture of both. The systems Type I and Type II errors need to be defined

For the OBM 1 situation, the approach is the same. Each diagnostic that detects the individual elements and that feeds into the symptom analysis can be wrong by itself with Type I and Type II error,

For the OBM 2, the verification requires a Monte Carlo simulation or other identification algorithms [13, 14]. As is known to be done based on new component tolerances, it is verified by the simulation what the chances are of a tolerance combination that can lead to tailpipe NO_x exceedance. Should this be the case, then either 1) the specific combination of tolerances is considered rare enough to be acceptable, 2) the specific combination of tolerances is made impossible, or 3) the tolerances that are most dominating in the analysis are reduced by demanding or developing elements with stricter tolerances. This approach is for OBM 2 repeated, however, with those tolerance deviations added caused by aging.

While practical experience with OBD has shown that starting later in the vehicle development cycle with designing OBD can sometimes result in challenges (e.g., sensor types and positions that have already been determined despite being sub-optimal for OBD) with OBM, this is a far more significant concern. If a component is chosen that has in certain situations aging to the point it would reach the OBM level, then every vehicle that is exposed to said situation would trigger an OBM warning. For an OEM to reach the demanded and internal targets, this may mean that said component cannot be used. Such information must be available as early as possible in the development cycle.

4.4. Integration and test

When applied for safety engineering, the safety methodologies can result in SW implementation of algorithms, failure rate (FIT) rate demands on hardware components, tolerance demands on mechanical components, and even redundancy in design. Also, they can demand testing from unit tests up to vehicle validation.

With OBD, this situation existed to a minor degree as apart from demanding sensors for measurements, OBD did not directly affect the hardware. Tolerances are a concern with OBD and may, at times, demand changes. Failure rates, however, are of no concern in OBD development.

OBM does take even the last step and does include failure rates, especially where it concerns aging effects that can trigger before the emissions durability or warranty term is passed. Despite the integration work and testing as demanded for OBD, for OBM, specific testing and/or simulation work is required in establishing the failure rate.

5. Conclusions

In order to fulfill the complex requirements of diagnostics development in the age of OBM new methods have to be introduced in the field. A lifecycle approach based on functional safety was proposed and described for emission system case. With a simplified system example the processes and analysis methods that make up the lifecycle were demonstrated. Each step of the lifecycle was either described or partly analysed in order to prove that the methods are fit for purpose. In authors opinion, the example and outcomes prove that such a systematic approach can handle the complexity of OBD development in the OBM environment providing additional benefits such as argumentation of completeness.

Nomenclature

AMOX	ammonia oxidation catalyst
CARB	California Air Resource Board
DOC	diesel oxidation catalyst
ECU	electronic control unit
EG	emission goal
EGR	exhaust gas recirculation
EMIL	emission integrity level
FIT	failure in time (per 10^9 hours)
FM	fault mode
FMEA	fault mode effect analysis
FMEDA	failure mode effects and diagnostic analysis
FTA	fault tree analysis
FuSa	functional safety
HARA	hazard analysis and risk assessment
HW	hardware
OBD	on board diagnostic
OBM	on board monitoring
OEM	original equipment manufacturer- car producer
PEMS	portable emission monitoring system
RDE	real driving emission
SCR	selective catalytic reductor
SDPF	SCR-catalysed diesel particle filter
SOTIF	safety of intended functionality
SW	software

Bibliography

[1] SASAKI, T. How the Japanese accelerated new car development. *Long Range Planning*. 1991, **24**(1), 15-25. https://doi.org/10.1016/0024-6301(91)90020-O

[2] VESTRENG, V., NTZIACHRISTOS, L., SEMB, A. et al. Evolution of NO_x emissions in Europe with focus on road transport control measures. *Atmospheric Chemistry and Physics*. 2009, **9**(4), 1503-1520. https://doi.org/10.5194/ACP-9-1503-2009

[3] Commission Regulation (EU) 2016/646 of 20 April 2016 amending Regulation (EC) No 692/2008 as regards emissions from light passenger and commercial vehicles (Euro 6) (Text with EEA relevance). *European Commission*. http://data.europa.eu/eli/reg/2016/646/oj

[4] Final Regulation Order for HD OBD II Regulation § 1968.2 Malfunction and Diagnostic System Requirements 2004 and Subsequent Model-Year Passenger Cars, Light-Duty Trucks, and Medium-Duty Vehicles and Engines. *California Air Resource Board* 2019.

[5] DILARA, P. The future of clean cars in Europe: EU Green Deal and EURO 7. *Sino-EU Workshop on New Emissions Standards and Regulations for Motor Vehicles* 2021. https://ec.europa.eu/jrc/sites/default/files/the_future_of_clean_cars_in_europe_eu_green_deal_and_euro_7.pdf

[6] WANG, J. China's next phase of automobile emission standards. *Sino-EU Workshop on New Emissions Standards and Regulations for Motor Vehicles* 2021. https://ec.europa.eu/jrc/en/science-update/sino-eu-workshop-presentations

[7] ISO 26262-2:2018 Road vehicles – Functional safety – Part 2: Management of functional safety. https://www.iso.org/standard/68384.html (accessed on 16.07. 2021).

[8] DE OLIVEIRA COSTA, L., ROSSIN, F. Optimizing the on board diagnostic system (OBD) to monitor for reduction of the SCR catalyst conversion efficiency using the NO_x sensor. *SAE Technical Paper* 2010-36-0198. 2010. https://doi.org/10.4271/2010-36-0198

[9] GU, Y., LI, J. Multi-state system reliability: a new and systematic review. *Procedia Engineering*. 2012, **29**, 531-536. https://doi.org/10.1016/J.PROENG.2011.12.756

[10] GELGELE, H.L., WANG, K. An expert system for engine fault diagnosis: development and application. *Journal of Intelligent Manufacturing*. 1998, **9**, 539-545. https://doi.org/10.1023/A:1008888219539

[11] ISERMANN, R. Supervision FDD methods – an introduction. *Control Engineering Practice*. 1997, **5**(5), 639-652. https://doi.org/10.1016/S0967-0661(97)00046-4

[12] GRAVES, S., BISGAARD, S., KULAHCI, M. et al. Accelerated testing of on-board diagnostics. *Quality and Reliability Engineering International*. 2007, **23**, 189-201. https://doi.org/10.1002/QRE.784

[13] DANTAN, J.-Y., QURESHI, A.-J. Worst-case and statistical tolerance analysis based on quantified constraint satisfaction problems and Monte Carlo simulation. *Computer-Aided Design*. 2009, **41**(1), 1-12. https://doi.org/10.1016/J.CAD.2008.11.003

[14] NIGAM, S.D., TURNER, J.U. Review of statistical approaches to tolerance analysis. *Computer-Aided Design*. 1995, **27**(1), 6-15. https://doi.org/10.1016/0010-4485(95)90748-5

Mateusz Kmieć, MEng. – Roben Automotive Poland.
e-mail: *mateusz.kmiec@roben-automotive.com*

Matthias Weber, Dipl.-Ing. – Roben Automotive Poland.
e-mail: *matthias.weber@roben-automotive.com*

Marcel Romijn, Dipl.-Ing. – Roben Automotive Netherlands.
e-mail: *marcel.romojn@roben-automotive.com*

Dave Matthews, MSc. – Roben Automotive USA.
e-mail: *dave.matthews@roben-automotive.com*

Article citation info:
SROKA, Z., PRAKASH, S., WLOSTOWSKI, R. Design of the turbocharger bearing arrangement to increase the overall efficiency of the combustion engine. *Combustion Engines*. 2022, **188**(1), 83-89. https://doi.org/10.19206/CE-142348

Zbigniew SROKA
Srinath PRAKASH
Radoslaw WLOSTOWSKI

Combustion Engines
Polish Scientific Society of Combustion Engines

Design of the turbocharger bearing arrangement to increase the overall efficiency of the combustion engine

ARTICLE INFO

Received: 27 July 2021
Revised: 16 September 2021
Accepted: 16 September 2021
Available online: 20 September 2021

The main objective of this study was to design a journal bearing, such that it can withstand the forces that arise in context to increasing the length of the shaft in an automotive turbocharger. The work will also provide information on how the design changes affect the overall performance of the bearing. The design changes include the thickness of the oil film, the number of grooves, the dimension of the grooves, the number of inlets and outlets, the dimension of the babbitt and mainly the length of the journal bearing. The simulation models were created using CATIA V5 and the analysis is done using ANSYS 19.2. The flow is considered to be laminar and is calculated using Reynold's Equation. The new concept gave insight on how the design considerations affect the pressure distribution and the pressure developed. From the results, it was interpreted that the new design can withstand the four times the pressure while distributing the pressure over twice the original design.

Key words: *turbocharger, journal bearing, design, simulation*

1. Introduction

The development of internal combustion engine has led to the discovery of new components which improve not only the power but the emission also. The thirst for power paved the way for the construction of turbochargers. Turbocharging has now become a very popular way of increasing the power output of internal combustion engines. This simple and compact piece of machinery is typically imparting a boost of 0.4 to 0.6 bar.

The turbocharger became popular due to fact they are light weight power packs, which not only improve the power but the emissions as well. But the turbocharger on its own is not that efficient. To increase the efficiency, intercoolers were provided to improve the density of air that is compressed using the turbocharger. The high operating temperature of a turbocharger causes the air to expand after compression [20]. The level of expansion determines the size of the intercoolers required. The increase in the temperature of the inlet gases, also increases the NO_x emissions due to peak in-cylinder temperatures [12]. The longer length of the exhaust system also tends to increase the pressure loss in the system. The longer exhaust system also increases the turbo-lag which is a primary concern in turbocharging.

The turbochargers are considered to be very inefficient at low speeds, which increases the turbo-lag. There is also a heat transfer from the turbine to the bearings, which causes damages due change in mechanical properties of the bearings [5, 15]. The oil properties are also varied extensively since it has been proved that the oil takes out about 30% of heat from the turbines [8, 20]. The insulation of the turbine is a solution which has been widely used to decrease the heat transfer between turbocharger components [18].

A solution to some of these problems were found out by Mercedes in the Formula-1 endeavours, as they introduced the first split turbocharger engine. The splitting of the turbine (hot) and the cold (compressor) side was done to reduce the heat interactions of the high temperate gases from the exhaust to the inlet air. This in turn helps in decreasing the exhaust system length. The split turbocharger system contains a longer shaft which increases the separation between the hot and cold side. The shaft is supported by a special bearing system, which sustains the load of the shaft which rotates by 50,000–250,000 rpm. The longer shaft also has given a possibility of introducing a special energy recovery system called MGU-H (Motor Generation Unit–Heat).

2. Turbocharger bearing systems

The arrangement of the bearings is based on where the turbocharger is installed and used. The regularly used arrangement of the bearings are in between the turbines as shown in Fig. 1A. This configuration makes it easier to supply oil, since all the housings are separated. The bearing access is provided by removing the turbine housing. The (B – Fig. 1) configuration decreases the need for a long shaft, thus decreases vibration and forces produced by the shaft. But the configuration also increases the problem of introducing a more complex lubrication system. The layout of the bearing system (C – Fig. 1) causes a large heat transfer between the turbines, which decreases the density of the compressed air [2, 14].

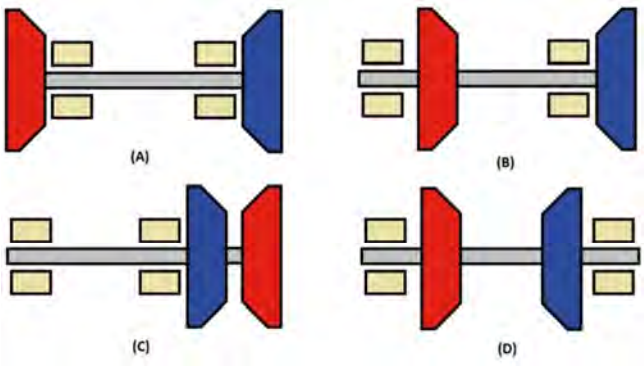

Fig. 1. The different bearing arrangements in a turbocharger [19]

The advantage of this configuration is the separation of the gases system and the lubrication system. The turbochargers used in marine or large-scale application uses the (D – Fig. 1) configuration. This configuration enables easy maintenance options, but the bearing capacity at high speeds are decreased.

3. Research methodology

This publication presents the results of design works of new slide bearing solutions. The research methodology was based on the characteristics of the oil film which, through the required pressure, can support the shaft. The starting point was standard bearing journal designs from one of the automotive turbochargers. The design changes included the thickness of the oil film, the number of grooves, the dimension of the grooves, the number of inlets and outlets, the dimension of the babbitt and mainly the length of the journal bearing.

The simulation models were created using CATIA V5 and the analysis is done using ANSYS 19.2 – education version [1]. The flow was considered to be laminar and was calculated using Reynold's Equation.

The journal bearings were designed to support the longer shaft, with pressures exceeding the twice the existing condition. The design concepts focused on decreasing the efficiency losses by improving rotor dynamic stability and pressure distribution [10, 24]. The journal bearings were designed in two parts, journal and the steel backing. Each of the parts were designed individually and were analyzed to understand more about how the parts work separately. The forces acting on the oil film were only radial forces. The same radial forces were administered on the face of the babbitt and the steel backing of journal bearing. The frictional forces or the axial forces were not considered here, since axial forces were supported by the thrust bearing and absence of the shaft nullifies the frictional force.

The bearing analysis was only considered for the inner oil film and whether the new design can sustain the pressure of oil film, even though the journal bearing used for the analysis is a fully floating bearing. The data which was experimentally found was used to estimate the pressure output of the oil film. The assumptions which were taken are as follows:

- the flow was considered to isoviscous [22],
- the pressure was taken as ambient,
- the outlet pressure was considered as zero,
- no external heat was added to the system,
- the property of the oil remained the same throughout the analysis,
- the oil was considered isotropic and incompressible [16].

The babbitt was designed such that the clearance between the babbitt and the shaft should produce the desired oil film. The babbitt was developed in 2 different dimensions, this was to test how the thickness of the babbitt influence the factor of design safety and deformations.

The final piece of the puzzle was the steel backing of the journal bearing. The dimension of this was decided by the thickness of the babbitt used. The steel backing was taken the shape of the outer surface of the babbitt to complement the stress distribution. Together with the babbitt and the steel backing, the whole design of journal bearing which produced the required oil film was completed.

The assumptions taken while using the methodology were, no lubricant flows in the axial direction, there is no eccentricity between the shaft and the bearing, and the oil film cannot support the load acting on it.

The research temperature ranges have been adopted from other publications [6, 13, 21] and were ranging from 310 K to 350 K. The viscosity of lubrication oil is termed to be a non-linear function in the range of 310–370 K [6]. In paper [21] states that the bearing temperature ranges from 290 K to 290 K during operation. Thus, it was assuming the case of 370 K as inlet temperature to avert any problems that may occur in the future. The inlet pressure was set 0.101325 MPa and velocity was 12.5 m/s during the initial setup [13]. The pressure under operating conditions reaches up to be 4.0 MPa at 60,000 rpm (based on the load acting). To support an excess load and excess pressure created, the journal bearings are to be designed for 12.0 MPa pressure and for a rpm of 200,000 to 250,000. Because it was very hard to have an overall good pressure distribution, the worst-case scenario was taken [17]. The oil is taken to have a density of 889 kg/m^3 and a dynamic viscosity of 1.06 kg/ms. This is the engine oil configuration used in ANSYS system. The specific heat of the oil is taken as 1845 J/kgK and the thermal conductivity is taken as 0.145 based on the literature [2, 21].

4. Model designing

The considered designs of oil films were introduced after different analysis which provided how the changes affect the pressure distribution. The one inlet design (Fig. 2) helps in reducing the complexity in production. This first design was simple, using one inlet around the circumference and using the periphery as the only outlets. Since the size of the outlet is small, the restriction for the flow was more hence the pressure increases significantly [3].

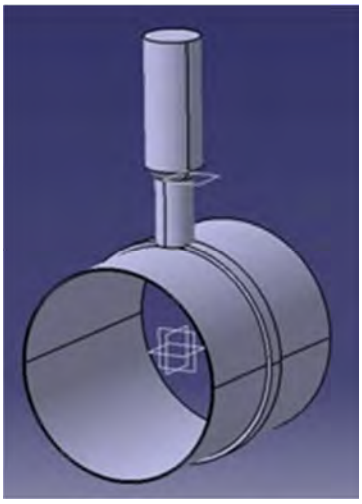

Fig. 2. Design of the oil film 1

The second model (Fig. 3) consists of 2 inlets and 2 outlets opposite to each other with a groove connecting them to regulate the flow of oil. The thickness of the oil film was reduced to by 25%.

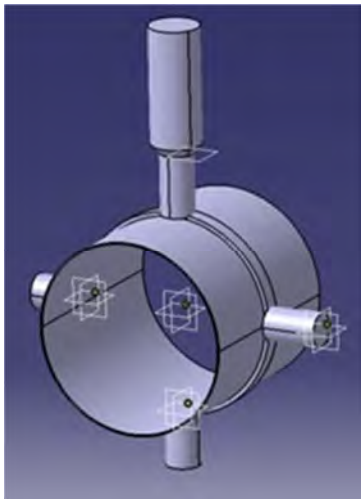

Fig. 3. Design of the oil film 2

The third oil film model (Fig. 4) consisted of 3 grooves instead of one, which was a design progression which was led by the previous analyses. The length of bearing was also increased from 12 mm to 20 mm.

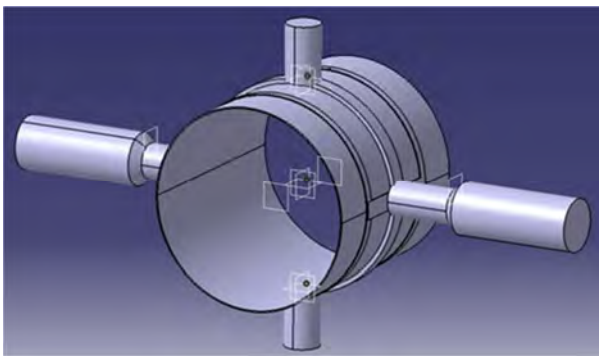

Fig. 4. Design of the oil film 3

The final design (Fig. 5) consists of 4 inlets and two outlets which are place perpendicular to each other. To incorporate the changes in pressure distribution due to increase in length, the inlets and outlets were modified.

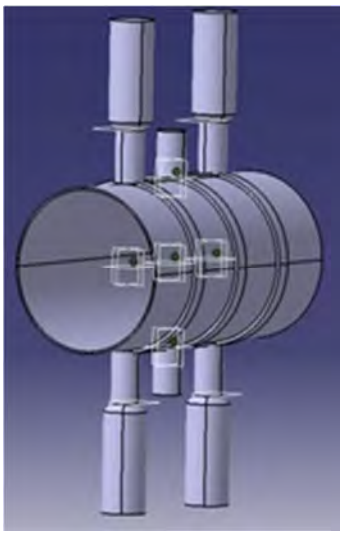

Fig. 5. Design of the oil film 4

The journal bearing (Fig. 6) was designed in according to last mentioned oil film design. The overlay is made in three thicknesses to check whether which thickness is suitable for the pressure distribution and oil flow. The three thicknesses where selected based on the data obtained on the commonly used thickness for the material. They are 100 µm, 50 µm, 35 µm and according to the thickness of the overlay, the thickness of the backing changes to reach the chosen diameter [23].

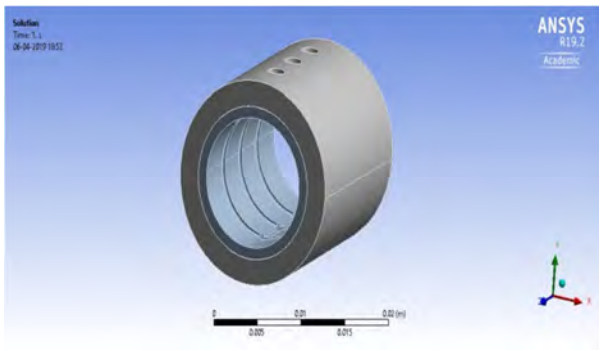

Fig. 6. Design of the bearing 1 (1 mm)

5. Data and results analysis

5.1. Computation

The simulation was done using the CFD/FEM software ANSYS. The available version was an education version which had several limitations in analysis. The maximum number of the nodes which were usable in the design was 512k nodes. The maximum number of faces that the model can have is 300 and the number of bodies was limited to 8.

5.2. Model meshing

The analysis for the oil film is done using the fluent analyser module of ANSYS 19.2. The element size was selected to 0.0007 mm for the accuracy. The mesh growth rate was program controlled. The model was set as solid structure with the material as babbitt. The babbitt was given boundary conditions, the ends are constrained in x, y, z axis for zero movements. The pressure was imported from the oil film analysis and is applied on the selected faces of the babbitt.

The number of nodes were 18609 and the elements were to be 8933. The whole journal bearing model with the steel backing was imported and meshed. The pressure is imported and is applied to the inside faces of the babbitt. The boundary condition remains same for the babbitt and the steel backing. The analysis is repeated for all the models of the babbitt.

5.3. Materials

The most sound operation of a journal bearing is obtained when the material used to make the bearing combine both high strength with softness [9, 11]. This in a little paradoxical but most of the bearing materials have the combination of these properties with a little compromise on their side. There were three components which required materials to consideration during the analysis, like the two parts of the journal bearing and the oil film. The overlay is a smooth material which can produce less wear and tear if there is any contact with the journal, the backing is usually a hard material which can absorb the load and withstand it for a long time.

The oil is taken as the lubricant for the operation. The materials which comes into contact with shaft was made of a metal matrix composite called babbitt [4, 7]. The material which is backing the babbitt was selected from three optional steels which are available in the market. The steels which were selected are AISI 1018, 1020, 1022, in which the AISI 1020 provided the required mechanical properties.

5.4. Oil film analysis

When considering the analysis of the first design, the oil film was having the highest pressure near to the inlet and was decreasing at a rapid rate while moving away from it. The groove has allowed the oil to produce some pressure at the bottom of the film. But it can be observed (Fig. 7) that the pressure is too high, reaching up to 50.0 MPa. This means there should be a change in velocity to decrease the pressure formed.

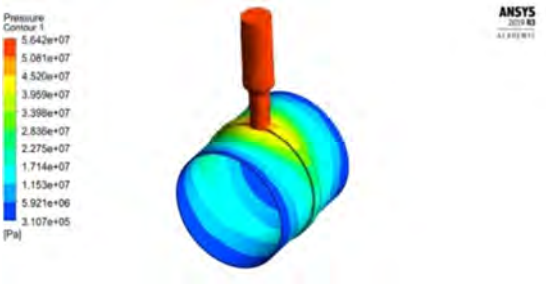

Fig. 7. Pressure distribution inside oil film 1

By introducing a second inlet parallelly opposite to the first one (Fig. 8), increase in the flow to all the circumference of the oil film. The overall bearing capacity was increased and there is less pressure losses in the film.

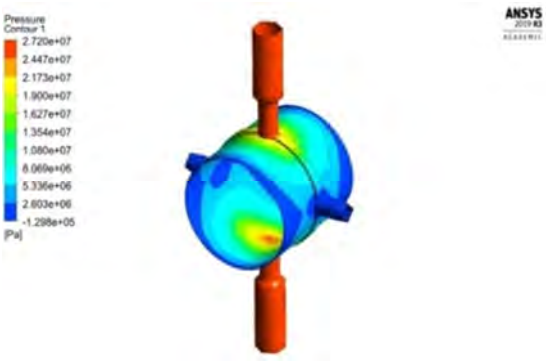

Fig. 8. Pressure distribution inside oil film 2

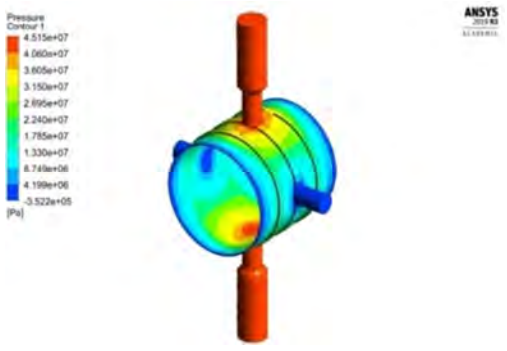

Fig. 9. Pressure distribution inside oil film 3

Next oil film had 3 grooves to flow which was used to transfer the oil to the extreme ends of the film (Fig. 9). By establish the new grooves, pressure was distributed in a more uniform manner.

The final design (Fig. 10) showed promising results compared to first one The pressure on the oil film was lesser than 10.0 MPa, which was the initially expected pressure. The placement of the inlets and holes ensures a wide range of support for the shaft without any significant reduction in pressure.

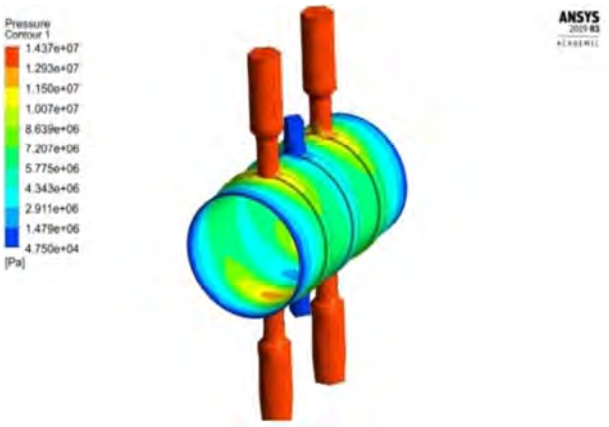

Fig. 10. Pressure distribution inside oil film 4

By placing the holes in between the inlets, more oil is removed and thus decreasing the pressure at the edges of the inlet. It was decide that this oil film design to be used for design of the actual journal bearing. There are here (Fig. 11) the diagram for the pressure formed in each oil film design. This is showing how each design affected the pressure, but the graph is for a soft visual comparison since a lot of design changes were experimented between different stages to verify the effectiveness.

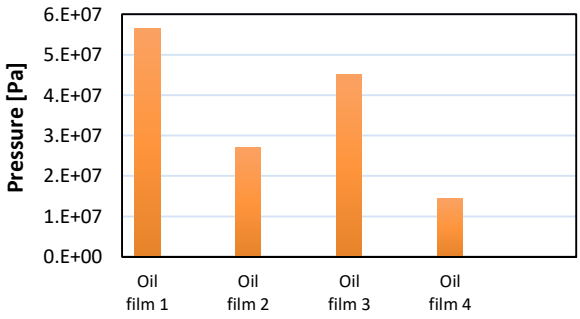

Fig. 11. Maximum pressure exerted by all the oil films

5.5. Babbitt analysis

The babbitt with 1 mm thickness was analysed using static structural analysis by applying the pressure exerted by the desired oil film. The result shows that, the highest pressure noted is near the inlet to the Babbitt (Fig. 12). The animation of the expansion due to the pressure shows, the babbitt expands at faster and higher rate near the inlet of the babbitt. This is due to pressure exerted at the inlet end was high in the oil film analysis. The holes in the babbitt design decreases the deformation at that point by a large value.

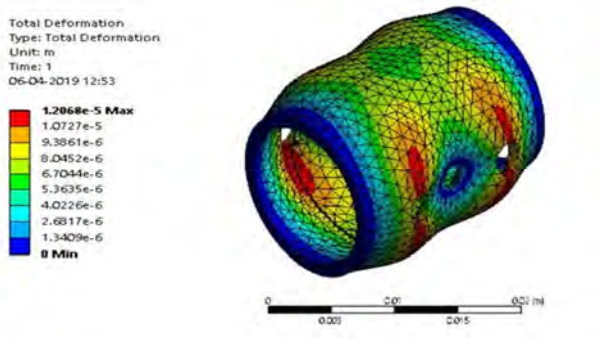

Fig. 12. Deformed babbitt 1 under pressure from oil film

In the 0.35 mm (Babbitt 2 – Fig. 13), the result showed a large difference in how the circumference, which is perpendicular to the inlet, deforms due to the pressure. This surface does not undergo a deformation compared to the other locations. The amount of deformation near the holes also increases which is a noted pattern as the thickness decreases. Since the material is a metallic, the stress-strain graph shows us that there can be an elastic deformation which changes to plastic after a certain value. This is noted here, the material deformation is easier near the inlet, thus it continues to deform to relieve the increase in pressure.

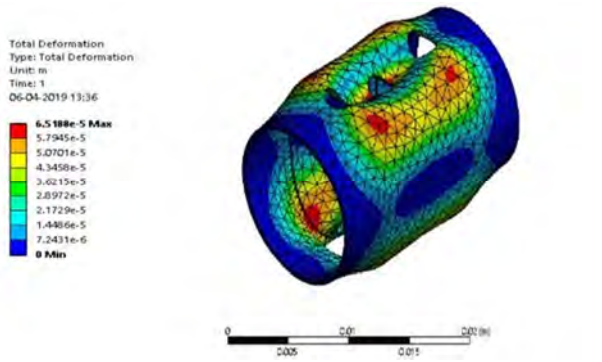

Fig. 13. Deformed babbitt 2 under pressure from oil film

The below table shows a comparison between the babbitts in mechanical properties.

Table 1. Comparison of the results for each Babbitt

Parameter		Unit	Design No	
			Babbitt 1 (1 mm)	Babbitt 2 (0.35 mm)
Maximum deflection		µm	1.21E–02	6.52E–02
Maximum stress		Pa	3.53E+08	1.64E+09
Maximum elastic strain		m/m	7.10E–03	3.31E–02
Total strain energy		J	2.14E–02	6.93E–02
Factor of Safety	Minimum	–	7.08E–01	1.50E–01
	Average	–	6.14E+00	2.69E+00

5.6. Full bearing analysis

The bearing with 1mm babbitt is seen considerable improvements in deformation due to support provided by the steel backing. The babbitt is deforming in a uniform manner starting from the inlet to the periphery. The maximum stress developed also decreased by 10 times compared to just the babbitt supporting the pressure. The other parameter were also decreased by a considerable value except Factor of Safety (FoS). The average FOS value as seen in the Table 2 is a very good value which reinforce the safety factor of the bearing under operation. The maximum deformation is seen on the corner edge of the grooves near the inlet of the oil supply, since the stress concentration is more due to sharp edges present at those points.

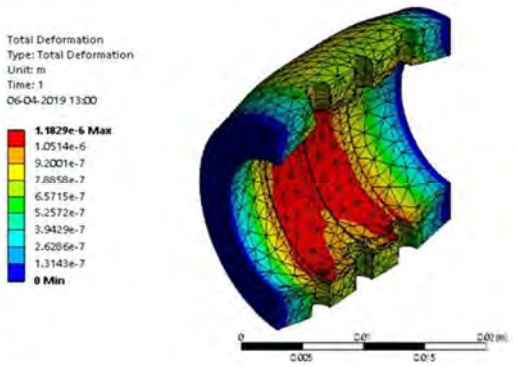

Fig. 14. Deformed bearing 1 under pressure from oil film

While analysing the bearing with 0.35 mm babbitt, the deflection further decreased in value, which means that as the thickness of the babbitt is decreased, the bearing properties are improved. Since the deflection was tending to decrease, we can see a relation which affects the strain energy acting on the bearing. The FOS value and the stress developed are closely related, thus the stress developed still remains the same.

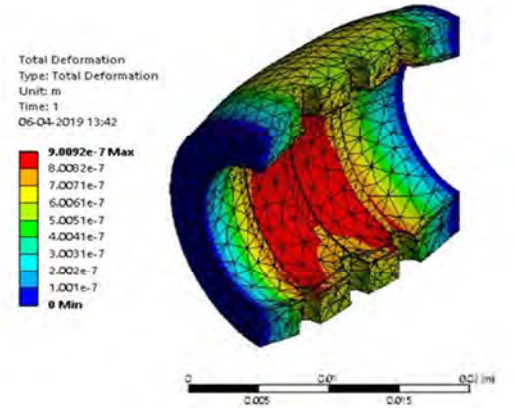

Fig. 15. Deformed bearing 2 under pressure from oil film

The table below shows a comparison of the bearings with their corresponding mechanical properties.

Table 2. Comparison of the results for each bearing

Parameter		Unit	Design No	
			Bearing 1 (1 mm)	Bearing 2 (0.35 mm)
Maximum deflection		µm	1.218–02	9.00E–03
Maximum stress		Pa	6.24E+07	5.85E+07
Maximum elastic strain		m/m	4.49E–04	3.98E–04
Total strain energy		J	2.62E–03	2.00E–03
Factor of Safety	Minimum	–	4.73E+00	5.04E+00
	average	–	1.44E+01	1.46E+01

5. Summary

It seems that the main objectives of the project which was to design a slide bearing, so that it can withstand the forces generated due to the increased length of the shaft in the turbocharger has been achieved. The paper introduces a series of modernization of the bearing structure, considering the most favorable oil pressure distribution. The study takes into account changes in thickness of the oil film, the number of grooves and their dimensions, the number of inlets and outlets and the length of the slide bearing. Simulation models were created using CATIA V5 and the analysis is performed using ANSYS 19.2. With the help of the oil film, the babbitt plate was designed. It was having a higher deformation near to the inlet due to the higher pressure which is formed. The grooves were producing sharp ends near the inlet which also increases the stress concentration. The irregularity in deformation of the babbitt is caused by the holes reducing the pressure in its zone. During the babbitt analysis, it was observed that as the thickness increased the babbitt showed better properties under the pressure acting on them.

The babbitt was supported by the steel backing and was analysed, which showed that the lesser the babbitt thickness the more better the journal bearings performance. This property can be explained by the transfer of stress from one material to the other. The stress transfer is high when the distance between the point of stress application and the location of the second material is less. As stress travels over a longer distance, the material absorbs the energy and deforms. This cause less energy to be transferred to the second material, and making too much stress allocation on the first material. Thus, after using the steel backing, the babbitt with 0.35mm proved to show more Factor of Safety and less deformation compared to the other bearings.

The currently constructed bearings can withstand about 150 bar of pressure in the oil film without having a significant change in dimensions. From the two bearings that were designed according to the oil film required, it can conclude that the 0.35 mm thick babbitt bearing is better than 1 mm. The length of the bearing can be increased to without compromising in the pressure exerted at different location by making changes to the oil film design. Removing the edges in the grooves can decrease the concentration of stress and increase the Factor of Safety. All of the mentioned above items directly affect to overall efficiency of the engine due to the fact that the energy necessary to overcome frictional resistance is reduced.

Acknowledgments:

This research was supported by using resources GEO-3EM Energy, Ecology, Education co-financed by the European Regional Development Fund.

Bibliography

[1] ANSYS Fluent Tutorial Guide. *Ansys Inc.* 2017.
[2] BAINES, N.C. Fundamentals of Turbocharging. *Concepts ETI, Inc.* 0933283148, 2005.
[3] BOMPOS, D.A., NIKOLAKOPOULOS, P.G. Tribological design of a multistep journal bearing. *Simulation Modelling Practice and Theory*. 2016, **68,** 18-32. https://doi.org/10.1016/j.simpat.2016.07.002
[4] CAMPO E.A. Plastic journal bearing design. *The Complete Part Design Handbook*, 2006, 335-376.
[5] CHEN, W.J. Rotordynamics and bearing design of turbochargers. *Mechanical Systems and Signal Processing*. 2012, **29**, 77-89. https://doi.10.1016/j.ymssp.2011.07.025
[6] CHUEPENG, S., SAIPOM, S. Lubricant thermo-viscosity effects on turbocharger performance at low engine load. *Applied Thermal Engineering*. 2018, **139**, 334-340. https://doi.org/10.1016/j.applthermaleng.2018.05.002
[7] CYPKO, E., KALDONSKI, T. Influence of lubricated sliding couple structural material type on generated potential difference value. *Journal of KONES Powertrain and Transport*. 2011, 18(1).
[8] DOWSON, D., TAYLOR, C.M., GODET, M. et al. Fluid film lubrication – Osborne Reynolds centenary. *Proceedings of 13th Leeds-Lyon Symposium on Tribology.* 1986, **11**. University of Leeds, England.
[9] KALDONSKI, T. Fundamentals of analysing od tribological processes. *WAT Publisher*. Warsaw 2015 (in Polish).
[10] KOUTSOVASILIS, P., DRIOT, N., DAIXING, L. et al. Quantification of sub-synchronous vibrations for turbocharger rotors with full-floating ring bearings. *Archive Applied Mechanics*. 2015, **85**(4), 481-502. https://doi.org/10.1007/s00419-014-0924-0
[11] LAWROWSKI, Z. Tribology. friction, wear and lubrication. *PWN Publisher*. Warsaw 1993 (in Polish).
[12] LI, C., WANG, Y., JIA, B. et al. Application of Miller cycle with turbocharger and ethanol to reduce NO_x and particulates emissions from diesel engine – a numerical approach with model validations. *Applied Thermal Engineering.* 2019, **150**, 904-911. https://doi.org/10.1016/j.applthermaleng.2019.01.056
[13] MANSHOOR, B., JAAT, M., IZZUDDIN, Z. et al. CFD analysis of thin film lubricated journal bearing. *Procedia Engineering*. 2013, **68**, 56-62. https://doi.org/10.1016/j.proeng.2013.12.147
[14] NICHOLAS, J., ALLAIRE, P., LEWIS, D. Stiffness and damping coefficients for finite length step journal bearings. *ASLE Transactions*. 2008, **23**(4), 353-362. https://doi.org/10.1080/05698198008982979
[15] ROMAGNOLI, A., MANIVANNAN, A., RAJOO, S. et al. A review of heat transfer in turbochargers. *Renewable and Sustainable Energy Reviews*. 2017, **79**, 1442-1460. https://doi.org/10.1016/j.rser.2017.04.119
[16] ROY L., LAHA, S. Steady state and dynamic characteristics of axial grooved journal bearings. *Tribology International*. 2009, **42**(5), 754-761, https://doi.org/10.1016/j.triboint.2008.10.010
[17] SCOTT, R. Journal bearings and their lubrication. *Machinery Lubrication*. Publish by Noria. 2005, 7, https://www.machinerylubrication.com/Read/779/journal-bearing-lubrication
[18] SCHWARZ, J.B., ANDREWS, D.N. Considerations for gas stand measurement of turbocharger performance. *Proceedings 11th International Conference on Turbochargers and Turbocharging*. 2014, 253-264. Institute of Mechanical Engineers, London.
[19] SEP, J., TOMCZEWSKI, L., GALDA, L. et al. The study on abrasive wear of grooved journal bearings. *Wear.* 2017, **376-377**, 54-62. https://doi.org/10.1016/j.wear.2017.02.034
[20] SHAABAN, S., SEUME, J. Impact of turbocharger non-adiabatic operation on engine volumetric efficiency and tur-

bo lag. *International Journal of Rotating Machinery*. 2011, **2012**. https://doi.org/10.1155/2012/625453

[21] SJOBERG, E. Friction characterization of turbocharger bearings. *Master of Science Thesis MMK*. 2013, **149**.

[22] STAHL, J., JACOBSON, B.O. Design function for hydrodynamics bearings. *Proceedings of the Institution of Mechanical Engineers, Part J: Journal of Engineering Tribology*. 2001, **215**(5), 405-416. https://doi.org/10.1243/1350650011543637

[23] SUMMER, F., GRÜN, F., OFFENBECHER, M. et al. Challenges of friction reduction of engine plain bearings – tackling the problem with novel bearing materials. *Tribology International*. 2018, **131**, 238-250. https://doi:10.1016/j.triboint.2018.10.042

[24] VANHAELST, R., KHEIR, A., CZAJKA, J. A systematic analysis of the friction losses on bearings of modern turbocharger. *Combustion Engines*. 2016, **164**(1), 22-31. https://doi.org/10.19206/CE-116485

Prof. Zbigniew Sroka, DSc., DEng. – Faculty of Mechanical Engineering, Wroclaw University of Science and Technology.
e-mail: *zbigniew.sroka@pwr.edu.pl*

Srinath Prakash, MEng. – Graduate of Faculty of Mechanical Engineering, Wroclaw University of Science and Technology.
e-mail: *srinath.p2@gmail.com*

Radoslaw Wlostowski, MEng. – Faculty of Mechanical Engineering, Wroclaw University of Science and Technology.
e-mail: *radoslaw.wlostowski@pwr.edu.pl*

Article citation info:
LABECKAS, G., SLAVINSKAS, S., MICKEVIČIUS, T. Experimental investigation of biodiesel-n-butanol fuels blends on performance and emissions in a diesel engine. *Combustion Engines*. 2022, **188**(1), 90-95. https://doi.org/10.19206/CE-142030

Gvidonas LABECKAS
Stasys SLAVINSKAS
Tomas MICKEVIČIUS

Combustion Engines
Polish Scientific Society of Combustion Engines

Experimental investigation biodiesel-n-butanol fuels blends on performance and emissions in the diesel engine

ARTICLE INFO

Received: 18 July 2021
Revised: 3 September 2021
Accepted: 8 September 2021
Available online: 23 September 2021

The paper presents the experimental test results reflecting the comparative changes in the performance efficiency and emissions of the exhaust of a naturally aspirated, four-stroke, single-cylinder, air-cooled diesel engine due to its transition from neat rapeseed oil biodiesel to fuel blends prepared by mixing in various proportion (by volume) rapeseed methyl ester (B) and butanol (Bu). The lubricity properties of biodiesel-n-butanol fuel blends were studied using HFRR method. In contrast to previous works, the undertaken investigation is performed with a totally renewable, binary liquid biofuel blends. The purpose of the research is to reduce simultaneously the production of NO_x emissions and the exhaust smoke with respect to neat biodiesel due to potentially improved homogeneity of combustible mixture and particulate matter emissions benefits suggested by the higher oxygen content (21.62 wt%) and the relatively lower carbon-to-hydrogen ratio (4.8) of the normal n-butanol. The tests revealed that the brake specific fuel consumption for the binary biodiesel-n-butanol fuel blends is always higher than that neat biodiesel produces under the same loading conditions. Maximum nitrogen oxide (NO_x) emissions were obtained with the engine running on neat biodiesel (2290 ppm). At full (100%) load conditions, the lowest NO_x emission was obtained with the engine running on a biofuel BBu20 blend. The lowest level of carbon monoxide emissions (CO) was observed, when engine running with the most butanol-oxygenated biofuel blend BBu20.The highest smoke opacity of the exhaust was obtained when the engine was fuelled with neat biodiesel and at full load.

Key words: *diesel engine, biodiesel, n-butanol, lubricity, brake specific fuel consumption, engine efficiency, emissions, smoke opacity*

1. Introduction

In the recent decades, the scientists continue to work on the rational global energy using as well as urgent ecological and environmental problems. The requirements stated by the EU parliamentarians to intensify the development of renewable energy sources, strict environmental requests associated with the reduction of greenhouse gas emissions and wastes in the municipal economy, agricultural and forestry sectors encourage the researchers to investigate alternative and renewable energy strategies including a wider use of biofuels. Up to now, the researchers have not offered new technological solutions that would completely replace internal combustion engines by other mechanical energy sources. For this reason, oil and the natural gas reserves rapidly decrease over the recent decades. Moreover, smoke and exhaust emissions produced by internal combustion engines cause serious damage to the ecological system. The Directive 2009/28/EC of the European Parliament and the Council on the promotion of the use of energy from renewable sources approved a target of a 20% of European energy consumption using renewable fuels in a cost-effective way [1]. This Directive fixes the minimum consumption of renewable fuel used in transport-sector and creates a challenge for both the scientists and the industry. Agriculture and transport sectors are among the largest fossil fuel consumers and therefore can be regarded as the biggest contributors to the environmental pollution. The mineral diesel fuel traditionally remains the most popular among the others motor fuels. Consumption of the diesel fuel has been growing steadily over the last two decades.

The physical properties of the fuel such as density, viscosity and bulk modulus of compressibility affect the delivery rate and the injection characteristics and thus the quality of the air and the fuel mixture, which in turn affects the combustion process, brake thermal efficiency and the ecological parameters of the diesel engine. Specific properties of alternative and renewable biofuels such as density, viscosity, calorific value, cetane number, freezing point, etc. differ from those of the normal diesel fuel. Keeping in a track with the newest trends to use lighter and more environment friendly biofuels for a diesel engine powering, Giakoumis et al. [2], Rakopoulos et al. [3], Labeckas et al. [4] tested n-butanol in diesel fuel blends. The research revealed [4], due to the longer auto-ignition delay period of a pilot portion of diesel-n-butanol fuel blends both the fuel-energy conversion efficiency representing burn angle MBF50, at which burns a half of the injected fuel portion, and the end of combustion occur earlier in an engine cycle after TDC. In result, the brake thermal efficiency increases to maximum value of 0.383 when running with diesel fuel blend involving n-butanol DB3 (3.0 wt% oxygen) at speed of 1800 rpm. While the NO_x, CO and THC emissions decrease by 5.1%, 29.5% and 3.7 times, respectively, when running with the most n-butanol involving blend DB4 (4.0 wt% oxygen) against analogous values a fully loaded straight diesel produces at a higher speed of 2500 rpm. The scientists Sukjit et al. progressed further with totally renewable and environment friendly binary, biodiesel-n-butanol biofuels adding to the intake manifold hydrogen to enhance combustion and drastically reduce CO and particulate matter (PM) emissions in compression ignition engines [5].

Normal butanol ($CH_3CH_2CH_2CH_2OH$) with molecular weight of 74.12 g/mol is an alcoholic-origin colourless liquid of medium volatility and a characteristic banana-like

odour. It is flammable enough with a flash point of around 35°C, contains 21.62 wt.% of fuel-bound oxygen with a boiling point of about 117.40°C at 760 mm Hg. This renewable biofuel added to widely known rapeseed oil methyl ester (RME) reduces density, viscosity, C/H atoms ratio and provides plenty of fuel-bound oxygen that along with its good evaporative properties improves both the air and fuel vapours mixing rate and the combustion of biofuel blends. Because biodiesel and n-butanol contain a lower number than traditional diesel fuel the carbon atoms in the molecules, the enhanced combustion takes the advantage to reduce the total amount of both CO_2 and CO emissions below the respective values of neat biodiesel or from a straight diesel could be expected. When being used as an oxygenator source in the above tests, anhydrous, 200 proof, ethanol (CH_3CH_2OH – 99.9 vol%) created more concern to the researchers than n-butanol in terms of the blends consistency, auto-ignition delay extension and combustion peculiarities. However, the presence of a lighter n-butanol in biodiesel also reduces the blended cetane number rating, net heating value and thus affects mass of biofuel consumed per unit of energy or effective power developed by an engine. A sensitive interaction between advantageous and disadvantageous operational properties of renewables with a widely differing nature, origin and production technology of biodiesel and n-butanol may lead to ambiguous development trends in the combustion attributes, net heat release rate and engine out emissions [4]. In contrast to ethanol, operational properties of n-butanol are much more similar to those of a straight diesel or biodiesel with the exception of lower density, viscosity and about twice as much lower CN rating the improvement of which rests on the higher cetane number of biodiesel [8]. Moreover, n-butanol provides operational advantages because its reasonable addition to biodiesel has the potential to drastically reduce the production of CO and smoke (PM) due to considerably lower C/H atoms ratio and high fuel-bound oxygen mass (wt, %) content. Next, the lower density and viscosity of n-butanol may have positive impact on biofuel injection, atomisation and vaporisation characteristics, the air and fuel vapours mixing rate in the hot in-cylinder compressed air charge, combustion attributes and thus engine out emissions when operating under steady and transient conditions [9].

Wei et al. [6] investigated and compared biodiesel-ethanol (BE) and biodiesel-n-butanol (BBu) blends-made effects on combustion, performance and emissions of a direct-injection diesel engine. Experiments were conducted on a straight diesel, biodiesel and BE5 (5% ethanol and 95% biodiesel, v/v), BE10, BE15 and BBu5, BBu10, BBu15 biofuel blends, at five engine loads and constant speed of 1800 rpm. The blended fuels lead to higher maximum heat release rate, higher maximum in-cylinder pressure, longer auto-ignition delay, and shorter combustion duration that all in a company evoked adverse effect on combustion noise and stability particularly when running with the BE blends. Moreover, on average of the five engine loads, the BBu and BE blends increased CO emission by 13.7% and 22.8% and HC emission by 5.6% and 29.2%, respectively; but reduced NO_x emission by 6.5% and 28.0%, particle mass concentration by 20.7% and 20.6% and particle number concentration by 22% and 21%, respectively. Thus the BE blends revealed themselves as being more effective in reducing particulate and NO_x emissions, while the BBu blends suggested less increase in CO and HC emissions [6].

Zöldy [7] conducted a wide-range chemical-analytical investigation on properties of butanol, hydrogenated vegetable oil and diesel fuel blends and measured nearly 20 chemical and physical parameters, especially such as flash point, cetane number, viscosity and cold filter plugging point (CFPP) to find out whether or not the three component blends are suitable for compression ignition engines. The researcher estimated that the viscosity decreases within the test range nearly liner and every 1% of butanol mass content (v/v%) added to the blend causes slight 1.4% decreasing effect on viscosity. He also noted that the added butanol decreases the blend's flash point to around 40°C that is under the standard DIN EN ISO 2719, revised in 2016, minimum. This decrease is critical from the point of view of transportation fire-safety and logistics security. Because butanol-diesel and/or n-butanol-biodiesel fuel blends are flammable, the security equipment needs to be used as in the gasoline supply chain. Through wide-range experimental tests, the author disclosed that there about a liner relationship exists and the increase by 1% of butanol in Hydro-treated Vegetable Oil (HVO) content decreases the blended CN rating with an average of 0.4 points [7].

A lot of the research and development performed on n-butanol using in a diesel engine, however, there is not completely clear what could be the rational renewable biodiesel and n-butanol mixing rate that could be acceptable for diesel-powered machines and power generators. To make a difference, the undertaken research intends to put more light on the changing trends in performance parameters of a diesel engine, biofuels energy conversion efficiency and emissions of the exhaust when running alternately on neat biodiesel (B) derived from rapeseed oil as a 'baseline' fuel and a totally, renewable binary liquid biodiesel-n-butanol blends.

2. Materials and methods

Regardless of both biodiesel (B) and n-butanol (Bu) are of the same renewable nature, nevertheless, the production of tested biofuels derives from different resources by using dissimilar technologies, therefore, these biofuels differ as having completely different origins with widely differing chemical and physical properties (Table 1). The totally renewable blends BBu10 (11.972 wt% oxygen) and BBu20 (12.336 wt% oxygen) were prepared by mixing 90 vol.% B/10% Bu (BBu10) and 80 vol.% B/20 vol.% Bu (BBu20), respectively.

The experimental investigation was carried out in the Engine testing laboratory of Power and Transport Machinery Engineering Institute, Faculty of Agricultural Engineering of Vytautas Magnus University – Agricultural Academy. For stroke, single-cylinder, direct injection, air cooled DEUTZ FL 511 diesel engine was used for these experiments. Load characteristics of an engine were taken when operating at gradually increasing load and constant engine speed of 2000 rpm at which an engine maximum torque develops. The test results of engine operation with various

biodiesel-n-butanol blends are analysed and compared with the respective parameters measured when running with neat biodiesel derived from rapeseed oil at the respective loads, with particular attention to full (100%) engine load, at constant speed of 2000 rpm.

Table 1. Chemical and physical properties of tested biofuels

Parameter	Rapeseed oil biodiesel (B)	n-butanol (Bu)
Density at 15°C, kg/m^3	884.7	810
Kinematic viscosity, mm^2/s	4.8	2.63
Lubricity (HFRR), wear scar diameter (wsd 1.4) at 60°C, µm	205	591
Flash point, open cup, °C	168	35
Initial / final boiling points, °C	346/366	117.7
Auto-ignition temperature °C	~342	~343
Cetane number	53.4	25
Oxygen content, max wt%	10.9	21.62
Carbon-to-hydrogen ratio (C/H)	6.49	4.8
Stoichiometric air/fuel ratio, kg/kg	12.62	11.12

Torque of an engine was measured with a magnetic powder brake dynamometer PT40M (0–60 N·m) with a definition rate of ±0.5 N·m and rotation speed with a mechanical tachometer (150–3000 rpm) with an accuracy of ±0.5% of the measured value. The air mass consumption was measured with a turbine type gas meter CGT-02 (10–100 m^3/h) with an accuracy of ±1% of the measured value, and fuel mass consumption by using electronic scale SK-1000 with an accuracy of ±0.5%.

Emissions of nitric oxide (NO), nitrogen dioxide (NO_2), carbon monoxide (CO) in parts per million (ppm) and carbon dioxide (CO_2) in vol% were measured with electrochemical cells installed in Testo 350 XL flue gas analyser. Total NO_x emissions were determined as a sum of both NO and NO_2 pollutants with an accuracy of ±5 ppm. Exhaust smoke was measured with a Bosch RTT 110 opacity meter with an accuracy of ±0.1% in a scale range of 0–100%. To improve reliability of the measured data the tests have been repeated no less than three times.

Lubricating properties of the fuels were determined by using the HFRR method. Tests were conducted according to the international standard ISO 12156. The temperature of the fuel was maintained to be of a constant value of about 30ºC during the lubricity tests.

3. Analysis of the results and discussions

3.1. Lubricity of biodiesel-n-butanol fuel blends

Columns in Fig. 1 show how the average wear scar of the test ball changed when using the neat biodiesel and biodiesel-n-butanol fuels blends.

The test results demonstrate that the average wear scar with maximum increase in the diameter of 0.395 mm was obtained when using biofuel BBu30 blend. While the minimum wear scar with the diameter of 0.280 mm was obtained with neat biodiesel. The Ball On-Cylinder or BOCLE tests showed that biodiesel derived from rapeseed oil has superior lubricity compared to low sulphur diesel fuel [10] and thus the wear-sensitive fuel system designs such as plunger-barrel and the needle-valve-barrel units are able to tolerate n-butanol additions to biodiesel.

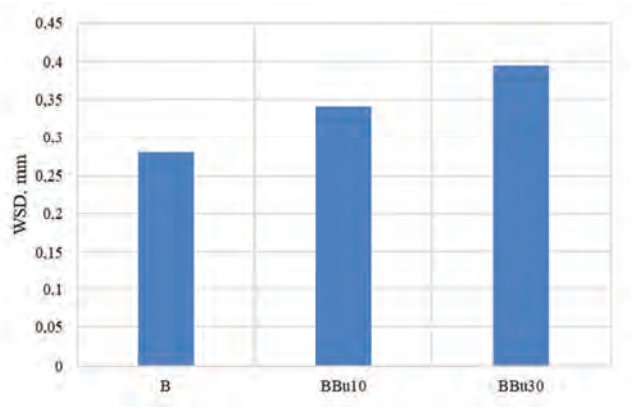

Fig. 1. The dependency of the average wear scar caused by the neat biodiesel and biodiesel-n-butanol fuel BBu10 and BBu30 blends

3.2. Performance efficiency and emissions from an engine powered with biodiesel-n-butanol fuel blends

Figure 2 shows the brake specific fuel consumption (bsfc) variations as a function of engine load. The summarised effect of the widely differing chemical and physical properties and net heating values of the biofuels studied along with the changes in the autoignition and combustion peculiarities have influence on the fuel mas burned over an hour (kg/h) and the fuel mass consumed per unit of effective power (g/kWh) developed by an engine. As can be seen in graphs, the brake specific fuel consumption (bsfc) for neat biodiesel are lower over the whole load-range tested compared to the engine running on less calorific biodiesel-n-butanol blends. The noted differences in the bsfc values are mainly observable when running at a light load, low pressure and temperature in the cylinder because the autoignition delay extends due to the presence of more volatile n-butanol with both the cooling effect and the reduced CN rating that may negatively affect the combustion of the blends. For the above reasons and slightly lower calorific value, the brake specific fuel consumptions for the respective blends BBu10 and BBu20 are up to 12.56% and 16.76% higher than, 798.7 g/kWh, neat biodiesel suggests for light-load operation.

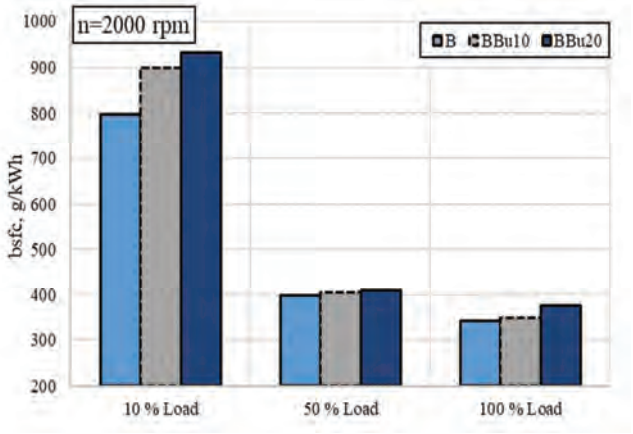

Fig. 2. The brake specific fuel consumption (bsfc) as a function of engine load when running at maximum torque speed of 2000 rpm

As soon as the temperature inside the cylinder increases with engine load increased to about medium (50% of full), the differences in brake specific fuel consumptions are also

less observable and the bsfc values for the respective blends BBu10 and BBu20 sustain at about 1.38–2.80% higher levels than, 398.4 g/kWh, the neat biodiesel consumes at considered test conditions.

As could be reasonably expected, the bsfc values remain relatively up to 1.39%–9.77% higher for n-butanol oxygenated biodiesel blends BBu10 and BBu20 when running at a full (100%) load as well than, 343.1 g/kWh, neat biodiesel suggests for the same loading conditions at maximum torque speed of 2000 rpm. The relatively higher brake specific fuel consumption of binary biofuels BBu10 and BBu20 can be mainly attributed to the lower net heating value of plenty oxygenated biodiesel-n-butanol blends.

Figure 3 shows the brake thermal efficiency variations as a function of engine load.

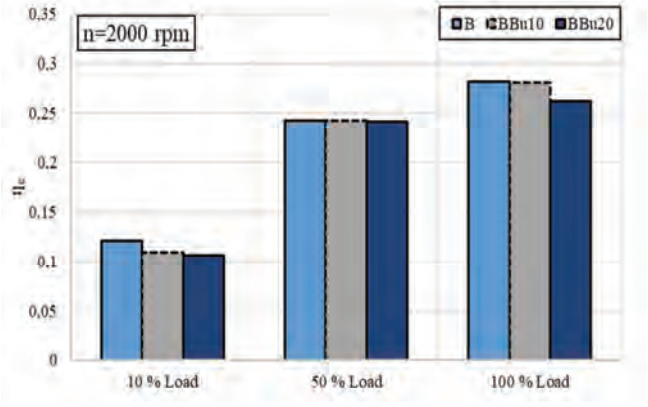

Fig. 3. The brake thermal efficiency as a function of engine load when running at maximum torque speed of 2000 rpm

The biggest relative decrease in the brake thermal efficiency of an engine reasonably obtained when running with neat biodiesel and biofuel blends tested under the low loads and thus not as high as would be needed for fuel-efficient combustion the temperature inside the cylinder. As shown in Fig. 3, an engine develops the lowest brake thermal efficiency value of 0.106 (14.15% lower) when running with the most n-butanol oxygenated blend BBu20 and the maximum one of 0.121 with neat biodiesel at the lowest (10%) load. The obtained energy conversion efficiencies of biofuel blends match well with obvious differences in the cetane number, negative changing trends in the combustion noise, engine performance stability and the respective bsfc values (Fig. 2) measured when running with blend BBu20 at the lowest load. The brake thermal efficiency gradually increased with engine load and the temperature inside the cylinder to reach for neat biodiesel the same maximum value of 0.282, remaining 3.28% and 7.33% lower engine efficiencies, 0.273 and 0.263, for the respective n-butanol blends BBu10 and BBu20 when running under full (100%) load conditions.

The variation of total emissions of nitrogen oxides (NO_x) with as a function of engine load and different biofuel blends is presented in Fig. 4. The total NO_x emissions sustain at a reasonable level when running at the lowest engine load varying within the narrow range from 434 ppm for neat biodiesel to 489 ppm for the biggest mass content of n-butanol containing biofuel BBu20. The relatively 12.5% higher NO_x emissions emanating from the combustion reaction of the most n-butanol involving blend BBu20 can be reasonably attributed to the fact that the temperature inside the cylinder is too low to keep smooth operation of an engine on plenty n-butanol oxygenated biodiesel blend at the lowest load. Therefore, the increased combustion instability accompanied by the high noise levels and the in-cylinder pressure oscillations contributed to the production of more NO_x emissions in this particular low-load conditions. High evaporative cooling effect and low calorific value of n-butanol can be realised in practise bearing in mind that the production of NO_x relies primary on the temperature inside the cylinder, local oxygen concentration, the residence time limited by the combustion reactions, and relative (overall) air/fuel ratio [11], but less depends on the availability of the local oxygen [12].

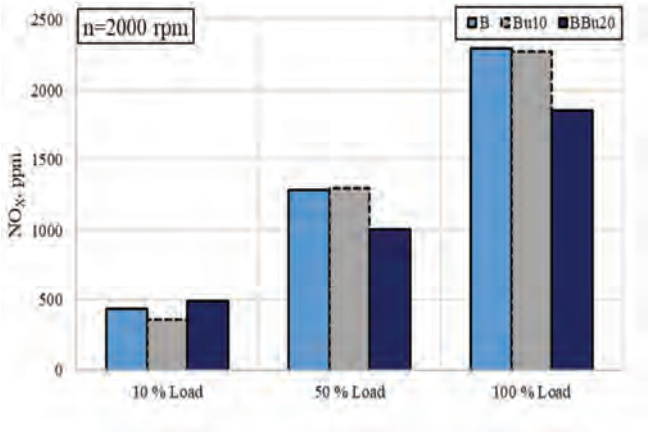

Fig. 4. The total nitrogen oxide (NO_x) emissions as a function of engine load when running at maximum torque speed of 2000 rpm

The production of NO_x emissions gradually increases with engine load and thus the temperature inside the cylinder reaching the lowest value, 1280 ppm, for neat biodiesel and 1273 ppm, for the combustion of biofuel blend BBu10 when running at about medium (50% of full) load.

As could be expected, the NO_x emissions increase to the maximum value of 2290 ppm for neat biodiesel sustaining at relatively 0.7% and 23.5% lower levels for the respective biodiesel-n-butanol blends BBu10 and BBu20 when running under the full (100%) load conditions. It is challenging to define the reasons, but in fact, the obtained result provides excellent finding revealing that the higher n-butanol mass content (v/v%) is added to biodiesel blend, the lower actually its contribution to the reduction intensity of maximum NO_x emissions can be expected. The potential answer to this intriguing question lies perhaps beyond the fact that the NO_x emissions emerge mainly during the first kinetic combustion phase under the high temperatures above 2000 K where a key role in the NO_x production plays the air-borne oxygen. While the biofuel-bound oxygen takes only a second-rate role coming into effect too late in the expansion stroke during the diffusion-controlled combustion phase and thus with a little help to contribute to the NO_x production. For this reason, the effect of the fuel-bound oxygen on the NO_x emissions changing trends can be ambiguous enough, hardly predictable and dependable on

the feedstock materials, origin and production technology of the biofuel as well as on the combustion chamber type and the test conditions of an engine, particularly on the relative (overall) air-fuel ratio.

The dependencies of carbon monoxide (CO) emission of engine load is shown in Fig. 5. At the beginning of engine loading, the CO emissions relatively decrease to be 6.0 and 25.3% lower mainly for the blends BBu10 and BBu20 case, than neat biodiesel, when running at the lowest load.

As soon as the engine load increases to about medium (50% of full) value and the temperature inside the cylinder boosts up, both most n-butanol oxygenated blends BBu10 and BBu20 reveal themselves as having strong potentials to drastically reduce the carbon monoxide (CO) emissions by 10.7% and 27.3%, respectively. The noted positive CO emissions changing trends with using the most n-butanol oxygenated biodiesel blends BBu10 and BBu20 actually remain in value after transition to full (100%) load operation as well. The enhanced combustion of the respective blends BBu10 and BBu20 produces the CO emissions 486 ppm and 374 ppm lower values than, 555 ppm, for the neat biodiesel under full (100%) load operation.

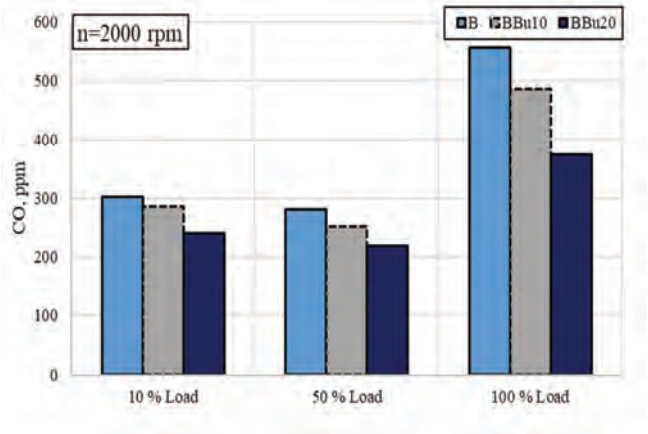

Fig. 5. Dependencies of carbon monoxide (CO) emissions on engine load when running at maximum torque speed of 2000 rpm

In contrast to ambiguous the NO_x emissions behaviour, the positive effect of the lower C/H atoms ratio strongly supported by both the absence of polycyclic aromatic hydrocarbons in the composition of biodiesel-n-butanol biofuels and the increased n-butanol-oxygen mass (wt, %) content, significantly contributes to enhance combustion and thus drastically reduce CO, CO_2 emissions and visible smoke of the exhaust.

Figure 6 shows dependencies of smoke opacity of the exhaust of engine load. Smoke opacity characteristics for the respective n-butanol oxygenated blends BBu10 and BBu20 is 52.9% and 23.5% higher comparison to the neat biodiesel produces, when running at low load and maximum torque speed of 2000 rpm. This phenomenon of smoke is the evidential fact that biofuel vapours do not burn completely at the low load, so they additionally affect transparency of the exhaust if or when the temperature inside the cylinder is not as high as would be needed to support efficient combustion and take under control the cyclic variability of operational parameters. As could be reasonably expected, the lowest smoke opacity produces the combustion of most n-butanol oxygenated blend BBu20 that is 26.7% lower than, neat biodiesel suggests when running at about medium (50% of full) load.

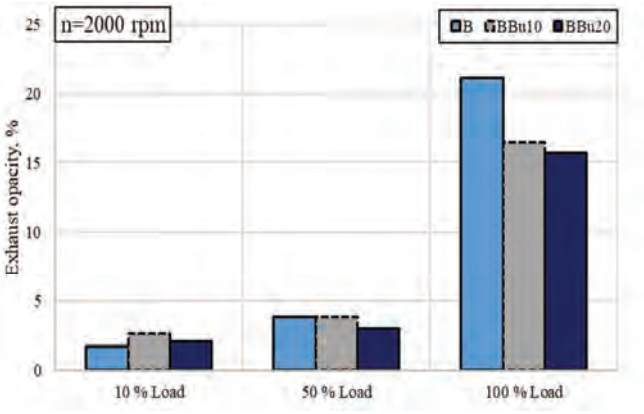

Fig. 6. Dependencies of smoke opacity of the exhaust on engine load when running at maximum torque speed of 2000 rpm

When running the engine on biofuel blends BBu10 and BBu20 at full (100%) load at maximum torque speed of 2000 rpm, the smoke opacity decreased by 28.5% and 35%, respectively, compared to the cases of using neat biodiesel.

Conclusions

1. Maximum mean diameter of the wear scar was equal to 0.395 mm when using biodiesel-n-butanol fuel BBu30 blend and the minimum value of the wear scar was measured when running with the neat biodiesel.
2. The brake specific fuel consumption using biodiesel-n-butanol fuel blends increased across at over the whole load range. At full engine load biofuel BBu10 and BBu20 blends, the break specific fuel consumption increased by 1.39%, and 9.77%, respectively, compared to neat biodiesel. The main reason of having relatively higher the bsfc for oxygenated blends is much lower net heating value of the added n-butanol.
3. Using a biofuel BBu20 blend, the break thermal efficiency was 7.33% lower, compared to the engine running on neat biodiesel, at full engine load.
4. The highest total NO_x emissions, 2290 ppm, produces the combustion of neat biodiesel, while the positive effect of n-butanol oxygenated biodiesel blends on the NO_x suppression is not as huge as could be expected. At full engine load and using biofuel BBu20 blend, the most environmentally and human harmful total emissions of nitrogen oxides decreased 23.5%, respectively.
5. When the engine running at low load, the highest the carbon monoxide emissions were obtained with the engine running on neat biodiesel (302 ppm) and the lowest using the biofuel BBu20 blend (241 ppm). Both most n-butanol oxygenated biodiesel blends BBu10 and BBu20 revealed themselves as having strong potentials to drastically reduce the carbon monoxide (CO) emissions for full load.
6. At the full engine load, using biofuel BBu10 and BBu20 blends, the smoke opacity was 28.5% and 35% lower, compared to the engine running on neat biodiesel.

Taking into account the above merits, renewable binary biodiesel-n-butanol blends are suitable for diesel engine powering to replace fossil-origin diesel fuels, reduce the climate change and safe the untouched nature for future generations. Because of the absence of polycyclic aromatic hydrocarbons in renewable biofuel blends, lower maximum NO_x and drastically reduced CO emissions and smoke opacity (PM) could reasonably be expected due to potentially improved homogeneity of combustible mixture and particulate matter (PM) emissions benefits suggested by higher n-butanol-oxygen mass content (21.62 wt%) and much lower carbon-to-hydrogen ratio (4.8).

Nomenclature

CN	cetane number
B	rapeseed methyl ester
Bu	n-butanol
BBu10	10 vol% n-butanol/80 vol% rapeseed oil methyl ester;
BBu20	20 vol% n-butanol/90vol% rapeseed oil methyl ester
WSD	wear scar diameter
bsfc	brake specific fuel consumption
bte	brake thermal efficiency
NO_x	total nitrogen oxides
CO	carbon monoxide

Bibliography

[1] Directive 2009/28/EC of the European Parliament and of the Council of 23 April 2009 on the promotion of the use of energy from renewable sources and amending and subsequently repealing Directives 2001/77/EC and 2003/30/EC. Available at: eur-lex.europa.eu

[2] GIAKOUMIS, E., RAKOPOULOS, C.D., DIMARATOS, A.M. et al. Exhaust emissions with ethanol or n-butanol diesel fuel blends during transient operation: A review. *Renewable and Sustainable Energy Reviews*. 2013, **17**(1), 170-190. https://doi.org/10.1016/j.rser.2012.09.017

[3] RAKOPOULOS, D.C., RAKOPOULOS, C.D., GIAKOUMIS, E.G. et al. Comparative evaluation of ethanol, n-butanol, and diethyl ether effects as biofuel supplements on combustion characteristics, cyclic variations, and emissions balance in light-duty diesel engine. *Journal of Energy Engineering*. 2017, **143**(2), 04016044-1-04016044-8. https://doi.org/10.1061/(ASCE)EY.1943-7897.0000399

[4] LABECKAS, G., SLAVINSKAS, S., RUDNICKI, J. et al. The effect of oxygenated diesel-n-butanol fuel blends on combustion, performance, and exhaust emissions of a turbocharged CRDI diesel engine. *Polish Maritime Research*. 2018, **25**, 1(97), 108-120. https://doi.org/10.2478/pomr-2018-0013.

[5] SUKJIT, E., HERREROS, J.M., DEARN, K.D. et al. Effect of hydrogen on butanol-biodiesel blends in compression ignition engines. *International Journal of Hydrogen Energy*. 2013, **38**(3), 1624-1635. https://doi.org/10.1016/j.ijhydene.2012.11.061

[6] WEI, L., CHEUNG, C.S., NING, Z. Effects of biodiesel-ethanol and biodiesel-butanol blends on the combustion, performance and emissions of a diesel engine. *Energy*. 2018, **155**, 957-970. https://doi.org/10.1016/j.energy.2018.05.049

[7] ZÖLDY, M. Fuel properties of butanol-hydrogenated vegetable oil blends as a diesel extender option for internal combustion engines. *Periodica Polytechnica Chemical Engineering*. 2020, **64**(2), 205-212. https://doi.org/10.3311/PPch.14153

[8] LABECKAS, G., SLAVINSKAS, S., KANAPKIENĖ, I. Study of the effects of biofuel-oxygen of various origins on a CRDI diesel engine combustion and emissions. *Energies*. 2019, **12**(7), 1241. https://doi.org/10.3390/en12071241

[9] RAKOPOULOS, D.C., RAKOPOULOS, C.D., GIAKOUMIS, E.G. Impact of properties of vegetable oil, bio-diesel, ethanol and n-butanol on the combustion and emissions of turbocharged HDDI diesel engine operating under steady and transient conditions. *Fuel*. 2015, **156**, 1-19, https://doi.org/10.1016/j.fuel.2015.04.021

[10] GRABOSKI M.S., MCCORMICK R.L. Combustion of fat and vegetable oil derived fuels in diesel engines. *Progress in Energy and Combustion Science*. 1998, **24**(2), 125-164. https://doi.org/10.1016/S0360-1285(97)00034-8

[11] SHAHIR, S.A., MASJUKI, H.H., KALAM, M.A. Performance and emission assessment of diesel–biodiesel– ethanol/bioethanol blend as a fuel in diesel engines: A review. *Renewable and Sustainable Energy Reviews*. 2015, **48**, 62-78. https://doi.org/10.1016/j.rser.2015.03.049

[12] PAPAGIANNAKIS, R.G., RAKOPOULOS, D.C., RAKOPOULOS, C.D. Evaluation of the air-oxygen enrichment effects on combustion and emissions of natural gas/diesel dual-fuel engines at various loads and pilot fuel quantities. *Energies*. 2018, **11**(11), 3028. https://doi.org/10.3390/en11113028

Prof. Stasys Slavinskas, DEng. – Institute of Power and Transport Machinery Engineering, Vytautas Magnus University.
e-mail: *stasys.slavinskas@vdu.lt*

Prof. Gvidonas Labeckas, DEng. – Institute of Power and Transport Machinery Engineering, Vytautas Magnus University.
e-mail: *gvidonas.labeckas@vdu.lt*

Tomas Mickevičius, DEng. – Institute of Power and Transport Machinery Engineering, Vytautas Magnus University.
e-mail: *tomas.mickevicius1@vdu.lt*

Article citation info:
LASKOWSKI, P., ZIMAKOWSKA-LASKOWSKA, M., ZASINA, D. Modelling of the air pollutants' cold-start emissions depending on average vehicles' speed. *Combustion Engines*. 2022, **188**(1), 96-103. https://doi.org/10.19206/10.19206/CE-142171

Piotr LASKOWSKI
Magdalena ZIMAKOWSKA-LASKOWSKA
Damian ZASINA

Combustion Engines
Polish Scientific Society of Combustion Engines

Modelling of the air pollutants' cold-start emissions depending on average vehicles' speed

ARTICLE INFO

Received: 14 July 2021
Revised: 10 August 2021
Accepted: 12 September 2021
Available online: 15 September 2021

The aim of the study is to present the results of mathematically modeled influence of the average speed on the pollutant released in the air during the cold-start process. There were taken into consideration the emission from the passenger cars (PCs) for the different fuel types, vehicles' segments (including hybrid), and the Euro standard. In the article the simulations was performed using the COPERT software, as well as WLTP-based research. The modelling results there are presented show that the change in average speed has a significant effect on air pollutant (CO_2, NO_x, NMVOC, CO) emissions released in cold-start process. Furthermore, the results show that pollutants' emissions are sensitive to average speed fluctuations.

Key words: *air pollutant, vehicle, cold-start emission, hybrid*

1. Introduction

Passenger cars' emissions are largely responsible for emissions from the road transport sector which is a significant source of air pollutants as: CO_2, NO_x, NMVOC and CO. All of these pollutants are harmful to the environment and human health, contribute to the greenhouse effect and affect air quality. Emissions from road transport is particularly troublesome in cities, where it significantly deteriorates the air quality. Emissions from motor vehicles arise mainly during two states of combustion engine operation: hot and cold-start emissions [5]. In modern vehicles emissions released into the air during the hot start (when the engine is at its normal operating temperature) are relatively small in comparison to cold-start emissions, and constantly decreasing during the trip. For this reason the cold-start emissions have become important [1, 8, 13, 16]. The cold-start emissions can be defined as the total mass of the individual pollutants generated under the operating conditions of a thermally unstable engine almost after the engine is started. [9]. Cold-start emissions can be also defined as 'excess' emissions, i.e. they are significant compared to the emissions produced when an engine is in a fully warmed-up operational state. However, taking into consideration the duration of any period of driving, the significance of cold-start emissions decreases as the duration and distance of a period of driving increase. Cold-start emissions arise at the initial start-up when the engine is cold – starting from the ambient temperature (Ta), their value can be expressed as a mass of pollutant(s) per the vehicle start [9]. During a hot start, the temperatures of the oil, coolant and all the elements of the engine are very close to those observed during a fully warmed-up operation (Tw). The term cool start can be used to refer to an engine's start in the intermediate temperatures, i.e. Ta < T < Tw, where T is the temperature of a given engine [9].

The bad air quality in urbanized areas is often dominated by these cold-start emissions which also contributes to formation of secondary aerosols [8, 13, 16]. It is especially important at low and average speed which are typical for cars usage in cities. It is also known that the emission of air pollutants depends on the type of fuel, and the Euro standard of the vehicles [2–4, 13].

2. Methodology

In this paper for purposes of simulation authors use the COPERT 5.4 software. The methodology used in the COPERT model are in accordance with the guidelines from EMEP Guidebook 2019 [5, 12] and widely applied in European countries. In the following Tier 3 approach, the total exhaust emissions from road transport are estimated as the sum of hot-start and cold-start emissions (during transient thermal engine operation) [5].

The general equation for the 'Tier 3' methodology is presented below:

$$E_{Total} = E_{Hot} + E_{Cold} \quad (1)$$

where: E_{Total} – total emissions [g] of any pollutant for the spatial and temporal resolution of the application, E_{Hot} – emissions [g] during stabilized (hot) engine operation, E_{Cold} – emissions [g] during transient thermal engine operation (cold start).

Additionally, cold-start emission occurring manly to urban driving condition, rarely in rural driving and in limited number of trips start at highway conditions. That's mean the total exhaust emission can by calculated by the equation [5]:

$$E_{Total} = E_{Urban} + E_{Rural} + E_{Highway} \quad (2)$$

where: E_{Urban}, E_{Rural}, $E_{Highway}$ – are the total emissions [g] of any pollutant the respective driving situations.

According to the 'tier 3' methodology cold-start emission is an additional emissions, which take place under all driving conditions (but most likely for urban and rural driving, as the number of starts in highway conditions is relatively limited).

Cold-start emission occur in all vehicles category, but in "EMEP/EEA air pollutant emission inventory guidebook 2019" there are available emission factors for petrol, diesel

and LPG passenger cars and light commercial vehicles, therefore only for these categories are covered by the methodology. Moreover, they are not considered to be a function of vehicle age.

According to the 'tier 3' methodology cold-start emissions are calculated as an extra emission over the emissions that would be expected if all vehicles were only operated with hot engines and warmed-up catalysts. A relevant factor, corresponding to the ratio of cold over hot emissions, is applied to the fraction of kilometres driven with a cold engine. This factor varies from country to country. Driving behaviour (varying trip lengths) and climatic conditions affect the time required to warm up the engine and/or the catalyst, and hence the fraction of a trip driven with a cold engine [5].

$$E_{Cold;|i,j} = \beta_{i,k} \cdot N_k \cdot M_k \cdot e_{Hot;i,k} \cdot \left(\frac{e^{Cold}}{e^{Hot}}\Big|_{i,k} - 1\right) \quad (3)$$

$E_{Cold;|i,j}$ – cold-start emissions of pollutant i (for the reference year), produced by vehicle technology k, $\beta_{i,k}$ – fraction of mileage driven with a cold engine or the catalyst operated below the light-off temperature for pollutant i and vehicle technology k, N_k – number of vehicles [veh] of technology k in circulation, M_k – total mileage per vehicle [km/veh] in vehicle technology k, $e_{Hot;i,k}$ – hot emission factor for pollutant i and vehicles of k technology, $\frac{e^{Cold}}{e^{Hot}}\Big|_{i,k}$ – cold/hot emission quotient for pollutant i and vehicles of k technology.

The β parameter depends on the ambient temperature (in COPERT software is using the average monthly temperature), the conditions (pattern) of the vehicle use that's means the average trip length l_{trip}. However, the information on l_{trip} is not available in Poland for all vehicle classes. According to the available statistical data and the default value of COPERT software author use the value of 12 km [5].

It should be emphasized that all of the emissions factors included in the COPERT model are determined on the basis of laboratory testing in accordance with the WLTP driving cycle [9].

In this paper, the authors investigated the impact of changes in average speed on the cold-start emissions of CO_2, NO_x, NMVOC and CO in passenger cars (PCs), for particular Euro standards, vehicles' segments and different fuel types. In the Table 1 there are shown the types of vehicles considered in the simulation.

Table 1. Types of the passenger cars considered in the simulation

Fuel	Segment	Euro Standard
Petrol	Mini, Small, Medium, Large-SUV-Executive	Euro 1 – Euro 6
Petrol HEV	Mini, Small, Medium, Large-SUV-Executive	Euro 4 – Euro 6
Diesel	Mini, Small, Medium, Large-SUV-Executive	Euro 1 – Euro 6
LPG Bifuel	Mini, Small, Medium, Large-SUV-Executive	Euro 1 – Euro 6
CNG Bifuel	Mini, Small, Medium, Large-SUV-Executive	Euro 4 – Euro 6

Calculations carried out using the COPERT software were based on the actual input data used for the compilation of Polish national emission inventory for 2019 [10]. The estimations are conducted for the basic assumptions on share per road class (urban, rural and highways) (Fig. 1), as well as the maximum and minimum temperatures occurring in Poland in 2019 [6, 7] (Table 2). The data is given below.

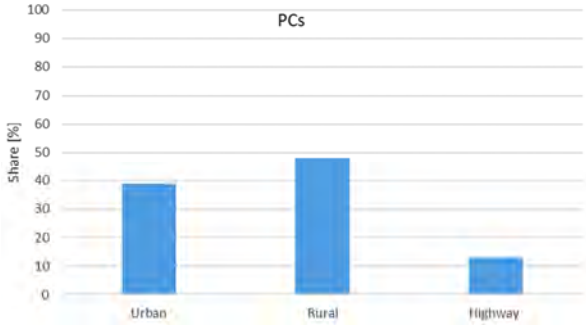

Fig. 1. Mileage share per road class

Table 2. Average monthly temperatures in Poland in 2019

Month	Min	Max
January	–8.5	1.2
February	–2.8	4
March	–2.9	7.2
April	0.8	11.2
May	1.9	13.8
June	12.5	23.3
July	9.7	20.3
August	11	21.2
September	5.7	15.2
October	4	11.5
November	–0.7	7.9
December	–3.1	4.8

Based on the various traffic situation in Polish cities authors want to check how big is the impact of the average speed on the cold-start emissions. The simulations are performed assuming average speed changing from 5 km/h to 45 km/h with 5 km/h intervals. The simulations were performed with the assumption that the engine warm-up time does not change.

3. Results

The comparison of cold-start emissions for CO_2, depending on average speed for the Euro standard is shown in the Figs 2–5, for the vehicle segment in the Figs 6–9 and for the fuel type in the Fig. 10.

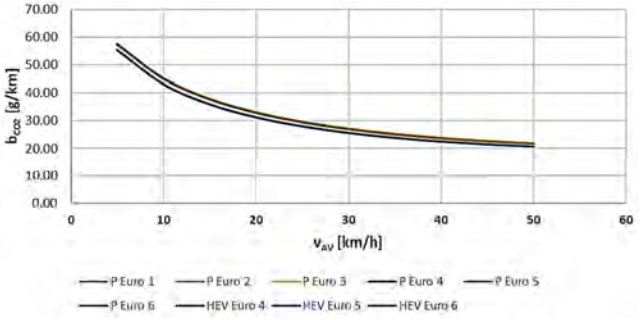

Fig. 2. CO_2 emission from petrol PCs for Euro standards depending on average speed

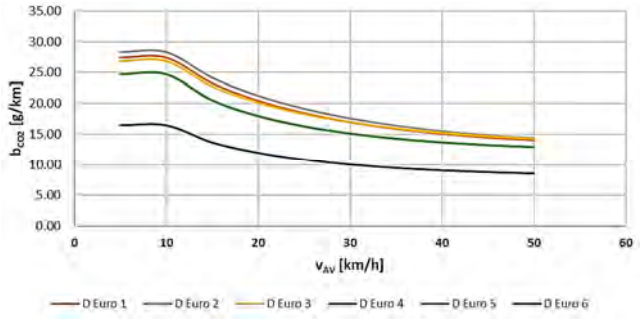

Fig. 3. CO_2 emission from diesel oil PCs for Euro standards depending on average speed

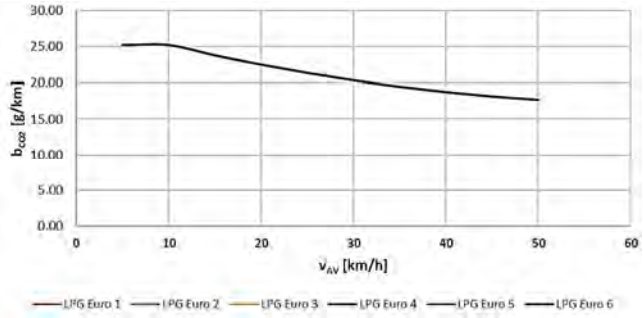

Fig. 4. CO_2 emission from LPG PCs for Euro standards depending on average speed

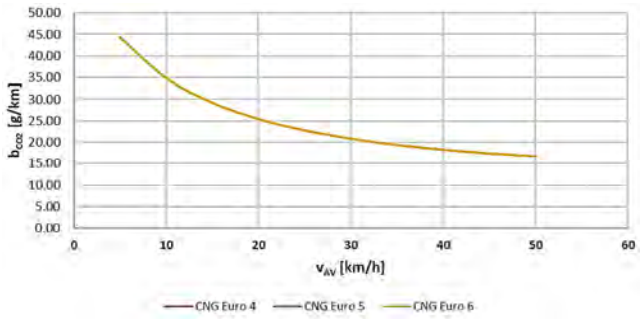

Fig. 5. CO_2 emission from CNG PCs for Euro standards depending on average speed

In the above figures it can be seen that for all fuels types, the CO_2 emissions decreases with the increase of the average speed. The cold start emission from PCs CNG and PCs LPG has the same value for all Euro standards, for PCs petrol there is small difference between the Euro standards, the greatest difference is visible for PCs diesel, where for the Euro 1 standard the cold start emission is the highest.

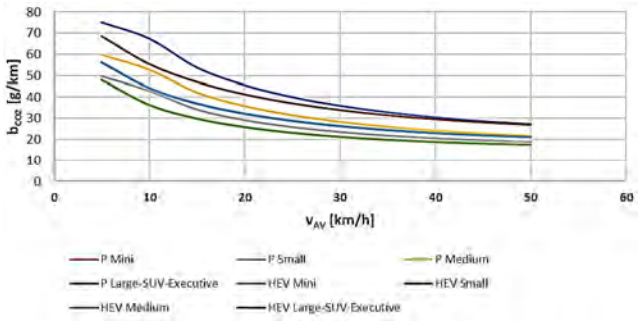

Fig. 6. CO_2 emission from petrol PCs for vehicle depending on average speed

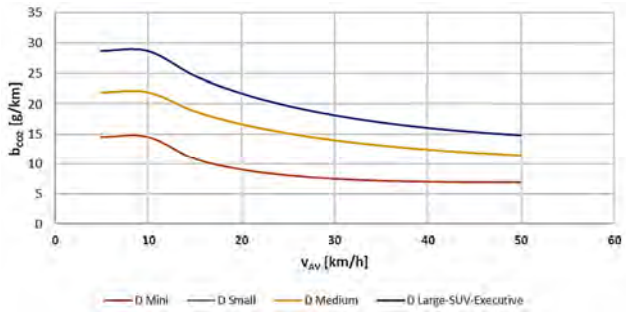

Fig. 7. CO_2 emission from diesel oil PCs for vehicle depending on average speed

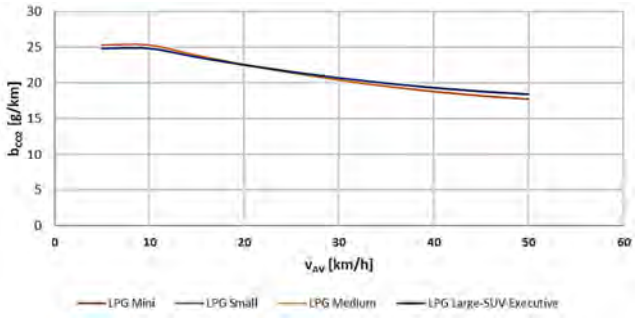

Fig. 8. CO_2 emission from LPG PCs for vehicle depending on average speed

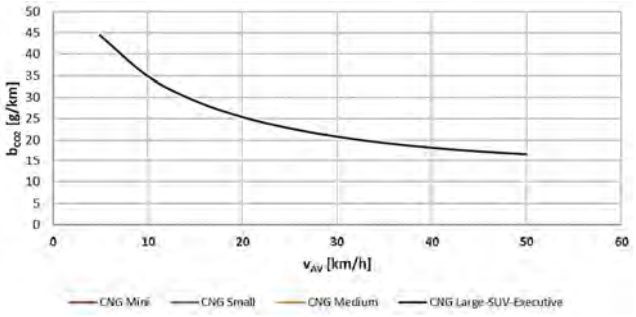

Fig. 9. CO_2 emission from CNG PCs for vehicle segments depending on average speed

The Figures 7–9 shows the dependence of CO_2 emissions on the average speed for the passenger car segments. The lowest emission is for the "Mini" and "Small" segment (for petrol, the emissions from the "Mini" and "Small" are the same, and for diesel, the emissions from the "Small" and "Medium" are the same). For CNG and LPG, there is no difference between the segments for cold start emissions.

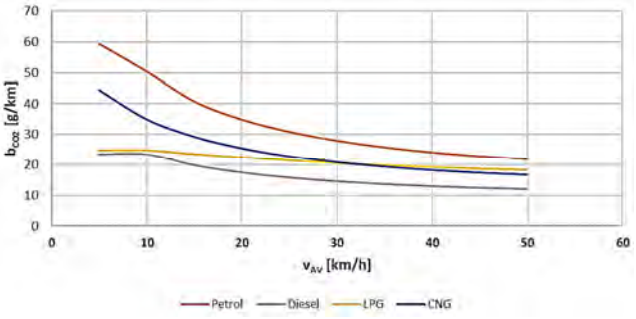

Fig. 10. CO_2 emission from PCs for fuel type depending on average speed

It is clearly visible that as the average speed increases, the cold-start emission decreases. The figure shows the sensitivity of cold-start emissions to the vehicle segment, moreover, that the lowest cold-start emission is for diesel oil and LPG.

In the Figures 11–14 are shown a comparison of NO_x cold-start emissions for Euro standard depending on the average speed, in the Figs are 15–18 for the vehicle segment and for the fuel type in the Fig. 19.

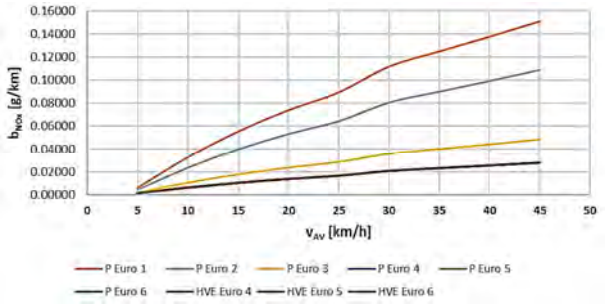

Fig. 11. NO_x emission from petrol PCs for Euro standards depending on average speed

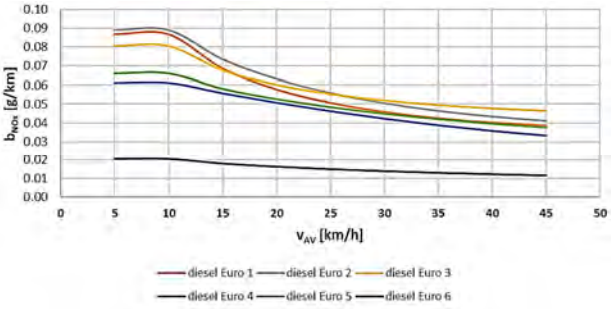

Fig. 12. NO_x emission from diesel oil PCs for Euro standards depending on average speed

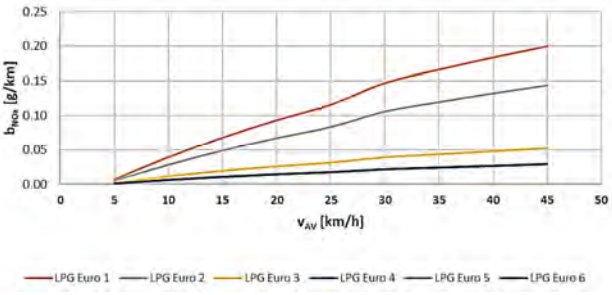

Fig. 13. NO_x emission from LPG PCs for Euro standards depending on average speed

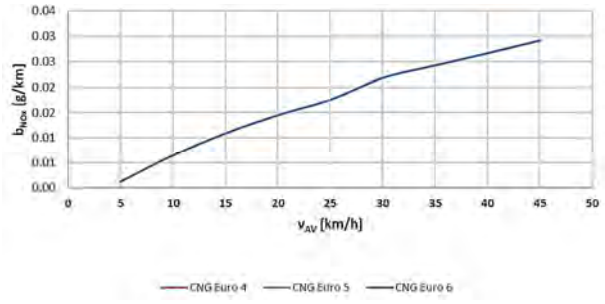

Fig. 14. NO_x emission from CNG PCs for Euro standards depending on average speed

In the Figures 11–14 it can be seen that for only for diesel the NO_x emissions decreases with the increase of the average speed and for petrol, CNG and LPG emission grows. The cold start emission from PCs CNG as the same value for all Euro standards.

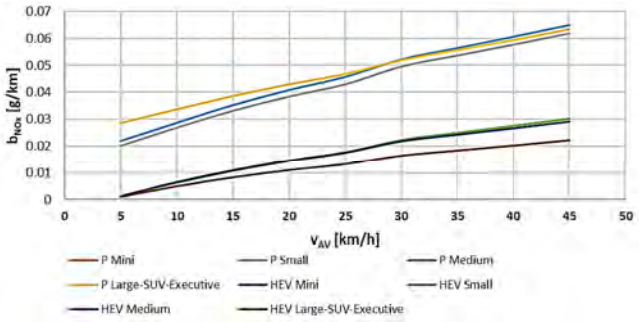

Fig. 15. NO_x emission from petrol PCs for vehicle segments depending on average speed

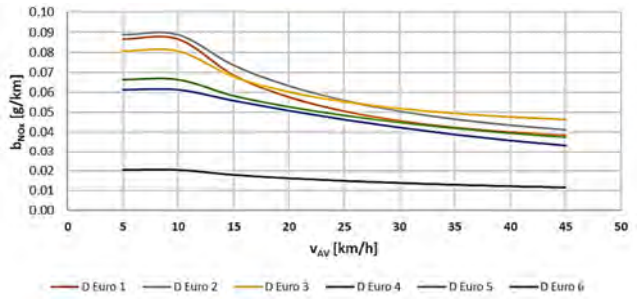

Fig. 16. NO_x emission from diesel oil PCs for vehicle segments depending on average speed

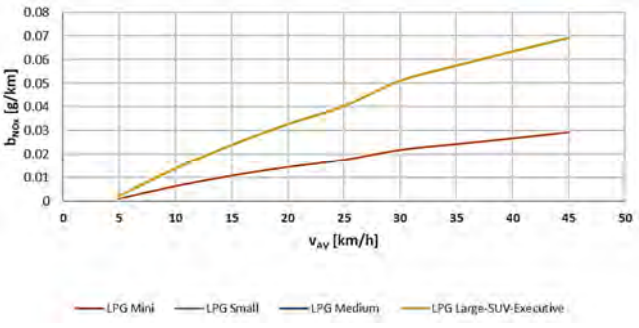

Fig. 17. NO_x emission from LPG PCs for vehicle segments depending on average speed

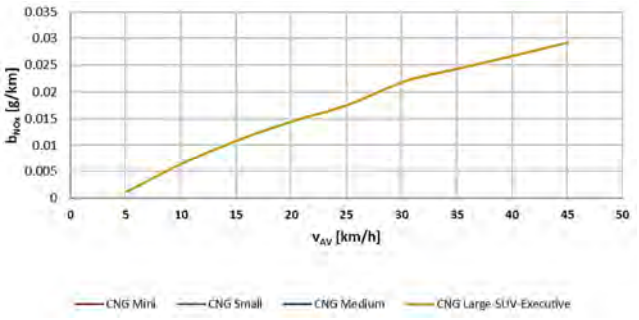

Fig. 18. NO_x emission from CNG PCs for vehicle segments depending on average speed

The Figure 16–18 shows the dependence of NO_x emissions on the average speed for the passenger car segments. For PCs CNG, there is no difference between the segments for cold start emissions.

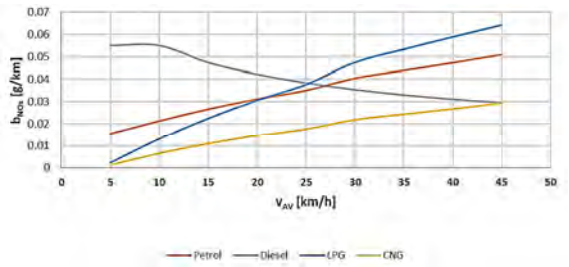

Fig. 19. NO_x emission from PCs for fuel type depending on average speed

Unlike CO_2 cold-start emissions, NO_x emissions increase with the average speed for all fuels types except diesel, this is the case for all euro standards and vehicles segments.

The comparison of cold-start emissions for CO_2, depending on average speed for the Euro standard is shown in the Figs 20–23, for the vehicle segment in the Figs 24–27 and for the fuel type in the Fig. 28.

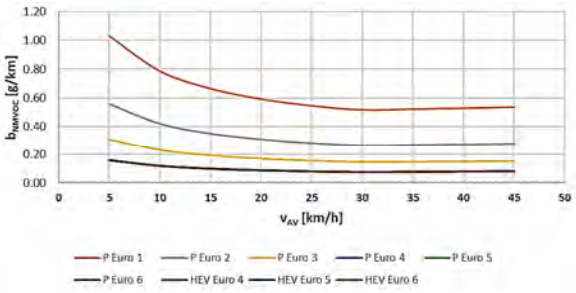

Fig. 20. NMVOC emission from petrol PCs for Euro standards depending on average speed

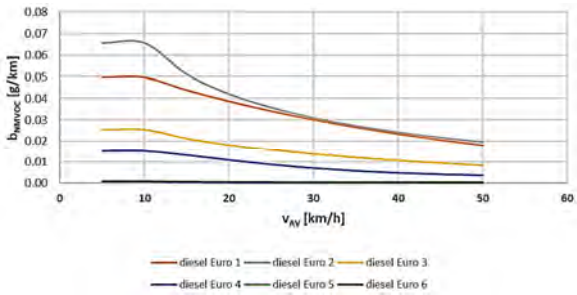

Fig. 21. NMVOC emission from diesel oil PCs for Euro standards depending on average speed

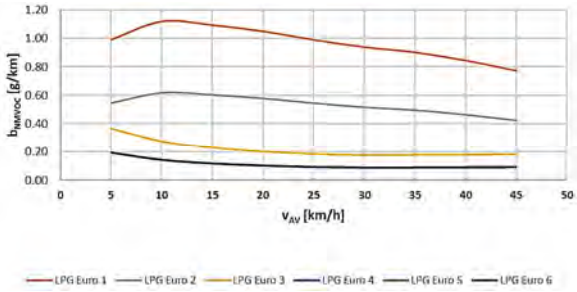

Fig. 22. NMVOC emission from LPG PCs for Euro standards depending on average speed

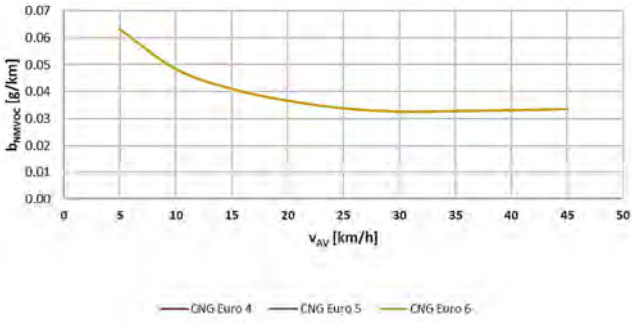

Fig. 23. NMVOC emission from CNG PCs for Euro standards depending on average speed

In the figures above it can be seen that for all fuels types NMVOC emissions decreases with the increase of the average speed for petrol, CNG and LPG emission grows. The cold start emission from PCs CNG as the same value for all Euro standards.

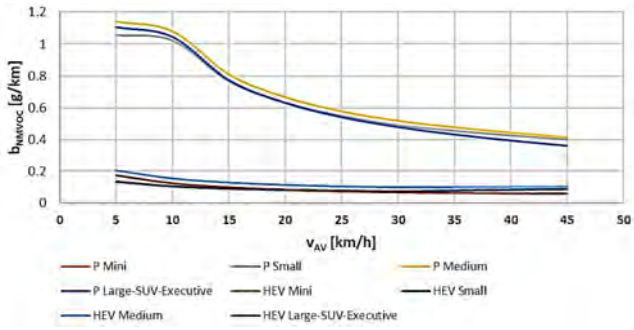

Fig. 24. NMVOC emission from petrol PCs for vehicle segments depending on average speed

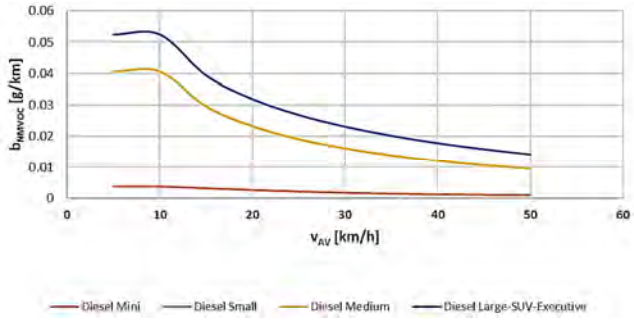

Fig. 25. NMVOC emission from diesel oil PCs for vehicle segments depending on average speed

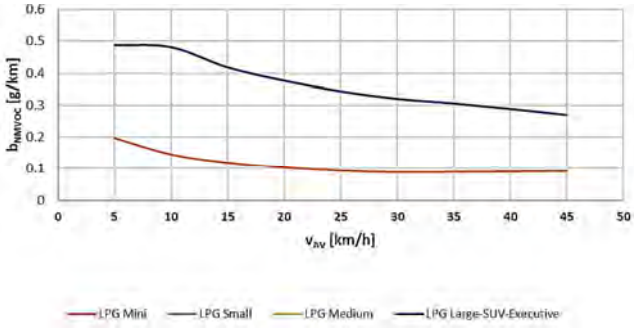

Fig. 26. NMVOC emission from LPG PCs for vehicle segments depending on average speed

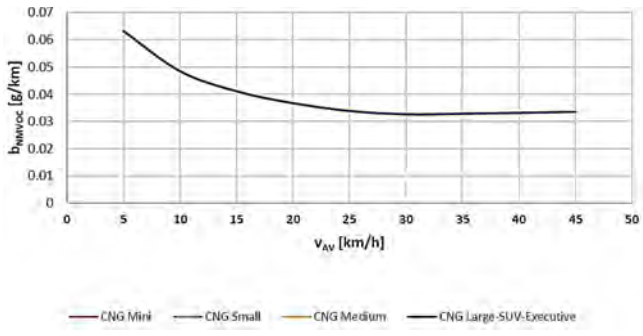

Fig. 27. NMVOC emission from CNG PCs for vehicle segments depending on average speed

On the Figure 24–27 it can be seen the dependence of NMVOC emissions on the average speed for PCs segments. For PCs CNG, there is no difference between the segments for cold start emissions.

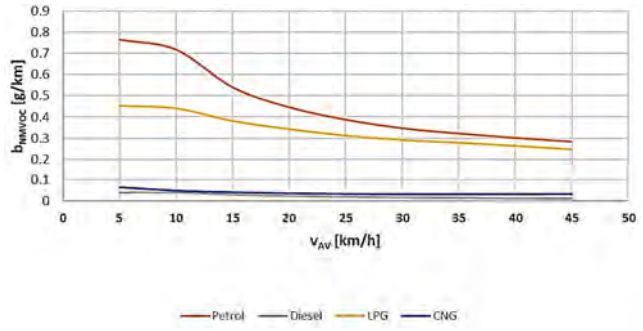

Fig. 28. NMVOC emission from PCs for fuel type depending on average speed

The figures above show that the NMVOC emissions decrease with speed for all types of fuel in all categories and segments. It should also be noted that standards for Euro 4–Euro 6 no difference in emissions.

In the Figures 29–32 are shown a comparison of NMVOC cold-start emissions for Euro standard depending on average speed, n the Figures are 33–36 for the vehicle segment and for the fuel type in the Fig. 37.

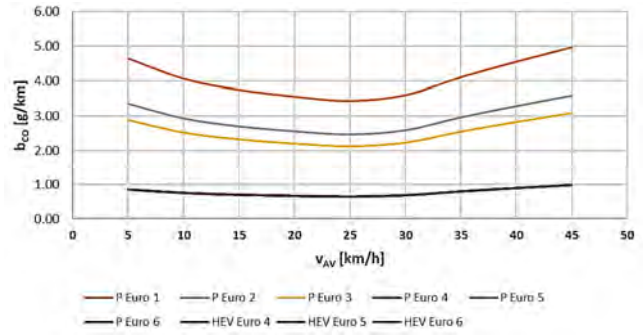

Fig. 29. CO emission from petrol PCs for Euro standards depending on average speed

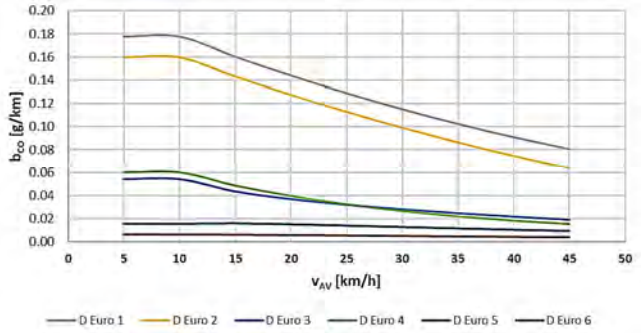

Fig. 30. CO emission from diesel oil PCs for Euro standards depending on average speed

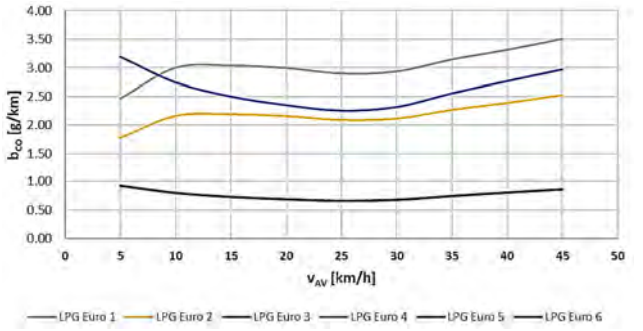

Fig. 31. CO emission from LPG PCs for Euro standards depending on average speed

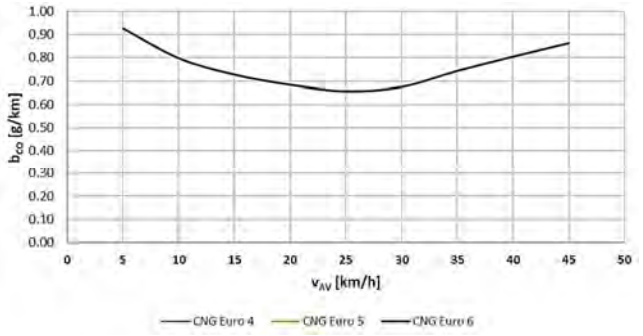

Fig. 32. CO emission from CNG PCs for Euro standards depending on average speed

The figures show the dependence of CO emissions for various euro categories on the average speed. The cold start emission from PCs CNG as the same value for all Euro standards.

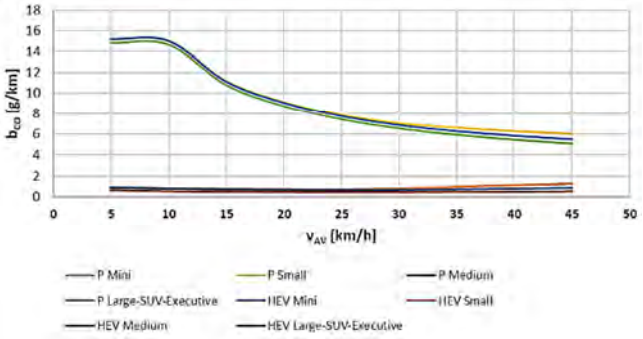

Fig. 33. CO emission from petrol PCs for vehicle segments depending on average speed

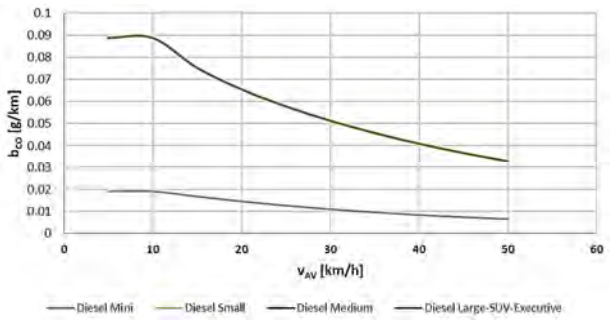

Fig. 34. CO emission from diesel oil PCs for vehicle segments depending on average speed

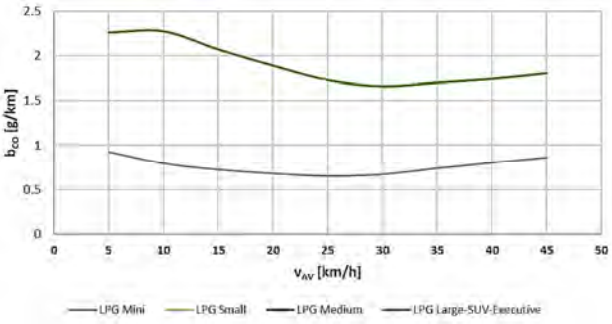

Fig. 35. CO emission from LPG PCs for vehicle segments depending on average speed

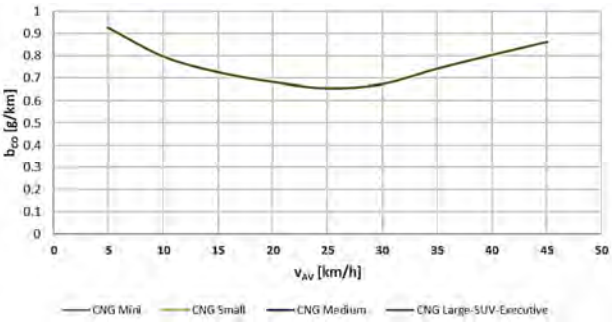

Fig. 36. CO emission from CNG PCs for vehicle segments depending on average speed

On the figure above it can be seen the dependence of CO emissions on the average speed for PCs segments. For "Mini" and "Small" and for " Medium" and "Large-SUV-Executive" for diesel and LPG the values are on the same level. For PCs CNG, there is no difference between the segments for cold start emissions.

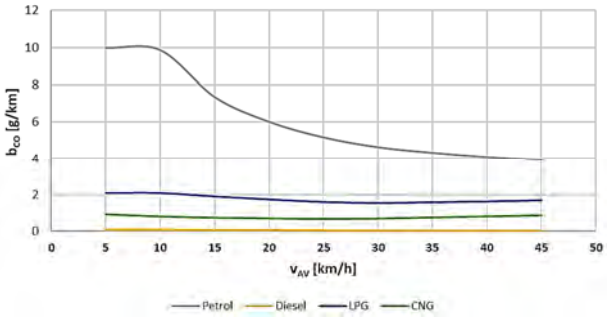

Fig. 37. CO emission from PCs for fuel type depending on average speed

The figures above show that the CO emissions decrease with speed for all types of fuel in all categories and segments. It should also be noted that standards for petrol CO cold-stare emission is higher than for another fuel.

4. Conclusions

The results of modelling indicate that in case of CO_2, NMVOC, CO are decreasing with the increasing of average speed. There is a difference between euro standard, for the Euro 1–3 cold-start emission is higher the for the Euro 4–6.

There is also a noticeable difference between the types of fuel. Cold-start emissions from gasoline combustion for all pollutants are higher than for other fuels.

The simulations carried out clearly show that increasing the average speed will reduce the cold-start emissions. The problem of emissions is particularly acute in cities during traffic congestion. It is important to strive to increase the average speed in cities, it will reduce the emission of pollutants from road transport.

The obtained modeling results would be worth comparing with measurements in real traffic conditions, the authors are in the process of conducting such tests.

Nomenclature

CNG	compressed natural gas
CO	carbon monoxide
CO_2	carbon dioxide
D	diesel oil
LPG	liquified petrolum gas
NMVOC	non-methane volatile organic compound
NO_x	nitrogen oxides
P	petrol
PCs	passenger cars
WLTP	Worldwide Harmonized Light-Duty Vehicles Test Procedure

Bibliography

[1] ANDRYCH-ZALEWSKA, M., MERKISZ J., PIELECHA J. The influence of the heating time of a catalyst-covered glow plug on the exhaust emissions from a diesel engine. *Combustion Engines*. 2021, **184**(1), 52-56. https://doi.org/10.19206/CE-134738

[2] BRADY, R.N. Internal Combustion (Gasoline and Diesel) Engines. *Reference Module in Earth Systems and Environmental Sciences*. 2013. https://doi.org/10.1016/B978-0-12-409548-9.01056-3

[3] BURR, M., GREGORY, C. Vehicular Exhausts. *Encyclopedia of Environmental Health (Second Edition)*. 2011, 335-343. https://doi.org/10.1016/B978-0-444-63951-6.00664-1

[4] CLAIROTTE, M., SUAREZ-BERTOA, R., ZARDINI, A.A. et al. Exhaust emission factors of greenhouse gases (GHGs) from European road vehicles. *Environmental Sciences Europe*. 2020, **32**, 125. https://doi.org/10.1186/s12302-020-00407-5

[5] EMEP/EEA air pollutant emission inventory guidebook 2019.
[6] GUS (2020). Statistical Yearbook of the Republic of Poland 2019. GUS, 2020.
[7] GUS T (2020). Transport – activity results in 2019. GUS, Warsaw 2020.
[8] LASKOWSKI, P., ZIMAKOWSKA-LASKOWSKA, M. The dependency between methane emissions and the trip length accounting the cold start engine conditions. *Proceedings of the Institute of Vehicles.* 2019, **1**(119), 25-33.
[9] LASKOWSKI, P., ZASINA, D., ZIMAKOWSKA-LASKOWSKA, M. et al. Modelling hydrocarbons cold-start emission from passenger cars. *Advances in Science and Technology Research Journal*. 2021, **15**(3), 117-125. https://doi.org/10.12913/22998624/138764.
[10] Ministry of Climate and Environment. 2021. Poland's Informative Inventory Report. Submission under the UNECE CLRTAP and NEC Directive. https://cdr.eionet.europa.eu/pl/eu/nec_revised/iir/envyei5sq/
[11] NTZIACHRISTOS, L., GKATZOFLIAS, D., KOURIDIS, C. et al. COPERT: a European road transport emission inventory model. ATHANASIADIS, I.N., RIZZOLI, A.E., MITKAS, P.A. et al. (eds) Information Technologies in Environmental Engineering. *Environmental Science and Engineering*. Springer, Berlin, Heidelberg. 2009. https://doi.org/10.1007/978-3-540-88351-7_37
[12] SENTOFF, K.M., ROBINSON, M.K., HOLMEN, B.A. Second-by-second characterization of cold-start gas-phase and air toxic emissions from a light-duty vehicle. *Transportation Research Record: Journal of the Transportation Research Board*. 2010, **2158**(1), 95-104. https://doi.org/10.3141/2158-12
[13] CHARLTON, S.J. Chapter 11 – Control Technologies for Compression–Ignition Engines. Handbook of Air Pollution From Internal Combustion Engines. *Academic Press*. 1998, 358-419. https://doi.org/10.1016/B978-012639855-7/50050-8
[14] SUAREZ-BERTOA, R., ASTORGA, C. Impact of cold temperature on Euro 6 passenger car emissions. *Environmental Pollution*. 2018, **234**, 318-329. https://doi.org/10.1016/j.envpol.2017.10.096
[15] WEILENMANN, M., FAVEZ, J.Y., ALVAREZ, R. Cold-start emissions of modern passenger cars at different low ambient temperatures and their evolution over vehicle legislation categories. *Atmospheric Environment*. 2009, **43**(15), 2419-2429. https://doi.org/10.1016/j.atmosenv.2009.02.005
[16] WEILENMANN, M., SOLTIC, P.. HAUSBERGER, S. The cold start emissions of light-duty-vehicle fleets: A simplified physics-based model for the estimation of CO_2 and pollutants. *Science of the Total Environment*. 2013, **444**, 161-176. https://doi.org/10.1016/j.scitotenv.2012.11.024

Piotr Laskowski, DEng. – Faculty of Automotive and Construction Machinery Engineering, Warsaw University of Technology.
e-mail: *piotr.laskowski@pw.edu.pl*

Magdalena Zimakowska-Laskowska, DEng. – Institute of Environmental Protection – National Research Institute.
e-mail: *magdalena.zimakowska-laskowska@kobize.pl*

Damian Zasina, DEng. – Faculty of Building Services, Warsaw University of Technology.
e-mail: *damian.zasina@pw.edu.pl*

Wrocław University of Science and Technology

X INTERNATIONAL
CONGRESS ON COMBUSTION ENGINES

POLISH SCIENTIFIC SOCIETY
OF COMBUSTION ENGINES

18th-20th June 2023

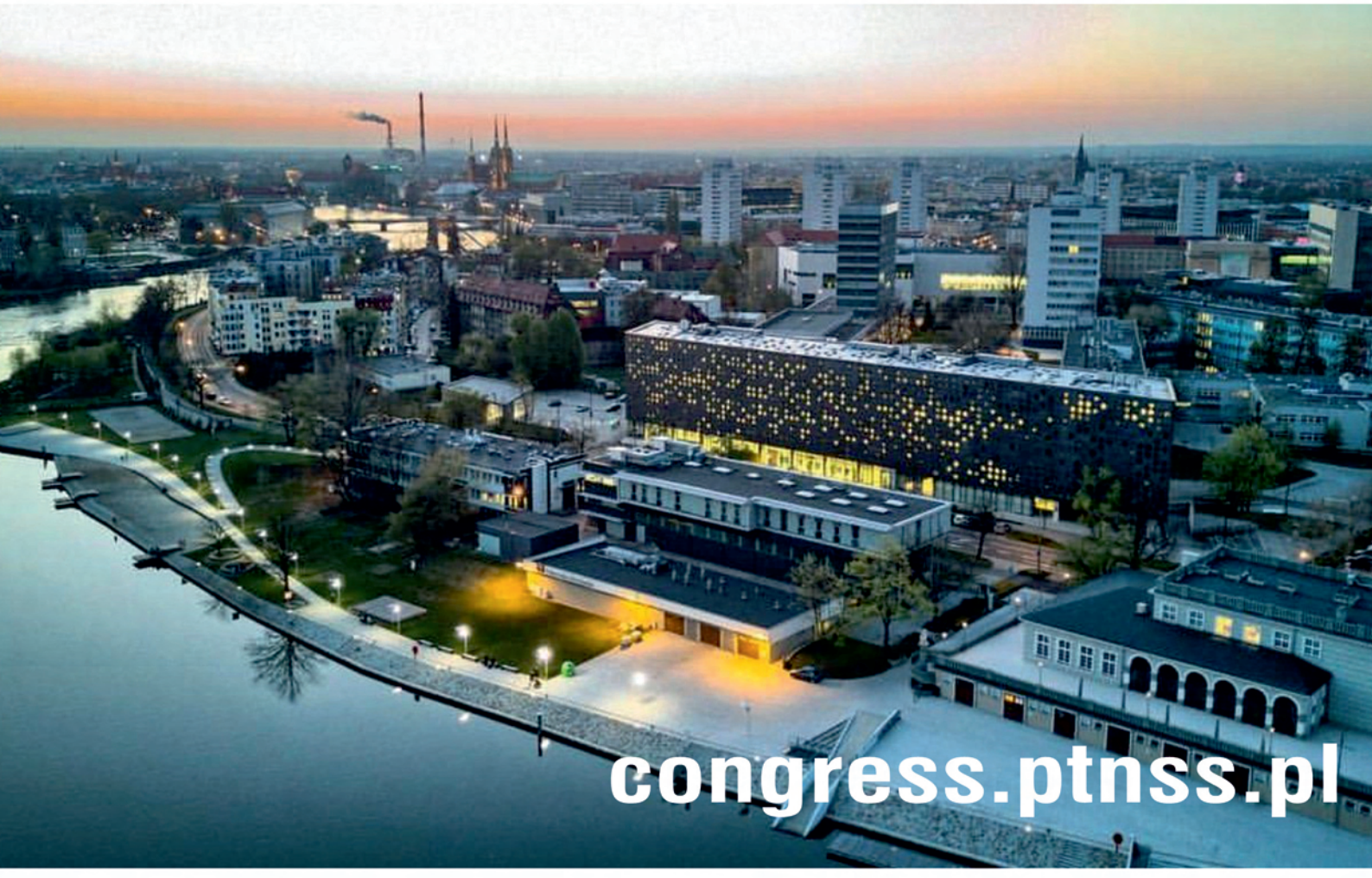

Wroclaw University of Science and Technology
Faculty of Mechanical Engineering
Wyb. St. Wyspianskiego 27, 50-370 Wroclaw, Poland

SAE INTERNATIONAL®

Join us in person in 2022!

Powertrains, Fuels and Lubricants Meeting and Exhibition

September 6-8, 2022
Krakow, Poland

SPONSORS:
BOSMAL
PTNSS

Call for Papers/Presentations

Share your innovative research by submitting an abstract for consideration as part of our 2022 technical program. It only takes 250 words to get started!

Contact: Dr. Piotr Bielaczyc, FSAE – Chair of the SAE 22 PF&L Organizing Committee
email: piotr.bielaczyc@bosmal.com.pl
phone: +48 33 8130598

Exhibit Space & Sponsorships Available

Contact Megan McCoy for information on exhibiting or sponsoring in Krakow.

o: +1.724.772.4037
e: megan.mccoy@sae.org

sae.org/pfl

P21835301

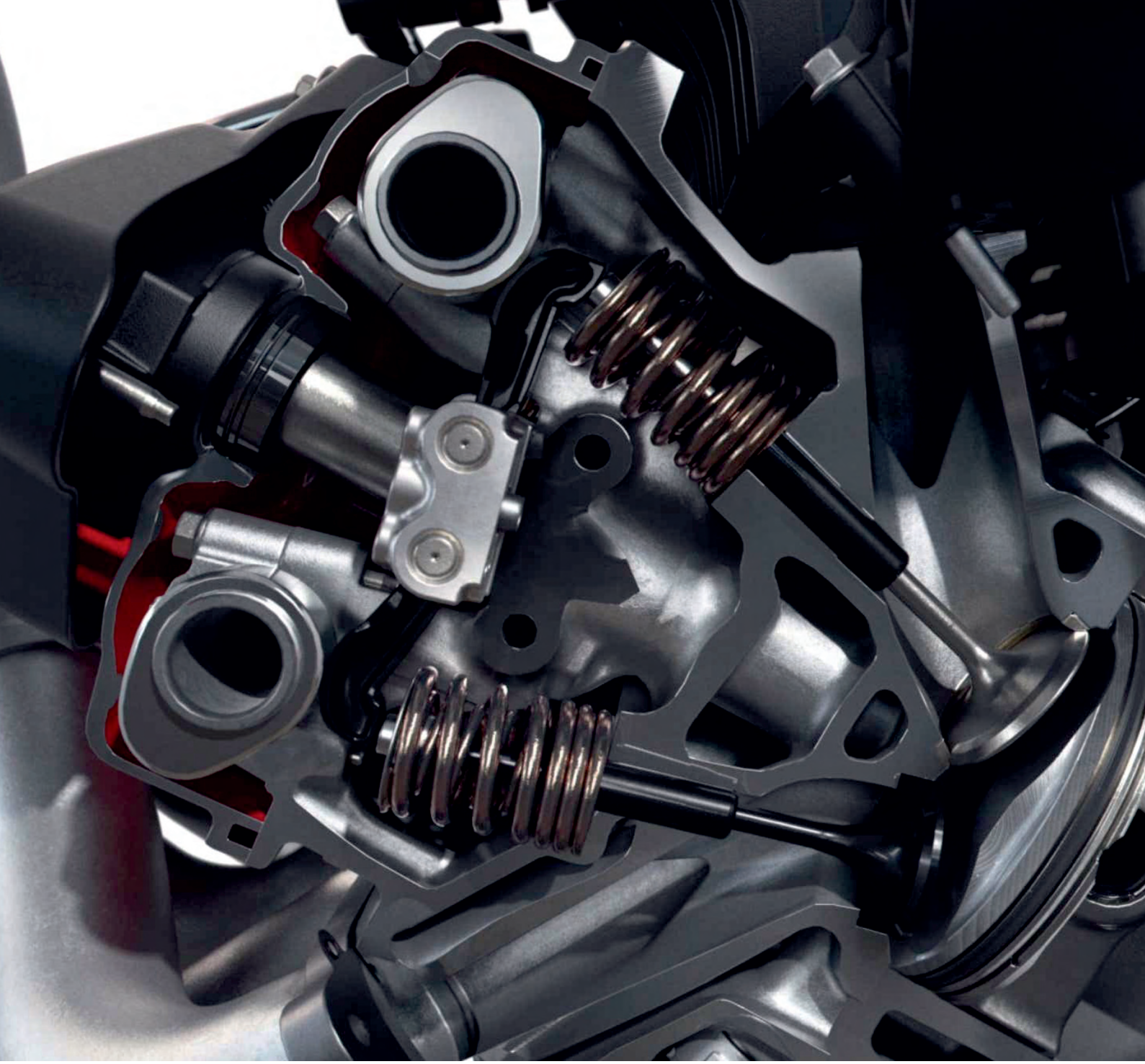

Publisher:

Polish Scientific Society of Combustion Engines

Combustion Engines

Polskie Towarzystwo Naukowe Silników Spalinowych

ISSN: 2300-9896
eISSN: 2658-1442

www.combustion-engines.eu